Mechanistic Studies on Palladium-Catalyzed C–N Cross-Coupling Reaction

By Pedro Luis Arrechea

B.S. Chemical Engineering, Massachusetts Institute of Technology, 2004

Submitted to the Department of Chemistry
in Partial Fulfillment of the
Requirement for the Degree of

Doctor of Philosophy in Organic Chemistry

at the

Massachusetts Institute of Technology

September 2016

© 2016 Massachusetts Institute of Technology

Signature of Author: ___ Signature redacted

Department of Chemistry
August 12, 2016
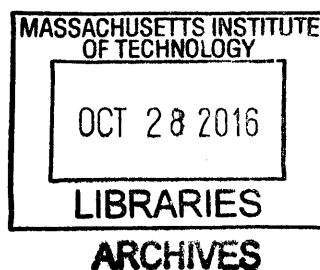
Certified by: _____ Signature redacted

Stephen L. Buchwald
Camille and Henry Dreyfus Professor of Chemistry
Thesis Supervisor

Accepted by: _____ Signature redacted

Robert W. Field
Haslam and Dewey Professor of Chemistry
Chairman, Departmental Committee on Graduate Students

This doctoral thesis has been examined by a committee of the Department of Chemistry as follows:

Signature redacted

Professor Timothy F. Jamison: _____

Thesis Committee Chair

Signature redacted

Professor Stephen L. Buchwald: _____

Thesis Supervisor

Signature redacted

Professor Jeremiah A. Johnson: ___

Mechanistic Studies on Palladium-Catalyzed C–N Cross-Coupling Reaction

By Pedro Luis Arrechea

B.S. Chemical Engineering, Massachusetts Institute of Technology

Submitted to the Department of Chemistry in Partial Fulfillment of the Requirement

for

the Degree of

Doctor of Philosophy in Organic Chemistry

September 2016

Abstract

Mechanistic studies on the palladium catalyzed C–N bond-forming reaction were carried out to generate a more complete understanding of the catalytic cycle. To understand this reaction, several kinetic studies employing simple aryl halide and amine coupling partners were performed to elucidate unknown reaction pathways.

Chapter 1. The resting state for the palladium catalyzed cross-coupling of various diarylamines and aryl halides is found to be the diphenylamido complex. Kinetic studies of the catalytic reaction are used to generate an Eyring plot. Hammett studies were performed for both the aryl halide and diarylamine coupling partners. The rates of reductive elimination for catalysts based on the biaryl ligands XPhos, CyJohnPhos, CPhos, BrettPhos, RuPhos, and SPhos were evaluated. Analogues of SPhos demonstrated that electron-donation of the lower aryl group is key to the stability of the amido complex in accordance with theoretical calculations. The methoxy substituent at the C3 position is demonstrated to retard the overall rate of reductive elimination for a RuPhos-BrettPhos hybrid ligand. These studies demonstrate that reductive elimination is likely not a problematic step for C–N cross-couplings.

Chapter 2. Kinetic experiments demonstrated an inverse dependence on the concentration of both amine and aryl halide coupling partners. These observations are demonstrated to be valid for several amine classes, aryl halides, and biaryl ligands. Some work is done to demonstrate mechanistic overlap with other bidentate ligands. Based on these studies, a simplified reaction

network for oxidative addition is proposed which reproduces key features of the experimental system.

Thesis Supervisor: Professor Stephen L. Buchwald
Title: Camille Dreyfus Professor of Chemistry

Preface:

Portions of this work have been excerpted or adapted form the following articles which were co-written by the author.

"Biaryl Phosphine Based Pd(II) Amido Complexes: The Effect of Ligand Structure on Reductive Elimination" Pedro Luis Arrechea and Stephen L. Buchwald. *J. Am. Chem. Soc.* Submitted.

"The role of oxidative addition towards the formation of "off-cycle" palladium and implications of C–N cross-coupling." Pedro Luis Arrechea, Yi-Ming Wang, and Stephen L. Buchwald. Manuscript in preparation.

Table of Contents

Introduction

The C–N palladium catalyzed cross-coupling reaction finds its greatest utility in the pharmaceutical industries. The coupling of aryl halides with various amines allows the medicinal chemist to quickly generate small and varied quantities of coupled products. These products can then be evaluated for their biological activity towards the identification of a therapeutic drug.

Given its application in drug development, much of the effort spent on improving this technology is oriented towards the development of wider substrate scope. This is often accomplished by screening supporting ligands, coupling partners, and palladium sources (e.g., $Pd_2(dba)_3$, $Pd(OAc)_2$). Based on the results of these experiments and with some chemical intuition, newer generations of supporting ligands (and new methods) are developed that facilitate the coupling of more challenging coupling partners.

Given the importance of this reaction, a multitude of different supporting ligands have been employed and/or developed. Some examples include BINAP, DPPF, XantPhos, JosiPhos, and trialkylphosphines.[1-8] The use of dialkylbiarylphosphines have been extensively developed for this application. This type of ligand was first introduced in 1998, and further work has led to a wide range of variations, some examples of which are given in the Scheme 0-1.[9]

Scheme 0-1 Examples of dialkylbiarylmonophosphine ligands developed by the Buchwald Group.
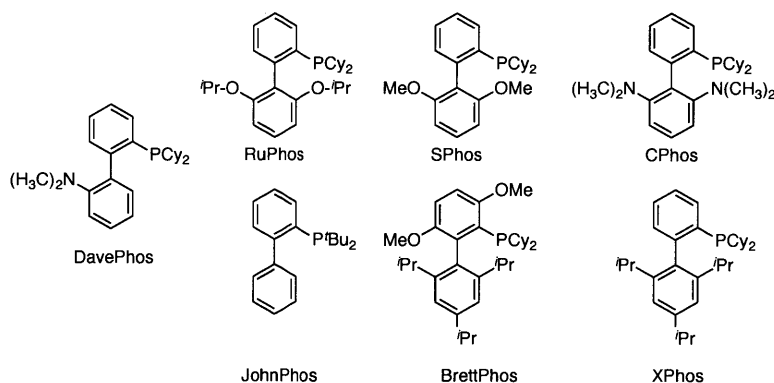
These ligands have found application in other cross-coupling reactions such as the Negishi,[10] Suzuki,[11-12] and Kumada cross-coupling reactions.[13] They have also found use in the formation of C–O and C–F bonds and aryl trifluoromethylation.[14-16]

Given the diversity of the supporting ligands used for this reaction, it is important to bring attention to the diversity of palladium sources. The most common examples are $PdCl_2$, $Pd(OAc)_2$, $Pd(dba)_2$, $Pd_2(dba)_3$, and $((cinnamyl)PdCl)_2$. In the case of Pd(II) complexes such as $Pd(OAc)_2$, the palladium must first be reduced *in situ* before it can enter the catalytic cycle. One such pathway involves the sacrificial oxidation of the phosphine ligand which requires excess ligand (relative to the palladium) and may not be desirable if the ligand is valuable. In the case of Pd(0) sources such as $Pd(dba)_2$, the coordination of the dibenzylideneacetone to the palladium can mitigate the activity of the palladium.

To address these problematic steps, pre-catalysts based on oxidative addition complexes that approximate "on-cycle" palladium intermediates have been developed. In principle, the employment of these reagents pre-empt the question of *in situ* reduction or the introduction of deleterious ligands. Several generations have been developed with emphasis on shelf-life, mild activation, and ease of preparation as driving rationales (Scheme 0-2).[17]

Scheme 0-2 Different Generations of Precatalysts Employed by Buchwald Group.

1st Generation   2nd Generation   3rd Generation   4th Generation
                                                          R- CH₃ or Ph
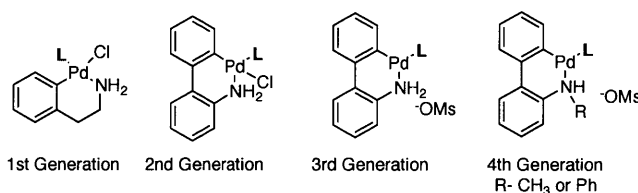
Given the breadth and utility of the dialkylbiaryl monophosphine ligand class and the mechanistically useful development of well-defined palladium sources, we felt that an in depth kinetic study with a goal of identifying unrecognized pathways for the C–N cross-coupling reaction was warranted.

References

1) Wolfe, J.P.; Wagaw S.; Buchwald S.L.; *J. Am. Chem. Soc.* **1996**, *118*, 7215.

2) Wolfe, J.P.; Buchwald S.L.; *J. Org. Chem.* **2000,** *65*, 1144.

3) Driver, M.S.; Hartwig J.F.; *J. Am. Chem. Soc.* **1996,** *118*, 7217.

4) Guari, Y.; van Es, D.S.; Reek, J.N.H.; Kamer P.C.J.; van Leeuwen, P. W. N. M. *Tetrahedron Lett.* **1999**, *40*, 3789.

5) Shen, Q.; Ogata T, Hartwig J.F.; *J. Am. Chem. Soc.* **2008**, *130*, 6586.

6) Marion N., Navarro O., Mei J.G.; Stevens E.D.; Scott N.M.; Nolan S.P. *J. Am. Chem. Soc.* **2006,** *128*, 4101.

7) Nishiyama M.; Yamamoto T.; Koie Y. *Tetrahedron Lett.* **1998**, *39*, 617.

8) Fleckenstein C.A.; Plenio H.; *Chem. Soc. Rev.* **2010,** *39*, 694.

9) a) Old, D.W.; Wolfe J.P.; Buchwald S.L.; *J. Am. Chem. Soc.* **1998**, *120*, 9722. b). Singer R.A.; Caron S.; McDermott R.E.; Arpin P.; Do N.M.; *Synlett.* **2003**, 1727. c) Rataboul F.; Zapf A.; Jackstell R.; Harkal S.; Riermeier T.; Monsees A.; Dingerdissen U.; Beller M. *Chem. Eur J.* **2004,** *10*, 2983. d) Singer R.A, Dore M.L.; Sieser J.E.; Berliner M.A. *Tetrahedron Lett.* **2006**, 47, 3727. e) Schwarz N.; Tillack A.; Alex K.; Sayyed I.A.; Jackstell R.; Beller M.; *Tetrahedron Lett.* **2007**, *48*, 2897. f) Doherty S.; Knight J.G.; Smyth C.H.; Jorgenson G.A.; *Adv. Synth. Catal.* **2008**, *350*, 1801. g) So C.M.; Zhou Z.; Lau C.P.; Kwong F.Y.; *Angew. Chem. Int. Ed.* **2008**, *47*, 6402. h) Suzuki K., Hori Y., Kobayashi T. *Adv. Synth. Catal.* **2008**, 350, 652. i) Withbroe G.J.; Singer R.A.; Sieser J.E. *Org. Process. Res. Dev.* **2008**, 12, 480. j) Pratap R.; Parrish D.; Gunda P.; Venkataraman D.; Lakshman M.K. *J. Am. Chem. Soc.* **2009,** *131*, 12240. k) Dai Q.; Gao W.Z.; Liu D.; Kapes L.M.; Zhang X.M. *J. Org. Chem.* **2006**, *71*, 3928. l). Ruan J.W.; Shearer L.; Mo J.; Bacsa J.; Zanotti-Gerosa A.; Hancock F.; Wu X.F.; Xiao J.L. *Org. Biomol. Chem.* **2009**, *7,* 3236. m) Suzuki K.; Hori Y.; Nishikawa T.; Kobayashi T. *Adv. Synth. Catal.* **2007**, *349*, 2089. n) Fleckenstein C.A.; Plenio H. *Chem. Eur. J.* **2007**, *13*, 2701.

10) Milne J. E.; Buchwald, S. L. *J. Am. Chem. Soc.*, **2004**, *126*, 13028.

11) Walker, S. D.; Barder, T. E.; Martinelli, J. R.; Buchwald, S. L. *Angew. Chem. Int. Ed.* **2004**, *43*, 1871. b) Barder, T. E.; Walker, S. D.; Martinelli, J. R.; Buchwald, S. L.. *J. Am. Chem. Soc.* **2005**, *127*, 4685.

12) Martin, R. Buchwald, S. L.; *Acc. Chem. Res.* **2008**, *41*, 1461.

13) Martin, R.; Buchwald, S.L.; *J. Am. Chem. Soc.* **2007**, *129*, 3844.

14) Cheung, C. W.; Buchwald, S. L.; *Org. Lett.* **2013**, *15*, 3998.

15) Campbell, M. G.; Ritter, T.; *Chem. Rev.* **2015**, *115*, 612.

16) Cho, E. J.; Senecal, T. D.; Kinzel, T.; Zhang, Y.; Watson, D. A.; Buchwald, S. L.; *Science.* **2010**, *328*, 1679.

17) a) Biscoe, M. R.; Fors, B. P.; Buchwald, S. L.; *J. Am. Chem. Soc.* **1996**, *118*, 7215. b) Bruno, N. C.; Tudge, M. T.; Buchwald, S. L. *Chem. Sci.* **2013**, *4*, 916. c) Bruno, N. C. Buchwald, S. L. *Org. Lett.* **2013**, *15*, 2876 d) Bruno, N. C.; Niljianskul, N.; Buchwald, S.L.; *J. Org. Chem.* **2014**, *79*, 4161.

1. Reductive Elimination of Biaryl Phosphine based Pd(II) Amido Complexes

1.1. Introduction

As shown in Figure 1-1, the palladium catalyzed C–N cross-coupling reaction mechanism is depicted as occurring through four palladium intermediates. An LPd^0 (**I**) complex undergoes oxidative addition with an aryl halide to afford complex **II** which undergoes ligand substitution with the amine substrate to form **III**. Intermediate **III** then reacts with a base, often referred to as a "deprotonation" step, to form a palladium amido complex **IV.**

Mechanistic studies based on biaryl supporting ligands would add significantly to our understanding of how this reaction works.[1] This ligand class is employed for not only the C–N cross coupling reaction, but also other bond forming reactions (e.g. C–F, C–CF$_3$, C–C, and C–O). Thus studies of C–N reductive elimination for this ligand class, may give insight into other coupling reactions.
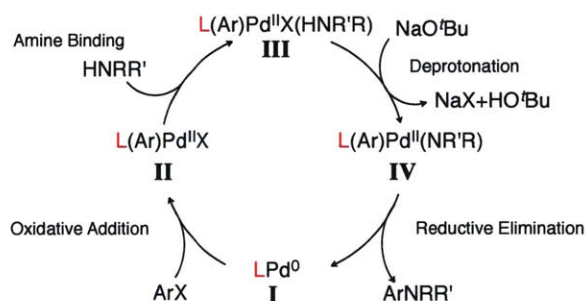
Figure 1-1 Prototype cycle for C–N coupling reaction

Since reductive elimination of **IV** is the implicated bond-forming step for the Buchwald-Hartwig C–N cross-coupling, studies of this elementary step are important for future development of these reactions. Shortly after the first publications on tin-free palladium catalyzed C–N cross-coupling,[2] Boncella was first to report the synthesis of a square planar *trans*-(PMe$_3$)$_2$PdPh(NHPh) complex.[3] For reductive elimination to occur, the complex must first isomerize so that the phenyl and anilide are in a *cis* configuration. However, thermolysis of this complex at 90 °C resulted in the loss of the volatile PMe$_3$ and the formation of a palladium dimer with bridging anilide ligands. Further heating at 110 °C, resulted in the reductive elimination of diphenylamine. Hartwig has published several studies investigating amido complexes based on the bidentate 1,1'-bis(diphenylphosphino)ferrocene (DPPF). DPPF, being bidentate naturally

enforces the *cis* configuration necessary for reductive elimination. A diarylamido complex employing DPPF as a supporting ligand underwent reductive elimination at 85 °C. Analogous anilide and alkylide complexes underwent reductive elimination at 25 °C and 0 °C in similar time frames. Hammett studies performed with diarylamido and anilide derivative complexes demonstrated that more nucleophilic amines and more electron deficient aryl groups favor greater rates of reductive elimination. These studies parallel conclusions drawn from different amine classes (diarylamines, *N*-alkyl aniline, dialkyamines, and alkyl amines), wherein amido complexes with more nucleophilic amines are less stable towards reductive elimination.[3]

Hartwig also successfully synthesized a T-shaped diarylamido palladium complex with P(^{t}Bu)$_3$ as the supporting ligand. This complex was derived from a diarylamine with four -CF$_3$ substituents and an aryl substituent containing a methoxy substituent in the para position of the aryl ring thus making the aryl coupling partner electron-rich. Even with the inherent biases of an extremely electron deficient amine and an electron rich electrophile this complex underwent reductive elimination at ambient temperatures thus providing a compelling experimental demonstration that three coordinate complexes readily undergo reductive elimination.[3e]

Prior to this particular example, Hoffman performed extended Hückel theory calculations which rationalized the difference in transition state energies. In modeling the ligands of a square planar complex as a set of s-orbitals (hydride model) of different energies and sizes, Hoffman found that the energy increase of the **a$_1$** symmetric molecular orbital is the major contributor to the reductive elimination activation energy. In the case of a three coordinate complex, the energy of the **a$_1$** molecular orbital at the transition state geometry is significantly decreased.[4]

These findings have significant implications for biaryl ligands. Though often referred to as monodentate, the "lower" aryl ring of dialkylbiarylphosphine behaves as a hemilabile coordinating group. Therefore these supporting ligands can reasonably be described as having bidentate characteristics. Due to the relatively poor coordinating ability of the bottom ring, we might rationalize that these biaryl supporting ligands will have rates of reductive elimination that are intermediate fully bidentate ligands such as DPPF and monodentate ligands such as P(^{t}Bu)$_3$.

1.2. Results

1.2.1. Recognition of rate-limiting step and Isolation of a diphenylamido complex

During studies of the *overall* kinetics of the C–N coupling reaction, we found that the rate of the coupling reaction of diphenylamine and 3-bromoanisole was independent of the concentration of all substrates (NaOtBu, diphenylamine, and 3-bromoanisole). Observation of the reaction by ^{31}P-NMR at room temperature indicated a single phosphine containing palladium species at 33 ppm. The observation of pseudo-zero order kinetics is consistent with several possible rate-determining steps- some examples are as follows:

1)   Formation of the active catalyst from a palladium dimer or aggregate

2)   Association of the supporting ligand **L1** with an "off-cycle" palladium complex to form the active catalyst.

3)   Intra-molecular isomerization

4)   Dissociative loss of a ligand

5)   C–N reductive elimination

The first possibility is not supported since the reaction was found to be directly proportional the catalyst loading. Additional ligand **L1,** did not appreciably affect the reaction thus ruling out the second scenario as a possibility. Isolation of the diphenylamido complex and comparison of its rate of reductive elimination with the values measured from studies of the catalytic reaction is the most reasonable manner in which to demonstrate that the 5th scenario is correct. We thus proceeded to derive a kinetic model of the reaction to indirectly calculate the stability of this complex.

Assuming reductive elimination is the rate-determining step, examination of the prototype reaction mechanism (Figure 1-1) allows us to derive a relationship between the time for the reaction to go to completion and the rate constant for reductive elimination k_{RE} (see experimental section). The quantity Pd_{ratio} is the molar ratio of palladium to the limiting reagent. The parameter c is the conversion of the limiting reagent and takes a value between 0 and 1. The parameter τ_{RXN} is the time at which the reaction ends.

$$k_{RE} = \frac{1}{(Pd_{ratio})} \frac{dc}{dt}$$

1.1a

$$k_{RE} = \frac{1}{(Pd_{ratio})\,\tau_{RXN}}$$

1.1b

Using the differential equation 1.1a, the reaction was monitored by GC measurements (see Section 1.4.5 for details). At 110, 100, and 90 °C, multiple catalyst loadings were used to obtain the rate constant for reductive elimination (Chart 1-1) at each of these temperature. At a temperature of 78 °C, the reaction was heterogeneous and thus the kinetic measurements employing the reaction vessels (5 mm NMR tubes which could not be equipped with stir bars) were unreliable. Calorimetry (which employs stirring) was instead used and the integral form of the rate law (equation 1.1b) was used to obtain the rate constant.

Chart 1-1 A) Reaction Kinetics for different catalyst loadings at 110 °C. B) Different catalyst loadings for 100 °C. C) Different Catalyst Loadings for 90 °C. D) Calorimetry was used to obtain last data points at 78 °C.
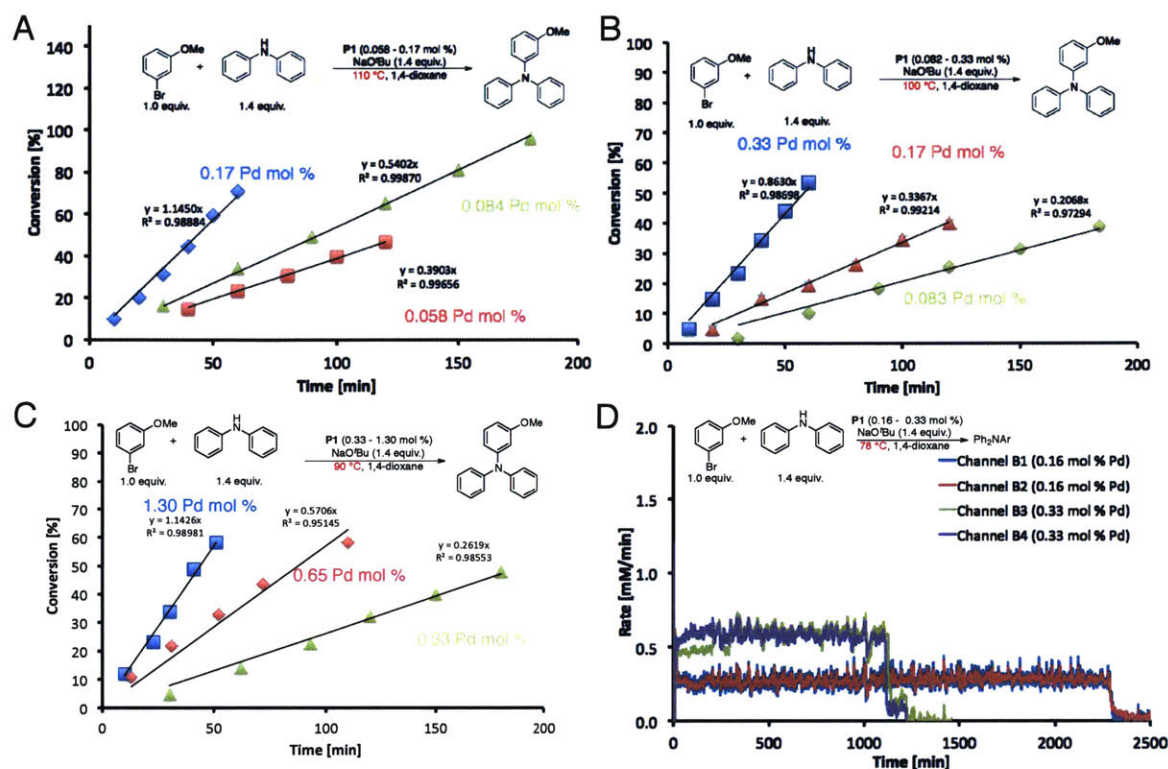
These data were then combined in the form of an Eyring Plot as shown in Figure 1-2. We should point out that this is an indirect measure of the rate constant for reductive elimination as the calculation assumes that *all* the palladium in the reaction exists as the diphenylamido complex (**IV**). We specifically chose a high yielding reaction (>95 %) in an attempt to avoid (or minimize) a scenario where the palladium is occupied in parasitic processes (for example dehalogenation of the aryl halide).

We should note that we do not see any curvature in the Eyring plot, which indicates that the reductive elimination is well-described by a single rate constant. Curvature would indicate more than one rate constant (with dissimilar enthalpies of activation) plays a role in the reductive elimination step.
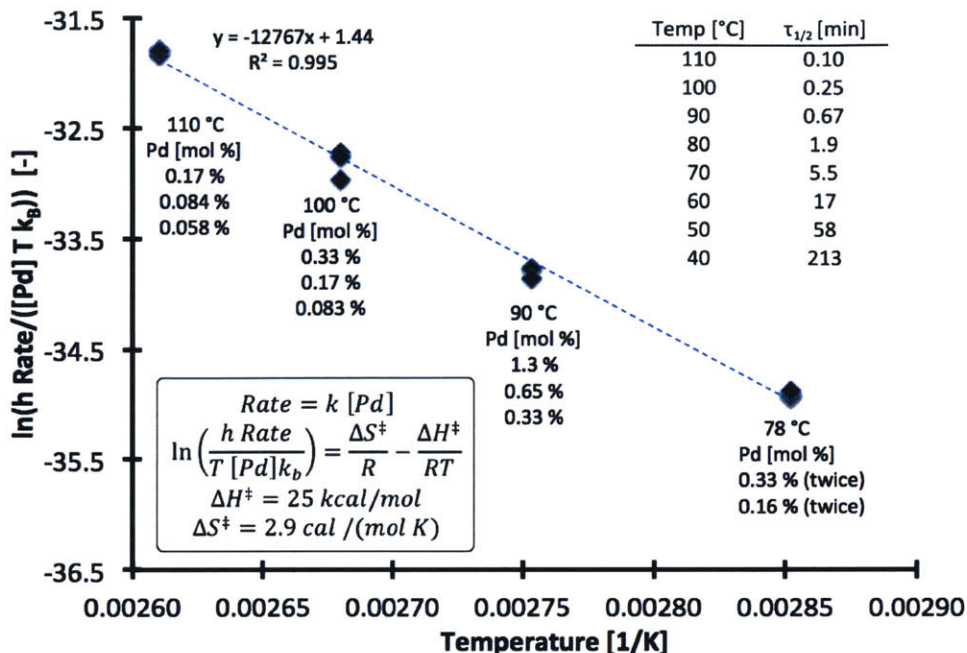
Figure 1-2 Eyring plot based on kinetic studies of the catalytic reaction. The table inset contains calculated half-lives for the amido complex (**A1a/IV**) based on the regression analysis

From this plot, we arrive at an enthalpy and entropy of activation comparable to that that seen for platinum based complexes.[5] These data allow for the indirect calculation of the half-life for the amido complex at various temperatures. As shown in the table inset for Figure 1-2, the half-life at ambient temperatures (>3 h at < 40 °C) indicates that **A1a** is stable to reductive elimination.

With this information in hand, we proceeded to synthesize an oxidative addition complex **OA1a** derived from **L1** and 3-bromoanisole. To this complex was added an excess of lithium diphenylamide which formed the diphenylamido complex **A1a** as a bright red solid. ^{31}P-NMR spectroscopy gave a single observable resonance at 33 ppm that matched the value taken from the catalytic reaction.

Scheme 1-1 Preparation of oxidative addition complex **OA1a** and corresponding diphenylamido complex **A1a**.
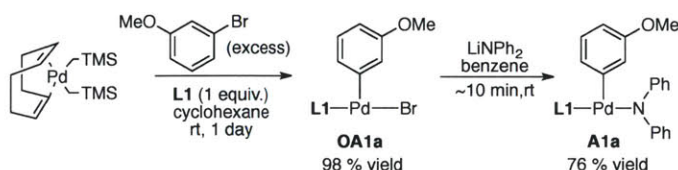
Having isolated **A1a** we then measured its rate of reductive elimination at 40 °C and 50 °C. We found that **A1a** underwent reductive elimination as a 1st order process with half-lives corresponding to 140 minutes and 42 minutes respectively. These half-lives compared

reasonably well to the predicted values (213 and 58 minutes) obtained from kinetic studies of the catalytic reaction (Figure 1-2). The reason for the discrepancy can be attributed to several factors:

1) The calculation of the rate constant under catalytic conditions inherently overestimates the stability of the amido complex since this does not consider other elementary steps such as oxidative addition, "off-cycle" palladium complexes, or low level impurities that may deactivate or occupy a portion of the catalyst.

2) The measurement of the rate constant from the catalytic studies is done at a temperature range of 78 to 110 °C. The measurement of the rate constant for reductive elimination of the isolated complex **A1a** was performed at 40 °C and 50 °C which is well outside the range of temperature for the catalytic reaction. Small changes or experimental errors in the linear regression for the catalytic reaction, will have larger effects the further the extrapolation.

3) The effect of changing solvent from 1,4-dioxane to benzene-d_6 (and solvated NaOtBu, diphenylamine, and 3-bromoanisole) has an unknown role on the measured rate of reductive elimination.

This complex was dissolved in a minimum of dichloromethane (~ 0.1 mL) to which pentane was layered. The solution was cooled to -20 °C and crystals grown that were suitable for x-ray analysis (Figure 1-3).
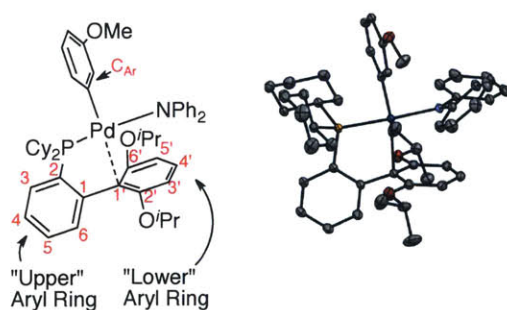
Figure 1-3 ORTEP Diagram for Amido Complex **A1a** and numbering scheme for biaryl motif.

As shown in Figure 1-3, the aryl group is *cis* to the coordinating phosphine. Given that phosphines and aryl substituents are both considered high trans-effect ligands, this is configuration is consistent with a "transphobic" effect.[6] The complex has a square planar geometry consistent with a 16-electron Pd(II) complex. The palladium is bound to the C1' carbon which is distorted from its expected sp^2 character. The deflection of C1, C1' and C4' from

17

linearity is 22°. The bond lengths between C1' and C2'/C6' atoms are longer than the typical length of aryl carbon-carbon bonds (1.42 Å vs. 1.39 Å).

Note that the lower aryl ring is a hemilabile-coordinating group. As we will see later in this thesis, the electron donating ability of the lower aryl ring is key to stabilizing the amido complex. However, since this is a weakly coordinating group that can br displaced to form a palladium reservoir. In attempting to study amine exchange of the **A1a** with *n*-propylamine, we synthesized a ^{15}N-enriched diphenylamine and used this starting material to synthesize and isolate an isotopically labeled **A1a**. This complex gave a similar ^{31}P-NMR spectrum where the dominant resonance was observed as a doublet at 33 ppm (J = 44 Hz) due to phosphorus coupling with the nitrogen-15. By exposing **A1a** to a benzene-d_6 solution of *n*-propylamine and bromobenzene, rapid ligand exchange of the lower aryl ring occurred (Scheme 1-2). A new complex was observed by ^{31}P-NMR at 48 ppm as a *doublet* (J= 50 Hz), which indicated the diphenylamine was still bound to the palladium complex. At ambient temperatures, this complex would (slowly) form an unobserved *n*-propylamido complex **A1'** that undergoes reductive elimination immediately. This process was estimated to have a half-life of 10 minutes so that within an hour the reaction would be near completion. The formation of this complex is reversible and attempts to isolate the complex by removing solvent (absent aryl halide) under vacuum failed with re-isolation of **A1a**. We found this to be a surprising example of a reversible palladium reservoir, which may serve to retard the overall rate of reductive elimination.

Scheme 1-2 Reversible displacement of lower aryl ring affords an observable room temperature stable intermediate.
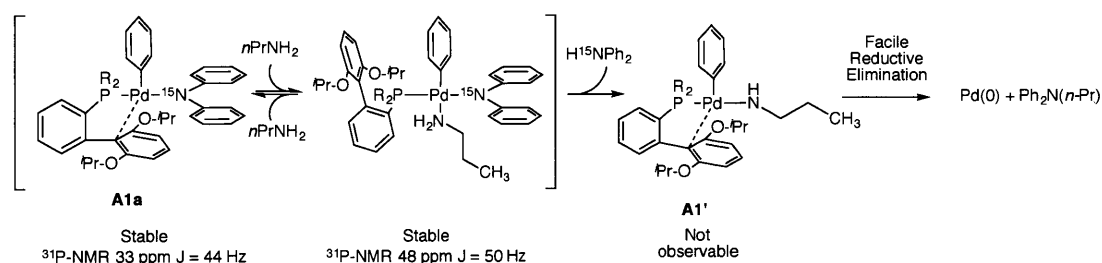
1.2.2. Hammett Studies

Having established that reductive elimination is the rate-determining step for the reaction of diphenylamine and 3-bromoanisole, we then investigated the role of aryl halide and diarylamine under both stoichiometric and catalytic reaction conditions. As was the case for the cross-

18

coupling reaction of diphenylamine and 3-bromoanisole, the kinetics of the catalytic reaction were compared to the kinetics of the corresponding amido complexes.

Variation of the substituents on the aryl halide and on the diarylamine facilitated the elucidation of the role of the electronic properties for the coupling partners. Finding that **P1** and **OA1a** gave identical results, we opted to use **OA1a** for these Hammett studies and varied the catalyst loading to obtain experimentally convenient reaction times. Since we were initially uncertain about the reliability of this experiment, we prepared separate batches of **OA1a** for each run.[7]

For every substituted diarylamine (-H, *p*-OMe, *m*-OMe, *p*-CH$_3$, and *p*-N(CH$_3$)$_2$) cross-coupled with bromobenzene at 80 °C, the rate law was consistent with reductive elimination as the rate-determining step (Chart 1-2). Within experimental error, variation of catalyst loading gave the same rate constant. For example, the coupling of 4-methyl-*N*-phenylaniline with bromobenzene, was performed at 2.33, 0.43, and 2.34 mol % **OA1a** concentrations. Respectively, these reactions gave rate constants of 1.22, 1.07 and 1.06 [1/min] by application of equation 1.1b. Most reactions were run with the amine in excess, however three examples were run with the amine as the limiting reagent as indicated in Chart 1-2.

Chart 1-2 Cross-coupling reactions of diarylamines with bromobenzene at 80 °C with **OA1a** at varied catalyst loadings.
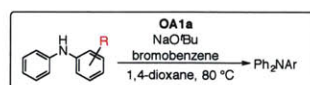
Amine	Run 1 (A) Pd [mol %] k_{RE} [1/min]	Run 2 (B) Pd [mol %] k_{RE} [1/min]	Run 3 (C) Pd [mol %] k_{RE} [1/min]
diphenylamine	2.31 (0.45)	2.37 (0.44)	2.46 (0.45)
4-methyl-N-phenylaniline	**2.33 (1.22)**	0.43 (1.07)	2.34 (1.06)
4-methoxydiphenylamine	0.40 (1.98)	**2.19 (1.99)**	0.44 (2.02)
3-methoxydiphenylamine	2.33 (0.30)	**3.25 (0.31)**	**4.06 (0.36)**
4-N,N-dimethylaminodiphenylamine	0.14 (4.03)	N/A	0.19 (4.19)

Note: Those entries which are **bolded** were run with the amine as the limiting reagent. (See tables 2-25, 2-31, 2-37 for details)
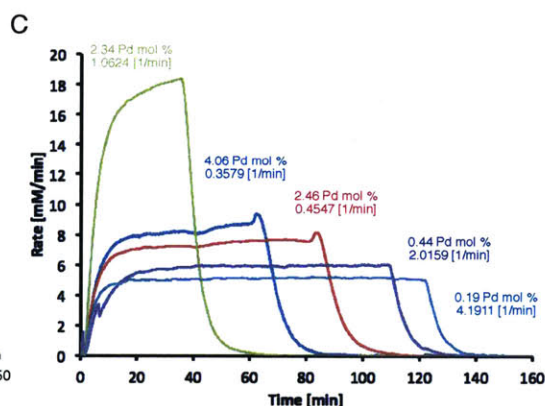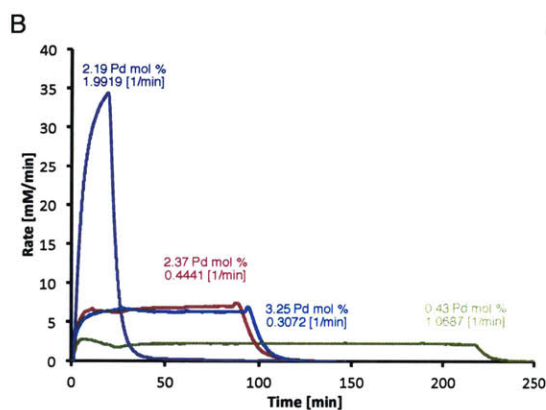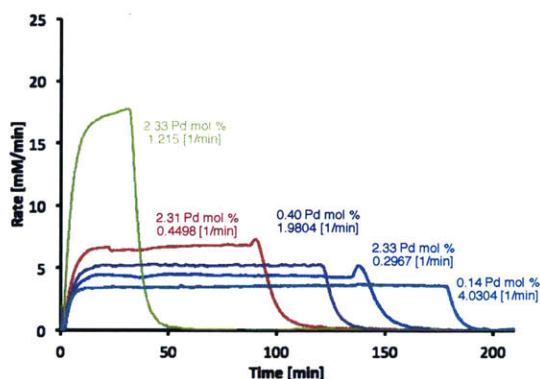
In parallel with the diarylamine studies, reactions were run in which the identity of the aryl halide was varied. It was found that the aryl chlorides gave slightly diminished rates when compared to the corresponding aryl bromides (3-bromoanisole and bromobenzene) despite the fact that these reactions also gave rate laws where reductive elimination was the dominant rate-determining step (Chart 1-3). Such a discrepancy can likely be attributed to processes involving the chloride. One such possibility is that the rate constant for reductive elimination is comparable to the rate constant for oxidative addition. Another possibility is that the chloride anion (from NaCl) may play a role in the catalytic cycle as has been shown in the work of Amatore.[8] We also cannot rule out simple catalyst decomposition as a possibility.

Chart 1-3 Coupling of various aryl halides with diphenylamines at 80 °C with **OA1a** at various catalyst loadings. Note Chart (D) with the 3-chloroanisole reactions was investigated with a single batch of **OA1a** in simultaneously.

ArX	Run 1 (A) Pd [mol %] k_{RE} [1/min]	Run 2 (B) Pd [mol %] k_{RE} [1/min]	Run 3 (C) Pd [mol %] k_{RE} [1/min]
4-chlorotoluene	2.50 (0.19)	3.32 (0.17)	2.96 (0.17)
chlorobenzene	2.76 (0.38)	3.39 (0.36)	2.90 (0.40)
3-bromoanisole	1.51 (0.37)	3.19 (0.34)	2.99 (0.36)
4-chloroanisole	2.68 (0.048)	3.07 (0.046)	2.92 (0.051)
4-chlorobenzotrifluoride	0.14 (4.03)	N/A	0.19 (4.19)
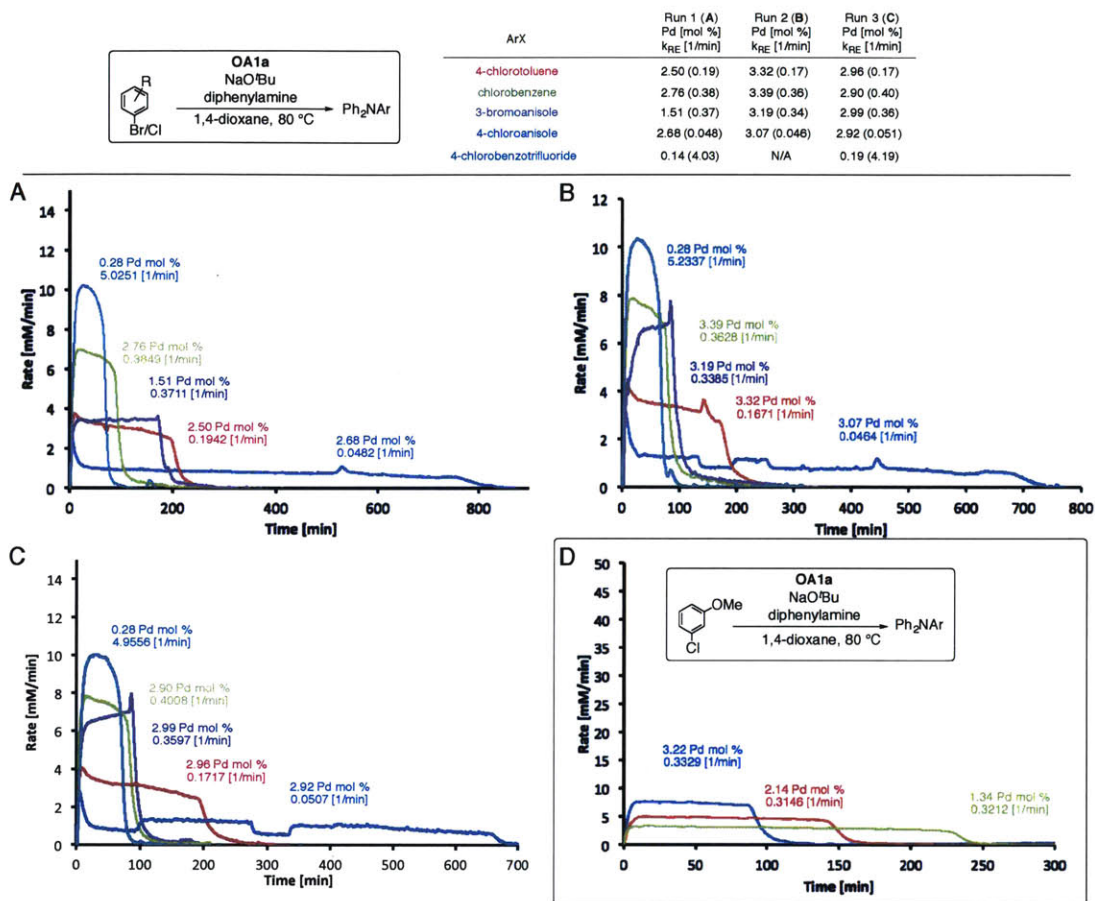
Having this data in hand, we prepared a series of oxidative addition complexes (**OA1b-OA1e**) corresponding to the different aryl halides (Table 1-1A). These OA complexes were stirred in the presence of the corresponding lithium diarylamide salt to afford the desired amido complexes (**A1b-A1i**) (Table 1-1B).

Table 1-1 Synthesis of different oxidative complexes and their corresponding amido complexes

A
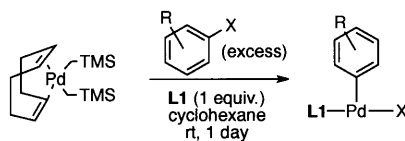
Complex	R	X	Yield [%]	Complex	R	X	Yield [%]
OA1b	p-CF$_3$	Br	89	**OA1d**	p-CH$_3$	Cl	79
OA1c	-H	Br	88	**OA1e**	p-OMe	Cl	75

B
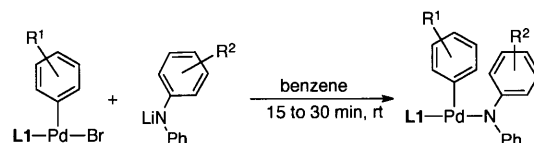
Complex	R^1	R^2	Yield [%]	Complex	R^1	R^2	Yield [%]
A1b	p-CF$_3$	-H	N/A[a]	**A1f**	-H	p-N(CH$_3$)$_2$	N/A[a]
A1c	-H	-H	56	**A1g**	-H	p-OMe	40
A1d	p-CH$_3$	-H	15	**A1h**	-H	p-CH$_3$	20
A1e	p-OMe	-H	64	**A1i**	-H	m-OMe	58

[a]Product could not be cleanly isolated at room temperature due to its instability towards reductive elimination

The amido complexes (with the exception of **A1b** and **A1f**) were found to be stable to reductive elimination at ambient temperatures. The complexes **A1b** and **A1f** could not be cleanly isolated due to their instability towards reductive elimination. Due to the limited solubility in 1,4-dioxane, the rate of reductive elimination of these complexes was monitored by ^{31}P-NMR at 40 °C in benzene-d_6 with a triphenylphosphine capillary standard. The results from the ^{31}P-NMR studies are summarized in Chart 1-4A (diarylamine) and Chart 1-4B (aryl halide).

Chart 1-4 ^{31}P-NMR studies of amido complexes based on substitute diarylamines (A) and substituted aryl groups (B)
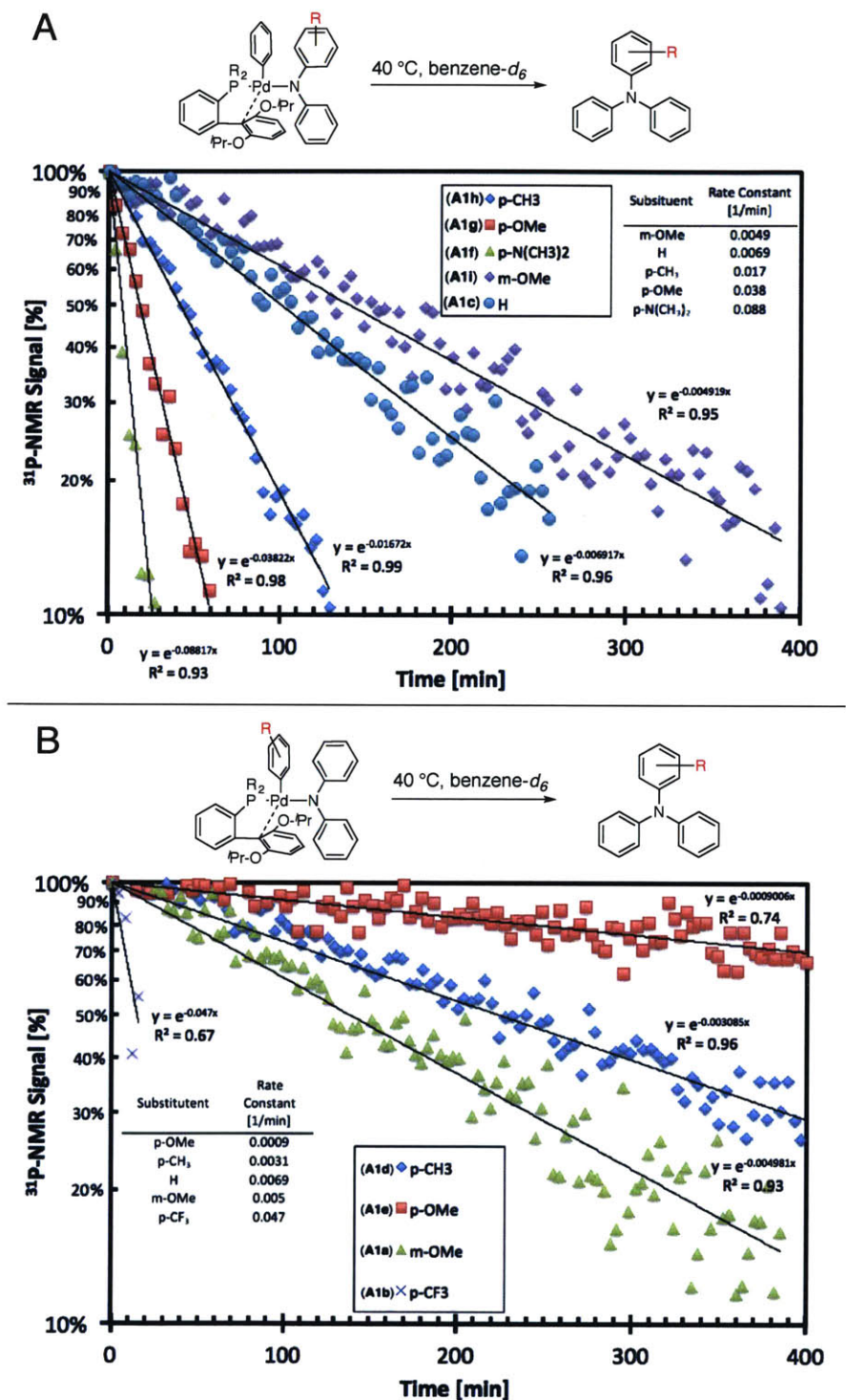
Having obtained rate constants for reductive elimination via studies of the catalytic reaction at 80 °C and the studies on the isolated amido complexes (**A1a-A1i**), we wanted to compare the

relative rates as a Hammett plot. As seen in Chart 1-5, the overlay for both the "stoichiometric" and "catalytic" studies is satisfactory. There is however a significant discrepancy for the reactions employing 4-chlorobenzotrifluoride 4-N,N-dimethylaminodiphenylamine. The half-life for the reductive elimination of **A1b** and **A1f** is on the order of 10 minutes, which made an accurate measurement by ^{31}P-NMR difficult and likely explains the discrepancy between the catalytic and stoichiometric-derived rate constants.
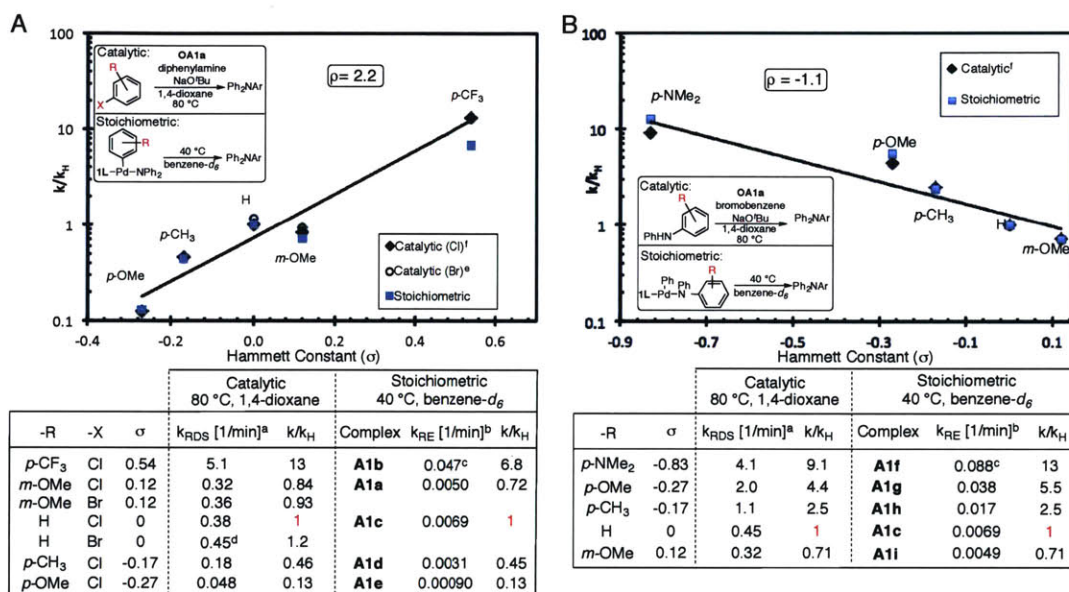
Chart 1-5 Hammett Plots comparing rate constants derived from studies of the catalytic reaction and kinetic studies of the corresponding amido complexes

-R	-X	σ	k_{RDS} [1/min][a]	k/k_H	Complex	k_{RE} [1/min][b]	k/k_H
p-CF$_3$	Cl	0.54	5.1	13	**A1b**	0.047[c]	6.8
m-OMe	Cl	0.12	0.32	0.84	**A1a**	0.0050	0.72
m-OMe	Br	0.12	0.36	0.93			
H	Cl	0	0.38	1	**A1c**	0.0069	1
H	Br	0	0.45[d]	1.2			
p-CH$_3$	Cl	-0.17	0.18	0.46	**A1d**	0.0031	0.45
p-OMe	Cl	-0.27	0.048	0.13	**A1e**	0.00090	0.13

-R	σ	k_{RDS} [1/min][a]	k/k_H	Complex	k_{RE} [1/min][b]	k/k_H
p-NMe$_2$	-0.83	4.1	9.1	**A1f**	0.088[c]	13
p-OMe	-0.27	2.0	4.4	**A1g**	0.038	5.5
p-CH$_3$	-0.17	1.1	2.5	**A1h**	0.017	2.5
H	0	0.45	1	**A1c**	0.0069	1
m-OMe	0.12	0.32	0.71	**A1i**	0.0049	0.71

[a]As determined from kinetics of the catalytic reaction at 80 °C. [b]Determined from the corresponding stoichiometric complex at 40 °C. [c]Corresponding complex could not be cleanly isolated. [d]Value taken from entry with R = H (catalytic) in Chart 1-5B. [e]The regression for Chart 1-5A excluded those values corresponding to aryl bromides. [f]Rate constants derived from experiments of the catalytic reaction are averaged values from several runs.

The ρ value determined from the kinetics of the catalytic reaction for different aryl halides was 2.2 while the corresponding study for different diarylamines was -1.1. These studies demonstrate that amido palladium intermediates with electron-deficient aryl groups and/or electron-rich diarylamido groups undergo reductive elimination at increased rates. These values are consistent with other studies of heteroatom cross-coupling reactions.[9]

1.2.3. Catalytic studies with different Ligands

Having demonstrated an ability to correlate kinetic studies of the catalytic reaction with kinetic studies of the corresponding amido complexes (**A1a-A1i**), we turned our attention to the question of ligand structure. In cases where reductive elimination is not the rate determining step, equation 1.2 can be used to calculate a *lower limit* for the rate constant.

$$k_{RE} > \frac{1}{(Pd_{ratio})} \max\left(\frac{dc}{dt}\right) \qquad\qquad 1.2a$$

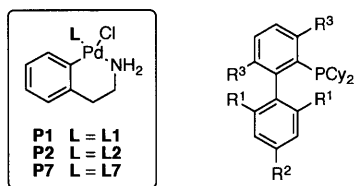$$k_{RE} > \frac{1}{(Pd_{ratio})\,\tau_{RXN}} \qquad\qquad 1.2b$$

Equation 1.2a can be applied by taking the value of the *maximum* reaction rate (in terms of conversion per unit time) for a particular reaction. The integral form (Eq. 1.2b) allows one to use the time for the reaction to go to completion to calculate a lower limit. In principle, equation 1.2a will always be more accurate (and thus compute a greater lower limit) when compared to equation 1.2b. However equation 1.2b is more straightforward to apply.

Employing the coupling of 3-bromoanisole and diphenylamine as a model reaction system, reactions were performed at 105 °C with NaO*t*Bu as the base. Because oxidative addition complexes similar to **OA1a** could not be synthesized for all biaryl ligands, several different precatalysts were employed. For XPhos (**L7**) and SPhos (**L2**), we used 1st generation precatalysts developed by Biscoe.[10] The SPhos OA complex (**OA2**) could be cleanly synthesized while an XPhos based OA complex could not. For the RuPhos-BrettPhos hybrid ligand (**L3**), CPhos (**L9**), MethoxySPhos (**L4**), and AminoSPhos (**L5**) oxidative addition complexes were successfully synthesized and employed (Table 1-2).
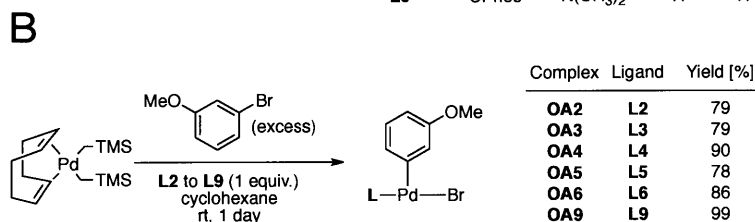
Fink reported that the oxidative addition complex of CyJohnPhos (**L8**) was unstable, as the complex undergoes cyclopalladation with the "lower" aryl ring of the phosphine ligand.[11] We thus prepared an $L_2Pd^{(0)}$ complex using CyJohnPhos (**L8**) for these studies.[12]

Table 1-2 Different ligands and corresponding oxidative complexes and precatalyst.

A

Ligand	Name	R¹	R²	R³
L1	RuPhos	-O*i*Pr	-H	-H
L2	SPhos	-OMe	-H	-H
L3	Hybrid	-O*i*Pr	-H	-OMe
L4	MethoxySPhos	-OMe	-OMe	-H
L5	AminoSPhos	-OMe	-N(CH₃)₂	-H
L6	BrettPhos	-*i*Pr	-*i*Pr	-OMe
L7	XPhos	-*i*Pr	-*i*Pr	-H
L8	CyJohnPhos	-H	-H	-H
L9	CPhos	-N(CH₃)₂	-H	-H

B

Complex	Ligand	Yield [%]
OA2	**L2**	79
OA3	**L3**	79
OA4	**L4**	90
OA5	**L5**	78
OA6	**L6**	86
OA9	**L9**	99

Having prepared a set of suitable catalyst sources (Table 1-2), we systematically measured the rates of reaction for the coupling of 3-bromoanisole and diphenylamine at 105 °C. For each ligand combination, a control experiment was simultaneously performed with **OA1a**. Equation 1.2b was used to establish the lower limit value for the rate constant of reductive elimination for those reaction not consistent with reductive elimination as a rate-determining step and this rate constant was indexed to the rate constant established with the **OA1a**-based control reaction. For those reactions where the rate law was consistent with reductive elimination as a rate-determining step equation 1.1b was used.
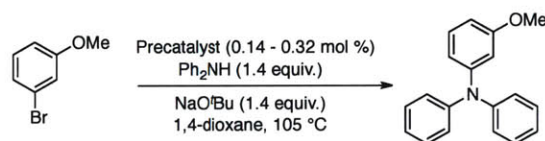
As summarized in Table 1-3, reactions based on BrettPhos (**L6**), XPhos (**L7**), CyJohnPhos (**L8**), and CPhos (**L9**) afforded rates that were not consistent with reductive elimination as the rate-determining step. Reactions based on SPhos (**L2**), MethoxySPhos (**L4**), and AminoSPhos (**L5**) afforded rates consistent with reductive elimination as the rate-determining step.

Given that the XPhos (**L7**) based catalyst afforded a rate that was 29 times faster than a RuPhos (**L1**) based reaction, we wondered whether only steric factors were playing a role. A comparison with the less sterically encumbered CyJohnPhos (**L8**) demonstrated that this reaction was 5.5 times faster than the reaction with a RuPhos (**L1**) based catalyst. Based on these two experiments, we could rule out steric factors as the sole reason for the increase in reaction rate relative to the RuPhos-based (**L1**) reaction.

In accordance with theoretical calculations,[4,13] we hypothesized that the electron-donating character of the lower aryl ring was responsible for the stabilization of the

diphenylamido complex (**IV**). The experiment with the SPhos (**L2**) based catalyst (**OA2**) gave a rate of reaction consistent with reductive elimination as the rate-determining step. Based on these results, we concluded that its corresponding amido complex (**A2**) had a rate constant for reductive elimination very close to that obtained for **A1a**. Given that methoxy- (SPhos/**L2**) and isopropoxy- (RuPhos/**L1**) substituents at the C2'/C6' positions should manifest similar electronic donating properties for the lower aryl ring, this result is not surprising. By adding substituents at the para position (C4') of SPhos **L2**, we synthesized two variants (MethoxySPhos/**L4** and AminoSPhos/**L5**) with electron donating bottom rings to test the theoretical predictions. Indeed, we found that the use of MethoxySPhos (**L4**) based catalyst gave a rate that less than half that of the SPhos (**L2**) based catalyst. Likewise, the AminoSPhos (**L5**) based catalyst gave a rate of reaction that was less than one-tenth that of the SPhos (**L2**) based catalyst.

<div align="center">

Table 1-3 Summary of different rate constants for various biaryl ligands

</div>

Precatalyst (0.14 - 0.32 mol %)
Ph$_2$NH (1.4 equiv.)

NaO^{t}Bu (1.4 equiv.)
1,4-dioxane, 105 °C

| Ligand	Precatalyst	Relative Rate[a] [-]	Ligand	Precatalyst	Relative Rate[a] [-]
L6	**OA6**	1.6	**L1**	**OA1a**	1
L7	**P7**	29	**L2**	**P2**	1.1
L8	**L$_2$Pd**	5.5	**L4**	**OA4**	0.42
L9	**OA9**	9.6	**L5**	**OA5**	0.087

Rate law not consistent with reductive elimination as the rate determining step
Relative rate is a *lower limit* for the rate of reductive elimination

Rate law consistent with reductive elimination as the rate determining step

[a]Relative rate refers to the time for the reaction to go to completion compared to the control reaction based on **OA1a**. A ratio of 0.5 means that the reaction takes twice as long compared to a reaction based on **OA1a** at the same catalyst loading

One anomalous example is the reaction with **OA9** (CPhos), where the rate was not consistent with reductive elimination as the rate-determining step. This reaction gave a rate that was 9.6 times faster than the reaction with **OA1a**. Given that CPhos **L9** has two dimethyl amino groups on the lower aryl ring, the observation that the reaction goes to completion in such a short time is surprising. It has been previously argued the dimethyl amino groups are unable to attain a planar conformation due to the steric interference of the "upper" aryl ring.[14] This may result in the nitrogen lone pairs being unable to donate their electron density info the π-system of the "lower" aryl ring. A second explanation is that the dimethylamino groups themselves may serve as coordination sites as depicted in the Scheme 1-3. The energy of the transition state for reductive elimination from such a configuration, maybe significantly lower than the transition state energy from the C1' position.

Such a geometry would be analogous to the binding configuration of a BINAP-based catalyst. Several amido complexes based on DPPF have been isolated and characterized.[3] However, no corresponding BINAP based amido complexes have been published despite the fact that BINAP is isolobal to DPPF. It seems likely that a BINAP based amido complex is less stable since the BINAP accommodates a skewed geometry. If this is true, the same reasoning may apply to the analogous CPhos (**L9**) based catalyst.

Scheme 1-3 Possible alternative binding mode which facilitates reductive elimination
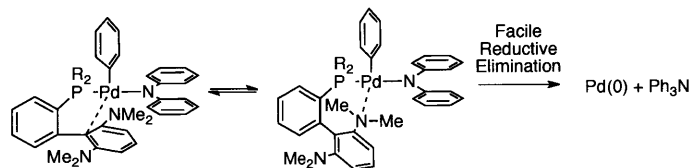
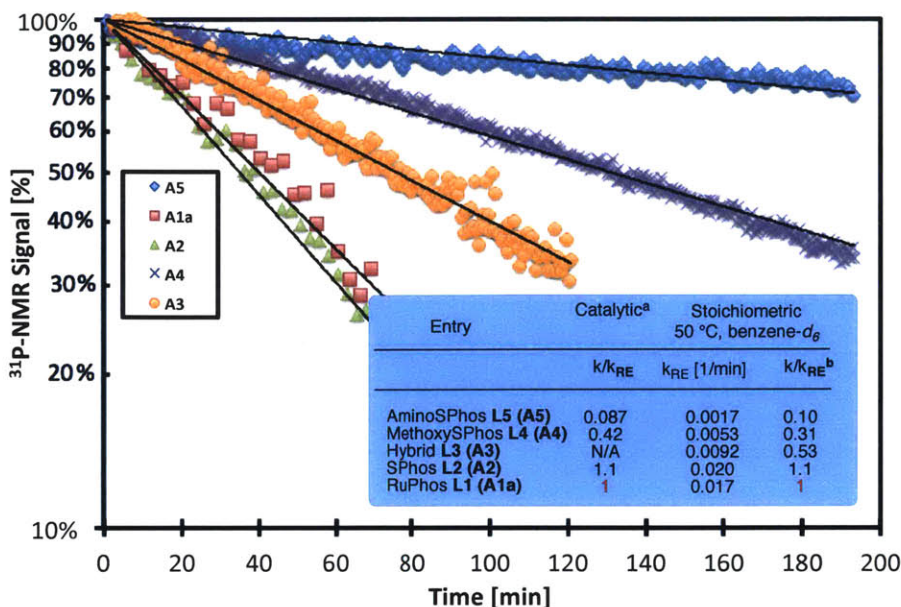### 1.2.4. Stoichiometric Studies with Different Biaryl Ligands

Having identified some ligand systems for which the rate law implies amido complex resting states, we synthesized the corresponding amido complexes (Table 1-4). Since the BrettPhos (**L6**) based amido complex could not be isolated due to its instability towards reductive elimination, a RuPhos-BrettPhos hybrid ligand (**L3**) was synthesized. The RuPhos-derived "lower" aryl ring of **L3** was used to stabilize the amido complex from reductive elimination while the BrettPhos-derived upper aryl ring probed the role of the methoxy substituent at C3 in reductive elimination.

Table 1-4 Synthesis of amido complexes based a different biaryl supporting ligands.
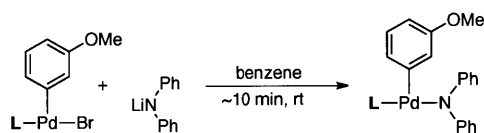
Complex	Ligand	Yield [%]	Complex	Ligand	Yield [%]
A2	L2	69	A4	L4	66
A3	L3	56	A5	L5	72

Having successfully synthesized these complexes, the rates of reductive elimination at 50 °C in benzene-d_6 by monitoring with ^{31}P-NMR (Figure 1-4). The measured rate constants of reductive elimination for **A2**, **A4**, and **A5** compared well with those values determined by studies of the catalytic reaction.

Figure 1-4 ^{31}P-NMR experiments for the rate of reductive elimination

The table embedded in the figure:

Entry	Catalytic[a]	Stoichiometric 50 °C, benzene-d_6	
	k/k_{RE}	k_{RE} [1/min]	k/k_{RE}[b]
AminoSPhos **L5 (A5)**	0.087	0.0017	0.10
MethoxySPhos **L4 (A4)**	0.42	0.0053	0.31
Hybrid **L3 (A3)**	N/A	0.0092	0.53
SPhos **L2 (A2)**	1.1	0.020	1.1
RuPhos **L1 (A1a)**	1	0.017	1

[a]Rates of the catalytic reaction are reproduced from Table 1-3. [b]Rate relative to reductive elimination of **A1a**.

BrettPhos-based palladium(II) complexes exist as observable rotamers in solution. For the oxidative addition complexes **OA6** and **OA3**, the ^{1}H- and ^{31}P-NMR spectra are consistent with interconverting *O*-bound and *C*-bound isomers. Likewise, the ^{1}H- and ^{31}P-NMR spectra of **A3** are consistent with interconverting *O*-bound (**A3-O**) and *C*-bound (**A3-C**) rotamers (Figure 1-5). The rate of reductive elimination for **A3** was approximately half that of the rate of reductive elimination for the **L1** based complex (**A1a**), which has the same "lower" aryl ring. A significant amount of complex **A3** exists as **A3-O**. Given that the rate constant for reductive elimination from the *C*-bound isomer **A3-C** should be similar to reductive elimination from **A1a** this would imply that rate constant for reductive elimination from the **A3-O** is significantly greater than the rate constant for reductive elimination from the **A3-C**. Thus, the rotamer **A3-O** acts as a palladium reservoir that retards the overall rate of reductive elimination.
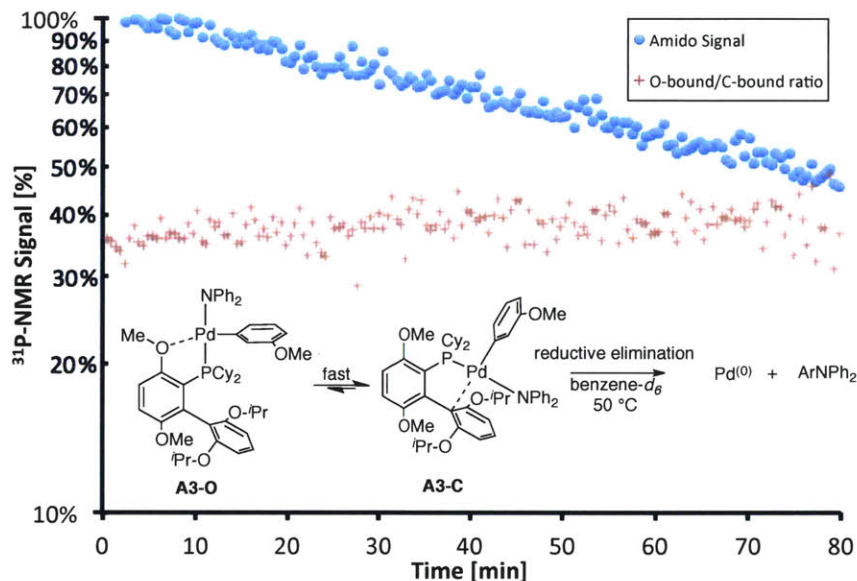
Figure 1-5 Rate of reductive elimination as measured by ^{31}P-NMR. Relative population of **A3-O** and **A3-C** is nearly constant.

To further bolster this argument, we obtained an X-ray crystal structure of **A3** to compare with **A1a**. As shown in Figure 1-6, there are no significant structural differences in bond length or bond angles. This suggests that the methoxy substituent has little role in altering the steric or electronic properties of the C-bound isomer (**A3-C**).
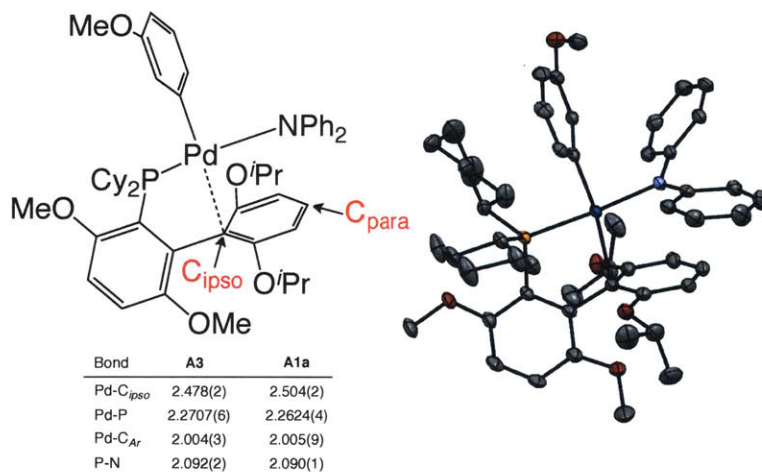

Bond	A3	A1a
Pd-C$_{ipso}$	2.478(2)	2.504(2)
Pd-P	2.2707(6)	2.2624(4)
Pd-C$_{Ar}$	2.004(3)	2.005(9)
P-N	2.092(2)	2.090(1)

Figure 1-6 ORTEP diagram for complex **A3.** Table compares bond length of **A3** and **A1a.** Bond lengths are reported in Angstroms.

1.3. Summary

Via kinetic studies of the catalytic reaction, we have by indirect means determined the rate constant for reductive elimination of several **L1** amido complexes (Figure 1-2). With the realization that these complexes are stable at room temperature (Figure 1-3), we were able to isolate several examples for the first time. Moreover, relative rates measured under catalytic and stoichiometric conditions were found to be in good agreement (Chart 1-5).

By measuring the rate of reaction using model substrates (diphenylamine/3-bromoanisole), we were able to calculate a lower limit for the rate constant of reductive elimination for catalysts based on different supporting ligands. This approach was valid even in cases where the corresponding amido complexes could not be isolated (Table 1-3). These studies also indicated that the electronic properties of the "lower" aryl ring were key to stabilizing these complexes toward reductive elimination. This finding was confirmed by isolating and characterizing the corresponding stable amido complexes and demonstrating corresponding rates of reductive elimination (Figure 1-4).

Surprisingly, the presence of a methoxy substituent at the C3 position (Figure 1-5) allowed the formation of an O-bound palladium isomer (**A3-O**), which retarded the overall rate of reductive elimination. As we will see in the next chapter of this thesis, the C–N cross-coupling reaction often forms "off-cycle" palladium species. It is quite likely that the methoxy substituent at the C3 position facilitates "return" to an "on-cycle" species via an intramolecular ligand substitution. Contrary to previous hypothesis, the methoxy substituent probably does not facilitate the reductive elimination step.

In the context of previously reported palladium(II) amido complexes, the **L1** based palladium(II) amido complexes investigated in this study underwent reductive elimination at rates between those previously observed for T-shaped palladium(II) amido complexes and DPPF-based palladium(II) amido complexes.[3e,4] Consistent with computational studies,[4,13] complexes that were stable at room temperature required an electron-rich "lower" aryl ring to maximize coordination with the palladium and an electron-deficient secondary amine. Based on work by Hartwig and coworkers, palladium(II) amido complexes based on **L1** with more nucleophilic amines, such as anilines, primary alkyl amines, alkyl N-substituted anilines, or secondary aliphatic amines, would undoubtedly undergo reductive elimination at room temperature.[9] Notably, this study implies that reductive elimination is not a kinetically difficult step for a significant number of palladium-catalyzed C–N cross-coupling reactions employing

biarylphosphine ligands. The work described in chapter 2 of this thesis will investigate the kinetics of other palladium-catalyzed amination reactions and the implications for the development of room temperature C–N cross-coupling reactions.

1.4. Experimental
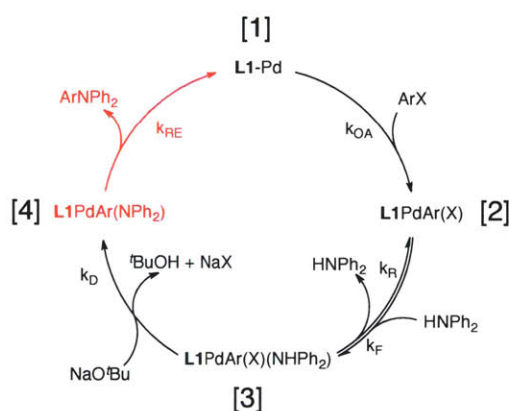
1.4.1. Derivation of rate law

Figure 1-7 Prototype reaction mechanism. The highlighted (red) step corresponds to the rate-determining step (reductive elimination).

We write three differential equations for the catalytic cycle and a fourth equation for the total palladium species balance. We make a steady state assumption concerning the first three differential equations by setting them equal to zero thus turning these differential equations into algebraic equations.

$$
\begin{bmatrix} 0 \\ 0 \\ 0 \\ [Pd]_0 \end{bmatrix} = \begin{bmatrix} \dfrac{d[2]}{dt} \\ \dfrac{d[3]}{dt} \\ \dfrac{d[4]}{dt} \\ [Pd]_0 \end{bmatrix} = \begin{bmatrix} k_{OA} & -k_F & k_R & 0 \\ 0 & k_F & -(k_D + k_R) & 0 \\ 0 & 0 & k_D & -k_{RE} \\ 1 & 1 & 1 & 1 \end{bmatrix} \begin{bmatrix} [1] \\ [2] \\ [3] \\ [4] \end{bmatrix} \qquad 1.4.1
$$

Application of Cramer's rule to the above matrix yields the solution for [4].

$$\frac{k_D k_F k_{OA}}{k_D k_F k_{OA} + k_D k_F k_{RE} + k_D k_{OA} k_{RE} + k_F k_{OA} k_{RE} + k_{OA} k_R k_{RE}} [Pd]_0 = [4] \qquad 1.4.2$$

Multiplication of [4] by k_{RE} gives the rate law in terms of production of arylated product or the consumption of aryl halides.

$$k_{RE} \frac{k_D k_F k_{OA} [Pd]_0}{k_D k_F k_{OA} + k_D k_F k_{RE} + k_D k_{OA} k_{RE} + k_F k_{OA} k_{RE} + k_{OA} k_R k_{RE}} = \frac{-d[ArX]}{dt} \qquad 1.4.3$$

We now insert substrate dependencies for k_{OA}, k_F, k_R, and k_D by writing them in terms of conversion, c, relative to a reference concentration $[ArX]_o$ and equivalents for amine A_o, aryl halide X_o, and base B_o as shown in equation 1.4.4.

$$k_D \to k_D'(B_o - c) \qquad 1.4.4a$$

$$k_{OA} \to k_{OA}'(X_o - c) \qquad 1.4.4b$$

$$k_F \to k_F'(A_o - c) \qquad 1.4.4c$$

$$k_R \to k_R \qquad 1.4.4d$$

$$k_{RE} \to k_{RE} \qquad 1.4.4e$$

$$[ArX] = [ArX]_0(X_o - c) \qquad 1.4.4f$$

Taking the above rate law (eq 1.4.3) and making the aforementioned substitutions (eq. 1.4.4) we rearrange the rate law to arrive at

$$\frac{1}{\frac{1}{k_{RE}} + \frac{1}{k_{OA}'(X_o - c)} + \frac{1}{k_F'(A_o - c)} + \frac{1}{k_D'(B_o - c)} + \frac{k_R}{k_D' k_F'(B_o - c)(A_o - c)}} = \frac{[ArX]_0}{[Pd]_0} \frac{dc}{dt} \qquad 1.4.5$$

While the above equation is analytically integrable, we now make an approximation where the reductive elimination rate constant is considered the smallest term so that

$$\frac{1}{k_{RE}} >> \left\{ \frac{1}{k_{OA}'(X_o - c)} + \frac{1}{k_F'(A_o - c)} + \frac{1}{k_D'(B_o - c)} + \frac{k_R}{k_D' k_F'(B_o - c)(A_o - c)} \right\} \qquad 1.4.6$$

which means we can write our equation as....

$$k_{RE} = \frac{[ArX]_0}{[Pd]_0} \frac{dc}{dt} \qquad 1.4.7$$

33

We call this the differential form of the rate law. We note that $\frac{[Pd]_0}{[ArX]_o}$ is the molar ratio of palladium relative to the reference concentration. We write this now as Pd_{ratio} and integrate the rate law

$$k_{RE}Pd_{ratio}\int_0^{\tau_{Rxn}} 1\,dt = \int_0^1 1\,dc \qquad\qquad 1.4.8$$

To arrive at the *integral form of the rate law* given in the earlier in this thesis.

$$\frac{1}{Pd_{ratio}\tau_{Rxn}} = k_{RE} \qquad\qquad 1.4.9$$

With this rate law in hand we proceeded to indirectly measure the rate determining step by variation of both the catalyst loading and temperature in a catalytic reaction.

1.4.2. General Procedures

Calorimetry experiments were performed using an Omnical Insight Parallel Reaction Calorimeter (Figure 1-8). Heating (or cooling) of the calorimeter was done via external recirculating baths (Anova A-25 Refrigerated and Heating Circulator). An internal thermocouple in the circulating bath was used to provide closed-loop temperature control for the recirculating bath. The reaction temperature was measured at the calorimeter and maintained to within ± 2 °C of the values reported in the manuscript.

Data processing was done in Microsoft® Excel. The area under the curve was integrated to arrive at an energy value for the reaction and this value in conjunction with the conversion from GC was used to convert the rate of reaction in power (milliwatts) to the rate of reaction in terms of concentration (mM/min). The rate (represented in terms of power [mW]) is converted to concentration via the following equation.

$$Rate(t)\left[\frac{mM}{min}\right] = \frac{Rate(t)\,[mW]}{\int_0^{\tau_{rxn}} Rate(t)[mW]dt}[Limiting\ Reagent]\rho * Conversion$$

The concentration of the reaction mixture for the limiting reagent is expressed in terms of molality. The density of several (heterogeneous) reaction mixtures was measured using a pre-weighed 5 mL volumetric flask. Multiple measurements indicated a variation of ±0.02 g/cm^3 thus an average density of 1.04 g/cm^3 was used for these calculations. The value of conversion or yield takes values between 0 and 1. Since all the reactions go to completion, a value of 1 is used. The curves generated by calorimetry have not been signal-processed for the response

behavior of the calorimeter.

Figure 1-8 Omnical Calorimeter with circulating cooling/heating baths. Note: The "brand names" of the circulating coolers have been edited out of the picture

Reagents and solvents were used as received from Sigma-Aldrich. All new compounds were characterized by NMR spectroscopy, IR-spectroscopy (if air stable), and elemental analysis. Compounds that did not pass elemental analysis were analyzed by mass spectrometry. ^{1}H-NMR, ^{13}C-NMR, and ^{31}P-NMR spectra were recorded on a Varian Inova 500 MHz spectrometer (except where noted). *Note: Many of the ^{1}H-NMR spectra indicate that the palladium amido complexes are fluxional.* ^{19}F-NMR and ^{31}P-NMR spectra were recorded on a Varian Inova 300 MHz spectrometer. ^{1}H-NMR and ^{13}C-NMR spectra were referenced to the residual solvent peak of the deuterated solvent. ^{31}P-NMR spectra were referenced to 85 wt % phosphoric acid (0 ppm). ^{19}F-NMR spectra were referenced to trifluorotoluene (-63.72 ppm). All heteronuclei NMR were collected with proton decoupling. ATR (diamond)-FTIR spectra were recorded on a Thermo Scientific Nicolet iS5 spectrometer. Melting points were measured for solids on a Mel-Temp capillary melting point apparatus. Elemental analyses were performed by Atlantic Microlabs Inc., Norcross, GA. Gas chromatography (GC) analyses were performed on an

Agilent 7890A gas chromatograph with an FID detector using a J&W DB-1 column (10 m, 0.1 mm I.D.).

1.4.3. General Calorimetry Procedure

In a nitrogen-filled glove box, a screw-cap sealable vial was charged with a stock solution of aryl halide, amine, base, and solvent. Aliquots were then loaded into 16 mL vials (Wheaton Vial, 16 mL E-C Vial, Cat # 224706) and the mass of each aliquot was recorded. The vials were equipped with a stir bar and then sealed with a silicon rubber/Teflon-laminated septum (ThermoScientific, 10/90 FOR18-400, B7995-18). (The part number for retaining cap for each septum/vial was manufactured by Kimble-Chase (part # 73804-18400).) The vials were removed from the glove box and loaded into the calorimeter that was preheated to the indicated reaction temperature. A reaction vial containing pure solvent was loaded into reference channel of the calorimeter.

Separately, solutions of an oxidative addition complex were prepared by the addition of the palladium complex into toluene or other appropriate solvent in a 4 mL Vial (Wheaton 4 mL E-C Vial Cat # 224742). The masses of the palladium complex and solvent were recorded. Syringes equipped with a 6-inch needle were then loaded with the catalyst solution and weighed. After equilibration of the reaction vials (~1 h) into the preheated calorimeter, the catalyst solution was injected through the septum to start the reactions. The syringes were weighed again to calculate the total amount of catalyst injected into the reaction. An equal mass of pure solvent was simultaneously injected into the reference channel.

The end of the reaction and thus the reaction time was determined by the return of the power output halfway to the baseline. At the end of the reaction, the 16 mL vial was removed from the calorimeter and allowed to cool before addition of n-dodecane as an internal standard. The reaction yield was quantified by GC analysis of the sample.

1.4.4. General Procedure for ^{31}P-NMR Kinetics

In a nitrogen-filled glove box, an amido complex (~20 mg) was placed into a NMR tube and dissolved in benzene-d_6 (~1 mL). A capillary with a solution of triphenylphosphine in benzene-d_6

was added to the NMR tube. The tube was sealed and removed from the glove box and then placed in a NMR instrument that was preheated to the indicated reaction temperature. Scans were taken continuously and the signal of the amido complex was referenced to the capillary signal. The decay was fitted as a first order process to calculate the rate of reductive elimination.

1.4.5. Procedure for Eyring Plot

An aluminum cylinder (15 cm diameter x 10 cm height) was custom-built with 18 holes arranged in a concentric pattern to provide uniform temperature to a set of (5 mm-O.D.) Wilmad-NMR tubes (Figure 1-9B). The block was heated using a pair of custom-made Watlow Mineral Insulated Band heaters with post terminals (https://www.watlow.com/products/heaters/mineral-insulated-band-heaters.cfm) (Figure 1-9A). Temperature control of the block was by use of a J-Kem Gemini controller (http://www.jkem.com/temperature-controllers/precision-controllers/gemini-multi-channel-controller) (Figure 1-9C).

In the glove box, stock solutions of anhydrous 1,4-dioxane, 3-bromoanisole, NaO*t*Bu, and diphenylamine were prepared. This solution was divided into three separate vials and to each aliquot was added precatalyst **P1** (or solution of **P1**) as indicated. The reaction solutions immediately became red. Each solution was then further partitioned into 6 reaction tubes (Sigma Aldrich Cat #Z274798-1PAK) for a total of 18 tubes. The tubes were then sealed with a polyethylene cap, the cap wrapped with parafilm, and the tube removed from the glovebox. The reaction tubes were then loaded into the preheated aluminum cylinder. Each reaction tube was removed after a predetermined time and immersed in a dry ice/acetone bath (-78 °C) to halt the reaction. Time points were selected so that the conversion would be at least 40 % for the last tube removed.

Each tube was opened and *n*-dodecane was added to each tube as an internal standard. The reaction mixture was analyzed by GC for 3-bromoanisole, *n*-dodecane, diphenylamine, and product. The integrated 3-bromoanisole signal was used to determine the conversion. A portion of the stock solution (taken before the addition of the catalyst) was also analyzed as a GC standard. For each catalyst loading, the conversion was plotted as a function of time. A linear regression was fitted to these points; the slope of the line gave rate of the

reaction as per equation 1.4.7. This experiment was repeated for temperatures at 110, 100, and 90 °C.
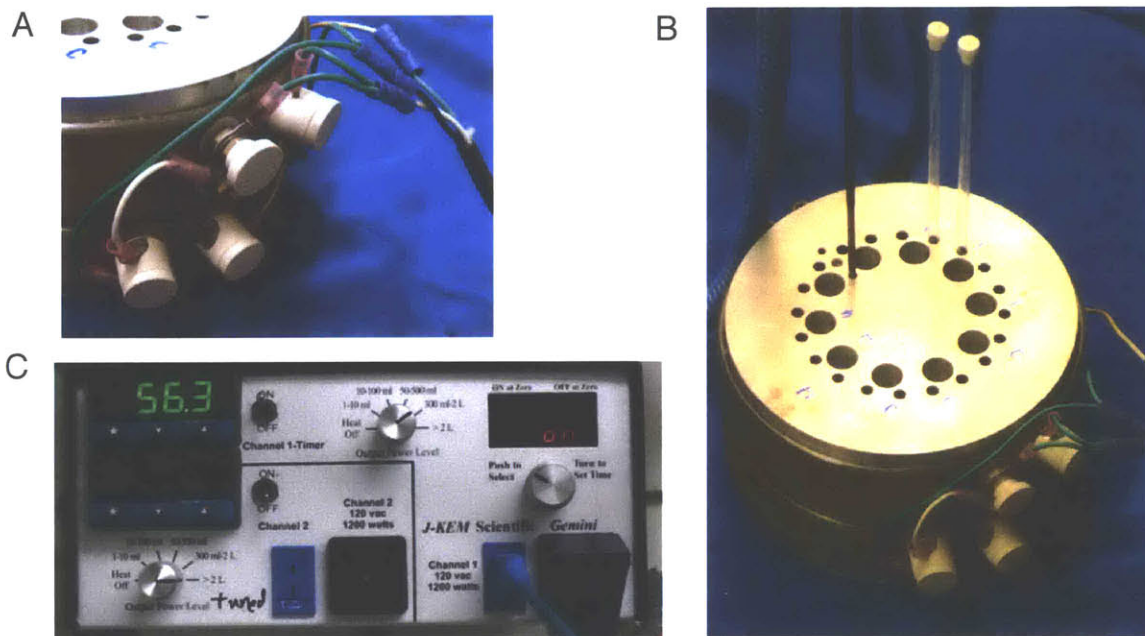

Figure 1-9 A) Closeup of band heaters connected to power supply and in contact with aluminum cylinder. B) Kinetics apparatus with thermocouple and 2 reaction tubes inserted. The device shown in the photograph has been modified with larger holes (10 total). These larger holes were not present for the experiments taken during this study. C) J-Kem Temperature controller.

1.4.5.1.   GC Measurements for Eyring Plot at 110 °C
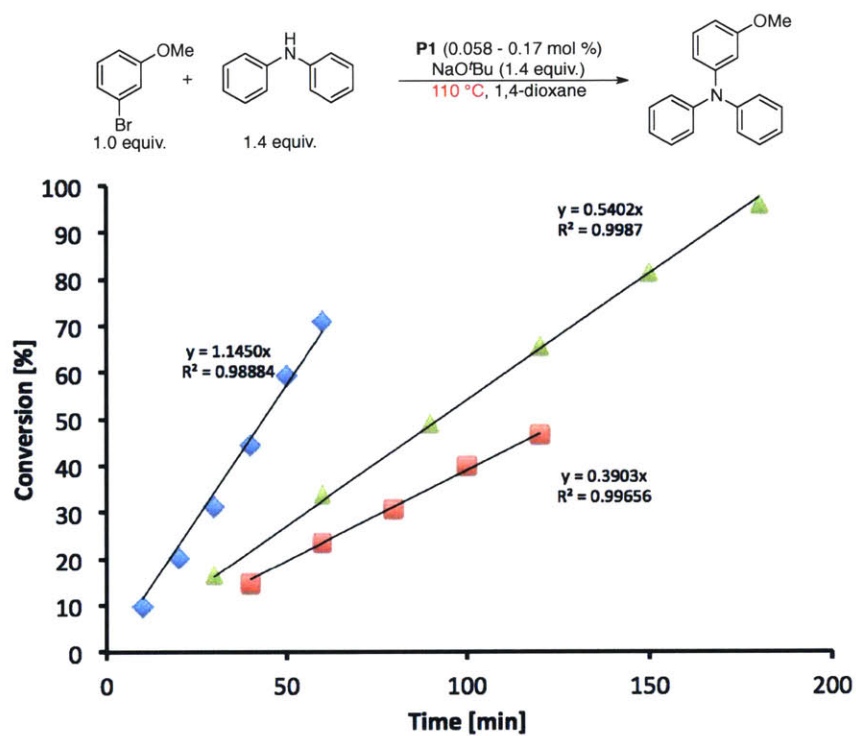
Figure 1-10 Rate of reaction at 110 °C

Table 1-5 Stock Solution

Reagent [g]	Name [-]	Conc. [mmol/g]
0.5198	NaO^{t}Bu	0.90
0.9188	Ph$_2$NH	0.91
0.7288	3-bromoanisole	0.65
3.8181	1,4-dioxane	

Table 1-6 Catalyst Solutions- (Note: Solutions B' and C' made from dilution of A')

ID	Catalyst	Toluene [g]	Concentration [mg/g]
Cat Sol A'	11.9 mg	0.5031	23.1
Cat Sol B'	0.1052 g of A'	0.1062	11.5
Cat Sol C'	0.0549 g of A'	0.1009	8.1

Table 1-7 Run Data

Solution	Stock Solution [g]	Catalyst Solution [mg]	Catalyst [mg]	ArX [mmol]	P1 [mol %]	ArX [mmol/g]	Amine [mmol]	NaO^{t}Bu [mmol/g]
A0	1.8064	62.6	1.45	1.18	0.169	0.629	0.877	0.873
B0	1.8025	62.4	0.72	1.17	0.084	0.629	0.877	0.873
C0	1.8061	61	0.50	1.18	0.058	0.630	0.878	0.874

Table 1-8 Data Summary

Data Summary

ID	ArX (2.02 min) [pA s]	C12 (2.15 min) [p As]	Amine (3.3 min) [pA s]	Prod (5.00 min) [pA s]	Time [min]	Solution [g]	Dodecane [g]	Mass Balance ArX [mmol]	Amine [mmol]	Base [mmol]	C12 [mmol]	GC Measurement ArX [mmol]	Amine [mmol]	Product [mmol]
A1	497.71	758.50	1307.08	191.26	10	0.2516	0.0189	0.158	0.221	0.220	0.111	0.143	0.206	0.019
A2	418.97	755.79	1188.84	371.62	20	0.2465	0.0194	0.155	0.216	0.215	0.114	0.124	0.193	0.037
A3	344.08	738.02	1038.80	512.23	30	0.2342	0.0189	0.147	0.205	0.205	0.111	0.101	0.168	0.051
A4	434.87	1040.89	1432.97	1089.13	40	0.2832	0.0206	0.178	0.248	0.247	0.121	0.099	0.179	0.084
A5	209.14	847.79	785.19	881.90	50	0.2423	0.0219	0.152	0.212	0.212	0.129	0.062	0.128	0.089
A6	129.69	574.78	591.50	908.31	60	0.2712	0.0192	0.171	0.238	0.237	0.113	0.050	0.125	0.119
B2	370.51	702.40	1005.48	206.10	40	0.2440	0.0216	0.154	0.214	0.213	0.127	0.131	0.195	0.025
B3	339.99	666.43	966.94	309.97	60	0.2440	0.0200	0.154	0.214	0.213	0.117	0.117	0.183	0.036
B4	401.42	818.27	1179.49	518.40	80	0.2473	0.0191	0.156	0.217	0.216	0.112	0.108	0.174	0.047
B5	258.18	732.03	800.98	468.25	100	0.2794	0.0260	0.176	0.245	0.244	0.153	0.106	0.180	0.065
B6	236.64	505.48	775.46	583.87	120	0.2492	0.0155	0.157	0.218	0.218	0.091	0.084	0.150	0.070
C1	322.67	985.50	876.27	195.41	30	0.2616	0.0365	0.165	0.230	0.229	0.214	0.138	0.205	0.028
C2	221.19	475.83	662.32	334.54	60	0.2423	0.0188	0.153	0.213	0.212	0.110	0.101	0.165	0.052
C3	148.87	481.52	505.18	423.33	90	0.2435	0.0219	0.153	0.214	0.213	0.129	0.078	0.145	0.075
C4	157.79	691.38	651.56	867.44	120	0.2515	0.0208	0.158	0.221	0.220	0.122	0.055	0.124	0.102
C5	54.10	404.78	321.16	653.43	150	0.2518	0.0194	0.159	0.221	0.220	0.114	0.030	0.097	0.123
C6	14.75	519.37	297.82	954.51	180	0.2518	0.0204	0.159	0.221	0.220	0.120	0.007	0.074	0.147
A0	272.27	486.47	681.32	0.00	N/A	0.2042	0.0195	0.128	0.179	0.178	0.114	0.126	0.172	N/A
B0	182.20	293.46	460.60	0.00	N/A	0.2138	0.0190	0.135	0.187	0.187	0.112	0.136	0.188	N/A
C0	265.64	471.27	675.17	0.00	N/A	0.1884	0.0184	0.119	0.165	0.165	0.108	0.119	0.166	N/A

1.4.5.2.   GC Measurements for Eyring Plot at 100 °C
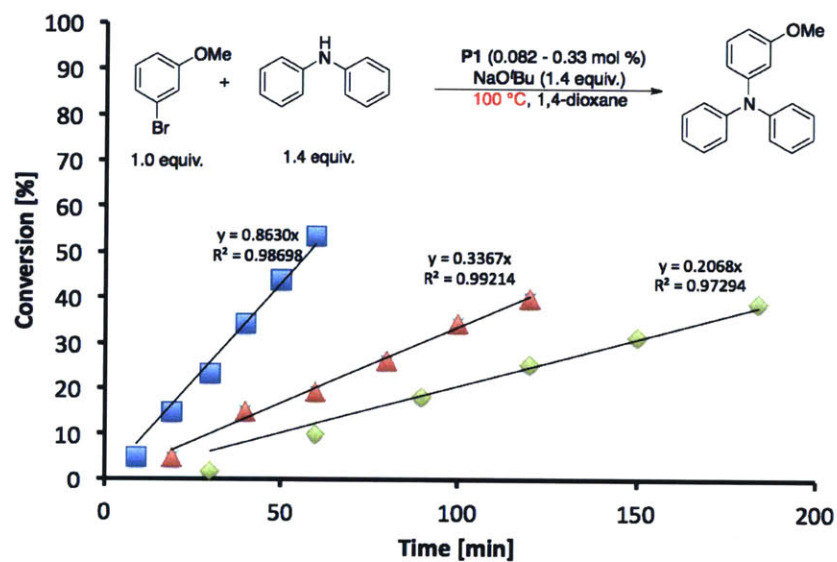
Figure 1-11 Rate of reaction at 100 °C

Table 1-9 Stock Solution

Reagent [g]	Name [-]	Conc. [mmol/g]
0.5193	NaO^{t}Bu	0.90
0.9199	Ph$_2$NH	0.90
0.7481	3-bromoanisole	0.66
3.8303	1,4-dioxane	

Table 1-10 Catalyst Solution

ID	Catalyst	Toluene [g]	Concentration [mg/g]
A & B	11.9 mg	0.5047	23.0
C	0.1072 g of A	0.1099	11.4

Table 1-11 Run Data

Solution	Stock Solution [g]	Catalyst Sol [mg]	Catalyst [mg]	ArX [mmol]	P1 [mol %]	ArX [mmol/g]	Amine [mmol/g]	NaO^{t}Bu [mmol/g]
A0	1.807	126.5	2.91	1.20	0.333	0.621	0.844	0.839
B0	1.809	63.0	1.45	1.20	0.166	0.642	0.873	0.868
C0	1.8142	63.7	0.72	1.21	0.083	0.642	0.873	0.868

Data Summary

Table 1-12 Data Summary

ID	ArX (2.02 min)	C12 (2.15 min)	Amine (3.3 min)	Prod (5.0 min)	Time [min]	Solution [g]	Dodecane	Mass Balance				GC Measurement		
								ArX [mmol]	Amine [mmol]	Base [mmol]	C12 [mmol]	ArX [mmol]	Amine [mmol]	Product [mmol]
A1	400.85	1114.00	1017.56	93.69	9	0.2471	0.0353	0.154	0.209	0.207	0.207	0.146	0.204	0.012
A2	337.41	1182.92	889.34	187.81	19	0.2242	0.0362	0.139	0.189	0.188	0.213	0.119	0.172	0.022
A3	290.63	823.32	799.55	284.90	30	0.2443	0.0286	0.152	0.206	0.205	0.168	0.116	0.175	0.039
A4	315.43	886.64	926.18	509.52	40	0.2669	0.0266	0.166	0.225	0.224	0.156	0.109	0.175	0.060
A5	244.94	887.06	765.57	583.59	50	0.2469	0.027	0.153	0.208	0.207	0.159	0.086	0.147	0.070
A6	184.13	765.56	628.69	634.72	60	0.2756	0.0288	0.171	0.233	0.231	0.169	0.080	0.149	0.093
B1	362.98	821.63	905.27	81.76	19	0.2321	0.0279	0.149	0.203	0.201	0.164	0.142	0.194	0.011
B2	270.64	820.59	696.99	128.36	40	0.2043	0.0294	0.131	0.178	0.177	0.173	0.112	0.158	0.018
B3	273.99	868.24	726.62	205.91	60	0.2176	0.031	0.140	0.190	0.189	0.182	0.113	0.164	0.029
B4	261.64	748.47	745.38	399.06	100	0.2617	0.0273	0.168	0.228	0.227	0.160	0.110	0.172	0.057
B5	262.14	764.97	715.16	286.62	80	0.2208	0.0265	0.142	0.193	0.192	0.156	0.105	0.156	0.039
B6	233.10	632.29	694.36	472.31	120	0.2517	0.0228	0.162	0.220	0.218	0.134	0.097	0.158	0.067
C1	311.94	703.23	785.30	61.69	30	0.2043	0.0252	0.131	0.178	0.131	0.148	0.129	0.178	0.009
C2	349.64	849.74	901.88	143.01	60	0.2492	0.0304	0.160	0.217	0.160	0.178	0.144	0.204	0.020
C3	350.13	716.60	930.26	237.25	90	0.254	0.0237	0.163	0.222	0.163	0.139	0.133	0.194	0.031
C4	289.58	740.46	792.12	284.31	120	0.247	0.0263	0.159	0.216	0.159	0.154	0.118	0.178	0.040
C5	310.76	816.00	882.30	419.98	150	0.2816	0.0282	0.181	0.246	0.181	0.166	0.124	0.192	0.057
C6	239.92	759.55	705.72	430.32	184	0.2453	0.0265	0.158	0.214	0.158	0.156	0.096	0.155	0.059
A0	290.28	676.87	717.13	0.00	N/A	0.207	0.0265	0.129	0.175	0.174	0.156	0.131	0.177	N/A
B0	182.02	342.77	447.28	0.00	N/A	0.2169	0.0233	0.139	0.189	0.188	0.137	0.142	0.192	N/A
C0	300.41	539.36	744.68	0.00	N/A	0.2561	0.0266	0.164	0.224	0.222	0.156	0.171	0.232	N/A

1.4.5.3. GC Measurements for Eyring Plot at 90 °C
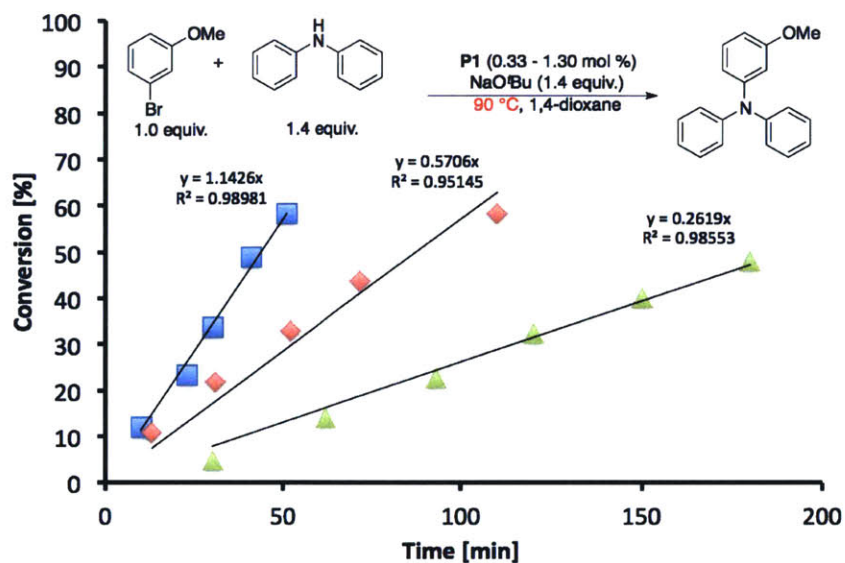
Figure 1-12 Rate of reaction at 90 °C

Table 1-13 Stock Solution

Reagent [g]	Name [-]	Conc. [mmol/g]
0.5443	NaO^{t}Bu	0.90
0.9818	Ph$_2$NH	0.92
0.7796	3-bromoanisole	0.66
4.0068	1,4-dioxane	

Table 1-14 Run Data

Solution	Stock Solution [g]	Catalyst [mg]	ArX [mmol]	P1 [mol %]	ArX [mmol/g]	Amine [mmol/g]	NaO^{t}Bu [mmol/g]
A0	1.866	11.7	1.225	1.304	0.656	0.913	0.892
B0	1.8529	5.8	1.220	0.651	0.658	0.916	0.894
C0	1.9733	3.1	1.301	0.327	0.659	0.918	0.896

44

Data Summary

Table 1-15 Data Summary

ID	ArX (2.02 min) [pA s]	C12 (2.15 min) [pA s]	Amine (3.3 min) [pA s]	Prod (5.0 min) [pA s]	Time [min]	Solution [g]	Dodecane	ArX [mmol]	Amine [mmol]	Base [mmol]	C12 [mmol]	ArX [mmol]	Amine [mmol]	Product [mmol]
									Mass Balance				**GC Measurement**	
A1	354.54	675.34	960.16	127.14	10	0.2135	0.0204	0.140	0.120	0.123	0.120	0.123	0.183	0.015
A2	277.81	664.49	796.89	241.99	23	0.2141	0.0224	0.140	0.132	0.108	0.132	0.108	0.170	0.032
A3	261.22	652.38	788.89	358.15	30	0.2094	0.0198	0.137	0.116	0.091	0.116	0.091	0.151	0.043
A4	337.54	944.46	1145.55	873.13	41	0.2456	0.02	0.161	0.117	0.082	0.117	0.082	0.153	0.072
A5	149.13	590.24	559.82	583.72	51	0.2091	0.0197	0.137	0.116	0.057	0.116	0.057	0.118	0.076
A6	205.16	659.63	780.19	826.20	62	0.2708	0.0204	0.178	0.120	0.073	0.120	0.073	0.152	0.100
B1	331.99	611.39	883.01	117.95	13	0.215	0.0202	0.142	0.119	0.126	0.119	0.126	0.184	0.015
B2	321.97	583.44	900.81	247.75	31	0.2406	0.0195	0.158	0.114	0.124	0.114	0.124	0.190	0.032
B3	220.91	611.10	657.84	313.60	52	0.1987	0.0211	0.131	0.124	0.088	0.124	0.088	0.143	0.042
B4	177.39	548.46	567.27	395.60	72	0.2073	0.0207	0.136	0.122	0.077	0.122	0.077	0.135	0.058
B6	136.77	502.93	501.27	536.72	110	0.2293	0.0202	0.151	0.119	0.063	0.119	0.063	0.127	0.084
C1	343.22	543.36	895.01	79.11	30	0.242	0.0209	0.160	0.123	0.152	0.163	0.152	0.217	0.012
C2	325.15	585.87	873.31	169.15	62	0.2383	0.0211	0.157	0.124	0.135	0.123	0.135	0.199	0.024
C3	208.31	485.91	582.08	181.17	93	0.1993	0.0206	0.131	0.121	0.102	0.124	0.102	0.156	0.030
C4	217.05	549.30	628.08	271.85	120	0.2082	0.0204	0.137	0.120	0.093	0.121	0.093	0.147	0.040
C5	204.80	533.45	627.19	388.69	150	0.2228	0.0199	0.147	0.117	0.088	0.120	0.088	0.148	0.057
C6	177.73	626.44	582.19	478.20	180	0.195	0.0205	0.129	0.120	0.067	0.117	0.067	0.120	0.061
A0	244.94	272.50	643.52	0.00	N/A	0.3548	0.0222	0.233	0.130	0.230	0.130	0.230	0.331	N/A
B0	270.65	277.97	707.64	0.00	N/A	0.3567	0.0202	0.235	0.119	0.226	0.119	0.226	0.325	N/A
C0	154.39	154.86	384.70	0.00	N/A	0.4871	0.0278	0.321	0.163	0.319	0.163	0.319	0.436	N/A

1.4.5.4.　Calorimetry Measurements for Eyring Plot at 78 °C

At 78 °C, the solution was not homogenous, therefore, kinetic measurements using GC experiments did not give reliable results. Consequently, we opted to perform a calorimetry experiment to measure the reductive elimination rate constant at 78 °C. Following general calorimetry procedure, a low catalyst loading was used (0.16 mol % - 0.33 mol %) and the experiment was performed in duplicate. Due to the long reaction time (> 17 h), the signal-to-noise ratio was poor but the end of the reaction was unmistakable. The integrated heat energy did not agree across the different time spans due to the low signal to noise ratio. This data was analyzed using equation 1.4.9 to calculate the reductive elimination rate constant.
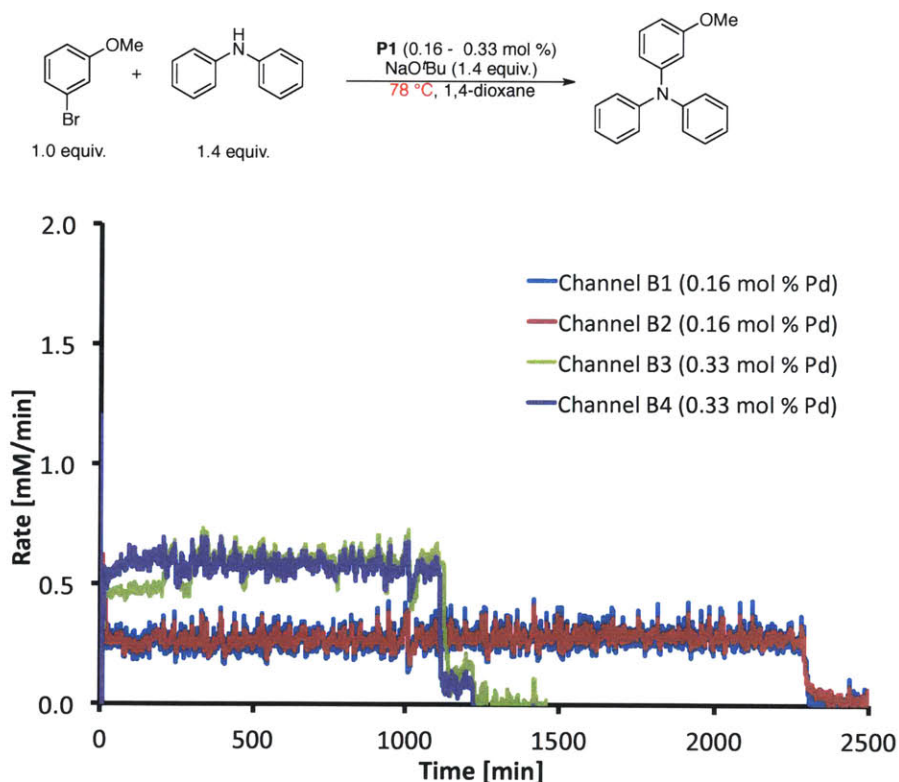
Figure 1-13 Rate of reaction at 78 °C

Table 1-16 Stock Solution

Reagent [g]	Name [-]	Conc. [mmol/g]
2.818	NaO^{t}Bu	0.91
4.9487	Ph$_2$NH	0.90
3.9209	3-bromoanisole	0.65
20.6923	1,4-dioxane	

Table 1-17 Catalyst Solution

P1 [mg]	Toluene [g]	Conc. [mg/g]
49.7	2.0249	23.96

Table 1-18 Run Summary

Channel [#]	Stock Solution [g]	ArX [mmol]	Loaded Syringe [g]	Post Injected Syringe [g]	Injected Mass [g]	Pd [mol %]	Rxn Time [min]	k [1/min]
B1	5.5012	3.56	2.8311	2.6537	0.1774	0.165	2294	0.2649
B2	5.5171	3.57	2.8098	2.6316	0.1782	0.165	2293	0.2646
B3	5.4996	3.56	2.9974	2.6447	0.3527	0.327	1127	0.2711
B4	5.5701	3.61	2.9844	2.6296	0.3548	0.325	1113	0.2764

Table 1-19 GC Summary

Channel [#]	Dodecane [mg]	Dodecane [pA s]	Product [pA s]	Yield [%]
B1	158.3	59.6	324.5	99
B2	131.1	74.0	500.1	>99
B3	156.8	64.7	353.4	98
B4	152.9	50.6	289.6	99

Table 1-20 Energy Summary

Channel [#]	Total Exotherm [J]	Limiting Reagent [mmol]	Energy Density [kJ/mol]
B1	600	3.56	168
B2	610	3.57	171
B3	789	3.56	221
B4	779	3.61	216

1.4.6. General Calorimetry Procedure for Hammett Studies

General Calorimetry Procedure (see section 1.4.3) was followed except the stock solution was prepared without the diarylamine. The appropriate amine was separately added to each reaction vessel. Note: For each diarylamine, the reaction was run multiple times (Run 1, Run 2, and Run 3) at different

catalyst loadings and the rate constant for reductive elimination was calculated using equation 9 (see corresponding Run Summary table (e.g., Table 1-25)). Three examples were run with the diarylamine as the limiting reagent (compared to bromobenzene). These examples did not give different rate constants. Comparing the different runs (which may look different) we did not find significant variation for the calculated rate constant.

For the Hammett series of aryl halides, the General Calorimetry Procedure (see section 1.4.3) was followed except the stock solution was prepared without the aryl halide. The appropriate aryl halide was added separately to each reaction vessel. Note: For each aryl halide the reaction was run three times (Run 1, Run 2, and Run 3) at various catalyst loadings and the rate constant for reductive elimination was calculated using equation 13 (see corresponding Run Summary table (e.g., Table 1-44)). Comparing the different runs (which may look different) we did not find significant variation for the calculated rate constant.

1.4.6.1. Hammett Series for Diarylamines - Run 1
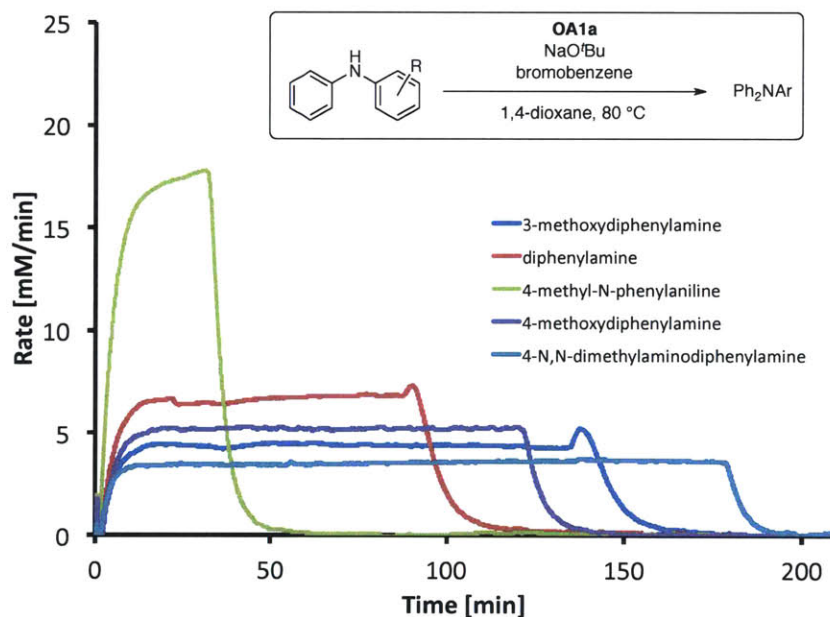
Figure 1-14 Rate of reaction for different diarylamines - Run 1

Table 1-21 Stock Solution

Reagent [g]	Name [-]	Conc. [mmol/g]
2.8569	bromobenzene	0.77
2.4925	NaO^{t}Bu	1.10
18.1966	1,4-dioxane	

Table 1-22 Catalyst Solution

Catalyst Label [-]	**OA1a** [g]	CH$_2$Cl$_2$ [g]	Conc. [mg/g]
A	0.2067	1.0599	163.19
B	0.0154	0.5164	28.96
C	0.0147	1.5094	9.65

Table 1-23 Run Summary

Catalyst Label [-]	Channel [#]	Amine	Loaded Syringe [g]	Post Injected Syringe [g]	Injected Mass [g]	Catalyst [mg]
A	A1	3-methoxydiphenylamine	2.8966	2.6776	0.2190	35.7
A	A2	diphenylamine	2.8747	2.6592	0.2155	35.2
A	A3	4-methyl-N-phenylaniline	2.8863	2.6685	0.2178	35.5
B	A4	4-methoxydiphenylamine	2.8797	2.6668	0.2129	6.2
C	B1	4-N,N-dimethylaminodiphenylamine	2.8568	2.6407	0.2161	2.1

Table 1-24 Run Summary

Channel	Added Stock Solution [g]	Amine [g]	Amine [name]	Amine [mmol]	ArX [mmol]	Pd [mol %]	Rxn Time [min]	k [1/min]
A1	2.6125	0.4285	3-methoxydiphenylamine	2.15	2.02	2.33	144.5	0.2967
A2	2.5900	0.3636	diphenylamine	2.15	2.00	2.31	96.05	0.4498
A3	2.5988	0.3216	4-methyl-N-phenylaniline	1.76	2.01	2.33	35.3	1.2150
A4	2.5977	0.4212	4-methoxydiphenylamine	2.11	2.01	0.40	124.8	1.9804
B1	2.5922	0.4500	4-N,N-dimethylaminodiphenylamine	2.12	2.00	0.14	181	4.0304

Table 1-25 GC Data

Channel	Name [-]	Dodecane [mg]	Aryl Halide [pA s]	Dodecane [pA s]	Product [pA s]	Limiting Reagent [mmol]	Product Yield [%]
A1	3-methoxydiphenylamine	122.3	0.00	206.99	841.34	2.02	>99
A2	diphenylamine	104.4	0.00	149.84	718.87	2.00	>99
A3	4-methyl-N-phenylaniline	105.6	17.88	121.66	490.26	1.76	95
A4	4-methoxydiphenylamine	111.7	0.00	105.80	469.21	2.01	>99
B1	4-N,N-dimethylaminodiphenylamine	113.3	0.00	113.03	517.44	2.00	>99

49

Table 1-26 Energy Density

Channel [#]	Total Exotherm [J]	Limiting Reagent [mmol]	Energy Density [kJ/mol]	Name [-]
A1	369	2.02	183	3-methoxydiphenylamine
A2	375	2.00	187	diphenylamine
A3	311	1.76	177	4-methyl-*N*-phenylaniline
A4	361	2.01	180	4-methoxydiphenylamine
B1	359	2.00	179	4-N,N-dimethylaminodiphenylamine

1.4.6.2. Hammett Series for Diarylamines - Run 2
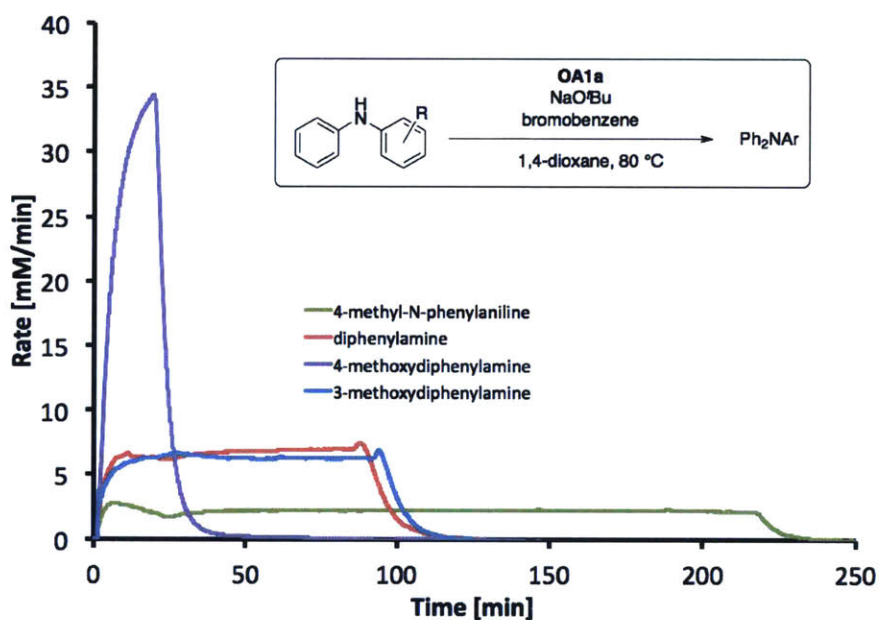
Figure 1-15 Rate of reaction for different diarylamines-Run 2

Table 1-27 Stock Solution

Reagent [g]	Name [-]	Conc. [mmol/g]
2.9576	bromobenzene	0.77
2.5400	NaO^{t}Bu	1.08
19.0100	1,4-dioxane	

Table 1-28 Catalyst Solution

Catalyst Label [-]	OA1a [g]	CH$_2$Cl$_2$ [g]	Conc. [mg/g]
A	0.2066	1.0107	169.72
B	0.0271	0.9322	28.25

Table 1-29 Run Summary

Catalyst Label [-]	Channel	Loaded Syringe [g]	Post Injected Syringe [g]	Injected Mass [g]	Catalyst [mg]
B	A1	2.8973	2.6761	0.2212	6.2
A	A2	2.8931	2.6887	0.2044	34.7
A	A3	2.8881	2.6733	0.2148	36.5
A	A4	2.8890	2.6684	0.2206	37.4
C	B1	2.8942	2.683	0.2112	2.0

Table 1-30 Run Summary

Channel [#]	Added Stock Solution [g]	Amine [g]	Amine [name]	Amine [mmol]	ArX [mmol]	Pd [mol %]	Rxn Time [min]	k [1/min]
A1	2.5100	0.3016	3-methoxydiphenylamine	1.52	1.93	3.25	100	0.3072
A2	2.5088	0.3644	diphenylamine	2.16	1.93	2.37	95	0.4441
A3	2.5183	0.3925	4-methyl-N-phenylaniline	2.14	1.94	0.43	220	1.0687
A4	3.0538	0.4360	4-methoxydiphenylamine	2.19	2.35	2.19	22.9	1.9919

Table 1-31 GC Data

Channel	Dodecane [mg]	Dodecane [pA s]	Product [pA s]	Yield [%]
A1	118	171.9	509.6	>99
A2	115.1	72.0	298.5	>99
A3	105.6	152.0	732.9	97
A4	116.2	114.5	521.7	>99

Table 1-32 Energy Density

Channel [#]	Total Exotherm [J]	Limiting Reagent [mmol]	Energy Density [kJ/mol]	Name [-]
A3	351	1.94	181	4-methyl-N-phenylaniline
A2	368	1.93	191	diphenylamine
A4	411	2.19	188	4-methoxydiphenylamine
A1	281	1.52	185	3-methoxydiphenylamine

1.4.6.3.   Hammett Series for Diarylamines- Run 3
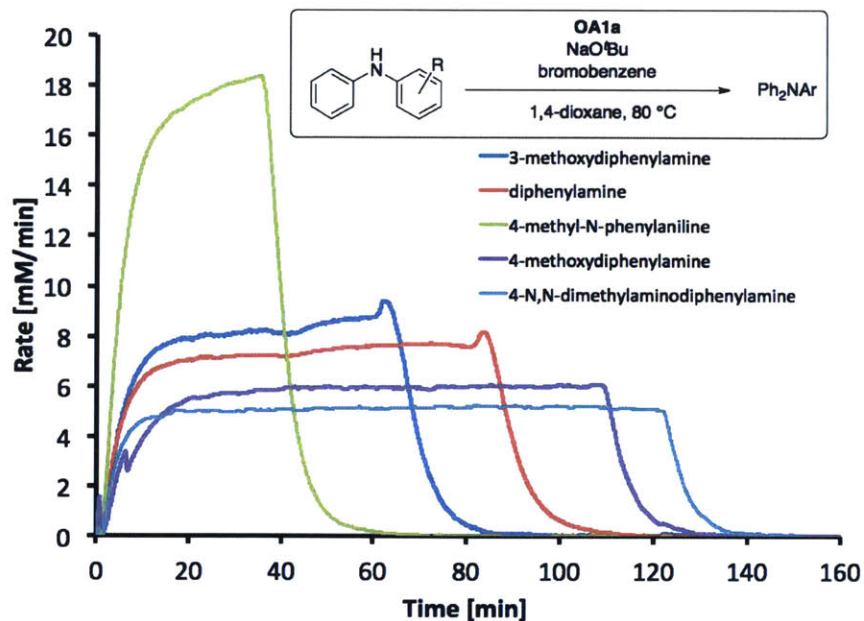
Figure 1-16 Rate of reaction for different diarylamines- Run 3

Table 1-33 Stock Solution

Reagent [g]	Name [-]	Conc. [mmol/g]
3.1460	bromobenzene	0.77
2.7392	NaO^{t}Bu	1.10
20.0395	1,4-dioxane	N/A

Table 1-34 Catalyst Solution

Catalyst Label [-]	OA1a [g]	CH$_2$Cl$_2$ [g]	Conc. [mg/g]
A	0.2059	1.0287	166.77
B	0.0304	1.0036	29.40
C	0.0199	1.5044	13.06

Table 1-35 Run Summary

Catalyst Label [-]	Channel [#]	Loaded Syringe [g]	Post Injected Syringe [g]	Injected Mass [g]	Catalyst [mg]
A	A1	2.8926	2.6769	0.2157	36.0
A	A2	2.8981	2.6807	0.2174	36.3
A	A3	2.8975	2.6825	0.2150	35.9
B	A4	2.8936	2.6718	0.2218	6.5
C	B1	2.9200	2.7053	0.2147	2.8

Table 1-36 Run Summary

Channel [#]	Added Stock Solution [g]	Amine [g]	Amine [name]	Amine [g/mol]	Amine [mmol]	ArX [mmol]	Pd [mol %]	Rxn Time [min]	k [1/min]
A1	1.5099	0.2027	3-methoxydiphenylamine	199	1.02	1.17	4.06	68.8	0.3579
A2	2.5148	0.3642	diphenylamine	169	2.15	1.94	2.46	89.5	0.4547
A3	2.6167	0.3928	4-methyl-N-aniline	183	2.14	2.02	2.34	40.3	1.0624
A4	2.5097	0.4321	4-methoxydiphenylamine	199	2.17	1.94	0.44	112	2.0159
B1	2.5030	0.4514	4-N,N-dimethylaminodiphenylamine	212	2.13	1.93	0.19	125	4.1911

Table 1-37 GC Data

Channel	Dodecane [mg]	Dodecane [pA s]	Product [pA s]	Yield [%]
A1	105.2	144.17	312.00	91
A2	106.2	101.23	465.14	>99
A3	102.7	35.26	183.84	>99
A4	106.3	62.49	278.93	>99
B1	100.7	83.33	409.16	>99

Table 1-38 Energy Density

Channel [#]	Total Exotherm [J]	Limiting Reagent [mmol]	Energy Density [kJ/mol]	Name [-]
A1	177	1.02	174	3-methoxydiphenylamine
A2	351	1.94	181	diphenylamine
A3	356	2.02	176	4-methyl-N-aniline
A4	334	1.94	172	4-methoxydiphenylamine
B1	372	1.93	192	4-N,N-dimethylaminodiphenylamine

1.4.6.4.   Hammett Series for Aryl Halides - Run 1
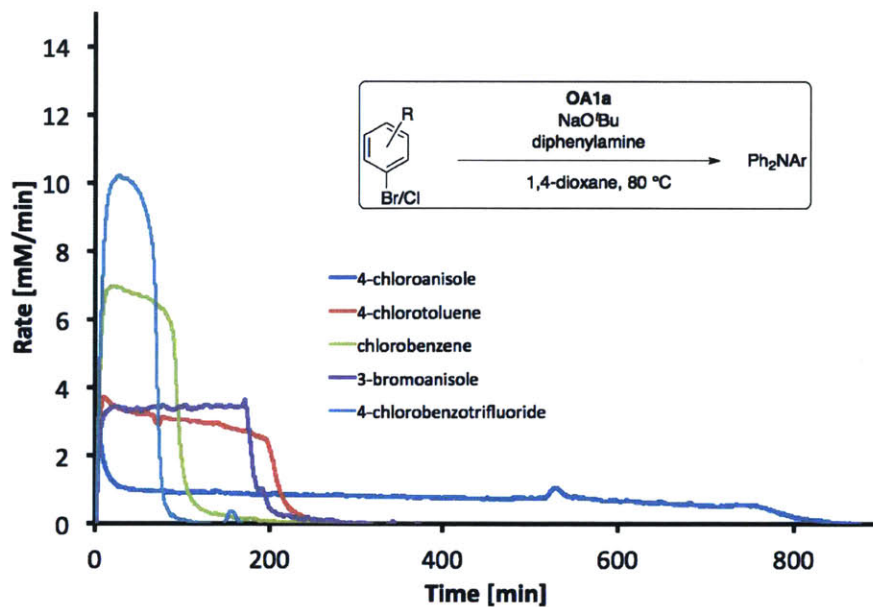
Figure 1-17 Rate of reaction for different aryl halides- Run 1

Table 1-39 Stock Solution

Reagent [g]	Name [-]	Conc. [mmol/g]
4.7449	Ph$_2$NH	1.02
2.6960	NaO^{t}Bu	1.02
20.00	1,4-dioxane	

Table 1-40 Catalyst Solution

Catalyst Label [-]	**OA1a** [g]	CH$_2$Cl$_2$ [g]	Conc. [mg/g]
A	0.3296	0.9989	248.10
B	0.0117	0.5011	22.82

Table 1-41 Run Summary

Catalyst Label [-]	Channel [#]	Loaded Syringe [g]	Post Injected Syringe [g]	Injected Mass [g]	Catalyst [mg]
A	A1	2.9281	2.6908	0.2373	58.9
A	A2	2.9202	2.6809	0.2393	59.4
A	A3	2.924	2.6793	0.2447	60.7
A	A4	2.8357	2.7019	0.1338	33.2
B	B1	2.9549	2.6786	0.2763	6.3

Table 1-42 Run Summary

Channel	Stock Solution [g]	ArX [g]	ArX [name]	Amine [mmol]	ArX [mmol]	Pd [mol %]	Rxn Time [min]	k [1/min]
A1	4.0188	0.4124	4-chloroanisole	4.11	2.89	2.68	774	0.0482
A2	4.0005	0.3961	4-chlorotoluene	4.09	3.13	2.50	206	0.1942
A3	4.0130	0.3257	chlorobenzene	4.11	2.89	2.76	94	0.3849
A4	4.0200	0.5433	3-bromoanisole	4.11	2.90	1.51	179	0.3711
B1	4.0036	0.5275	4-chlorobenzotrifluoride	4.10	2.92	0.28	70	5.0251

Table 1-43 GC Data

Channel [#]	Dodecane [mg]	Dodecane [pA s]	Product [pA s]	Yield [%]
A1	108.4	55.27	347.45	>99
A2	100.7	45.31	326.84	91
A3	108.4	51.87	343.76	>99
A4	136.3	75.34	399.10	>99
B1	149.3	85.24	406.50	95

Table 2-44 Energy Density

Channel [#]	Exotherm [J]	Limiting Reagent [mmol]	Energy Density [kJ/mol]	Name [-]
A1	619	2.89	214	4-chloroanisole
A2	594	3.13	190	4-chlorotoluene
A3	589	2.89	204	chlorobenzene
A4	550	2.90	189	3-bromoanisole
B1	568	2.92	194	4-chlorobenzotrifluoride

1.4.6.5.   Hammett Series for Aryl Halides- Run 2
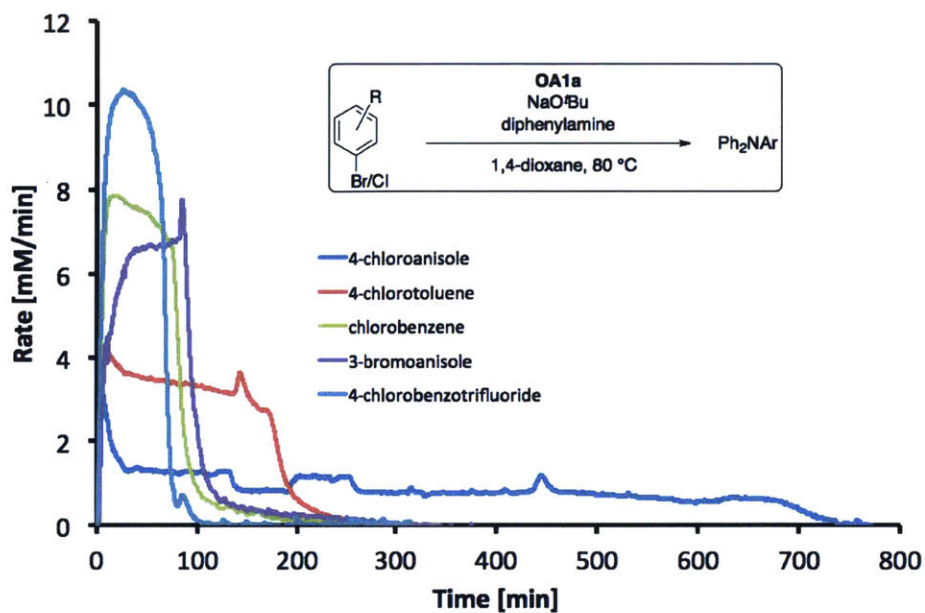
Figure 1-18 Rate of reaction of different aryl halides - Run 2

Table 1-45 Stock Solution

Reagent [g]	Name [-]	Conc. [mmol/g]
4.7390	Ph$_2$NH	1.02
2.6944	NaO^{t}Bu	1.02
20.0138	1,4-dioxane	

Table 1-46 Catalyst Solution

Catalyst Label [-]	OA1a [g]	CH$_2$Cl$_2$ [g]	Conc. [mg/g]
A	0.3572	1.2047	228.70
B	0.0146	0.7244	19.76

Table 1-47 Run Summary

Label [-]	Channel [#]	Loaded Syringe [g]	Post Injected Syringe [g]	Injected Mass [g]	Catalyst [mg]
A	A1	2.9144	2.7073	0.2071	47.4
A	A2	2.8894	2.6698	0.2196	50.2
A	A3	2.9077	2.6869	0.2208	50.5
A	A4	2.8719	2.6587	0.2132	48.8
B	B1	2.8780	2.6592	0.2188	4.3

Table 1-48 Run Summary

Channel [#]	Added Stock Solution [g]	ArX [g]	ArX [name]	Amine [mmol]	ArX [mmol]	Pd [mol %]	Rxn Time [min]	k [1/min]
A1	2.7539	0.2897	4-chloroanisole	2.81	2.03	3.07	702	0.0464
A2	2.742	0.2519	4-chlorotoluene	2.80	1.99	3.32	180	0.1671
A3	2.7742	0.2207	chlorobenzene	2.83	1.96	3.39	81.25	0.3628
A4	2.7483	0.3768	3-bromoanisole	2.81	2.01	3.19	92.65	0.3385
B1	2.7483	0.363	4-chlorobenzotrifluoride	2.81	2.01	0.28	67.45	5.2337

Table 1-49 GC Data

Channel	Dodecane [g]	Dodecane [pA s]	Product [pA s]	Yield [%]
A1	121.30	79.22	302.48	97
A2	108.30	98.16	453.69	99
A3	108.80	144.87	605.89	95
A4	109.00	127.98	582.52	>99
B1	111.90	171.00	768.45	97

Table 1-50 Energy Density

Channel [#]	Total Exotherm [J]	Limiting Reagent [mmol]	Energy Density [kJ/mol]	Name [-]
A1	404	2.03	199	4-chloroanisole
A2	443	1.99	223	4-chlorotoluene
A3	433	1.96	221	chlorobenzene
A4	418	2.01	207	3-bromoanisole
B1	390	2.01	194	4-chlorobenzotrifluoride

1.4.6.6. Hammett Series for Aryl Halides- Run 3
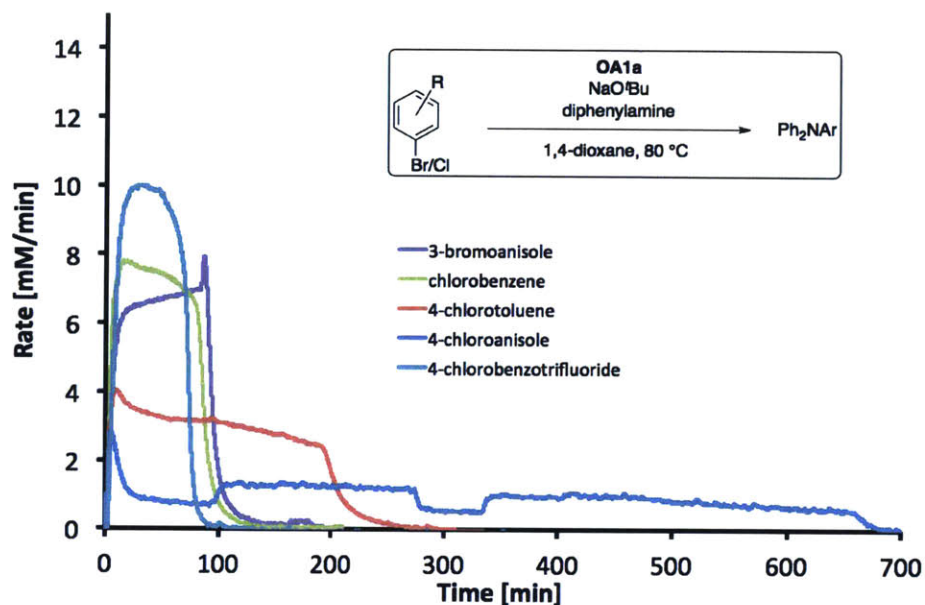
Figure 1-19 Rate of reaction for different aryl halides - Run 3

Table 1-51 Stock Solution

Reagent [g]	Name [-]	Conc. [mmol/g]
4.7483	Ph$_2$NH	1.02
2.6926	NaO^{t}Bu	1.02
19.99	1,4-dioxane	

Table 1-52 Catalyst Solution

Catalyst Label [-]	OA1a [g]	CH$_2$Cl$_2$ [g]	Conc. [mg/g]
A	0.3286	1.2194	212.27
B	0.0149	0.7275	20.07

Table 1-53 Run Summary

Label [-]	Channel	Loaded Syringe [g]	Post Injected Syringe [g]	Injected Mass [g]	Catalyst [mg]
A	A1	2.8717	2.6672	0.2045	43.41
A	A2	2.8944	2.6783	0.2161	45.87
A	A3	2.8938	2.6839	0.2099	44.56
A	A4	2.8972	2.6853	0.2119	44.98
B	B1	2.8664	2.6562	0.2102	4.22

58

Table 1-54 Run Summary

Channel	Added Stock Solution [g]	ArX [g]	ArX [name]	ArX [mmol]	Amine [mmol]	Pd [mol %]	Rxn Time [min]	k [1/min]
A1	2.7411	0.2219	chlorobenzene	1.97	2.81	2.90	86	0.4008
A2	2.772	0.3781	3-bromoanisole	2.02	2.84	2.99	93	0.3597
A3	2.7465	0.2513	4-chlorotoluene	1.99	2.81	2.96	197	0.1717
A4	2.7812	0.2894	4-chloroanisole	2.03	2.85	2.92	675	0.0507
B1	2.7808	0.3608	4-chlorobenzotrifluoride	2.00	2.85	0.28	72.55	4.9556

Table 1-55 GC Data

Channel	Dodecane [g]	Dodecane [pA s]	Product [pA s]	Yield [%]
A1	105.3	47.90	216.89	>99
A2	116.3	28.87	132.95	92
A3	111.7	39.07	177.56	100
A4	104.4	68.53	304.29	>99
B1	107.5	46.64	223.00	>99

Table 1-56 Energy Density

Channel [#]	Total Exotherm [J]	Limiting Reagent [mmol]	Energy Density [kJ/mol]	Name [-]
A1	385	1.97	195	chlorobenzene
A2	383	2.02	189	3-bromoanisole
A3	434	1.99	219	4-chlorotoluene
A4	415	2.03	204	4-chloroanisole
B1	390	2.00	195	4-chlorobenzotrifluoride

1.4.6.7. Hammett Series 3-chloroanisole/diphenylamine kinetics
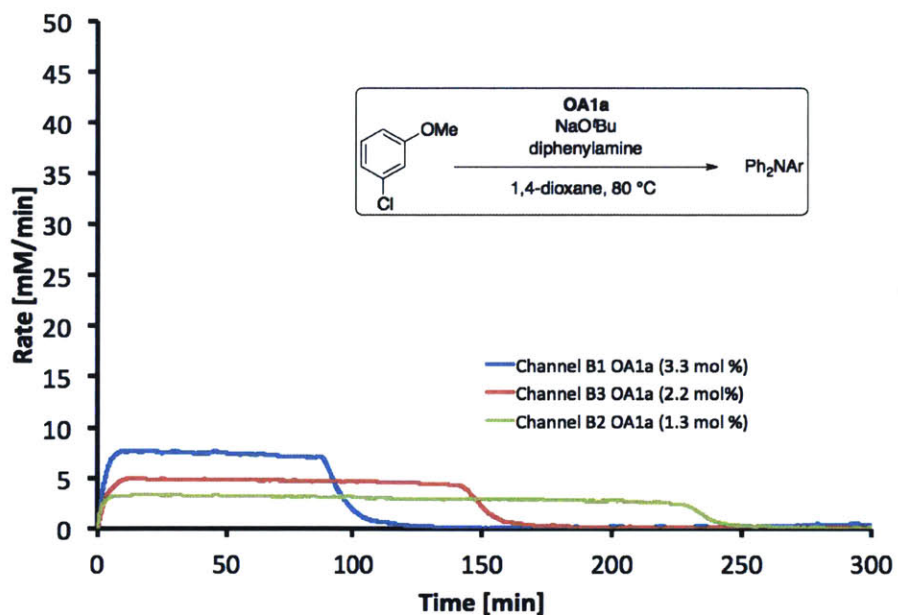
Figure 1-20 Rate of reaction for three different catalyst loadings. Note: These reaction employed the same "batch" of **OA1a** unlike the other Hammett Studies

Table 1-57 Stock Solution

Reagent [g]	Name [-]	Conc. [mmol/g]
1.0108	3-chloroanisole	0.67
0.9643	NaO^{t}Bu	0.94
1.6577	Ph$_2$NH	0.92
7.0156	1,4-dioxane	

Table 1-58 Catalyst Solution

OA1a [mg]	CH$_2$Cl$_2$ [g]	Conc. [mg/g]
200.6	0.6974	223.4

Table 1-59 Run Summary

Channel [#]	Stock Solution [g]	Loaded Syringe [g]	Post Injected Syringe [g]	Injected Mass [g]	ArX [mmol]	Pd [mol %]	Rxn Time [min]	k [1/min]
B1	3.0446	2.8953	2.6735	0.2218	2.03	3.22	93.2	0.3329
B2	2.9962	2.7874	2.6967	0.0907	2.00	1.34	232.5	0.3212
B3	3.0057	2.8472	2.7016	0.1456	2.00	2.14	148.3	0.3146

Table 1-60 GC Data

Channel [#]	Dodecane [mg]	Dodecane [pA s]	Product [pA s]	Yield [%]
B1	135.3	70.62	256.30	99
B2	144.1	78.57	267.34	>99
B3	154.1	77.67	242.03	98

60

Table 1-61 Energy Density

Channel [#]	Total Exotherm [J]	Limiting Reagent [mmol]	Energy Density [kJ/mol]
B1	417	2.03	206
B2	410	2.00	205
B3	405	2.00	202

1.4.7. General Calorimetry Procedure for different ligand based catalyst

In a nitrogen-filled glove box, a stock solution of aryl halide, amine, base, and solvent was charged to a screw cap sealable vial. Aliquots were then loaded into 16 mL vials (Wheaton Vial, 16 mL E-C Vial, Cat # 224706) and the mass of each aliquot was recorded. The vials were equipped with a stir bar and then sealed with a silicon/Teflon septum. The vials were removed from the glove box and loaded into the calorimeter that was preheated to the indicated reaction temperature. A reaction vial containing pure solvent was loaded into reference channel of the calorimeter.

Separately, solutions of the pre-catalysts were prepared by the addition of the palladium complex into toluene or other appropriate solvent in a 4 mL Vial (Wheaton 4 mL E-C Vial Cat # 224742). The masses of the palladium complex and solvent were recorded. Syringes equipped with a 6-inch needle were then loaded with the catalyst solution and weighed. After equilibration of the reaction vials (~1 h) into the preheated calorimeter, the catalyst solution was injected through the septum to start the reactions. The syringes were weighed again to calculate the total amount of catalyst injected into the reaction. An equal mass of pure solvent was injected into the reference channel.

The end of the reaction and thus the reaction time was determined by the return of the power output to 20 % of the baseline. The 16 mL vial was removed from the calorimeter and allowed to cool before addition of n-dodecane as an internal standard and the reaction yield was quantified by GC analysis of the sample.

These reactions were run simultaneously with a control reaction employing **OA1a** as a catalyst source. In this manner the control reaction based on RuPhos **L1** (**OA1a**) is exposed to the identical temperature conditions as the reactions employing the other ligand types. The rate constant for each reaction was calculated according to equation 1.4.9. Thus the rate constants were indexed to the control reaction rate constant and these ratios are reported in table 1-3.

1.4.7.1. CPhos (L9) and RuPhos (L1)
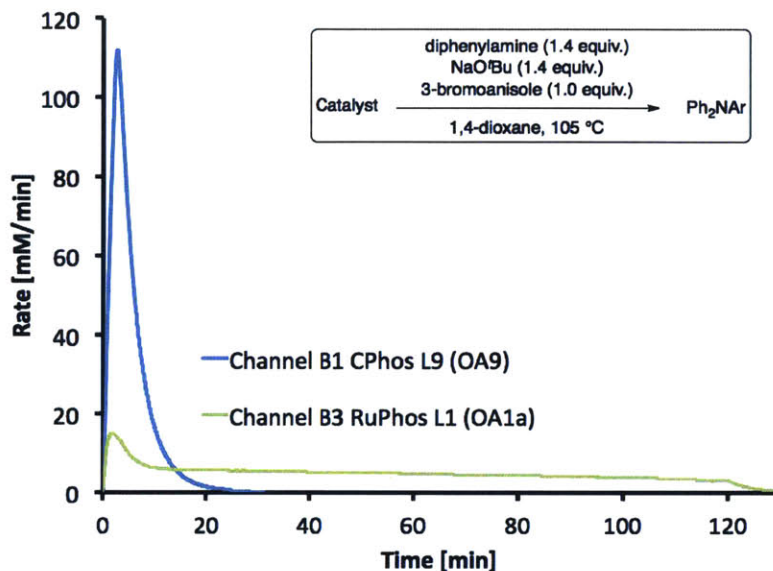
Figure 1-21 Rate of reaction for CPhos (**L9**) based catalyst

Table 1-62 Stock Solution

Reagent [g]	Name [-]	Conc. [mg/g]
3.5146	HNPh$_2$	0.89
2.0875	NaO^{t}Bu	0.93
2.7838	3-bromoanisole	0.64
14.9235	1,4-dioxane	

Table 1-63 Catalyst Solution

Catalyst Label [-]	Name [-]	Catalyst [mg]	THF [g]	Conc. [mg/g]
A	**OA9**	14.3	0.5206	26.7
B	**OA1a**	14.7	0.5129	27.9

Table 1-64 Run Summary

Catalyst Label [-]	Channel [#]	Stock Solution [g]	Loaded Syringe [g]	Post Injected Syringe [g]	Injected Mass [g]	ArX [mmol]	Pd [mol %]	Rxn Time [min]	k [1/min]
A	B1	3.0022	2.7304	2.6318	0.0986	1.92	0.19	13.4	39.57
B	B3	3.0038	2.7265	2.6226	0.1039	1.92	0.20	122	4.12

Table 1-65 GC Data

Channel [#]	Dodecane [mg]	Dodecane [pA s]	Product [pA s]	Yield [%]
B1	112.4	49.57	201.21	97
B3	109.3	91.41	388.76	99

62

Table 1-66 Energy Density

Channel [#]	Total Exotherm [J]	ArX [mmol]	Energy Density [kJ/mol]
B1	368	1.92	192
B3	447	1.92	233

1.4.7.2. RuPhos (L1), SPhos (L2), and XPhos (L7)
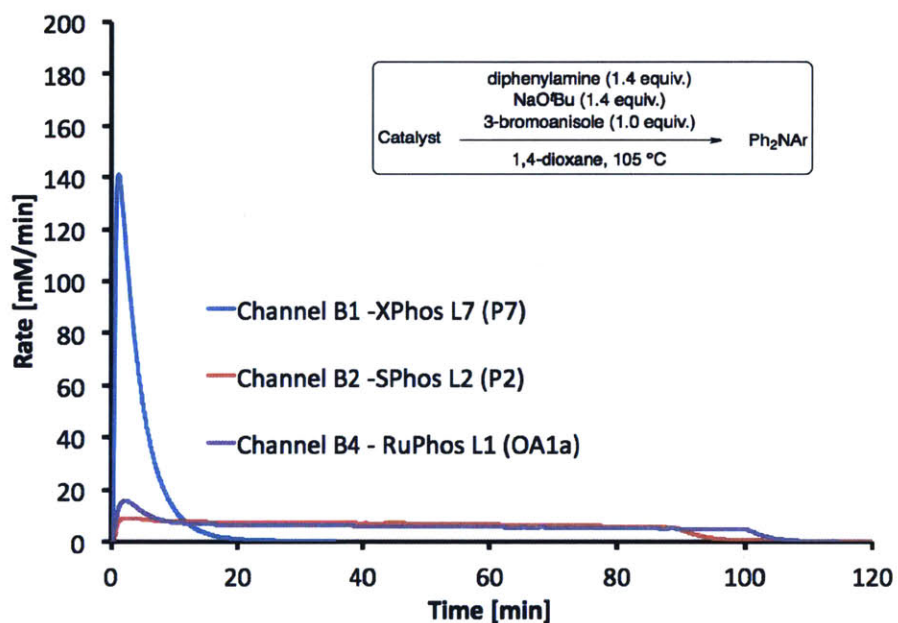
Figure 1-22 Rate of reaction for XPhos (**L7**) and SPhos (**L2**) based catalysts

Table 1-67 Stock Solution

Reagent [g]	Name [-]	Conc. [mmol/g]
3.5023	HNPh$_2$	0.89
2.0416	NaO^{t}Bu	0.91
2.7781	3-bromoanisole	0.64
14.9063	1,4-dioxane	

Table 1-68 Catalyst Solution

Catalyst Label [-]	Name [-]	Catalyst [mg]	THF [g]	Conc. [mg/g]
A	**P7**	15.4	0.5682	26.4
B	**P2**	14.7	0.5727	25.0
C	**OA1a**	14.4	0.4957	28.2

63

Table 1-69 Run Summary

Catalyst Label (-)	Channel (#)	Stock Solution (g)	Loaded Syringe (g)	Post Injected Syringe (g)	Injected Mass (g)	ArX (mmol)	Pd (mol %)	Rxn Time (min)	Rate Constant (1/min)
A	B1	2.9935	2.7371	2.6354	0.1017	1.91	0.191	7.10	73.87
B	B2	2.9994	2.7392	2.6323	0.1069	1.91	0.204	91.2	5.37
C	B4	2.9642	2.7350	2.6327	0.1023	1.89	0.202	101.9	4.86

Table 1-70 GC Data

Channel	Dodecane [mg]	Dodecane [pA s]	Product [pA s]	Yield [%]
B1	160.0	226.28	675.69	>99
B2	130.6	149.49	530.14	99
B4	124.6	124.59	460.56	>99

Table 1-71 Energy Summary

Channel	Total Exotherm [J]	ArX [mmol]	Energy Density [kJ/mol]
B1	343	1.91	180
B2	406	1.91	213
B4	415	1.89	220

1.4.7.3. RuPhos (L1) and BrettPhos (L6)
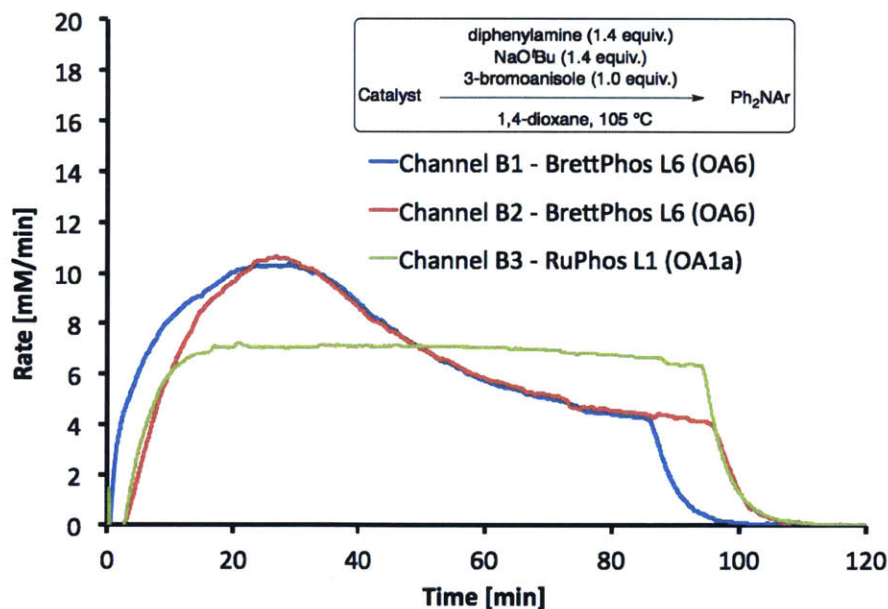
Figure 1-23 Rate of reaction for BrettPhos (**L6**) based catalyst

Table 1-72 Stock Solution

Reagent [g]	Name [-]	Conc. [mmol/g]
2.6478	Ph$_2$NH	0.90
1.5023	NaO^{t}Bu	0.90
2.1023	3-bromoanisole	0.64
11.2119	1,4-dioxane	

Table 1-73 Catalyst Solution

Catalyst Label [-]	Name [-]	Catalyst [mg]	THF [g]	Conc. [mg/g]
A	**OA6**	23.5	1.0165	22.6
B	**OA1a**	16.5	0.5313	30.1

Table 1-74 Run Summary

Catalyst Label [-]	Channel [#]	Stock Solution [g]	Loaded Syringe [g]	Post Injected Syringe [g]	Injected Mass [g]	ArX [mmol]	Pd [mol %]	Rxn Time [min]	k [1/min]
A	B1	3.0035	2.7043	2.6014	0.1029	1.93	0.15	88.40	7.80
A	B2	3.0322	2.7383	2.6397	0.0986	1.95	0.14	98.34	7.39
B	B3	3.0037	2.7715	2.6650	0.1065	1.93	0.22	96.45	4.74

Table 1-75 GC Data

Channel	Dodecane [mg]	Dodecane [pA s]	Product [pA s]	Yield [%]
B1	93.3	88.81	439.19	98
B2	117.5	121.41	485.01	98
B3	151.6	125.45	400.26	>99

Table 1-76 Energy Density

Channel	Energy [J]	ArX [mmol]	Energy Density [kJ/mol]
B1	340	1.93	176
B2	290	1.95	149
B3	332	1.93	172

1.4.7.4. RuPhos (L1) and CyJohnPhos (L8)
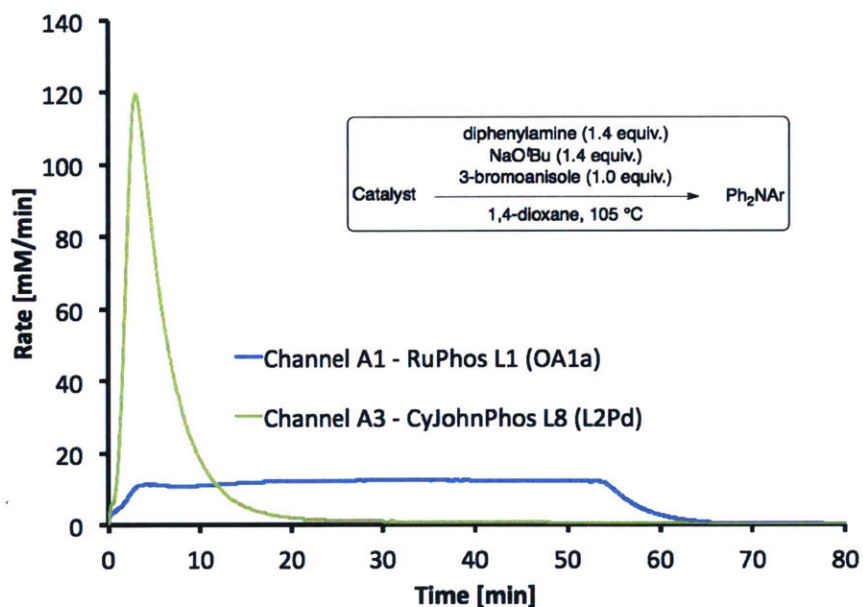
Figure 1-24 Rate of reaction for CyJohnPhos (**L8**) based catalyst

Table 1-77 Stock Solution

Reagent [g]	Name [-]	Conc. [mmol/g]
2.9530	3-bromoanisole	0.64
2.1232	NaO^{t}Bu	0.90
3.7490	Ph$_2$NH	0.90
15.7852	1,4-dioxane	

Table 1-78 Catalyst Solution (Note: Included in the benzene (for L$_2$Pd) is 30 mg of 3-iodoanisole)

Catalyst Label [-]	Name [-]	Catalyst [g]	Benzene [g]	Conc. [mg/g]
A	**OA1a**	16.6	0.6094	26.52
B	**L$_2$Pd**	21.3	0.5074	40.29

Table 1-79 Run Summary

Catalyst Label [-]	Channel	Stock Solution [g]	Loaded Syringe [g]	Post Injected Syringe [g]	Injected Mass [g]	ArX [mmol]	Pd [mol %]	Rxn Time [min]	k [1/min]
A	A1	4.0408	2.8544	2.635	0.2194	2.59	0.30	57	5.9264
B	A3	4.0265	2.7853	2.6281	0.1572	2.58	0.30	10	32.8809

Table 1-80 GC Data

Channel	Dodecane [mg]	Dodecane [pA s]	Product [pA s]	Yield [%]
A1	105.70	118.90	728.07	>99
A3	108.20	117.28	696.17	>99

Table 1-81 Energy Density

Channel	Total Exotherm [J]	Limiting Reagent [mmol]	Energy Density [kJ/mol]
A1	424	2.59	164
A3	471	2.58	182

1.4.7.5. RuPhos (L1), MethoxySPhos (L4), and AminoSPhos (L5)
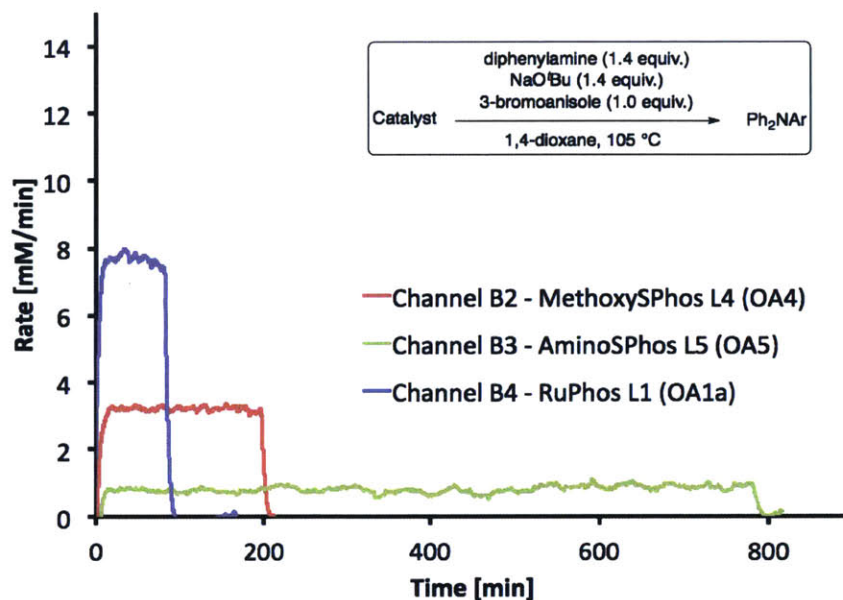
Figure 1-25 Rate of reaction for MethoxySPhos (**L4**) and AminoSPhos (**L5**) based catalyst

Table 1-82 Stock Solution

Reagent [g]	Name [-]	Conc. [mmol/g]
3.5126	Ph$_2$NH	0.891
2.0758	NaO^{t}Bu	0.927
2.7945	3-bromoanisole	0.641
14.9365	1,4-dioxane	

Table 1-83 Catalyst Solution

Catalyst Label [-]	Name [-]	Catalyst [mg]	THF [g]	Conc. [mg/g]
A	**OA4**	9.5	0.2587	35.4
B	**OA5**	12.0	0.2594	44.2
C	**OA1a**	10.5	0.2649	38.1

Table 1-84 Run Summary

Catalyst Label [-]	Channel [#]	Stock Sol [g]	Loaded Syringe [g]	Post Injected Syringe [g]	Injected Mass [g]	ArX [mmol]	Pd [mol %]	Rxn Time [min]	k [1/min]
A	B2	2.9948	2.7588	2.6556	0.1032	1.92	0.26	199.1	1.93
B	B3	2.9957	2.7322	2.6279	0.1043	1.92	0.32	783	0.40
C	B4	3.0568	2.7285	2.6272	0.1013	1.95	0.26	84	4.55

Table 1-85 GC Data

Channel	Dodecane [mg]	Dodecane [pA s]	Product [pA s]	Yield [%]
B2	107.5	100.73	420.70	96
B3	135.8	74.30	240.59	94
B4	144.2	95.98	312.37	98

Table 1-86 Energy Density

Channel	Energy [J]	ArX [mmol]	Energy Density [kJ/mol]
B2	295	1.92	154
B3	305	1.92	159
B4	309	1.95	159

1.4.7.6.   XPhos (L7) and RuPhos (L1)
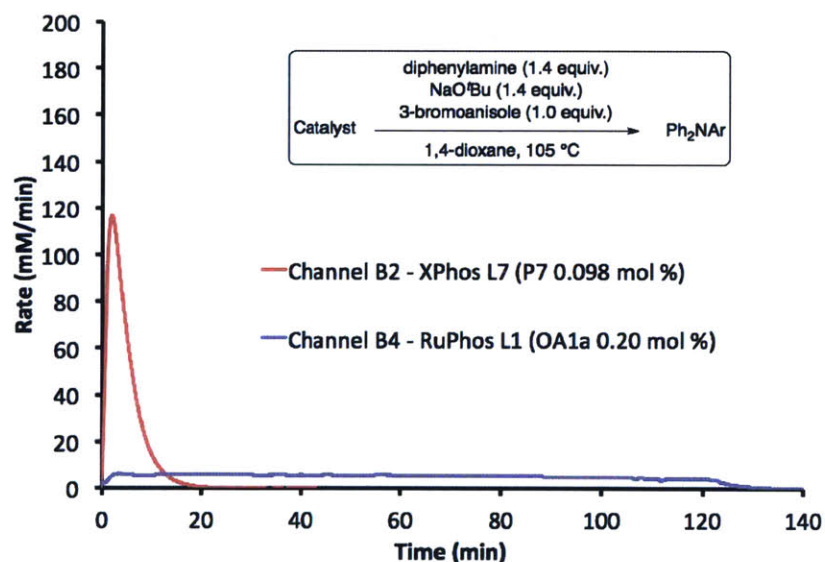
Figure 1-26 Rate of Reaction for XPhos (**L7**) based catalyst

Table 1-87 Stock Solution

Weight (g)	Name (-)	Conc. (mmol/g)
2.7830	3-bromoanisole	0.64
3.4720	Ph_2NH	0.89
2.0207	NaO^tBu	0.91
14.9012	1,4-dioxane	

Table 1-88 Catalyst Solution

Catalyst Label (-)	Catalyst (mg)	Name (-)	THF (g)	Conc. (mg/g)
A	16.9	**OA1a**	0.5971	27.5
B	19.1	**P7**	1.4229	13.2

Table 1-89 Run Summary

Catalyst Label (-)	Channel (#)	Stock Solution (g)	Loaded Syringe (g)	Post Injected Syringe (g)	Injected Mass (g)	ArX (mmol)	Pd (mol %)	Rxn Time (min)	Rate Constant (1/min)
B	B2	2.7461	2.7692	2.6725	0.0967	1.76	0.0983	8.60	118.30
A	B4	2.7637	2.7552	2.6573	0.0979	1.77	0.200	122.2	4.09

Table 1-90 GC Data

Channel (#)	Energy (J)	Limiting Reagent (mmol)	Energy Density (kJ/mol)
B2	345	1.76	196
B4	356	1.77	201

Table 1-91 Energy Density

Channel (#)	n-dodecane (mg)	n-dodecane (pA s)	Product (pA s)	Yield (%)
B2	100.2	123.4	505.6	95
B4	113.3	227.0	835.1	96

1.4.8. X-ray data for A1a and Procedure

In a nitrogen-filled glove box, the isolated complex (~ 20 mg) was dissolved in a minimum of dichloromethane (~ 0.1 mL) and pentane (~ 2 mL) was added. The solution was cooled to -20 °C in the glove box freezer overnight to yield crystals suitable for diffraction. Crystals were mounted for x-ray crystallography within a week's time.

Amido Complex based on **L1** as Supporting Ligand

1.4.9. X-ray data for A3

In a nitrogen-filled glove box, the isolated complex (~ 20 mg) was dissolved in a minimum of benzene (~0.1 mL) and pentane (~ 2 mL) was added. The solution was cooled to -20 °C in the glove box freezer overnight to yield crystals suitable for x-ray diffraction.
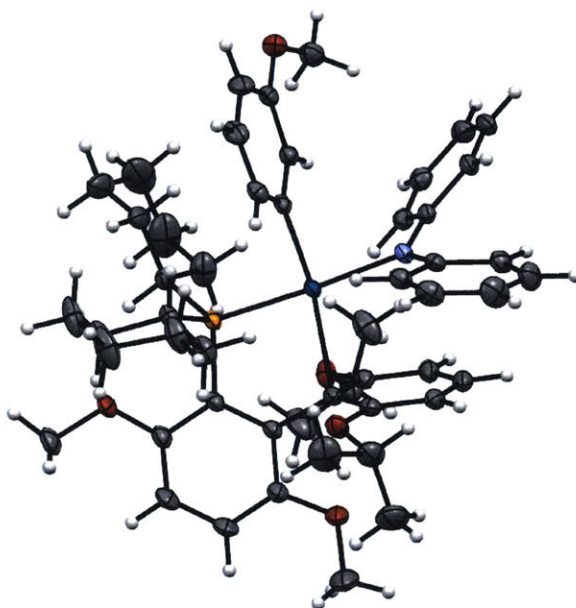
Amido Complex based on **L3** as Supporting Ligand

X-ray data for this compound is given in a separate file.

1.4.10. GC calibrations for triarylamines and diarylamines

Gas chromatography response factors for analytes were done by taking a mass of the pure compound and adding this to a comparable mass of n-dodecane in a solution of ethyl acetate. This solution was analyzed by gas chromatography and the response factors calculated using the equation below. The table below summarizes these results.

$$\frac{Analyte(pA\ s)/Analyte(mg)}{Dodecane(pA\ s)/Dodecane(mg)} = Ratio\ (-)$$

Diarylamines	Weight [mol/g]	Cmpd [mg]	C12 [mg]	Analyte [pA s]	Std [pA s]	Ratio [-]
pCF$_3$	237	65.3	74.3	757.68	1187.09	0.726
mOMe	199	53.9	70.1	701.2	1126.79	0.809
pOMe	199	56.3	78.1	633.44	1083.21	0.811
pCH3	183	58.9	67.1	904.68	1078.22	0.956
pN(CH$_3$)$_2$	212	68.9	82.2	800.6	1176.54	0.812
H	169	66.4	78.9	1022.88	1271.47	0.956
Triarylamine						
pCF$_3$	313	49.4	53.4	377.57	496.2	0.823
mOMe	275	28.9	83.2	257.25	833.09	0.889
pOMe	275	50.7	70.4	430.58	702.3	0.851
pCH3	259	56.6	74.4	546.4	731.43	0.982
pN(CH$_3$)$_2$	288	52	77.4	499.15	855.83	0.868
H	245	53.9	73.7	594.07	817.69	0.993

1.4.11. Synthesis of RuPhos (L1) Oxidative Addition (OA) Complexes

1.4.11.1.   General Procedure for OA Complex Synthesis

In a nitrogen-filled glove box, a large screw cap test tube (Fisherbrand 14-959-37C) was charged with codPd(CH$_2$TMS)$_2$, phosphine ligand, and an excess of aryl halide. A minimum amount of cyclohexane (~ 4 mL) was added to dissolve the solids. The test tube was then closed with a silicon/Teflon septum and cap, and the solution was then stirred 12 to 24 h with a PTFE coated stir bar at rt. The solid precipitate was washed multiple times with pentane, decanted, and dried under vacuum to provide the product.

1.4.11.2.   RuPhos(Pd)(Ar-mOMe)Br Complex OA1a
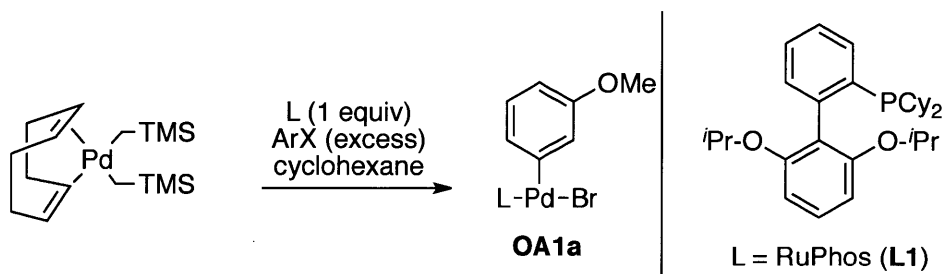
Following General Procedure in section 1.4.11.1, using codPd(CH$_2$TMS)$_2$ (496 mg, 1.28 mmol), **L1** (580 mg, 1.24 mmol) and 3-bromoanisole (278 mg, 1.5 mmol). The product was washed with pentane (3 x 20 mL) and dried under vacuum. The product was an off-white solid (920 mg, 98 % yield, 1.21 mmol). **^{1}H NMR** (500 MHz, CD$_2$Cl$_2$) δ 7.63 (m, 2H), 7.44 (m, 1H), 7.39 (m, 1H), 6.88 (ddd, J = 7.7, 3.0, 1.3 Hz, 1H), 6.81 (m, 1H), 6.70 (m, 1H), 6.64 (m, 3H), 6.41 (dd, J = 8.0, 2.4 Hz, 1H), 4.62 (m, 2H), 3.73 (s, 3H), 2.19 (m, 2H), 1.95 – 1.53 (m, 12H), 1.39 (d, J = 5.9 Hz, 6H), 1.31 – 1.07 (m, 6H), 1.02 (d, J = 5.9 Hz, 6H), 0.84-0.66 (m, 2H). **^{13}C{^{1}H} NMR** (126 MHz, CD$_2$Cl$_2$) δ 159.50 (br), 157.99, 157.97, 145.30, 145.16, 137.46, 135.10, 134.05, 133.77, 132.99, 132.91, 131.50, 131.04, 131.02, 130.75, 130.72, 126.80, 126.76, 126.69, 126.68, 122.97, 122.94, 111.79, 111.76, 109.48, 107.75, 107.70, 71.34, 55.52, 34.63, 34.29, 34.08, 28.56, 28.17, 28 to 27 (multiple overlapping peaks), 26.7 to 26.4 (br), 22.86, 22.37, 21.88, 14.36. **^{31}P{^{1}H} NMR** (202 MHz, CD$_2$Cl$_2$) δ 31.65. **ATR-IR** (cm^{-1}): 2970, 2930, 2840, 1570, 1450, 1250, 1110, 1070, 1040, 847, 809, 758. **Elemental**: Calculated, C(58.47) H(6.63) Found, C(58.76), H(6.47).

1.4.11.3. RuPhos(Pd)(Ar-pCF$_3$)Br Complex OA1b
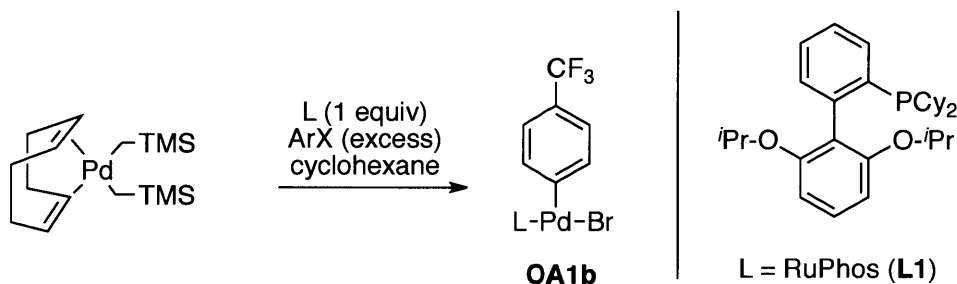
Following General Procedure in section 1.4.11.1, using codPd(CH$_2$TMS)$_2$ (502 mg, 1.29 mmol), **L1** (603 mg, 1.29 mmol) and bromobenzotrifluoride (332 mg, 1.48 mmol). The product was washed with pentane (2 x 20 mL) and dried under vacuum. The product was a white solid (918.7 mg, 89 %, 1.15 mmol).**^{1}H NMR** (500 MHz, CDCl$_3$) δ 7.66 (t, J = 8.4 Hz, 1H), 7.57 (t, J = 7.4 Hz, 1H), 7.47 (m, 1H), 7.37 (m, 1H), 7.28 (d, J = 7.4 Hz, 2H), 7.15 (d, J = 8.1 Hz, 2H), 6.90 (ddd, J = 7.7, 3.0, 1.1 Hz, 1H), 6.68 (d, J = 8.5 Hz, 2H), 4.63 (hept, J = 6.0 Hz, 2H), 2.18 – 1.99 (m, 2H), 1.83 – 1.48 (m, 12H), 1.37 (d, J = 6.0 Hz, 6H), 1.29 – 1.05 (m, 6H), 1.01 (d, J = 6.0 Hz, 6H), 0.81 – 0.62 (m, 2H). **^{13}C{^{1}H} NMR** (126 MHz, CD$_3$Cl) δ 158.76, 145.44 (br), 144.70, 144.57, 137.01, 136.98, 134.96, 132.73, 132.65, 132.61, 132.31, 130.81, 130.74, 130.72, 126.62, 126.57, 125.98, 125.72, 123.82, 123.11 (br), 111.59, 111.56, 107.57, 71.11, 33.76,

33.55, 28.24 (br), 27.65, 27.64, 27.25, 26.15, 26.91, 26.82, 26.09, 26.09, 22.27, 21.59. ^{31}P{^{1}H}

NMR (121 MHz, CDCl$_3$) δ 30.65 .^{19}F{^{1}H} **NMR** (282 MHz, CDCl$_3$) δ -63.17. **ATR-IR** (cm^{-1}):
2970, 2920, 2850, 1580, 1560, 1450, 1420, 1380, 1370, 1310, 1240, 1150, 1110, 1060, 1020,
938, 850, 786. **Elemental**: Calculated, C(55.68) H(5.94) Found, C(55.84) H(6.08)

1.4.11.4. RuPhos(Pd)(Ph)Br Complex OA1c
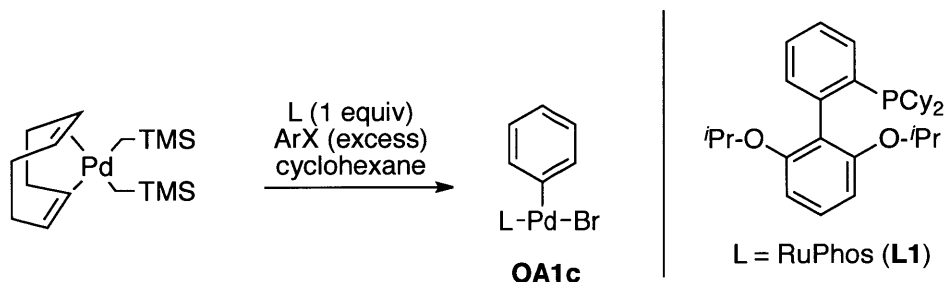
Following General Procedure in section 1.4.11.1, using codPd(CH$_2$TMS)$_2$, (497.6 mg, 1.28
mmol), **L1** (602.1 mg, 1.29 mmol), and bromobenzene (230 mg, 1.47 mmol). The product was
washed with pentane (15 mL) and dried under vacuum. The product was white solid (825.6 mg,
88 %, 1.13 mmol). ^{1}**H NMR** (500 MHz, CD$_2$Cl$_2$) δ 7.63 (t, J = 8.4 Hz, 2H), 7.49 – 7.41 (m, 1H),
7.41 – 7.35 (m, 1H), 7.07 (ddd, J = 8.2, 2.1, 1.1 Hz, 2H), 6.91 (t, J = 7.5 Hz, 2H), 6.87 (ddd, J =
7.7, 3.1, 1.3 Hz, 1H), 6.85 – 6.81 (m, 1H), 6.65 (d, J = 8.5 Hz, 2H), 4.61 (hept, J = 6.0 Hz, 2H),
2.32 – 2.04 (m, 2H), 1.76 (d, J = 10.4 Hz, 6H), 1.70 – 1.52 (m, 6H), 1.39 (d, J = 6.0 Hz, 6H),
1.31 – 1.06 (m, 6H), 1.02 (d, J = 6.1 Hz, 6H), 0.73 (m, 2H). ^{13}C{^{1}H} **NMR** (126 MHz, CD$_2$Cl$_2$) δ
159.51, 145.30, 145.16, 138.17, 138.14, 136.73, 134.99, 134.02, 133.74, 133.01, 132.93,
131.50, 131.02, 131.01, 127.17, 127.16, 126.80, 126.76, 123.52, 112.01, 111.98, 107.75, 71.36,
34.65, 34.23, 34.02, 28.61, 28.03, 28.02, 27.76, 27.66, 27.37, 27.28, 26.52, 26.51, 22.38, 21.90.
^{31}P{^{1}H} **NMR** (202 MHz, CD$_2$Cl$_2$) δ 31.41. **ATR-IR** (cm^{-1}): 3060, 3050, 2970, 2920, 2850, 1580,
1560, 1440, 1250, 1110, 1070, 1060, 1020, 760. **Elemental**: Calculated, C(59.23) H(6.63)
Found, C(59.34) H(6.61)

1.4.11.5. RuPhos(Pd)(Ar-pCH₃)Cl Complex OA1d

L = RuPhos (L1)
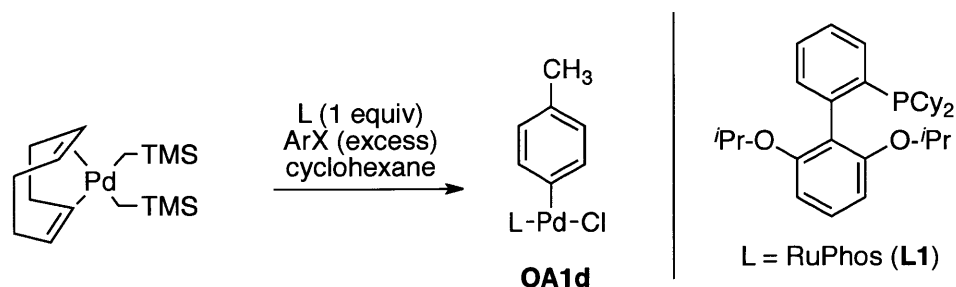
Following general procedure in section 1.4.11.1, using codPd(CH₂TMS)₂ (107.2 mg, 0.28 mmol), **L1** (131.2 mg, 0.28 mmol), and 4-chlorotoluene (41.2 mg, 0.33 mmol). The product was washed with pentane (3 x 5 mL) and dried under vacuum. The yield was a white solid (152 mg, 79 %, 0.22 mmol). **¹H NMR** (500 MHz, CD₂Cl₂) δ 7.62 (t, J = 8.4 Hz, 2H), 7.46 – 7.41 (m, 1H), 7.41 – 7.34 (m, 1H), 6.95 – 6.88 (m, 2H), 6.86 (ddd, J = 7.7, 3.1, 1.4 Hz, 1H), 6.79 – 6.73 (m, 2H), 6.63 (d, J = 8.5 Hz, 2H), 4.62 (m, 2H), 2.21 (s, 3H), 2.13 (m, 2H), 1.82 – 1.47 (m, 12H), 1.38 (d, J = 6.0 Hz, 6H), 1.31 – 1.04 (m, 6H), 1.01 (d, J = 6.0 Hz, 6H), 0.86 – 0.65 (m, 2H). **¹³C{¹H} NMR** (126 MHz, CD₂Cl₂) δ 159.43, 151.47, 145.50, 145.36, 137.09, 137.07, 135.05, 134.38, 134.22 (br), 134.10, 133.05, 132.92, 132.84, 131.50, 130.99, 130.97, 128.36, 128.34, 126.79, 126.74, 107.50, 71.26, 34.28, 34.06, 28.71, 28.21, 28.19, 27.74, 27.63, 27.40, 27.31, 26.58 (br), 22.41, 21.87, 20.82. **³¹P{¹H} NMR** (121 MHz, CD₂Cl₂) δ 32.90. **ATR-IR** (cm⁻¹): 2940, 2910, 2850, 1590, 1450, 1250, 1110, 1060, 1000, 847, 796, 776. **HRMS (ESI):** Calculated for C₃₇H₅₀ClO₂PPd [M-Cl]⁺, 663.2583 Found: 663.2587

1.4.11.6. RuPhos(Pd)(Ar-pOMe)Cl Complex OA1e

L = RuPhos (L1)
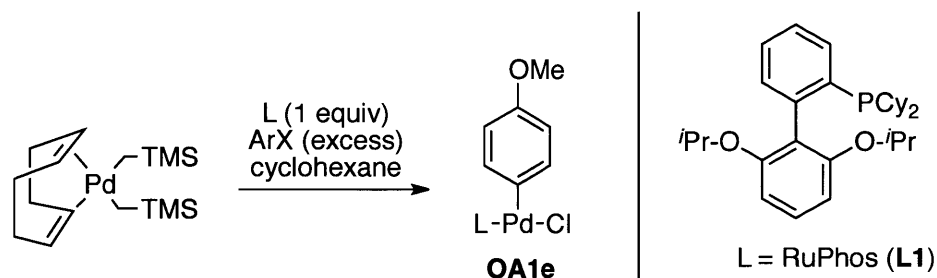
Following general procedure in section 1.4.11.1, using codPd(CH₂TMS)₂ (106.2 mg, 0.27 mmol), **L1** (128.9 mg, 0.28 mmol), and 4-chloroanisole (41.2 mg, 0.29 mmol). The product was

washed with pentane (3 x 15 mL) and dried under vacuum. The product was a solid (147 mg, 75 %, 0.21 mmol). ^{1}H NMR (500 MHz, CD$_2$Cl$_2$) δ 7.62 (t, J = 8.4 Hz, 2H), 7.49 – 7.33 (m, 2H), 7.03 – 6.76 (m, 3H), 6.62 (dd, J = 13.8, 8.6 Hz, 4H), 4.73 – 4.54 (m, 2H), 3.71 (s, 3H), 2.25 – 1.95 (m, 2H), 1.89 – 1.48 (m, 12H), 1.38 (d, J = 6.0 Hz, 6H), 1.28 – 1.07 (m, 6H), 1.01 (d, J = 6.0 Hz, 6H), 0.85 – 0.69 (m, 2H). ^{13}C{^{1}H} NMR (126 MHz, CD$_2$Cl$_2$) δ 159.44, 157.36, 137.16, 135.07, 132.94, 132.85, 131.49, 130.99, 126.81, 126.76, 126.45, 113.56, 107.54, 71.30, 55.61, 34.30, 34.08, 28.75, 28.23 (br), 27.75, 27.65, 27.40, 27.31, 26.60 (br), 22.41, 21.86. ^{31}P{^{1}H} NMR (121 MHz, CD$_2$Cl$_2$) δ 33.13. **ATR-IR** (cm^{-1}): 3050, 2930, 2984, 1590, 1450, 1260, 1240, 1220, 1170, 1110, 1050, 1030, 1000, 848, 827, 791, 776. **Elemental**: Calculated, C(62.10) H(7.04) Found, C(62.22) H(7.20)

1.4.12. RuPhos (L1) Amido Complexes

1.4.12.1.   General Procedure for amido complex synthesis

In a nitrogen-filled glove box, a screw cap test tube was charged with an oxidative addition complex followed by the appropriate lithium diarylamide. Anhydrous benzene (~1 mL) was added and the mixture vigorously stirred with a PTFE stir bar for the indicated time. The mixture was then filtered through a PTFE syringe filter (0.45 micron). The filtrate was frozen by placing in the glovebox freezer (-20 °C). The solvent was removed under vacuum (freeze drying) after which the solid product was washed multiple times with pentane and dried under vacuum. *Note: Many of the ^{1}H-NMR spectra indicate that the palladium amido complexes are fluxional in benzene-d_6.*

#### 1.4.12.2.   RuPhos(Pd)(Ar-*m*OMe)NPh$_2$ Complex A1a
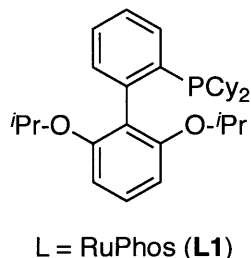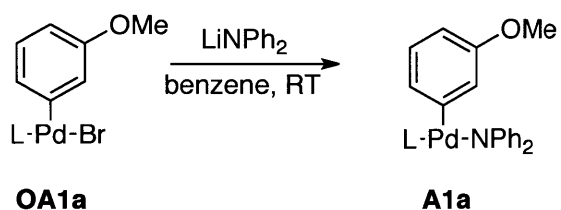
Following general procedure in section 1.4.12.1, using **OA1a** (100.6 mg, 0.13 mmol) and LiNPh$_2$ (46 mg, 0.26 mmol). The mixture was stirred for 15 min and the red product was washed with pentane (9 x 4 mL) and dried under vacuum. The product was a red solid (85.5 mg, 76 %, 0.10 mmol). ^{1}**H NMR** (500 MHz, benzene-d_6) δ 7.70 – 7.45 (br, 4H), 7.31 (t, J = 7.0 Hz, 1H), 7.25 – 7.01 (m, 6H), 6.96 (t, J = 7.3 Hz, 1H), 6.87 – 6.65 (m, 5H), 6.64 – 6.56 (m, 1H), 6.52 (dd, J = 8.0, 2.3 Hz, 1H), 6.40 – 5.70 (br, 2H), 4.60 – 4.28 (br, major), 4.21 (br, minor), 3.55 (s, minor), 3.34 (s, major), 2.56 – 0.46 (m, 34H). ^{13}**C{^{1}H} NMR** (126 MHz, benzene-d_6) δ 158.40 (br), 157.77, 157.13, 156.66 (br), 147.16, 146.99, 144.60, 144.55, 143.64, 137.10, 136.84, 136.45, 131.78, 131.70, 131.21, 130.61, 130.59, 129.55, 128.59, 128.54, 126.49, 126.43, 126.39, 124.77, 122.95 – 122.14 (br), 121.13, 119.68, 119.66, 118.20, 118.14, 115.59 – 115.01 (br), 111.97, 111.46, 111.19, 106.90- 106.32 (br), 70.44, 54.88, 29.18 – 28.88 (br), 28.01 – 27.15 (br), 27.00 – 26.40 (br), 22.70, 22.36, 21.77, 21.15. ^{31}**P{^{1}H} NMR** (202 MHz, benzene-d_6) δ 33.50. **Elemental**: Calculated, C(69.37) H(7.13) Found, C(69.28) H(7.12)

1.4.12.3. RuPhos(Pd)(Ph)NPh$_2$ Complex A1c
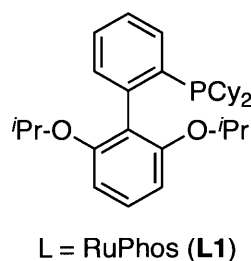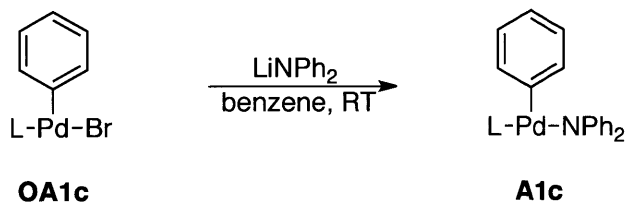
Following general procedure 1.4.12.1, **OA1c** (98.9 mg, 0.14 mmol) and LiNPh$_2$ (100 mg, 0.57 mmol) were combined. The mixture was stirred for 20 min and the red product was washed with pentane (3 x 4 mL) and dried under vacuum. The yield was 62.3 mg (56 %, 0.076 mmol). ^{1}**H NMR** (500 MHz, benzene-d_6) δ 7.59 (d, J = 8.3 Hz), 7.39 – 7.18 (m), 7.13 – 6.58 (m), 6.09 (d, J

= 8.5 Hz), 5.17 − 5.02 (br, free amine), 4.56 − 4.33 (m, major), 4.27 − 4.11 (m, minor), 2.40 − 0.61 (m, 34H). ^{13}C{^{1}H} NMR (126 MHz, benzene-d_6) δ 158.37, 157.15, 155.80, 147.18, 147.01, 144.22, 144.16, 137.10, 136.83, 136.24, 135.96, 135.93, 131.81, 131.73, 131.18, 130.61 (br), 129.56, 128.36, 126.76, 126.44 (br), 124.65, 123.55, 122.49 (br), 121.13, 118.22, 115.47, 111.69 (br), 106.69, 70.46, 33.97, 33.77, 28.88, 28.59, 28.56, 27.57, 27.47, 27.35, 27.26, 26.60, 22.72, 22.34 (br), 21.79 (br), 21.17. ^{31}P{^{1}H} NMR (202 MHz, benzene-d_6) δ 33.19. **MS (ESI):** Calculated for $C_{36}H_{48}O_2PP^+$ [M-NPh$_2$]$^+$, 649.242 Found: 649.247

1.4.12.4. RuPhos(Pd)(Ph-pCH₃)NPh₂ Complex A1d
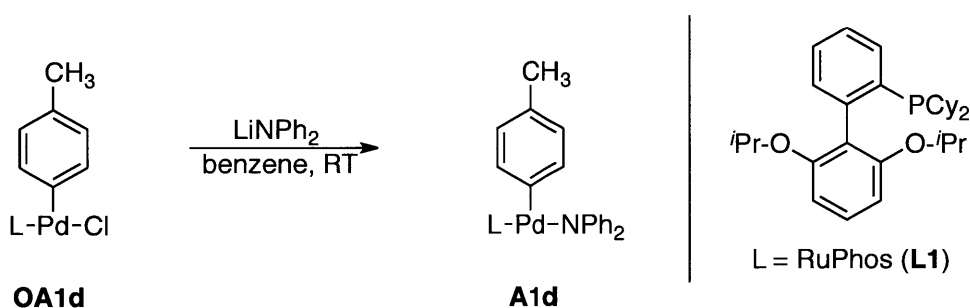
Following general procedure in section 1.4.12.1, **OA1d** (87.5 mg, 0.13 mmol) and LiNPh₂ (100 mg, 0.57 mmol) were combined. The mixture was stirred for 30 min and the red product was washed with pentane (2 x 4 mL) and dried under vacuum. The yield was 15.2 mg (15 %, 0.018 mmol). *Note: The ^{13}C spectra was collected on a 600 mHz Bruker Avance Spectrometer.* ^{1}H **NMR** (500 MHz, benzene-d_6) δ 7.64 − 7.59 (m), 7.57 (d, J = 8.3 Hz), 7.36 − 7.29 (m), 7.29 − 7.25 (m), 7.20 (t, J = 7.7 Hz), 7.14 (d, J = 7.9 Hz), 7.09 − 7.02 (m), 6.99 − 6.90 (m), 6.89 − 6.81 (m), 6.81 − 6.78 (m), 6.74 (t, J = 7.1 Hz), 6.64 (d, J = 7.9 Hz), 6.61 − 6.59 (m), 6.53 − 6.49 (m), 6.05 (d, J = 8.4 Hz), 5.11 − 5.03 (m), 4.41 (dt, J = 12.0, 5.9 Hz), 4.24 − 4.09 (m), 2.19 (s), 2.05 (s, 1H), 1.97 (s), 1.91 − 1.37 (m), 1.29 − 0.63 (m). ^{13}C{^{1}H} **NMR** (151 MHz, benzene-d_6) δ 158.30, 157.21, 155.78, 143.66, 137.23, 137.01, 136.23, 135.64, 132.27, 131.81, 131.18, 130.55, 129.54, 126.38, 122.47 (br), 121.12, 118.23, 115.39, 111.79 (br), 106.68, 70.44, 34.05, 33.88, 28.95, 28.67 (br), 27.57 (br), 27.49 (br), 27.35, 27.27, 26.82, 26.64, 22.74 (br), 22.30 (br), 22.04, 21.78, 21.17, 21.12, 20.70. ^{31}P{^{1}H} **NMR** (121 MHz, benzene-d_6) δ 33.15. **MS (ESI):** Calculated for $C_{37}H_{50}O_2PPd^+$ [M-NPhAr]$^+$, 663.26 Found: 663.27

1.4.12.5. RuPhos(Pd)(Ar-*p*OMe)NPh₂ Complex A1e

OA1e → **A1e**

L = RuPhos (**L1**)
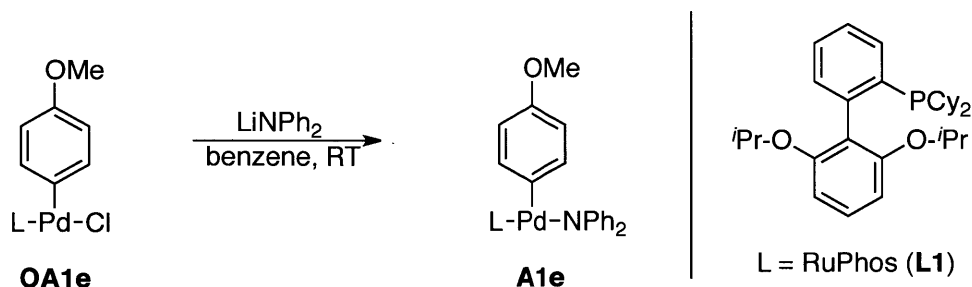
Following general procedure in section 1.4.12.1, **OA1e** (181.0 mg, 0.25 mmol) and LiNPh₂ (100 mg, 0.57 mmol) were combined. The mixture was stirred for 15 min and the red product was washed with pentane (6 x 4 mL) and dried under vacuum. The yield was 137.7 mg (64%, 0.162 mmol). ^{1}H NMR (500 MHz, benzene-d_6) δ 7.61 (d, J = 7.6 Hz), 7.35 (t, J = 6.9 Hz), 7.28 – 7.21 (m), 7.14 (d, J = 8.6 Hz), 7.12 – 7.06 (m), 7.00 (t, J = 7.5 Hz), 6.87 (t, J = 8.3 Hz), 6.85 – 6.81 (m), 6.78 (t, J = 7.1 Hz), 6.66 – 6.61 (m), 6.56 (d, J = 8.7 Hz), 6.09 (d, J = 8.5 Hz), 5.09 (br, free amine), 4.45 (m,major), 4.32 – 4.17 (m, minor), 3.45 (s, minor), 3.22 (s, major), 2.16 – 0.67 (m). ^{13}C{^{1}H} NMR (126 MHz, benzene-d_6) δ 158.35, 157.45, 155.81, 147.22, 147.05, 137.31, 137.04, 136.29, 135.72, 135.69, 131.79, 131.70, 131.31, 131.25, 131.18, 130.58, 130.57, 129.55, 128.35, 126.43, 126.40, 122.44, 122.43, 121.12, 118.21, 115.40, 113.00, 111.62, 111.59, 106.64, 70.44, 54.47, 34.45, 34.05, 33.84, 28.95, 28.70, 28.67, 27.56, 27.45, 27.36, 27.27, 26.64, 22.75, 22.72, 22.37, 21.81, 21.16, 14.31. ^{31}P{^{1}H} NMR (202 MHz, benzene-d_6) δ 33.45. **Elemental**: Calculated, C(69.37) H(7.13) Found, C(69.17) H(6.98).

1.4.12.6. RuPhos(Pd)(Ph)(N(Ph)Ar-*p*OMe) Complex A1g

OA1c → **A1g**

L = RuPhos (**L1**)
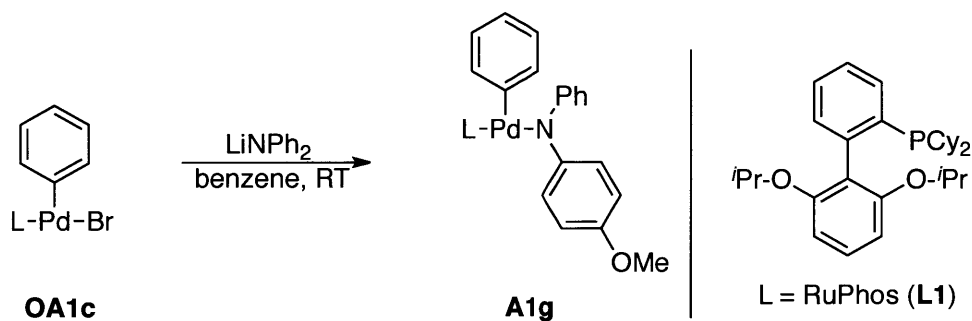
Following general procedure in section 1.4.12.1, **OA1c** (103.0 mg, 0.14 mmol) and Li(N(Ph)Ar-*p*OMe) (100 mg, 0.49 mmol) were combined. The mixture was stirred for 15 min. The red

product was washed with pentane (3 x 4 mL) and dried under vacuum. Yield was 48 mg (40 %, 0.057 mmol). ^{1}H NMR (500 MHz, benzene-d_6) δ 7.55 (d, J = 7.7 Hz), 7.39 (d, J = 8.9 Hz), 7.34 – 7.28 (t), 7.25 – 7.18 (t), 7.09 – 6.56 (m), 6.18 – 6.04 (b), 4.55 – 4.30 (br, 2H), 3.47 (s), 3.30 (s), 3.23 (s), 2.30 – 0.33 (m, 34H). ^{13}C{^{1}H} NMR (126 MHz, benzene-d_6) δ 158.58 – 157.77 (br), 156.61, 151.58, 149.71, 148.84, 147.18, 147.01, 145.15, 145.09, 137.10, 136.83, 136.09, 136.03 – 135.57 (br), 131.82, 131.73, 131.19, 130.54, 130.52, 129.58, 129.49, 128.59, 126.71 (br), 126.43, 126.39, 123.59, 123.58, 123.44, 123.41, 122.65, 122.20, 121.63, 121.61, 119.74, 115.98, 115.22, 114.95, 114.32, 113.81, 112.11 (br), 107.06 (br), 106.40 (br), 70.47 (br), 55.47, 55.09, 54.99, 34.45, 34.28 – 33.42 (br),33.00-31.75 (br), 29.50 – 28.50 (br), 28.52 – 27.75 (br), 27.57, 27.46, 27.34, 27.25, 26.60, 22.81, 22.74, 22.70, 22.16, 21.19 (br), 14.30. ^{31}P{^{1}H} NMR (202 MHz, benzene-d_6) δ 31.23. MS (ESI): Calculated for $C_{49}H_{60}NO_3PPd^+$ [M]$^+$, 847.335 Found 847.338

1.4.12.7. RuPhos(Pd)(Ph)(NPhAr-pCH$_3$) Complex A1h
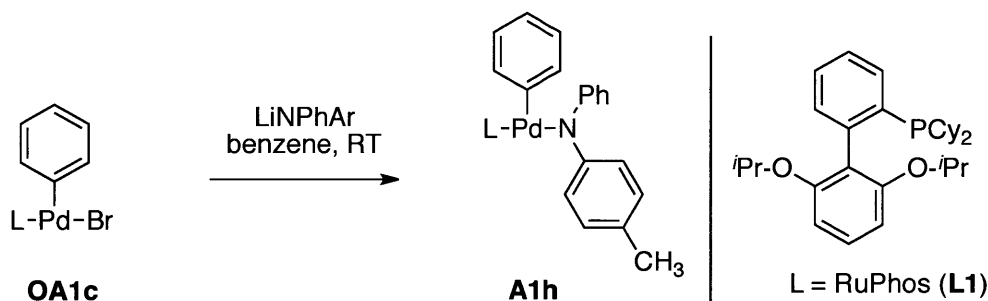
Following general procedure in section 1.4.12.1, OA1c (102 mg, 0.14 mmol) and the Li(N(Ph)Ar-pCH$_3$) (40 mg, 0.21 mmol) were combined. The mixture was stirred for 15 min and the red product was washed with pentane (5 x 4 mL) and dried under vacuum. The yield was 23 mg (20 %, 0.028 mmol). ^{1}H NMR (500 MHz, benzene-d_6) δ 7.57 (d, J = 7.6 Hz), 7.44 (d, J = 8.4 Hz), 7.36 – 7.28 (m), 7.24 – 7.17 (m), 7.09 – 6.64 (m), 6.62 – 6.58 (m), 6.18 – 6.00 (m), 4.97 (br, free amine), 4.50 – 4.36 (m, major), 4.22 – 4.12 (m, minor), 2.29 (s, major), 2.10 (s, minor), 2.08 – 0.62 (m). ^{13}C{^{1}H} NMR (126 MHz, benzene-d_6) δ 158.51 (br), 156.55, 153.56, 147.51, 147.34, 144.88, 144.82, 137.44, 137.17, 136.46, 136.35 – 136.10 (br), 132.12, 132.03, 131.48, 130.86 (br), 130.63, 130.40, 129.86, 129.83, 128.96, 128.90, 128.65, 127.04, 126.73, 126.70, 126.34,

125.76, 124.42, 124.23, 123.78, 122.98, 122.96, 122.47, 122.45, 120.78, 119.65, 117.57, 115.16, 112.24 − 112.09 (br), 107.2-106.9 (br), 70.85 − 70.52 (br), 34.76, 34.37 − 33.83 (br), 29.47 − 28.5 (multiple overlapping peaks), 27.88, 27.78, 27.65, 27.56, 26.90, 23.05, 23.04, 22.63, 22.07, 21.67 − 21.26 (br), 21.08, 14.61. $^{31}P\{^1H\}$ NMR (202 MHz, benzene-d_6) δ 33.08. **Elemental**: Calculated, C(70.70) H(7.27), Found, C(70.86) H(7.35)

1.4.12.8. RuPhos(Pd)(Ph)(NPhAr-mOMe) Complex A1i

OA1c   **A1i**   L = RuPhos (**L1**)
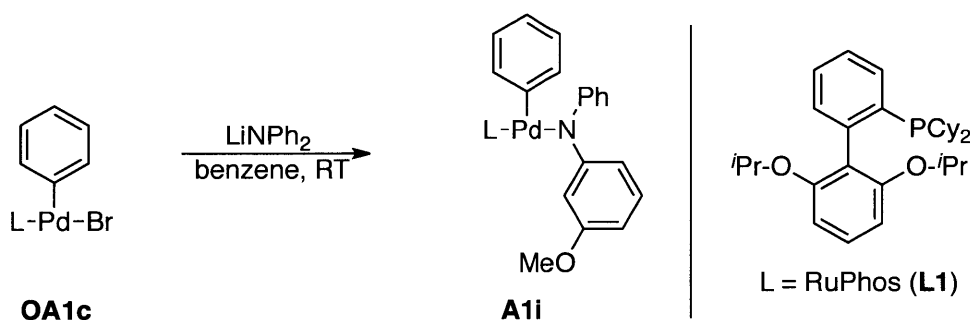
Following general procedure in section 1.4.12.1, **OA1c** (100.5 mg, 0.14 mmol) and Li(N(Ph)Ar-mOMe) (100 mg, 0.21 mmol) were combined. The mixture was stirred for 20 min and the red product was washed with pentane (5 x 4 mL) and dried under vacuum. The yield was 68 mg (58 %, 0.080 mmol). ^1H NMR (500 MHz, benzene-d_6) δ 7.58 (d, J = 7.7 Hz, 1H), 7.34 (d, J = 6.9 Hz, 1H), 7.28 − 7.19 (m, 2H), 7.16 (s, 1H), 7.13 − 7.05 (m, 2H), 7.00 (t, J = 7.5 Hz, 1H), 6.91 (t, J = 8.4 Hz, 1H), 6.87 − 6.72 (m, 3H), 6.69 − 6.62 (m, 1H), 6.43 − 6.36 (m, 1H), 6.18 − 6.09 (m, 1H), 4.61 − 4.38 (m, 1H), 3.50 (s, 1H), 2.20 − 1.86 (m, 3H), 1.86 − 1.37 (m, 11H), 1.37 − 0.55 (m, 18H). $^{13}C\{^1H\}$ NMR (126 MHz, benzene-d_6) δ 160.84, 158.39, 158.32 (br), 157.12, 155.74, 147.19, 147.01, 144.12, 144.07, 137.08, 136.81, 136.16, 135.97, 135.94, 131.83, 131.74, 131.18, 130.60 (br), 128.35, 126.75, 126.43, 126.39, 123.52, 122.76, 122.74, 116.09, 115.55, 111.75, 111.72, 108.28, 106.97, 106.59, 101.37, 70.44, 54.86, 34.77 − 33.43 (br), 29.00 − 28.84 (br), 28.80 − 28.29 (br), 27.57, 27.47, 27.34, 27.25, 26.59, 22.71, 21.50 − 20.91 (br). $^{31}P\{^1H\}$ NMR (202 MHz, benzene-d_6) δ 33.32. **MS (ESI)**: Calculated for $C_{36}H_{48}O_2PPd^+$ [M-NPhAr]$^+$, 649.24 Found: 649.27

1.4.13. Ligand Series Oxidative Addition Complexes

1.4.13.1. SPhos(Pd)(Ar-*m*OMe)Br Complex OA2
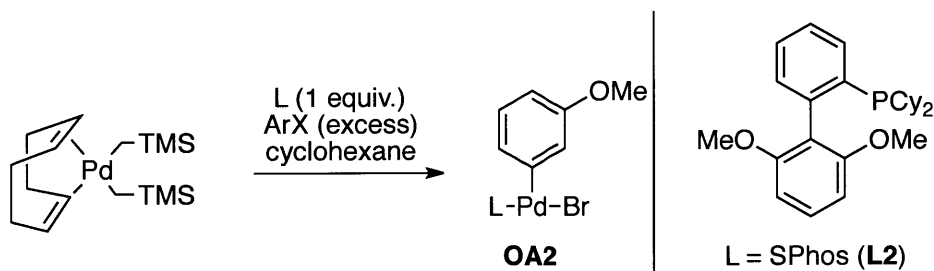
Following general procedure in section 1.4.11.1, codPd(CH$_2$TMS)$_2$ (98 mg, 0.25 mmol), SPhos **L2** (100.7 mg, 0.25 mmol), and 3-bromoanisole (90 mg, 0.48 mmol) were combined. The product was washed with pentane (2 x 4 mL). The yield of the white, solid complex was 136 mg (79 %, 0.19 mmol). **^{1}H NMR** (500 MHz, CD$_2$Cl$_2$) δ 7.75 (t, J = 8.4 Hz), 7.70 − 7.64 (m), 7.51 − 7.37 (m), 7.30 (t, J = 8.4 Hz), 7.22 − 7.06 (m), 6.87 − 6.81 (m, 3H), 6.72 − 6.67 (m), 6.64 (d, J = 8.4 Hz), 6.47 − 6.41 (m), 6.34 − 6.27 (m), 3.94 − 3.85 (br), 3.78 (s), 3.74 (s), 3.45 − 3.37 (br), 2.36 − 0.49 (m). **^{13}C{^{1}H} NMR** (126 MHz, CD$_2$Cl$_2$) δ 161.23 (br), 158.20, 158.18, 157.58 (br), 144.73, 144.58, 136.69, 136.28, 136.27, 135.98, 134.75 − 134.43 (br), 133.75 − 133.46 (br), 132.31, 132.21, 131.71, 131.69, 131.13, 130.59, 130.56, 129.82, 129.33 − 128.89 (br), 127.31, 127.27, 126.86, 126.84, 126.63 − 126.37 (br), 126.31 (br), 126.29 − 126.19 (br), 122.99, 122.96, 109.58, 109.26, 108.50, 107.08 − 106.40 (br), 100.35, 56.39, 55.63, 54.94, 39.24 − 38.30 (br), 35.08 − 34.51 (br), 33.48 − 32.64 (br), 31.11 − 30.88 (br), 29.12 − 26.27 (multiple overlapping peaks, very broad). **^{31}P{^{1}H} NMR** (202 MHz, CD$_2$Cl$_2$) δ 40.04 − 39.07 (br), 34.50 . **ATR-IR** (cm^{-1}): 2920, 2840, 1600, 1580, 1440, 1410, 1330, 1220, 1200, 1150, 1120, 809. **Elemental**: Calculated C(56.30), H(6.01) Found, C(56.59), H(6.11).

1.4.13.2. Hybrid(Pd)(Ar-*m*OMe)Br Complex OA3

OA3 L-Pd-Br
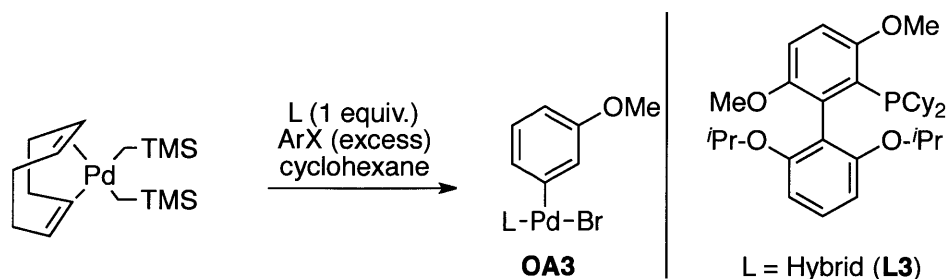
L = Hybrid (**L3**)

Following general procedure in section 1.4.11.1, codPd(CH₂TMS)₂ (29.4 mg, 0.075 mmol), HybridPhos **L3** (39.8 mg, 0.076 mmol), and 3-bromoanisole (90 mg, 0.48 mmol) were combined. The product was washed with pentane (3 x 5 mL) and dried under vacuum. The yield was 48.8 mg (79 %, 0.060 mmol) as a white solid. **¹H NMR** (500 MHz, CDCl₃) δ 7.75 (t, *J* = 8.4 Hz, 1H-minor), 7.24 (d, *J* = 8.3 Hz, 2H-minor), 7.05-6.9 (m, major and minor), 6.89-6.7 (m, major and minor), 6.59 (d, *J* = 8.3 Hz, 2H-major), 6.46 (d, *J* = 8.4 Hz, 2H-minor), 6.40 – 6.34 (m, major and minor), 4.62 – 4.51 (m, 2H-minor), 4.35 (s, 3H-major), 4.35 – 4.25 (m, 2H-major), 3.80 (s, 3H-minor), 3.73 (s, 3H-minor), 3.71 (s, 3H-major), 3.61 (s, 3H-major), 3.41 (s, 3H-minor), 2.88 – 2.70 (m, 2H-minor), 2.07 – 0.75 (m, major and minor). **¹³C{¹H} NMR** (126 MHz, CDCl₃) δ 158.46, 153.68, 137.74, 137.33, 131.55, 131.30, 131.28, 130.28, 130.08 (br), 127.42 – 125.82 (br), 123.54 – 123.39 (br), 123.41 – 123.24 (br), 114.74, 113.33, 113.32l, 112.40 (br), 110.02, 108.95, 106.45, 106.35, 103.97, 100.50, 73.19, 70.46, 63.04, 56.75, 56.33, 55.71, 55.53, 36.86, 36.68, 34.83, 30.60 – 30.12 (br), 30.02, 29.99, 28.53, 27.58, 27.47, 27.24, 27.13, 26.15, 26.14, 23.70, 23.05, 22.78, 22.42, 14.78. **³¹P{¹H} NMR** (202 MHz, CDCl₃) δ 46.46 (major), 46.15 (minor). **ATR-IR** (cm⁻¹): 2920, 2850, 1570, 1450, 1420, 1240, 1110, 994, 816. **Elemental**: Calculated, C(57.11) H(6.64), Found, C(56.84) H(6.56).

1.4.13.3. MethoxySPhos(Pd)(Ar-*m*OMe)Br Complex OA4

OA4 L-Pd-Br
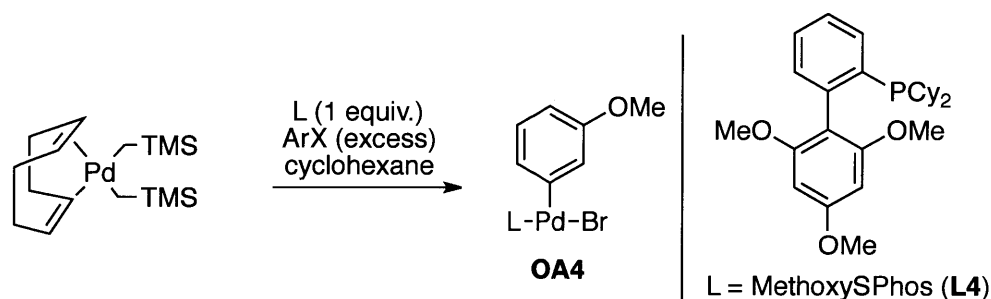
L = MethoxySPhos (**L4**)

Following general procedure in section 1.4.11.1, using codPd(CH₂TMS)₂ (91.0 mg, 0.23 mmol), MethoxySPhos **L4** (104.1 mg, 0.24 mmol), and 3-bromoanisole (90 mg, 0.48 mmol). The product was washed with pentane (3 x 5 mL) and dried under vacuum. The yield was 155.4 mg (90 %, 0.21 mmol). **¹H NMR** (500 MHz, CDCl₃) δ 7.61 (t, J = 7.0 Hz, 1H), 7.44 (t, J= 7.4 Hz, 1H), 7.38 (t, J = 7.4 Hz, 1H), 6.89-6.79 (m, 2H), 6.77 (m, 1H), 6.70 (s, 1H), 6.44-6.40 (dd, J= 8 Hz, 1.5 Hz, 1 H), 6.20 (s, 2H), 3.98 (s, 3H), 3.76 (s,3H), 3.74 (s, 6H), 2.27-2.12 (m, 2H), 2.06-1.96 (m, 1H), 1.90-1.52 (m, 11 H), 1.32-1.01 (m, 6H), 0.80-0.48 (m, 2H) **¹³C{¹H} NMR** (126 MHz, CDCl₃) 169.86, 163.28, 163.14, 157.69,157.67, 145.13, 144.98, 137.61, 137.60, 136.72, 136.43, 132.00, 131.90, 131.35, 131.32 (overlapping peaks), 130.23, 130.20, 126.70, 126.66, 126.61, 126.60, 122.20, 122.18, 109.70, 97.81, 97.78, 93.42, 93.35, 56.57, 55.86, 55.26, 34.43, 34.27, 34.22, 34.06, 27.98 − 27.07 (multiple overlapping peaks), 27.03, 26.11, 25.97. **³¹P{¹H} NMR** (202 MHz, CDCl₃) δ 35.59 **ATR-IR** (cm⁻¹): 2920, 2840, 1600, 1570, 1450, 1240, 1220, 1200, 1120, 821, 805, 763 **HRMS (ESI):** Calculated for $C_{34}H_{44}BrNaO_4PPd^+$ [M+Na]⁺, 755.1088 Found: 755.1090

1.4.13.4. AminoSPhos(Pd)(Ar-*m*OMe)Br Complex OA5
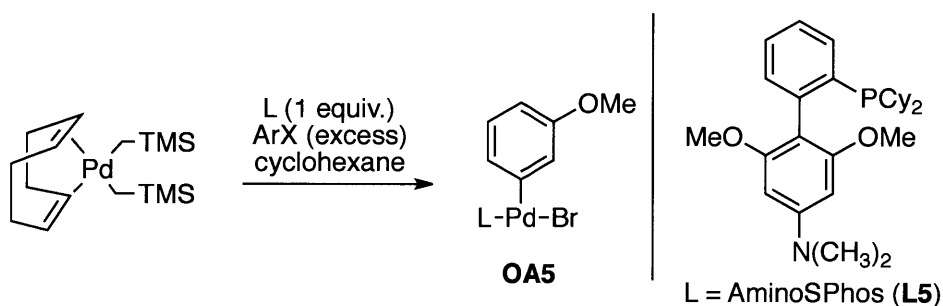
Following general procedure in section 1.4.11.1, using codPd(CH₂TMS)₂ (149 mg, 0.38 mmol), AminoSPhos **L5** (175.1 mg, 0.39 mmol), and 3-bromoanisole (100 mg, 0.53 mmol). The product was washed with pentane (3 x 5 mL) and dried under vacuum. The yield was 222.9 mg (78 %, 0.30 mmol). **¹H NMR** (500 MHz, CDCl₃) δ 7.57 (t, J = 7.0 Hz, 1H), 7.40 (t, J = 7.0 Hz, 1H), 7.34 (t, J = 7.0 Hz, 1H), 6.81 (m, 3H), 6.75 (s, 1H), 6.46 − 6.36 (m, 1H), 5.86 − 5.75 (m, 2H), 3.75 (s, 3H), 3.72 (s, 6H), 3.11 (s, 6H), 2.28 − 2.10 (m, 2H), 2.10 − 1.97 (m, 1H), 1.95 − 1.46 (m, 12H), 1.41 − 0.96 (m, 6H), 0.86 − 0.71 (m, 1H), 0.67 − 0.49 (m, 1H).**¹³C{¹H} NMR** (126 MHz, CDCl₃) δ

165.19, 165.02, 160.00, 157.60, 157.58, 147.24, 147.07, 139.93, 139.92, 137.95, 137.65, 131.87, 131.77, 131.11, 130.93, 130.90, 126.37, 126.35, 126.29, 126.25, 122.43, 122.40, 109.51, 89.68, 89.62, 55.47, 55.26, 41.48, 34.54, 34.32, 34.28, 34.08, 28.23 – 27.02 (multiple overlapping peaks), 26.20, 26.02. ^{31}P{^{1}H} NMR (202 MHz, CDCl$_3$) δ 38.07 **Elemental**: Calculated, C(56.27) H(6.34), Found, C(56.05) H(6.27).

1.4.13.5. BrettPhos(Pd)(Ar-*m*OMe)Br Complex OA6
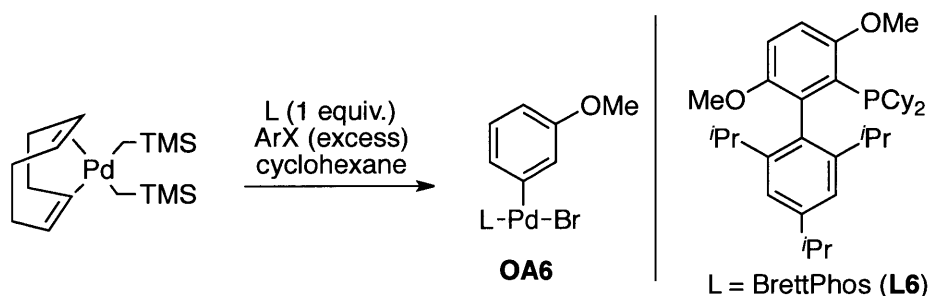
Following general procedure in section 1.4.11.1, using codPd(CH$_2$TMS)$_2$ (548.8 mg, 1.41 mmol), BrettPhos **L6** (746.7 mg, 1.39 mmol), and 3-bromoanisole (0.5 mL, 3.9 mmol). The product was washed with pentane (2 x 20 mL). The yield was 1.001 g (86%, 1.2 mmol). ^{1}H NMR (500 MHz, CD$_2$Cl$_2$) δ 7.07 (s), 6.95 – 6.89 (m), 6.86 (d, J = 8.9 Hz), 6.82 – 6.75 (m), 6.67 (d, J = 7.5 Hz), 6.62 (s), 6.39 – 6.34 (m), 4.35 (s, minor), 3.81 (s, major), 3.71 (s, major), 3.68 (s, minor), 3.61 (s, minor), 3.34 (s, major), 3.18 – 3.02 (m, major), 3.00 – 2.92 (m, minor), 2.86 – 2.79 (m, major), 2.60 – 2.46 (m, major), 2.43 – 2.33 (m, minor), 2.10 – 0.55 (40H). ^{13}C{^{1}H} NMR (126 MHz, CD$_2$Cl$_2$) δ 157.87,157.85, 157.65, 157.63, 157.27, 157.13, 157.06, 155.41, 155.39, 154.45, 154.40, 152.55, 152.51, 152.39, 149.56, 147.43, 139.22, 138.66, 138.50, 136.75 – 136.39 (br), 133.57, 131.46, 131.43, 131.15 (br), 130.95, 130.92, 126.40, 126.39, 125.30, 125.09, 124.12, 123.91, 123.88, 123.61, 123.58, 122.04, 118.84, 117.74, 114.00-113.80 (multiple overlapping peaks),111.94, 111.89, 111.55, 111.52, 109.18, 108.96, 62.47, 55.56, 55.48, 55.39, 55.29, 54.88, 36.98, 36.80, 35.72, 35.58, 35.51, 35.38, 34.88, 31.91, 31.41, 31.35, 31.33, 29.97 – 29.85 (multiple overlapping peaks), 29.74, 29.38 – 29.27 (multiple overlapping peaks), 28.51, 28.44, 28.40, 28.33, 28.23, 27.29, 27.17, 26.97,26.88, 26.72 – 26.68 (multiple overlapping peaks), 26.63 – 26.55 (multiple overlapping peaks), 25.81, 25.80, 25.76, 25.57, 25.05, 25.02, 24.73, 24.28, 23.69 . ^{31}P{^{1}H} NMR (202 MHz, CD$_2$Cl$_2$) δ 45.71, 37.73. **ATR-IR** (cm^{-1}): 2920, 2840, 1570, 1560, 1460, 1420, 1260, 1230, 1010, 817, 767. **Elemental**: Calculated, C(60.76) H(7.28), Measured C(60.98) H(7.38).

1.4.13.6. CPhos(Pd)(Ar-*m*OMe)Br Complex OA9
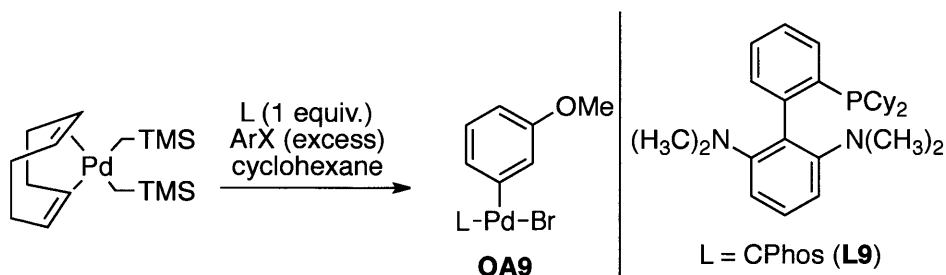
Following general procedure in section 1.4.11.1, using codPd(CH₂TMS)₂ (90.4 mg, 0.23 mmol), CPhos **L9** (102.4 mg, 0.23 mmol), and 3-bromoanisole (90 mg, 0.48 mmol). The product was washed with pentane (3 x 5 mL) and dried under vacuum. The yield was 169 mg (99%, 0.23 mmol). ^{1}**H NMR** (500 MHz, CDCl₃) δ 7.68 (t, *J* = 7.0 Hz, 1H), 7.61 (t, *J* = 8.1 Hz, 1H), 7.42 (t, *J* = 7.5 Hz, 1H), 7.33 (t, *J* = 7.3 Hz, 1H), 7.14 – 7.06 (m, 1H), 6.90 (d, *J* = 8.1 Hz, 3H), 6.81 (t, *J* = 7.8 Hz, 1H), 6.74 (d, *J* = 7.5 Hz, 1H), 6.70 (s, 1H), 6.40 (dd, *J* = 7.9, 1.8 Hz, 1H), 3.71 (s, 2H), 2.59 (s, 12H), 2.37 – 2.23 (m, 2H), 2.15 – 1.92 (m, 2H), 1.87 – 1.60 (m, 8H), 1.54 – 1.45 (m, 2H), 1.29 – 1.02 (m, 6H), 1.00 – 0.81 (m, 2H). ^{13}C{^{1}H} **NMR** (126 MHz, CDCl₃) δ 157.69 (br), 155.96 (br), 136.67 (br), 134.51 (br), 134.01, 133.92 (br), 133.48 (br), 130.65 (br), 129.41 (br), 126.71 (br), 125.96 (br), 122.02, 121.99 ,117.27 (br), 115.80 (br), 109.31, 55.20, 45.15, 36.84 (br), 36.64 (br), 29.34 (br), 28.01 (br), 27.91 (br), 27.71, 27.62 (br), 26.03 (br). ^{31}P{^{1}H} **NMR** (202 MHz, CDCl₃) δ 31.04 . **ATR-IR** (cm^{-1}): 2920, 2850, 2820, 2780, 1570, 1560, 1470, 1450, 1280, 1220, 1030, 1000, 760. **Elemental**: Calculated, C(57.58) H(6.63), Measured C(57.45) H(6.66).

1.4.14. Ligand Series Amido Complexes

1.4.14.1. SPhos L2 Based Amido Complex A2
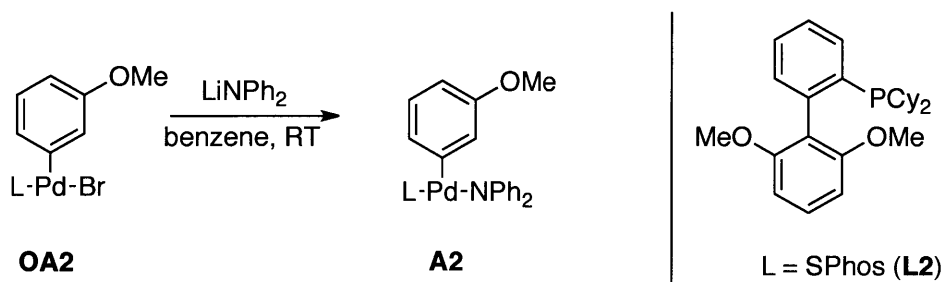
Using general procedure in section 1.4.11.2, **OA2** (77.1 mg, 0.11 mmol) and LiNPh$_2$ (33 mg, 0.19 mmol) were combined. The mixture was stirred for 15 min and the red product was washed with pentane (3 x 4 mL) and dried under vacuum. The yield was 59.7 mg (69 %, 0.075 mmol). **^{1}H NMR** (500 MHz, benzene-d_6) δ 7.78 – 6.48 (m), 6.22 – 5.88 (br), 5.13 – 4.98 (br, free amine), 3.88 – 2.99 (m), 2.78 – 0.75 (m), 0.29 (s). **^{13}C{^{1}H} NMR** (126 MHz, benzene-d_6) δ 158.08, 146.21, 146.05, 144.19, 144.14, 143.93, 137.12, 137.06, 136.85, 132.52, 132.43, 131.97, 131.40 (br), 129.86, 127.00, 126.97, 126.87, 123.04 (br), 121.44, 120.05, 120.02, 118.50, 115.91 (br), 111.58, 110.24, 105.13 (br), 55.18, 35.67 – 33.22 (multiple overlapping peaks), 30.42 – 25.25 (multiple overlapping peaks). **^{31}P{^{1}H} NMR** (202 MHz, benzene-d_6) δ 33.46. **MS (ESI):** Calculated for NaC$_{45}$H$_{52}$NO$_3$PPd [M-Na]$^+$, 814.26 Found: 814.27

1.4.14.2. RuPhosBrettPhos Hybrid L3 Based Amido Complex A3
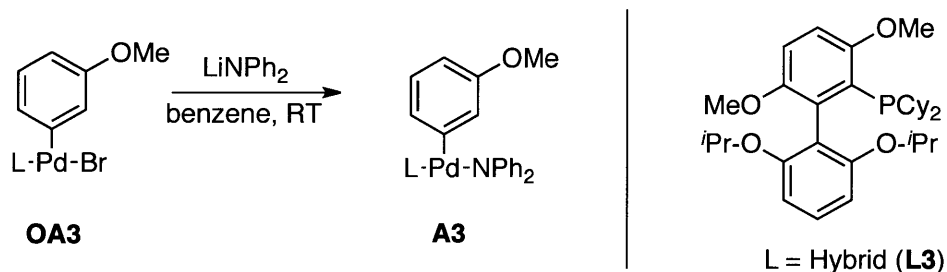
Using general procedure in section 1.4.12.1, **OA3** (95.5 mg, 0.12 mmol) and the LiNPh$_2$ (40 mg, 0.23 mmol) were combined. The mixture was stirred for 15 min and the red product was washed with pentane (3 x 4 mL) and dried. Yield was 59.2 mg (56 %, 0.065 mmol). **^{1}H NMR** (500 MHz, benzene-d_6) δ 8.01 – 5.70 (19H, major and minor), 5.17 – 5.07 (br, free amine), 4.65 – 3.93 (m, 2H- major and minor), 3.83 – 2.72 (m, 9H), 2.59 – 0.51 (m, 34H). **^{13}C{^{1}H} NMR** (126 MHz, benzene-d_6) δ 160.73, 158.34, 157.42, 156.10, 155.68, 155.04, 155.02, 151.27, 151.15, 147.28, 147.25, 138.92, 138.75, 137.54, 129.54, 129.34, 129.32, 129.18, 128.35, 126.09, 122.87 (br), 121.43 (br), 121.09, 120.72, 120.70, 118.19, 116.43, 115.34 – 114.40 (br), 112.75 (br), 110.93, 110.43 (br), 109.97 (br), 108.98, 106.05 (br), 72.71, 70.05 (br), 58.68, 55.28, 54.94, 54.89, 54.64, 54.39, 35.98, 35.80, 34.45, 33.48 (br), 30.71 (br), 30.17 (br), 29.02, 28.83 (br), 28.13 – 27.90 (br), 27.90 – 27.78 (br), 27.31, 27.20, 26.99, 26.28, 23.00, 22.79, 22.75, 21.78, 20.93, 14.30. **^{31}P{^{1}H} NMR** (202 MHz, benzene-d_6) δ 45.40, 44.32 **MS (ESI):** Calculated for C$_{39}$H$_{54}$O$_5$PPd [M-NPh$_2$]$^+$, 739.27 Found: 739.29

1.4.14.3. MethoxySPhos L4 based Amido Complex A4

L = MethoxySPhos (**L4**)
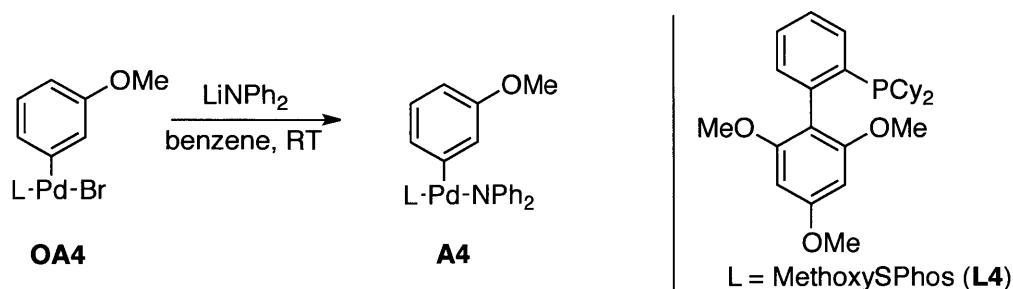
Using general procedure in section 1.4.12.1, **OA4** (95.6 mg, 0.13 mmol) and the LiNPh$_2$ (45 mg, 0.26 mmol) were combined. The mixture was stirred for 15 min and the red product was washed with pentane (9 x 4 mL). The yield was 71.1 mg (66 %, 0.086 mmol). ^{1}**H NMR** (300 MHz, benzene-d_6) δ 8.11 − 7.23 (m), 7.13 − 6.42 (m), 6.18 − 5.87 (m), 5.12 (dd, J = 1.2, 0.4 Hz), 3.47 (s), 3.46 (s), 3.40 (s), 3.36 (s), 2.73 − 0.67 (m,). ^{13}**C{^{1}H} NMR** (151 MHz, benzene-d_6) δ 159.23 − 158.92 (br), 158.26, 157.52, 157.36, 155.26 (br), 145.63, 145.49, 143.62, 143.58, 143.40, 136.48 (br), 136.30, 131.91 (br), 131.38 (br), 130.83, 129.29, 126.43, 126.40, 126.29, 122.47 (br), 120.86, 119.50 (br), 117.95, 115.33 (br), 111.00, 109.71, 109.68, 104.60, 55.10, 54.62, 34.19, 30.10 − 26.75 (multiple overlapping peaks), 26.29, 22.48, 14.03. ^{31}**P{^{1}H} NMR** (121 MHz, benzene-d_6) δ 33.49. **Elemental**: Calculated, C(67.19) H(6.62), Found, C(66.90) H(6.60).

1.4.14.4. AminoSPhos L5 Based Amido Complex A5

L = AminoSPhos (**L5**)
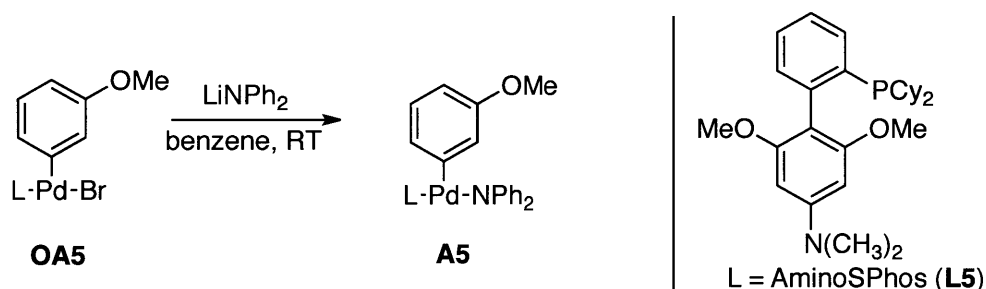
Using general procedure in section 1.4.12.1, **OA5** (104.1 mg, 0.14 mmol) and LiNPh$_2$ (50 mg, 0.29 mmol) were combined. The mixture was stirred for 60 min and the orange product was washed with pentane (2 x 4 mL). The yield was 83.3 mg (72 %, 0.10 mmol). ^{1}**H NMR** (500 MHz, benzene-d_6) δ 7.64 − 7.33 (m), 7.26 − 6.95 (m), 6.95 − 6.73 (m), 6.64 (dd, J = 9.1, 4.8 Hz, 0H), 6.53 (dd, J = 8.0, 2.1 Hz), 5.56 − 4.93 (m), 3.41 (d, J = 19.9 Hz), 2.76 (s), 2.42 − 1.90 (m), 1.91

– 1.60 (m), 1.60 – 1.46 (m), 1.45 – 0.90 (m), 0.90 – 0.76 (m). $^{13}C\{^1H\}$ **NMR** (126 MHz, benzene-d_6) δ 157.72, 156.24, 156.01 – 155.75 (br), 148.97, 148.79, 147.89, 147.85, 138.80, 138.51, 132.40, 132.31, 131.23, 130.99, 130.98, 129.55, 129.37, 129.34, 126.34, 126.29, 126.25, 122.21 (br), 121.14, 120.89, 120.86, 118.18, 116.34 – 113.99 (br), 110.70, 91.07, 91.04, 88.40, 54.80, 54.24, 41.27, 39.68, 35.74 – 32.49 (br), 28.54 (br), 28.19 – 27.73 (br), 27.67, 27.58, 26.64 (br), 22.75, 14.31. $^{31}P\{^1H\}$ **NMR** (202 MHz, benzene-d_6) δ 37.62 **Elemental**: Calculated, C(56.27) H(6.34), Found, C(56.51) H(6.42).

1.4.15. Ligand Synthesis

1.4.15.1. AminoSPhos L5

1.4.15.1.1. AminoSPhos (L5) "Lower" Ring
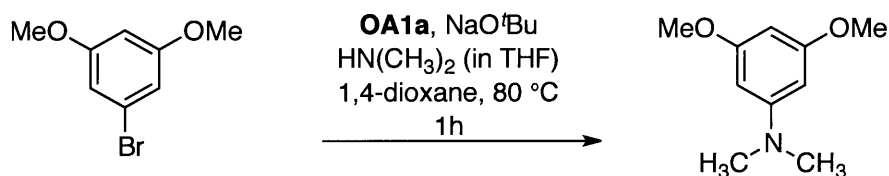
A round bottom flask was charged with 3,5-dimethoxybromobenzene (1.04 g, 4.8 mmol) and NaOtBu (1.5491 g, 6.6 mmol). The flask was fitted with a rubber septum (VWR Cat No. 89097-544), and evacuated and backfilled with nitrogen (this process was repeated a total of three times). Anhydrous dioxane (10 mL) was added via syringe followed by dimethyl amine (4 mL; 2.0 M in THF). A solution of **OA1a** (53 mg, 0.07 mmol, dissolved in a minimum of CH_2Cl_2 (~ 0.1 mL)) was added and the vessel heated to 80 °C for 1 h. The reaction was allowed to cool to rt and water (50 mL) was added. The reaction was then extracted with EtOAc (3 x 50 mL). The organic layers were combined. For purification by dry loading chromatography, silica gel was added (~ 5 g), and the solvent removed by rotary evaporation. The residue was then purified by silica gel chromatography (EtOAc/hexanes). The isolated yield was 0.7080 g (82 %, 3.9 mmol). **Melting Point**. 73.4-73.6. ^1H **NMR** (500 MHz, CD_2Cl_2) δ 5.87 (overlapping) (s, 3H), 3.75 (s, 6H), 2.91 (s, 6H). $^{13}C\{^1H\}$ **NMR** (126 MHz, CD_2Cl_2) δ 162.14, 153.11, 92.13, 89.12, 55.59, 40.93 .

1.4.15.1.2.   AminoSPhos (L5) Biaryl Subunit

1) *n*BuLi at -78 °C
2) ZnCl$_2$ in 2-methyl-THF at 25 °C
3) XPhos G1 and 2-bromoiodobenzene at 65 °C
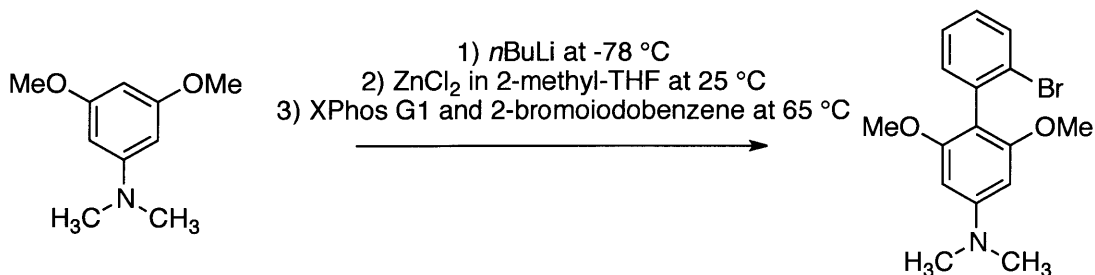
Using Schlenk techniques, 3,5-dimethoxy-*N,N*-dimethylaniline (225.1 mg, 1.24 mmol) was loaded into a screw cap test tube, sealed with a rubber septum, and then evacuated and backfilled with nitrogen (this process was repeated a total of three times). Anhydrous THF (5 mL) was added via syringe. The solution was cooled to -78 °C and *n*BuLi (0.55 mL; 2.5 M hexanes) was added via syringe. The solution was allowed to warm to rt and stirred for an additional 30 min before addition of ZnCl$_2$ (0.75 mL; 1.9 M Methyl-THF). A separate solution of a first generation XPhos precatalyst (10.9 mg, 0.015 mmol) (see reference 16b in the manuscript) and 2-bromoiodobenzene (335.0 mg, 1.2 mmol) in THF (2 mL) was then added via syringe. The reaction solution was heated to 65 °C and stirred for an additional 2 h. After cooling to rt, the reaction was quenched by the addition of MeOH (0.25 mL) and then water (50 mL) was added. The reaction mixture was extracted with EtOAc (3 x 50 mL). The combined organic extracts were dried over MgSO$_4$ and filtered. The residual MgSO$_4$ was rinsed with EtOAc. For purification by dry loading chromatography, silica gel (10 mL dry volume) was added to the filtrate and the solvent removed with the aid of a rotary evaporator. The residue was purified by silica gel chromatography (EtOAc/hexanes) to give the product as a white solid (185.9 mg, 45 % yield). ^{1}H NMR (500 MHz, CDCl$_3$) δ 7.65 (d, *J* = 8.0 Hz, 1H), 7.38 – 7.31 (m, 2H), 7.30 – 7.25 (m, 2H), 7.22 – 7.15 (m, 1H), 6.01 (s, 2H), 3.75 (d, *J* = 1.2 Hz, 8H), 3.05 (d, *J* = 1.1 Hz, 9H). ^{13}C{^{1}H} NMR (126 MHz, CDCl$_3$) δ 158.40, 151.93, 136.73, 135.14, 133.23, 132.30, 128.20, 127.75, 126.88, 126.50, 108.41, 89.17, 55.96, 40.75, 22.48, 14.21.

1.4.15.1.3.   Synthesis of AminoSPhos L5
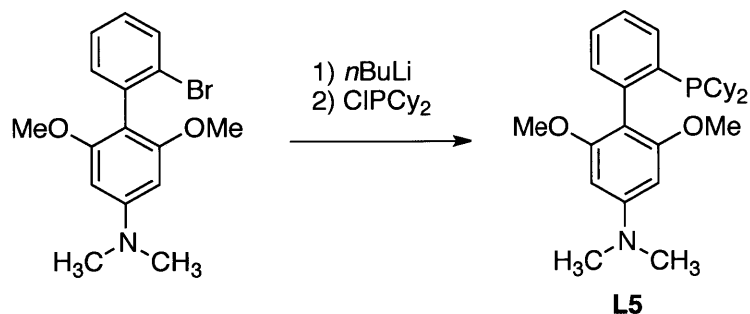
In a nitrogen-filled glove box, a large screw cap test tube, equipped with a stir bar, was charged with the biaryl precursor from above (185 mg, 0.55 mmol) and diethyl ether (4 mL) was added. The reaction tube was capped and nBuLi (0.25 mL; 2.5 M in hexanes) was added via syringe. The reaction mixture was stirred at rt for 30 min before the addition of Cy_2PCl (0.12 mL, 0.54 mmol). The reaction mixture was stirred for an additional 3 h and the reaction tube was removed from the glove box. For purification by dry loading chromatography, silica gel was added to the reaction mixture and the solvent removed under vacuum. The residue was then purified by silica gel chromatography (EtOAC/hexanes). The yield obtained was 185.4 mg (75 %, 0.41 mmol). **Melting Point.** 155.4-156.3 °C. **^{1}H NMR** (500 MHz, $CDCl_3$) δ 7.54 (d, J = 7.5 Hz, 1H), 7.37 (t, J = 7.3 Hz, 1H), 7.33 − 7.27 (m, 1H), 7.20 − 7.17 (m, 1H), 5.93 (s, 2H), 3.68 (s, 6H), 3.02 (s, 6H), 1.79 (t, J = 11.9 Hz, 2H), 1.75 − 1.50 (m, 10H), 1.35 − 0.99 (m, 10H). **^{13}C{^{1}H} NMR** (126 MHz, $CDCl_3$) δ 158.05, 158.04, 151.49, 143.75, 143.50, 136.71, 136.58, 132.38, 132.35, 131.92, 131.87, 131.49, 128.25, 128.24, 127.63, 125.85, 109.32, 109.27, 88.28, 55.91, 55.15, 40.74, 34.09, 33.98, 30.16, 30.02, 29.17, 29.10, 27.75, 27.66, 27.57, 27.51, 26.72. **^{31}P{^{1}H} NMR** (202 MHz, $CDCl_3$) δ -8.68. **ATR-IR** (cm^{-1}): 2920, 2850, 1610, 1560, 1440, 1360, 1240, 1120, 1010, 995, 850, 797. **HRMS (ESI)**: Calculated for $C_{28}H_{41}NO_2P^+$ [M+H]$^+$, 454.2869, Found: 454.2867.

1.4.15.2. RuPhosBrettPhos Hybrid Ligand (L3)

1.4.15.2.1. Synthesis of lithiated lower aryl ring
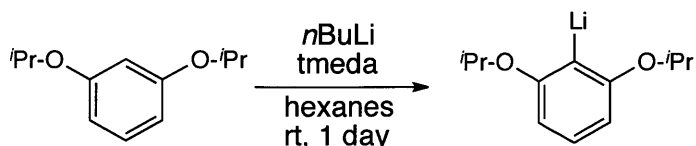
In a nitrogen-filled glove box, 1,3-isopropoxybenzene (0.558 g, 2.9 mmol) was charged to a screw cap test tube. Anhydrous pentane (~10 mL) was added along with TMEDA (0.1 mL, 1.1 mmol) and nBuLi (1.15 mL, 2.5 M in hexanes). The solution was allowed to sit for 24 h after which the aryl lithium salt precipitated. The solvent was then decanted and the white crystalline product washed with pentane (~5 mL) and dried under vacuum. The yield was 550 mg (96 %, 2.75 mmol). The intermediate was used in the subsequent step without further purification or characterization.

1.4.15.2.2. Hybrid (L3) Biaryl Precursor
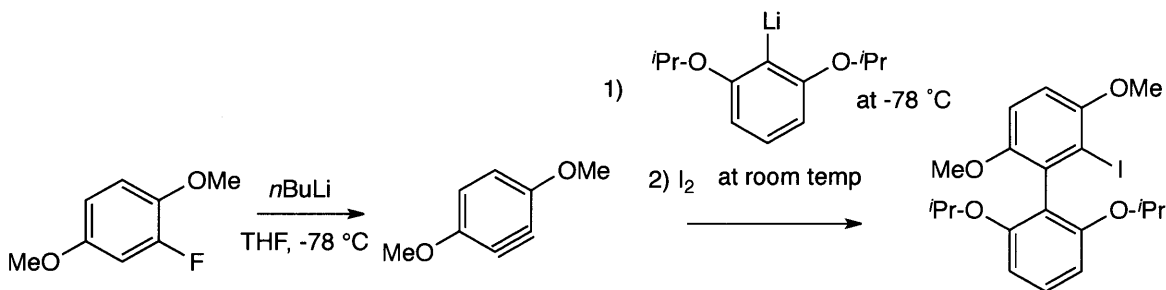
In a nitrogen-filled glove box, 3,6-dimethoxyfluorobenzene (0.5565 g, 3.6 mmol) was added to anhydrous THF (~10 mL) in a screw cap test tube equipped with a stir bar. The vessel was then sealed with a silicon/Teflon septum. In a second vessel the aryl lithium salt (706 mg, 3.53 mmol) was dissolved in anhydrous THF (~7 mL) and sealed with a silicon/Teflon septum. Both vessels were removed from the glove box. The first vessel was cooled to -78 °C at which point nBuLi (1.5 mL, 2.5 M in hexanes) was added to the solution. This reaction mixture was allowed to stir for an additional 30 min before the addition of the aryl lithium salt solution via syringe. The ensuing reaction mixture was then stirred for 1 h at -78 °C, and warmed slowly to rt over 45 min and stirred for an additional 45 min. Iodine (0.88 g, 3.5 mmol) was dissolved in a minimum of anhydrous THF and added via syringe to the reaction mixture, then stirred for an additional 45

min before quenching with water (10 mL). The crude product was extracted with CH_2Cl_2 (3 x 50 mL). The extracts were combined and the solvent removed via rotary evaporator. The residue was purified by silica gel chromatography (EtOAc/hexanes) and the product crystallized from hexane. The yield was 420.5 mg (26 %, 0.92 mmol). **Melting Point**: 76.5-76.8 °C. **^{1}H NMR** (500 MHz, CDCl$_3$) δ 7.26 (t, J = 8.3 Hz, 1H), 6.89 (d, J = 8.9 Hz, 1H), 6.78 (d, J = 8.9 Hz, 1H), 6.61 (d, J = 8.3 Hz, 2H), 4.38 (hept, J = 6.0 Hz, 2H), 3.88 (s, 3H), 3.66 (s, 3H), 1.14 (dd, J = 22.9, 6.0 Hz, 12H). **^{13}C{^{1}H} NMR** (126 MHz, CDCl$_3$) δ 156.49, 152.78, 152.61, 132.82, 128.92, 122.25, 111.77, 109.57, 107.16, 95.58, 70.73, 57.10, 57.05, 22.45. **HRMS (ESI)**: Calculated for $C_{20}H_{26}IO_4^+$ [M+H]$^+$ 457.0871, Found: 457.0877

1.4.15.2.3.   Synthesis of RuPhosBrettPhos Hybrid L3

L3
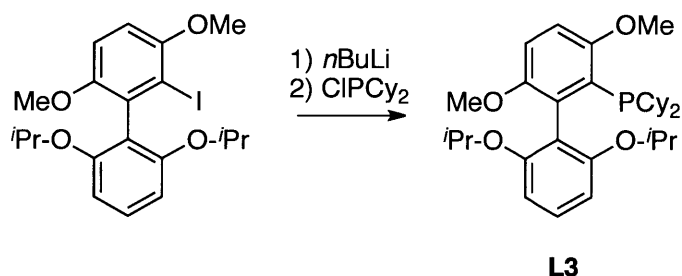
In a nitrogen-filled glove box, the iodobiaryl precursor shown above (200.1 mg, 0.44 mmol) was added to a small screw cap test tube along with diethyl ether (2 mL). The vessel was then sealed with a silicon/Teflon septum. To this was added nBuLi (0.2 mL, 2.5 M in hexanes) and the resulting solution was allowed to stir for 30 min. Cy$_2$PCl (0.10 mL, 0.45 mmol) was added via syringe. After 2 h, the reaction vessel was taken out of the glove box and water (10 mL) was added.   The resulting mixture was extracted with CH_2Cl_2 (3 x 20 mL). The extracts were combined and the solvent removed with the aid of a rotary evaporation. Hexanes (~3 mL) were added to the residue to induce rapid crystallization. The product was then dried under vacuum. The yield was 167 mg (72 %, 0.32 mmol). **Melting Point**: 138.0-140.0 °C. **^{1}H NMR** (500 MHz, CDCl$_3$) δ 7.21 (t, J = 8.3 Hz, 1H), 6.82 (d, J = 8.8 Hz, 1H), 6.74 (d, J = 8.8 Hz, 1H), 6.51 (d, J = 8.3 Hz, 2H), 4.39 (hept, J = 5.7 Hz, 2H), 3.81 (s, 3H), 3.58 (s, 3H), 2.25 (m, 2H), 1.86 – 1.53 (m, 8H), 1.46 – 0.95 (m, 24H). **^{13}C{^{1}H} NMR** (126 MHz, CDCl$_3$) δ156.50, 156.49, 156.42, 156.39, 151.87, 151.79, 135.59, 135.31, 128.05, 127.54, 127.34, 119.92, 119.85, 111.49, 111.48, 108.67, 105.80, 70.06, 56.19, 55.31, 35.27, 35.17, 33.04, 32.85, 30.53, 30.45, 27.68, 27.62,

27.59, 27.48, 26.73, 26.72, 22.58, 22.27 . ^{31}P{^{1}H} **NMR** (202 MHz, CDCl$_3$) δ 2.30 **ATR-IR** (cm$^-$^{1}): 2970, 2920, 2830, 1580, 1570, 1460, 1430, 1380, 1370, 1260, 1240, 1110, 1060, 1030, 1020, 793. **HRMS** (ESI): Calculated for C$_{32}$H$_{48}$O$_4$P$^+$ [M+H]$^+$ 527.3285, Found: 527.3287

1.4.16. NMR Data

1.4.16.1.   RuPhos L1 OA Complexes

1.4.16.1.1.   RuPhos(Pd)(Ar-*m*OMe)Br Complex OA1a
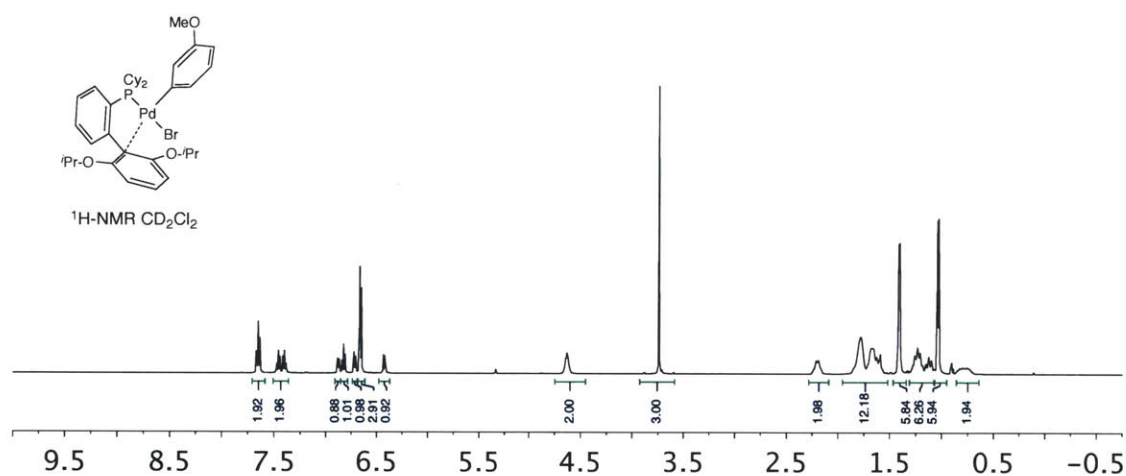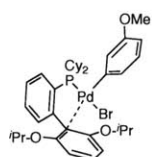
$^{13}C\{^1H\}$-NMR CD$_2$Cl$_2$
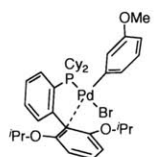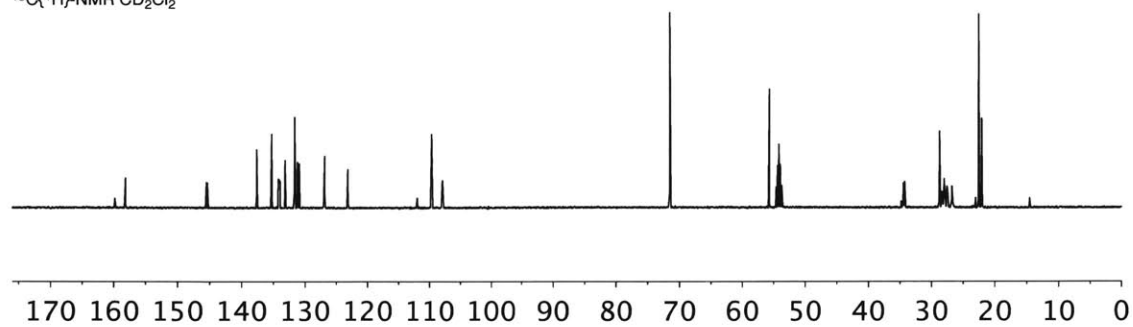
$^{31}P\{^1H\}$-NMR CD$_2$Cl$_2$
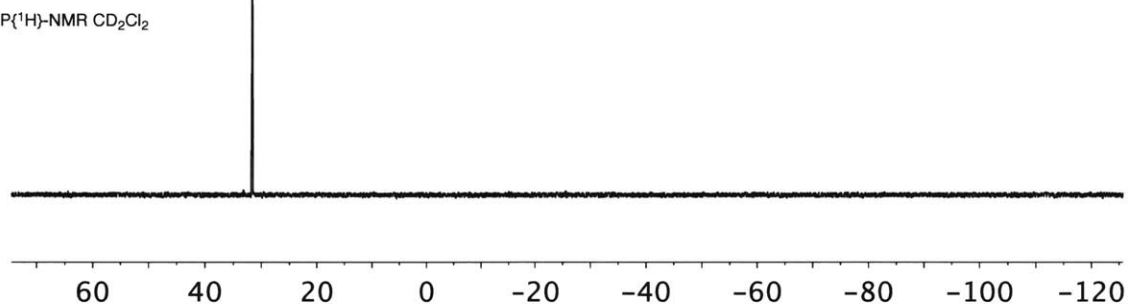
1.4.16.1.2.   RuPhos(Pd)(Ar-pCF$_3$)(Br) Complex OA1b

¹H-NMR CDCl₃

8.0 7.5 7.0 6.5 6.0 5.5 5.0 4.5 4.0 3.5 3.0 2.5 2.0 1.5 1.0 0.5 0.0

¹³C{¹H}-NMR CDCl₃

170 160 150 140 130 120 110 100 90 80 70 60 50 40 30 20 10 0

³¹P{¹H}-NMR CDCl₃

70 60 50 40 30 20 10 0 −10 −20
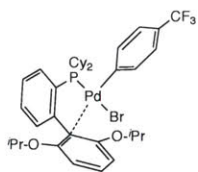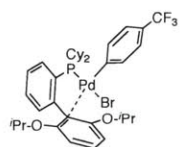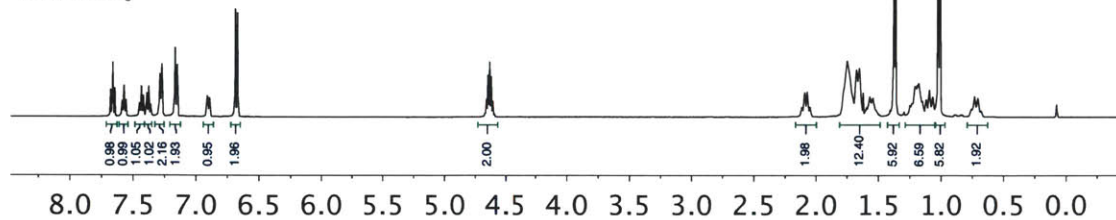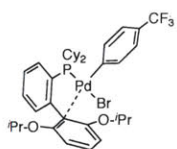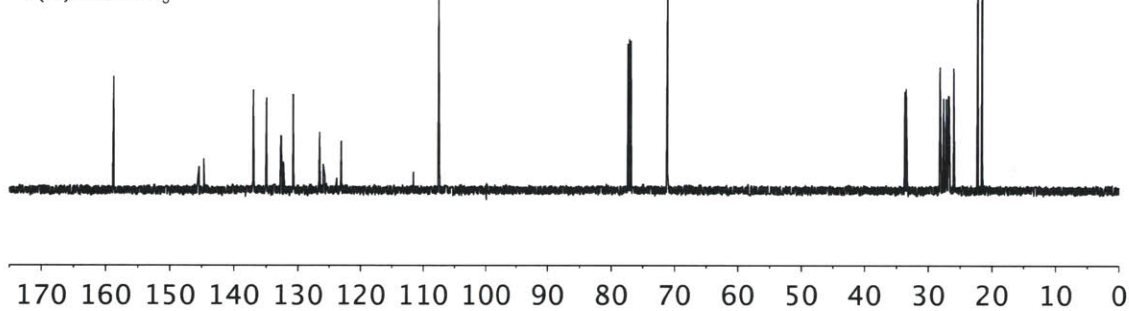
^{31}F{^{1}H}-NMR CDCl$_3$
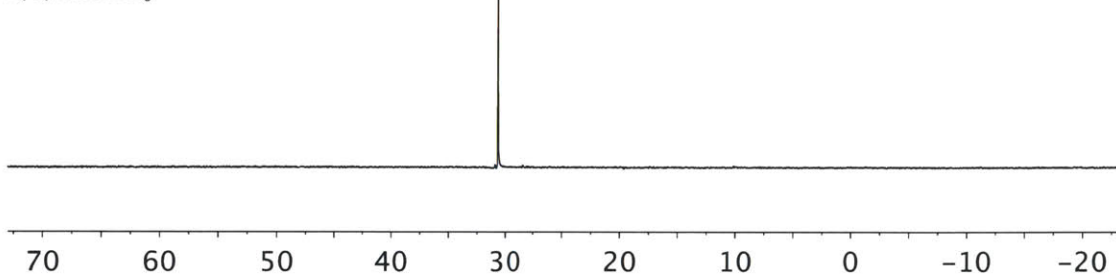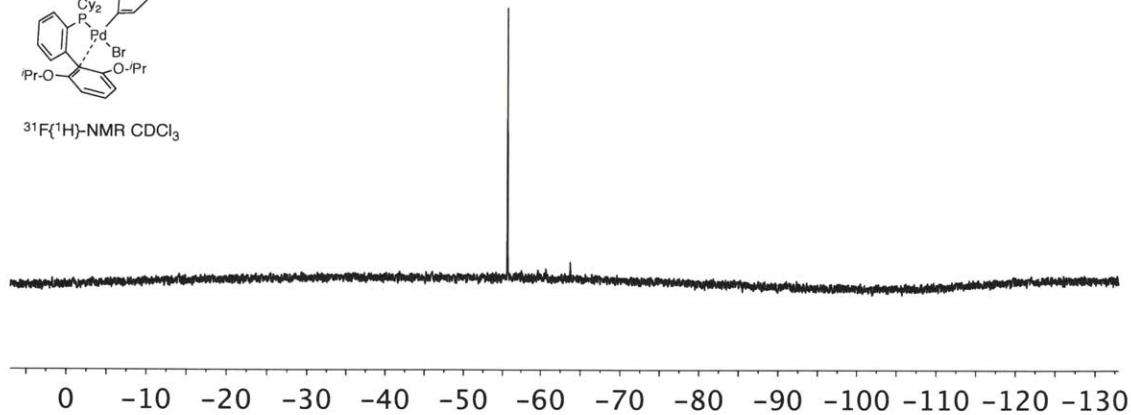
1.4.16.1.3.   RuPhos(Pd)(Ph)(Br) Complex OA1c

^{1}H-NMR CD$_2$Cl$_2$

$^{13}C\{^1H\}$-NMR CD$_2$Cl$_2$

170 160 150 140 130 120 110 100 90 80 70 60 50 40 30 20 10 0

$^{31}P\{^1H\}$-NMR CD$_2$Cl$_2$

60 40 20 0 -20 -40 -60 -80 -100 -120
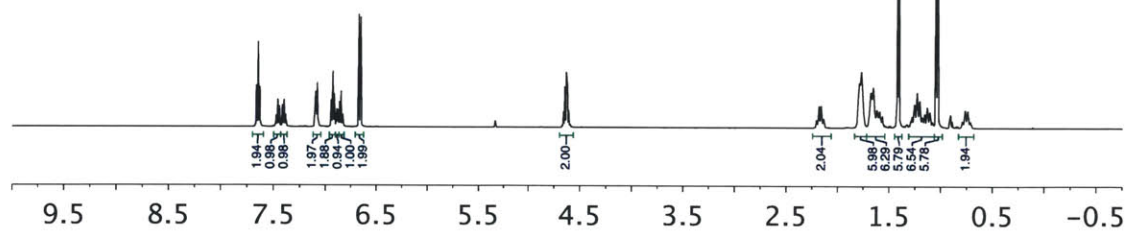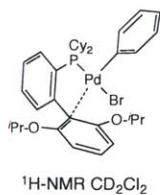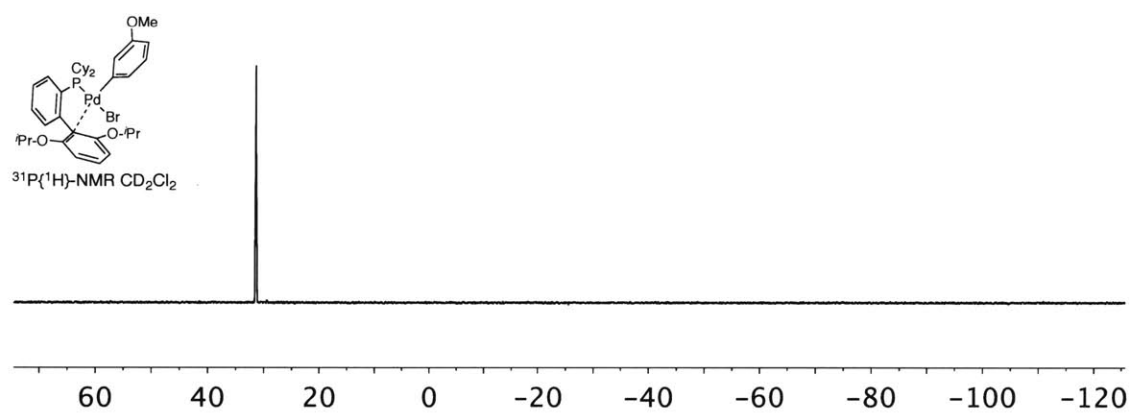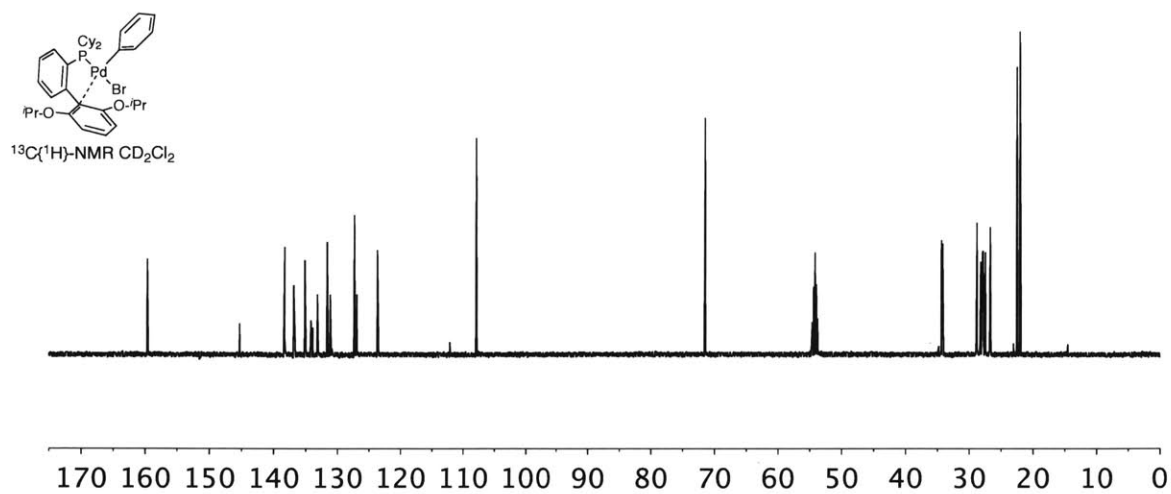
1.4.16.1.4.   RuPhos(Pd)(Ar-pCH$_3$)(Cl) Complex OA1d
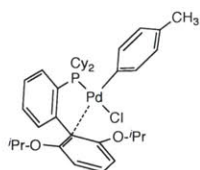
¹H-NMR CD₂Cl₂
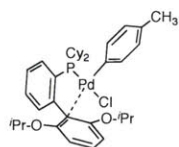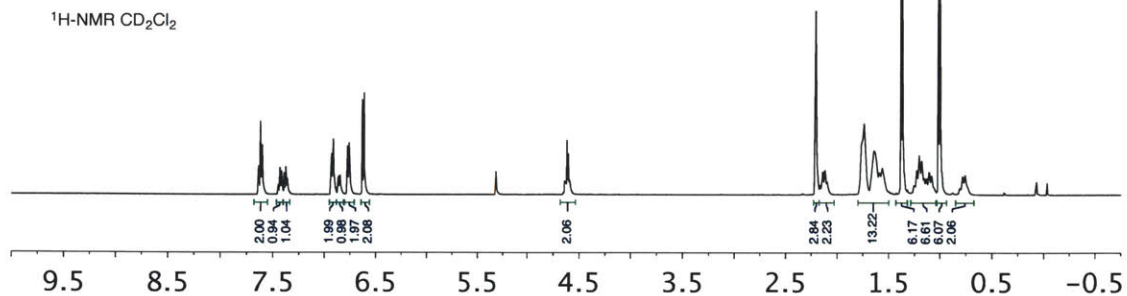
¹³C{¹H}-NMR CD₂Cl₂
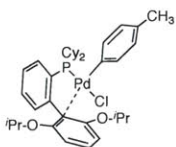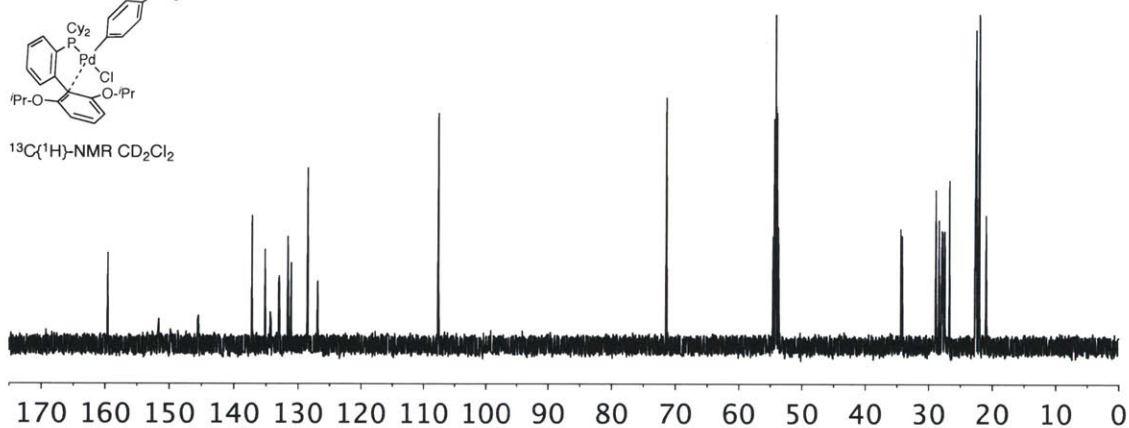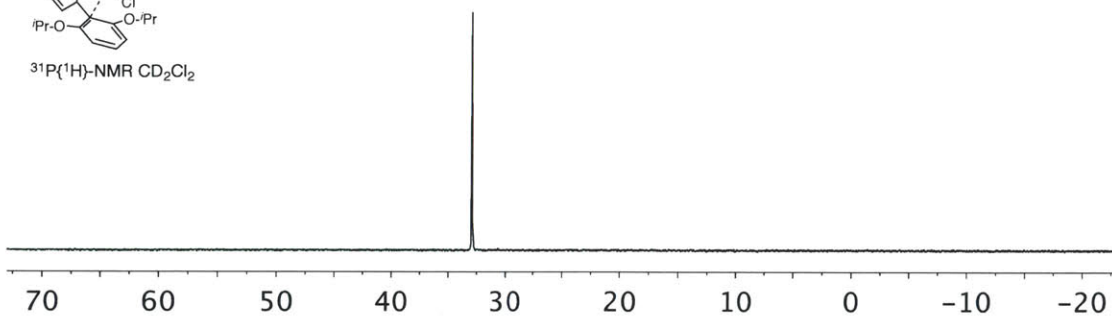
³¹P{¹H}-NMR CD₂Cl₂

1.4.16.1.5.   RuPhos(Pd)(Ar-pOMe)(Br) Complex OA1e
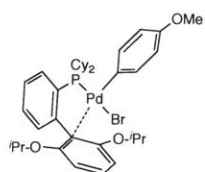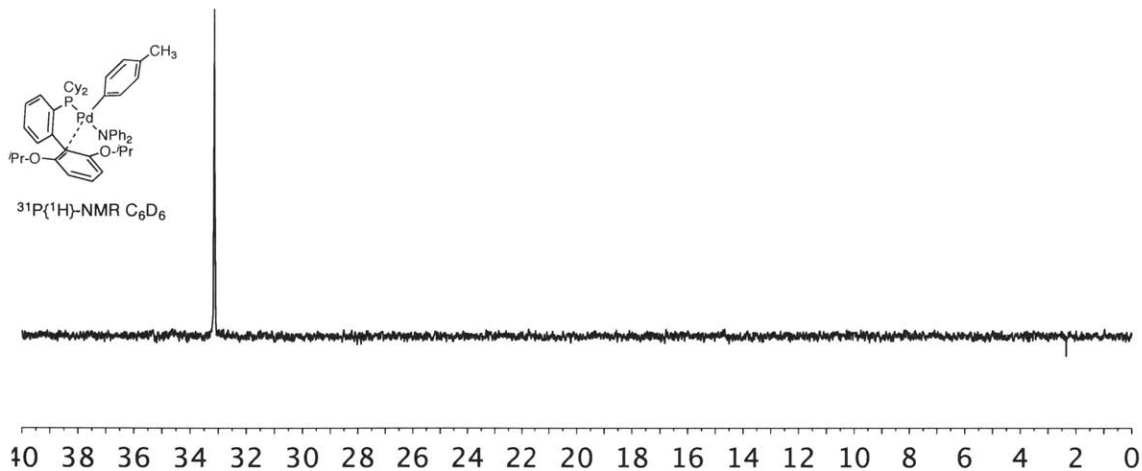

¹H-NMR CD₂Cl₂
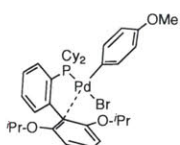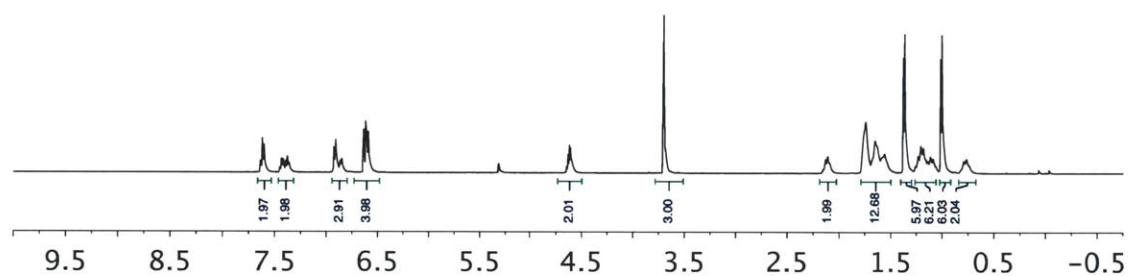
¹³C{¹H}-NMR CD₂Cl₂
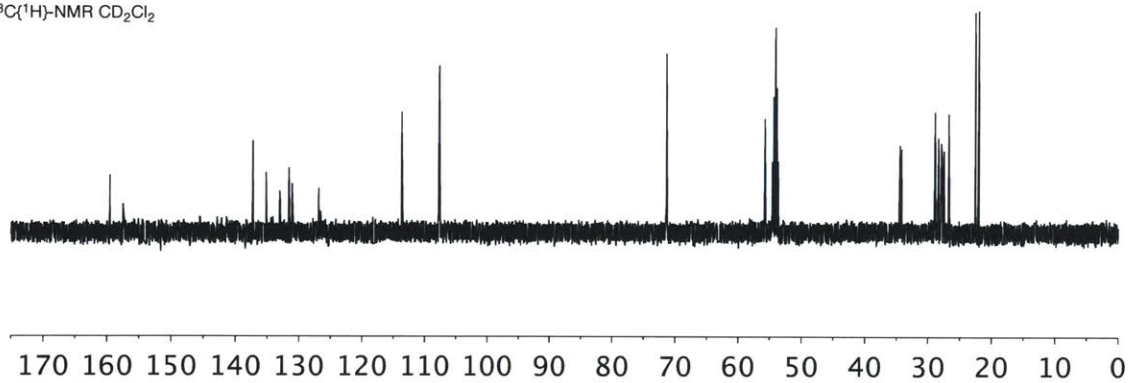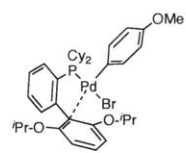
$^{31}P\{^1H\}$-NMR CD_2Cl_2
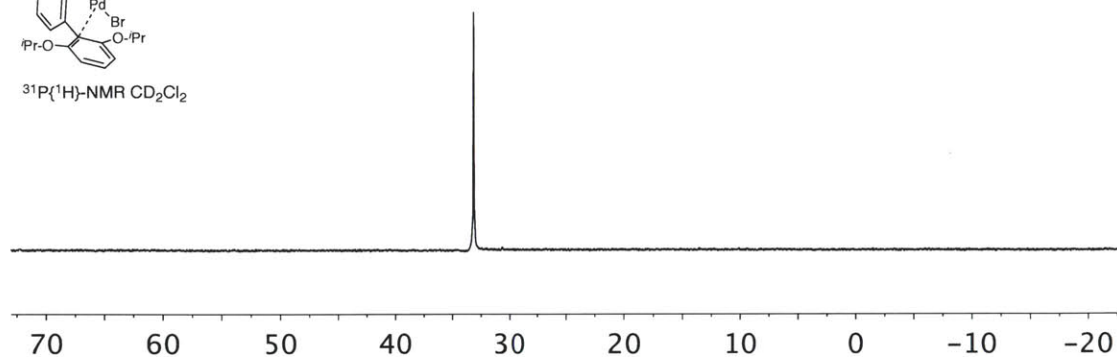
1.4.16.2. RuPhos L1 Based Amido Complexes

1.4.16.2.1. RuPhos(Pd)(Ar-*m*OMe)(NPh$_2$) Complex A1a

^1H-NMR C_6D_6
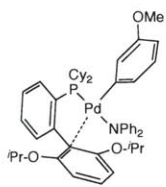
$^{13}C\{^1H\}$-NMR C_6D_6
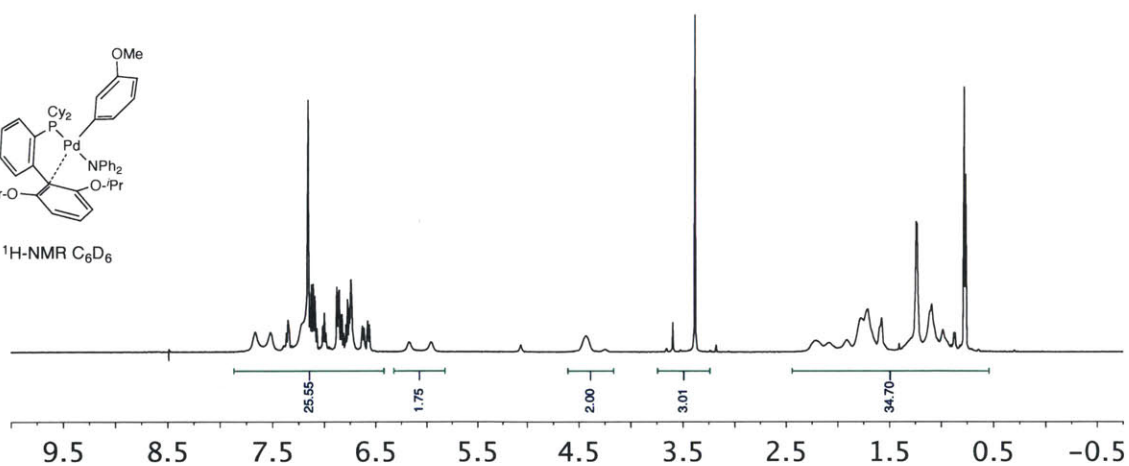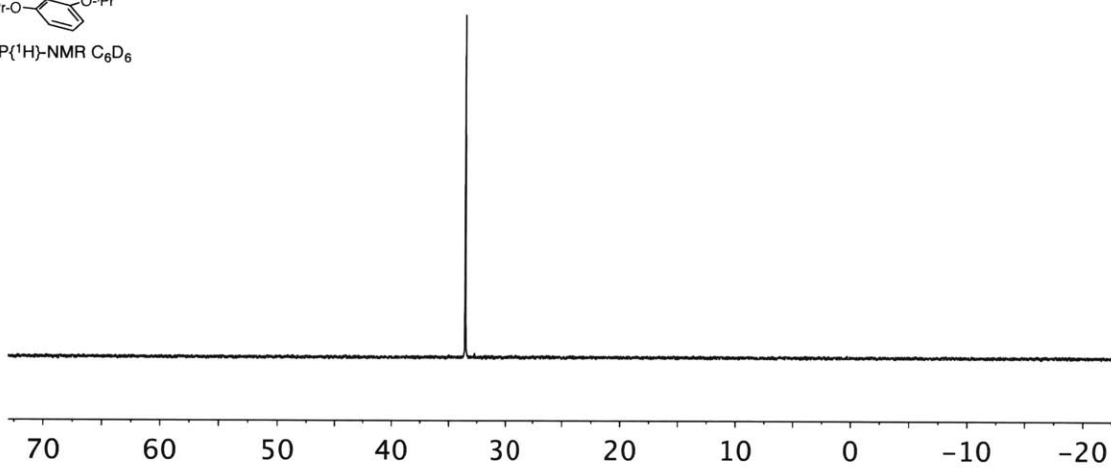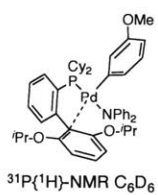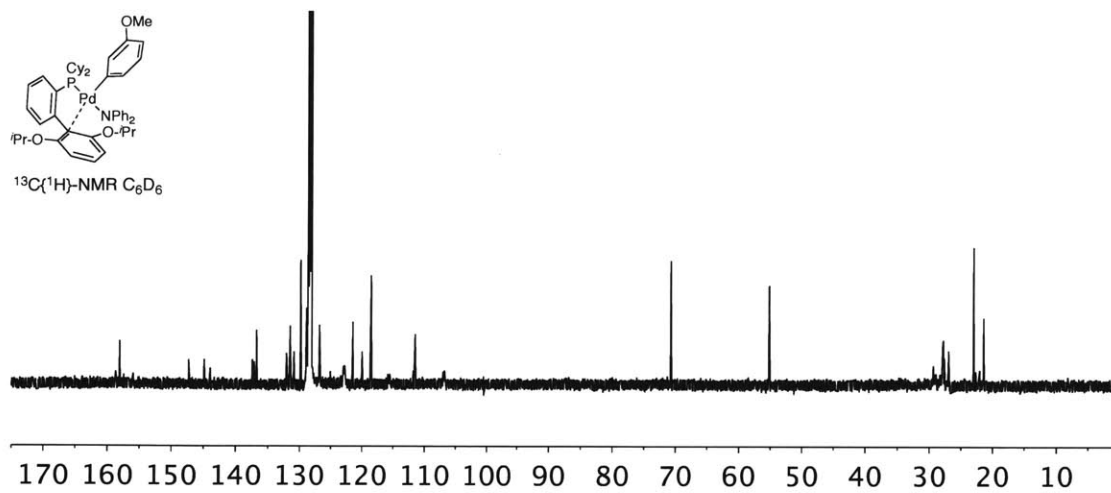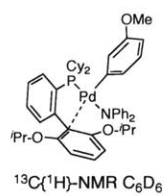
$^{31}P\{^1H\}$-NMR C_6D_6

1.4.16.2.2.   RuPhos(Pd)(Ph)(NPh$_2$) Complex A1c
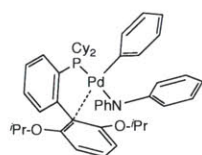
^{1}H-NMR C$_6$D$_6$
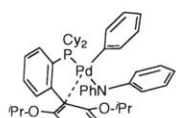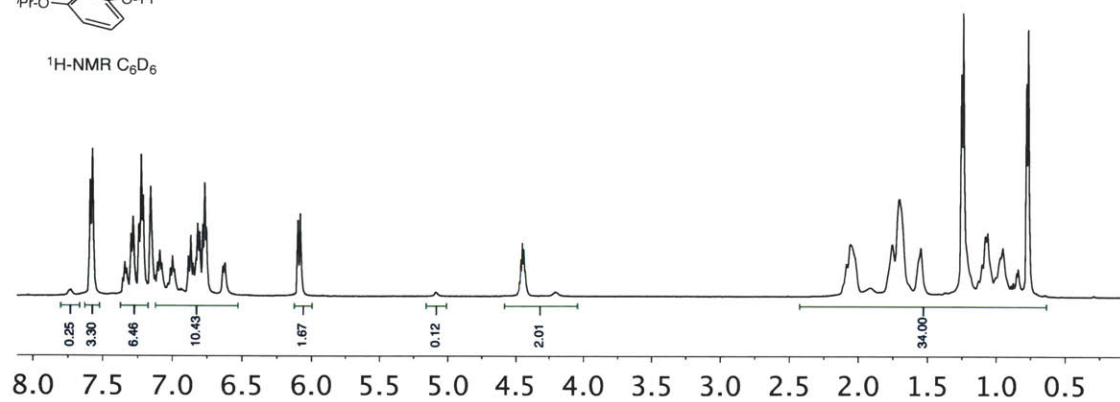
^{13}C{^{1}H}-NMR C$_6$D$_6$
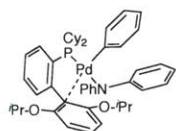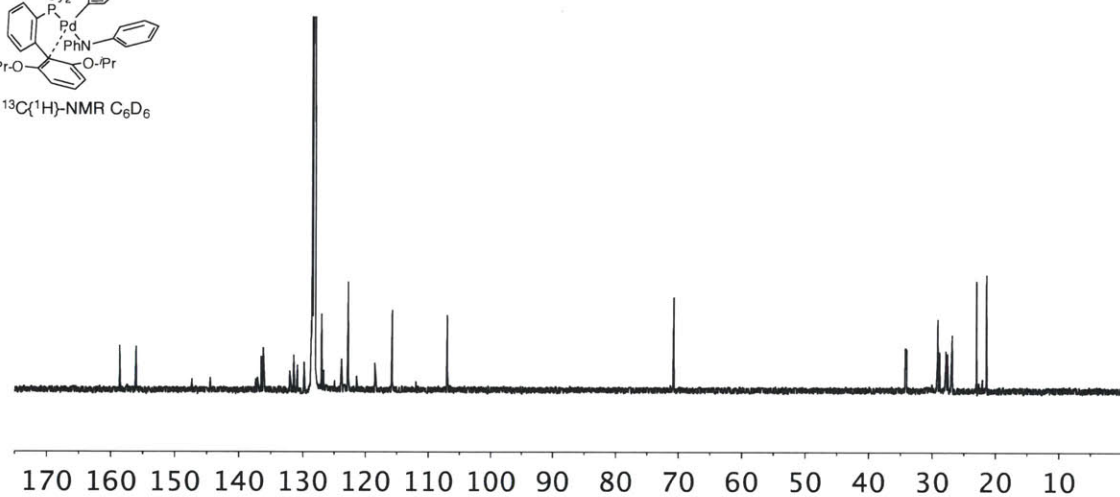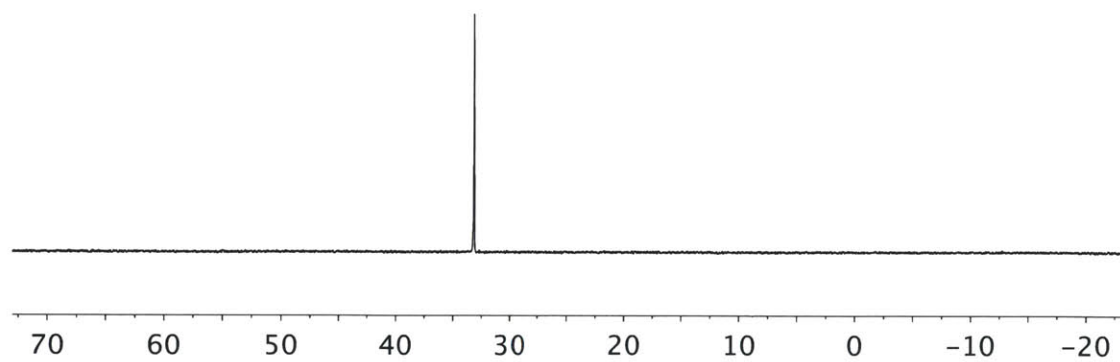
^{31}P{^{1}H}-NMR C$_6$D$_6$

1.4.16.2.3. RuPhos(Pd)(Ar-*p*CH₃)(NPh₂) Complex A1d
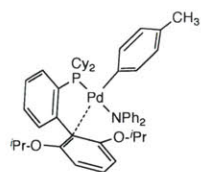
¹H-NMR C₆D₆
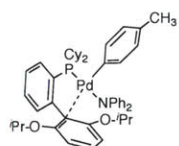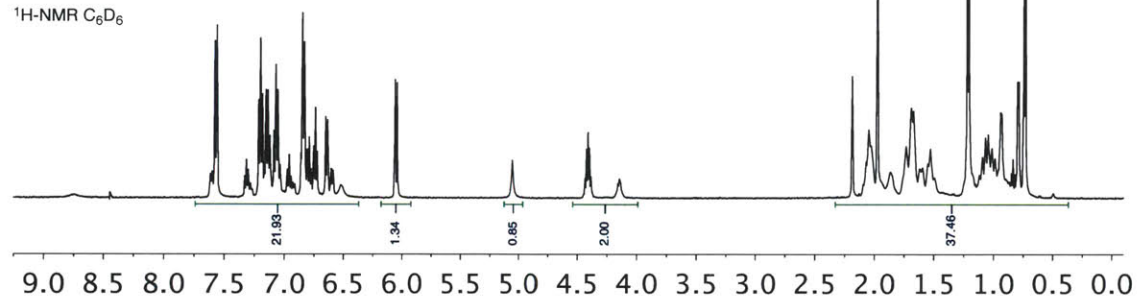
¹³C{¹H}-NMR C₆D₆

$^{31}P\{^1H\}$-NMR C_6D_6
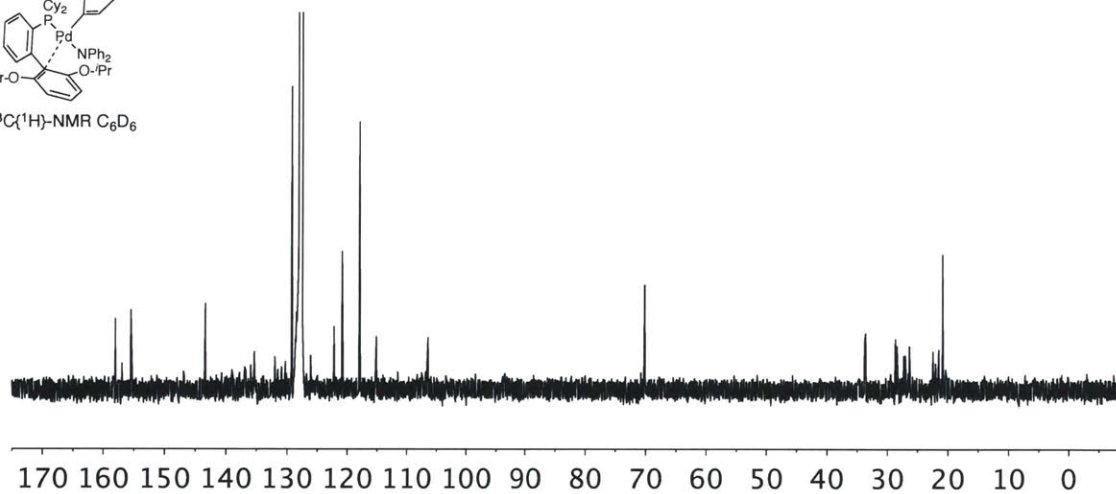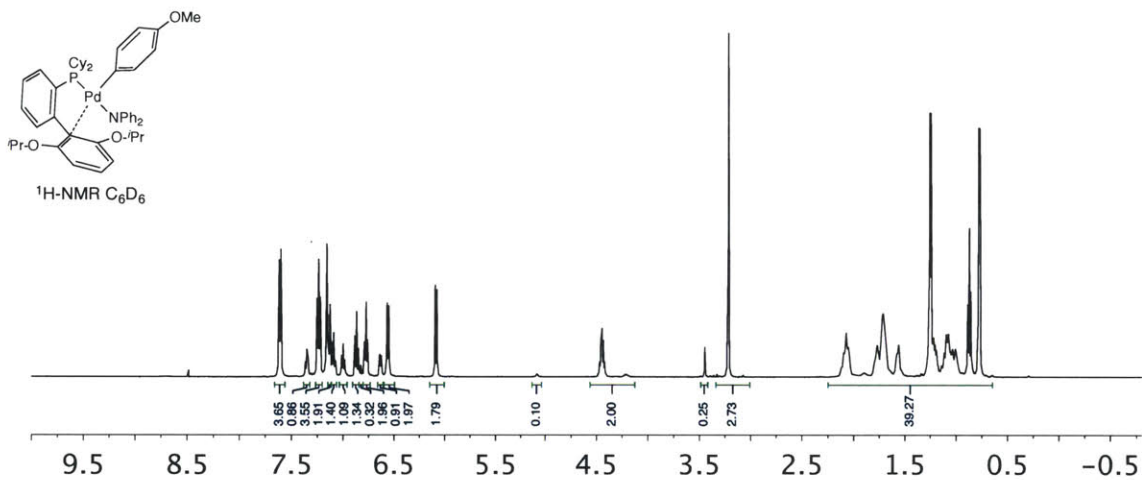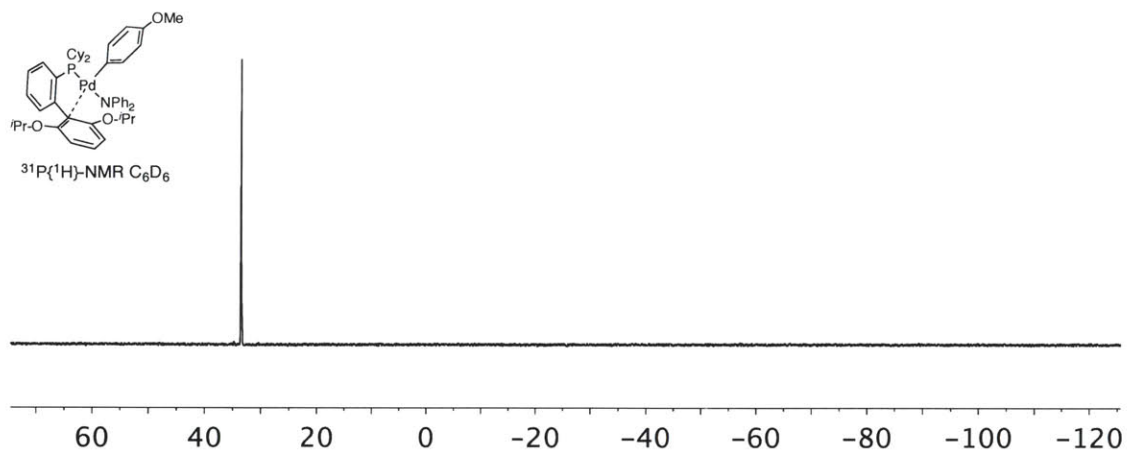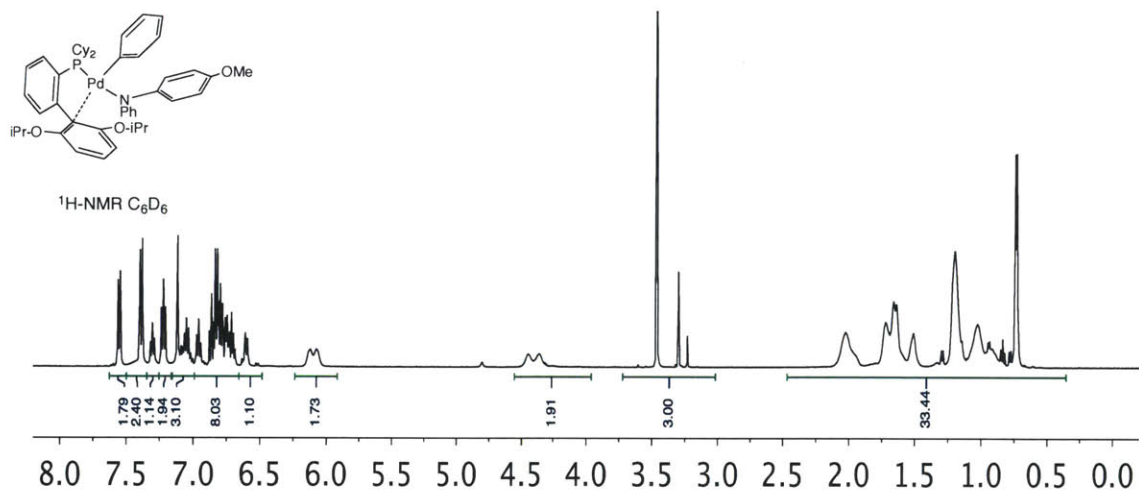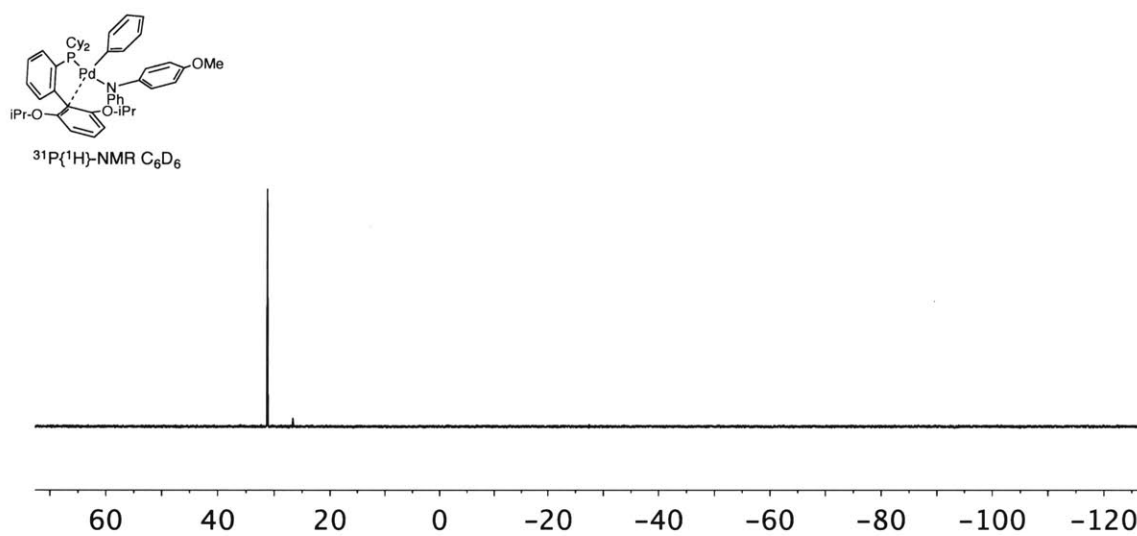

1.4.16.2.4. RuPhos(Pd)(Ar-*p*OMe)(NPh₂) Amido Complex A1e

^1H-NMR C_6D_6

$^{13}C\{^1H\}$-NMR C_6D_6
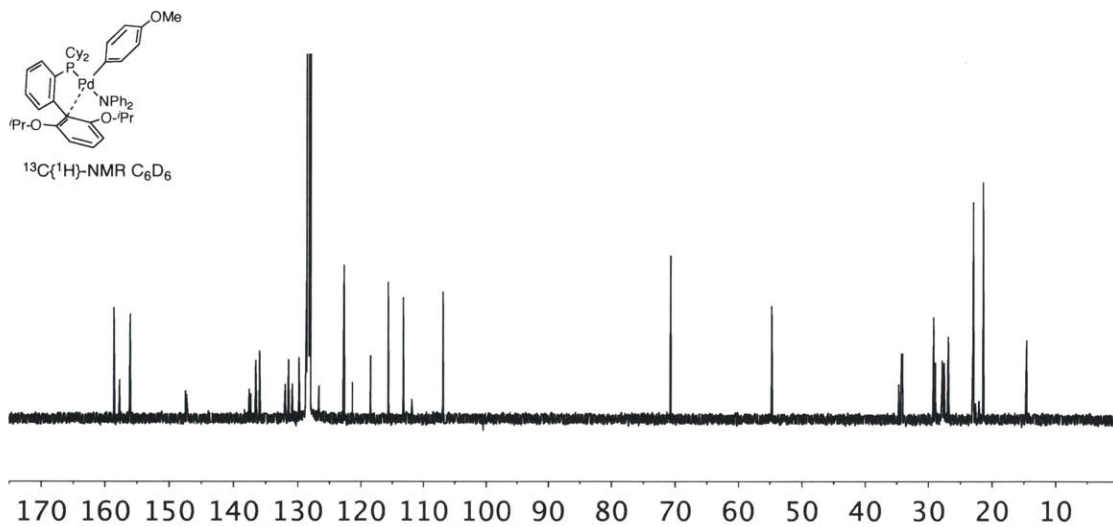
$^{31}P\{^1H\}$-NMR C_6D_6

1.4.16.2.5. RuPhos(Pd)(Ph)(NPhAr-*p*OMe) Amido Complex A1g

^1H-NMR C_6D_6

$^{13}C\{^1H\}$-NMR C_6D_6
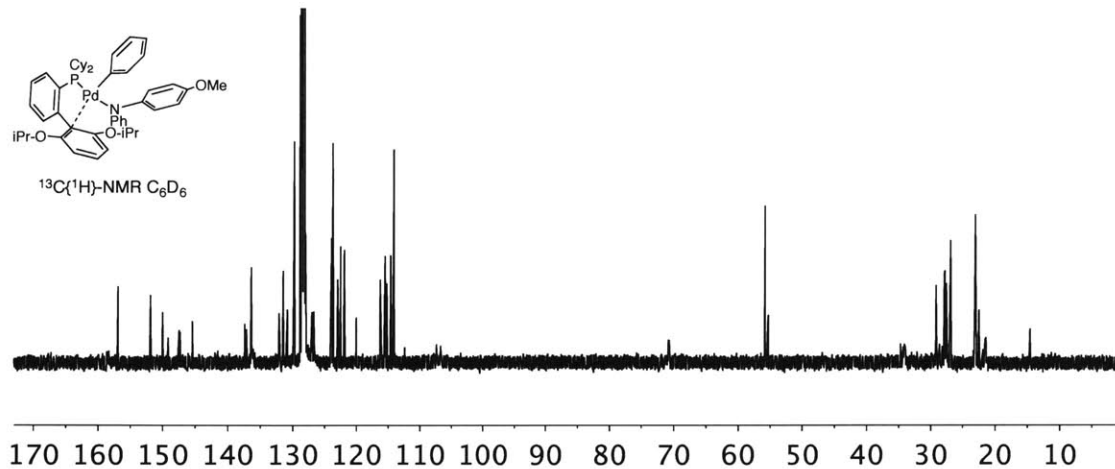
$^{31}P\{^1H\}$-NMR C_6D_6

1.4.16.2.6.   RuPhos(Pd)(Ph)(NPhAr-pCH$_3$) Amido Complex A1h

^{1}H-NMR C$_6$D$_6$

^{13}C{^{1}H}-NMR C$_6$D$_6$
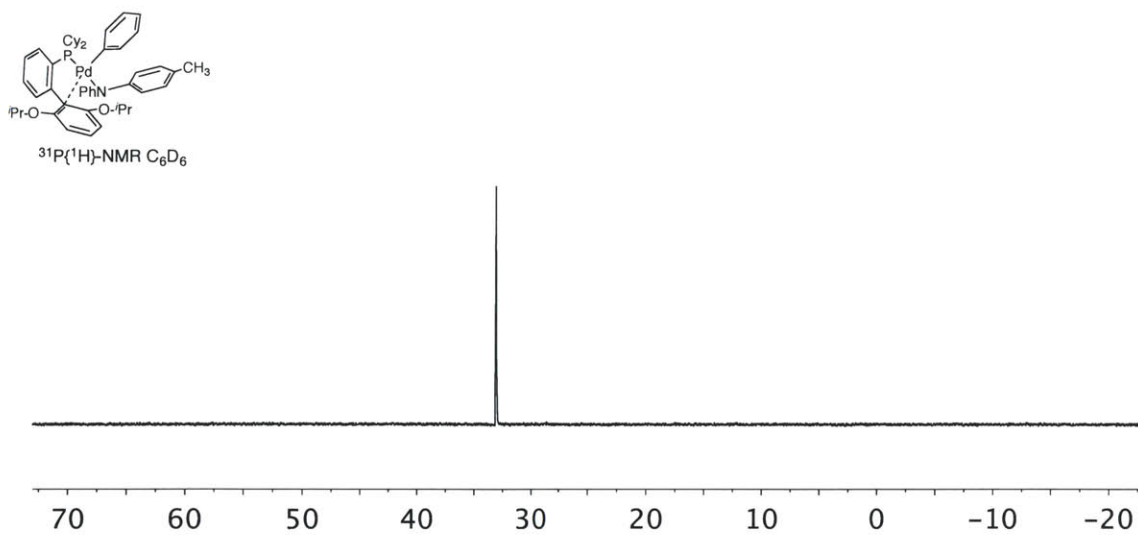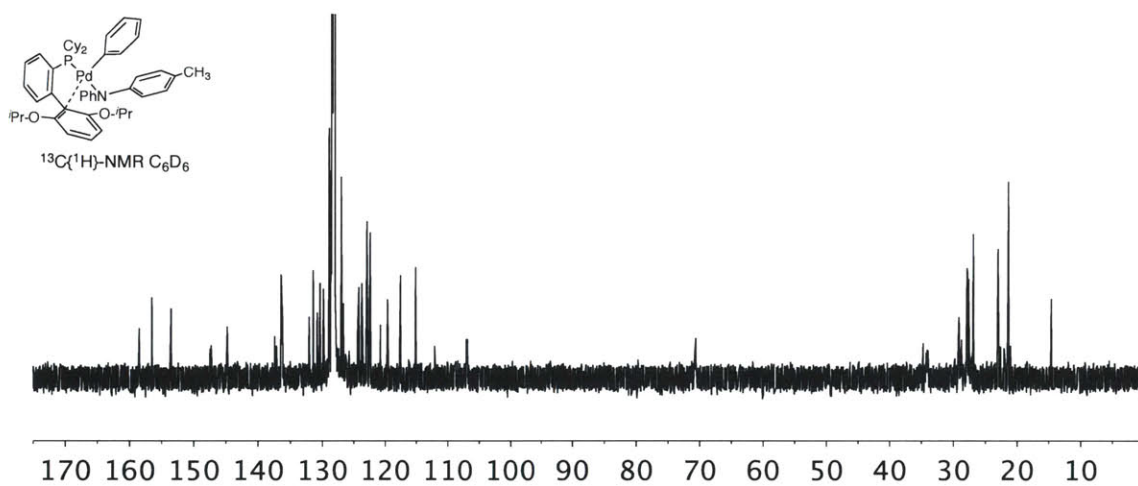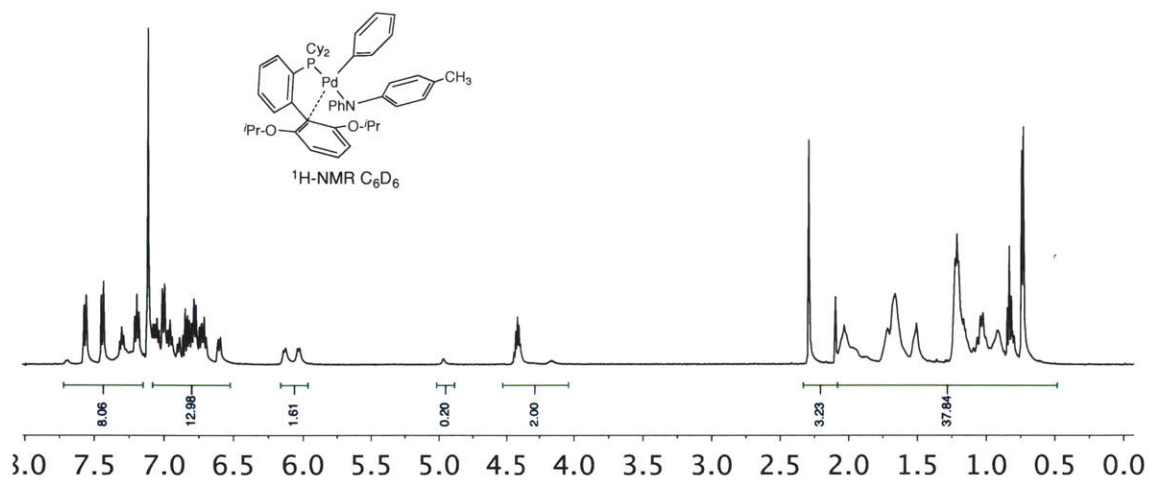
^{31}P{^{1}H}-NMR C$_6$D$_6$

1.4.16.2.7.   RuPhos(Pd)(Ph)(NPhAr-*m*OMe) Amido Complex A1i

^{1}H-NMR C$_6$D$_6$

^{13}C{^{1}H}-NMR C$_6$D$_6$

^{31}P{^{1}H}-NMR C$_6$D$_6$

| | | | | | | | | | |
|70|60|50|40|30|20|10|0|−10|−20|
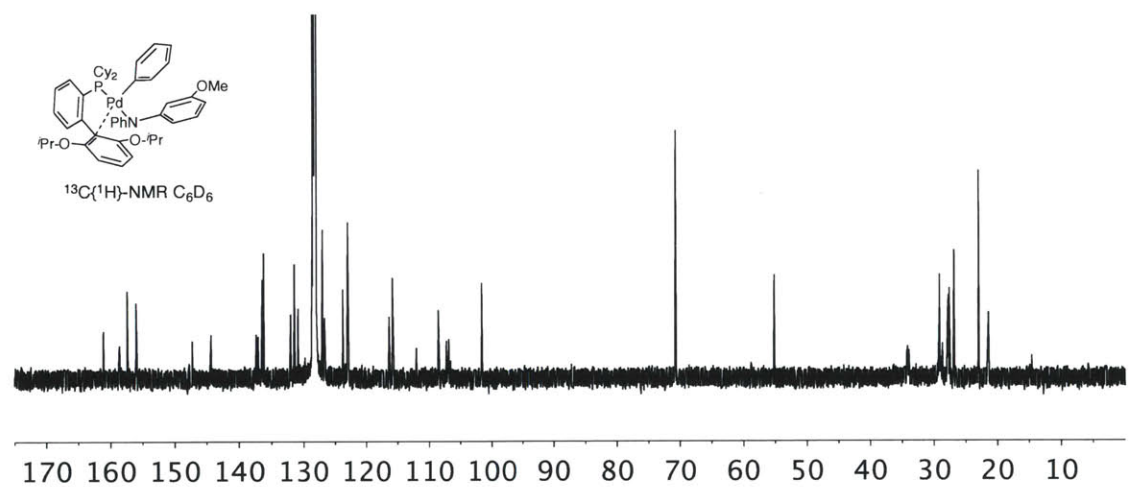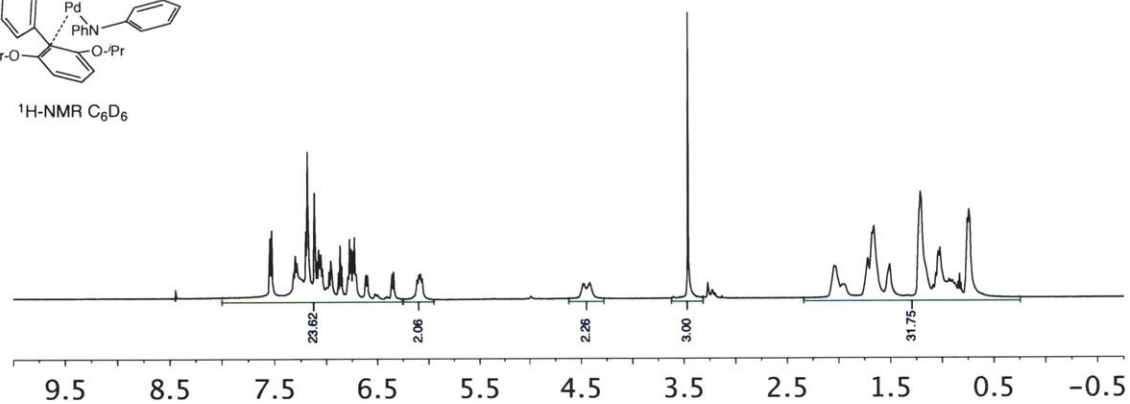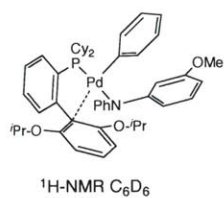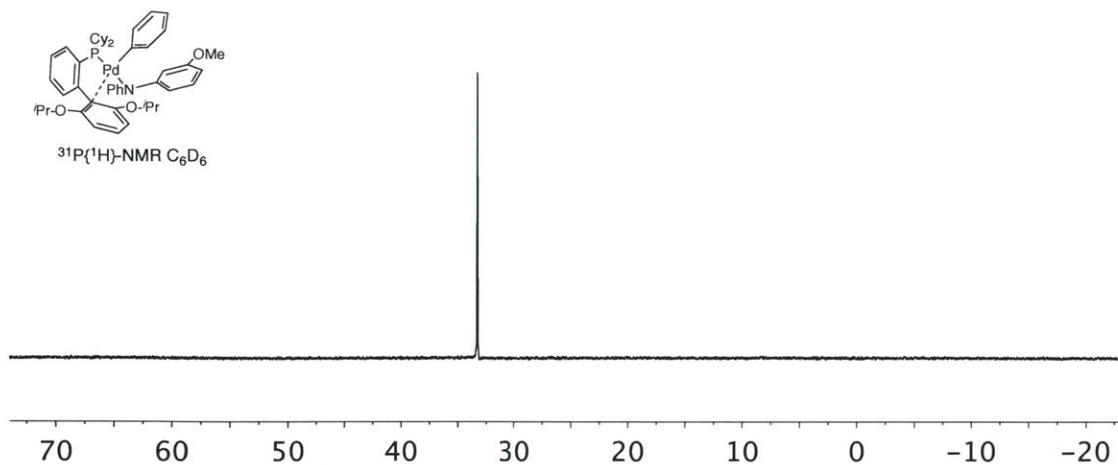
1.4.16.3. Ligand OA Complexes

1.4.16.3.1. SPhos(Pd)(Ar-*m*OMe)Br Complex OA2

^{1}H-NMR CD$_2$Cl$_2$

| | | | | | | | | | | |
|9.5|8.5|7.5|6.5|5.5|4.5|3.5|2.5|1.5|0.5|−0.5|

11.33   9.00   0.46   21.77
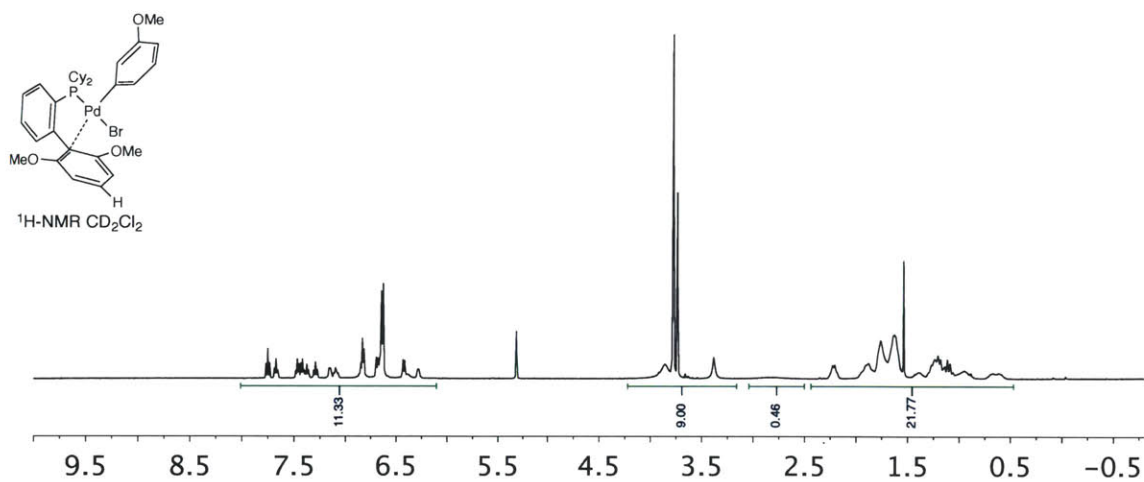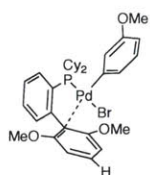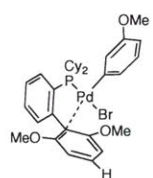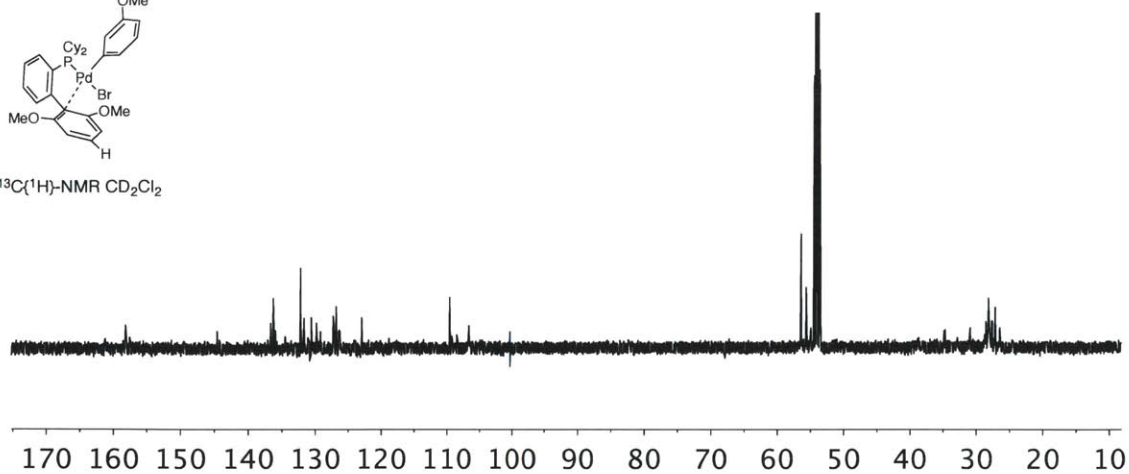
^{13}C{^{1}H}-NMR CD$_2$Cl$_2$

^{31}P{^{1}H}-NMR CD$_2$Cl$_2$

1.4.16.3.2. **Hybrid(Pd)(Ar-*m*OMe)(Br) Complex OA3**

MeO
Cy₂
P
Pd
Br
O-ⁱPr
ⁱPr-O

MeO

MeO

¹H-NMR CDCl₃

0.37
0.85
4.12
3.24
2.02
0.86
1.28
0.86
5.00
1.46
4.21
2.97
1.10
0.75
56.05

9.5   8.5   7.5   6.5   5.5   4.5   3.5   2.5   1.5   0.5   -0.5

OMe

MeO
Cy₂
P
Pd
Br
O-ⁱPr
ⁱPr-O

MeO

¹³C{¹H}-NMR CDCl₃

170 160 150 140 130 120 110 100 90 80 70 60 50 40 30 20 10 0

OMe

MeO
Cy₂
P
Pd
Br
O-ⁱPr
ⁱPr-O

MeO

³¹P{¹H}-NMR CDCl₃

70   60   50   40   30   20   10   0   -10   -20
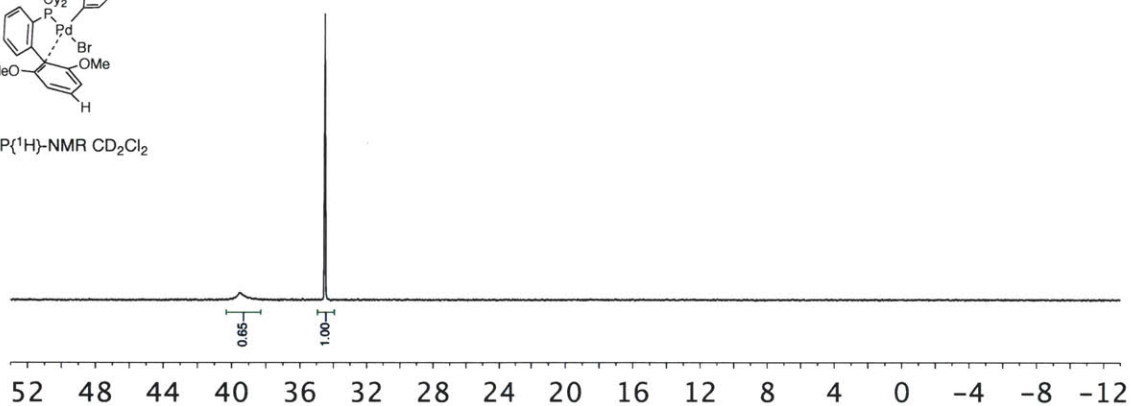
1.4.16.3.3.   MethoxySPhos(Pd)(Ar-*m*OMe)(Br) Complex OA4
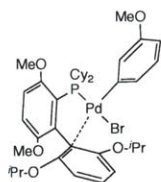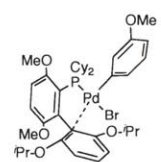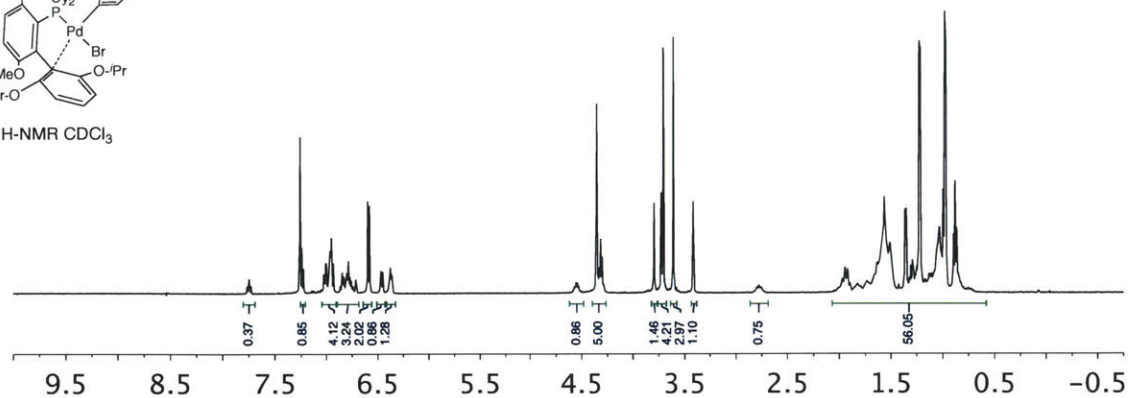
^{1}H-NMR CDCl$_3$
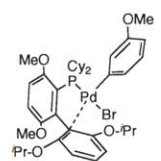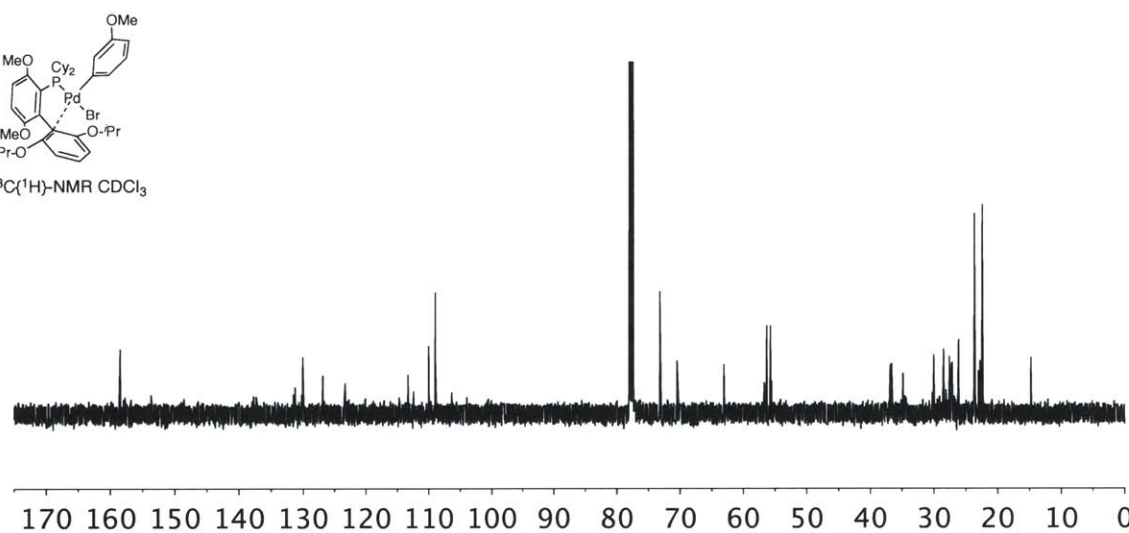
^{13}C{^{1}H}-NMR CDCl$_3$

^{31}P{^{1}H}-NMR CDCl$_3$

1.4.16.3.4.   AminoSPhos(Pd)(Ar-*m*OMe)(Br) Complex OA5

¹H-NMR CDCl₃

¹³C{¹H}-NMR CDCl₃
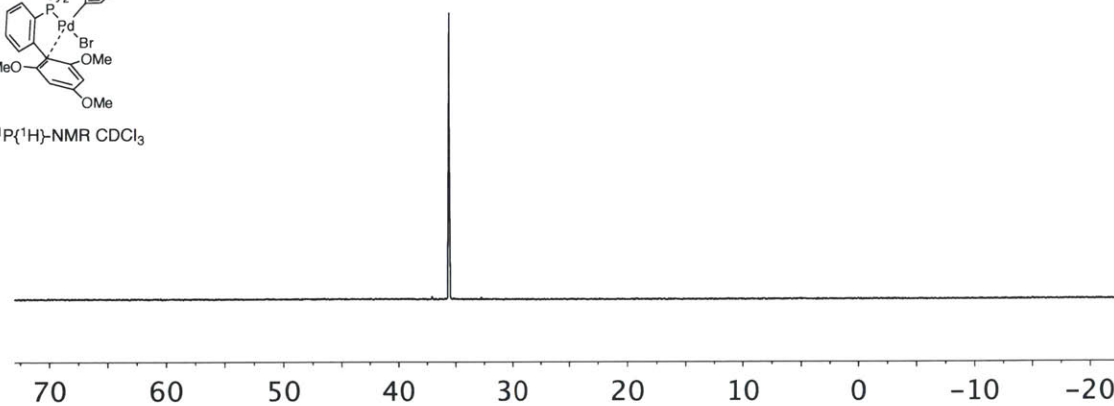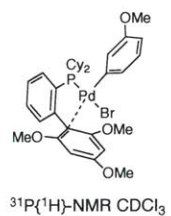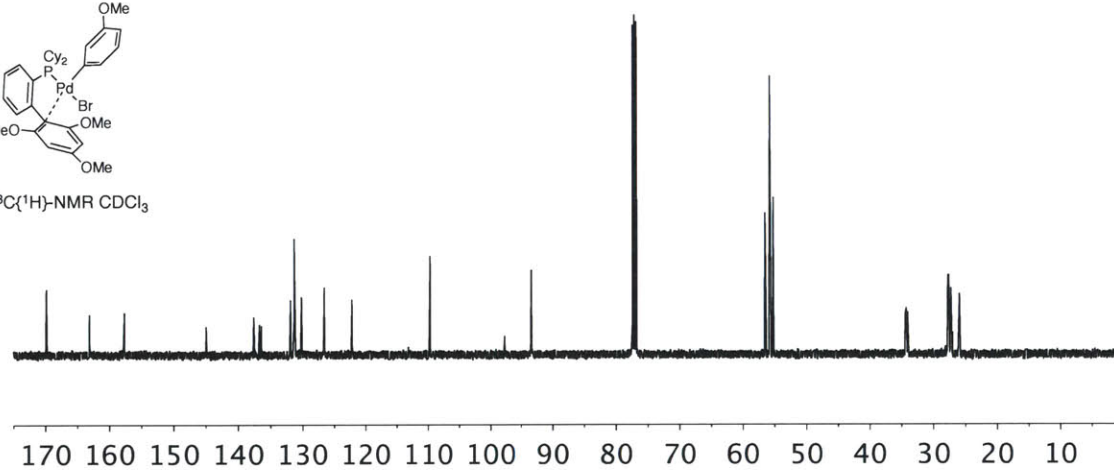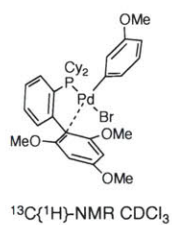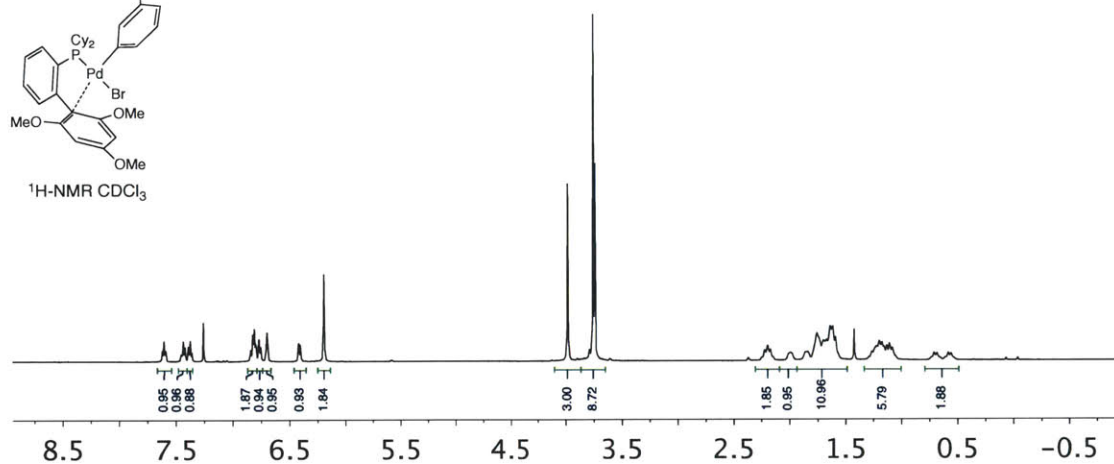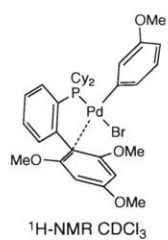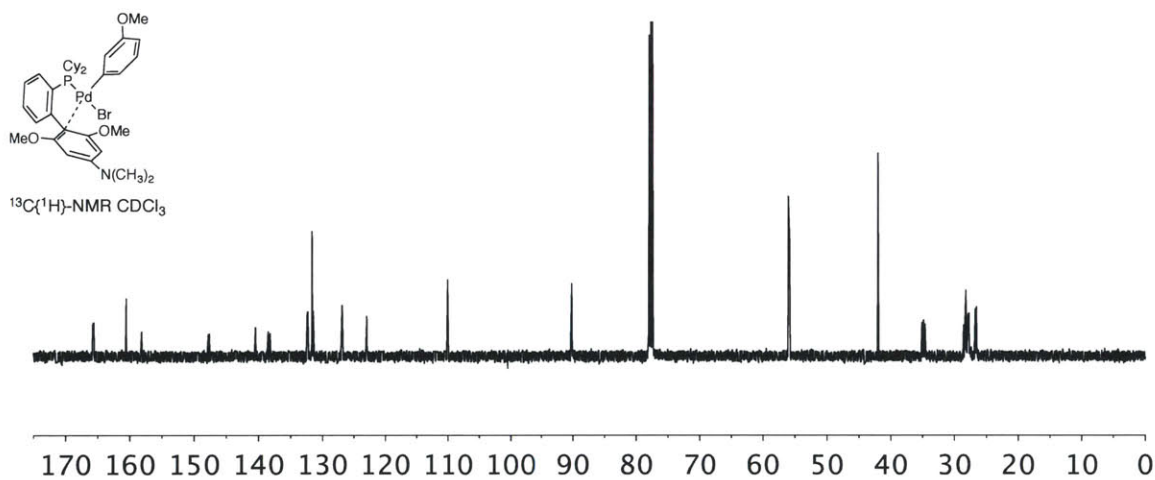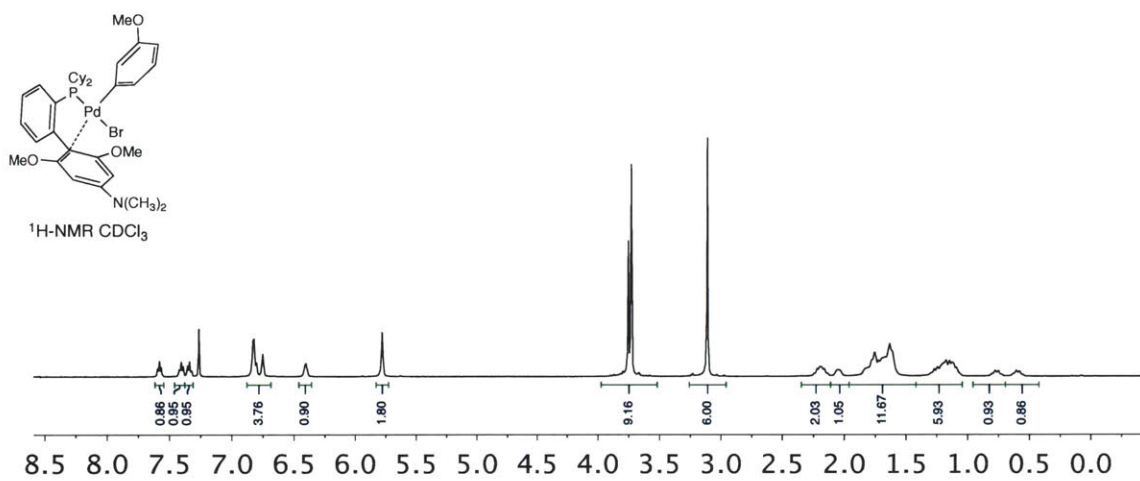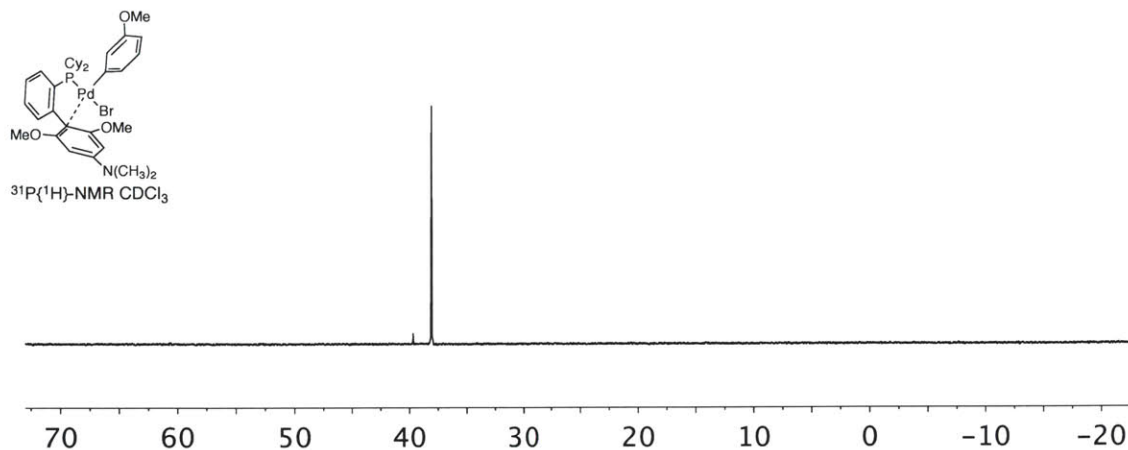
1.4.16.3.5. BrettPhos(Pd)(Ar-*m*OMe)Br Complex OA6

$^{31}P\{^1H\}$-NMR CD_2Cl_2

1.4.16.3.6.　　CPhos(Pd)(Ar-*m*OMe)(Br) Complex OA9

^1H-NMR $CDCl_3$

$^{13}C\{^1H\}$-NMR CDCl$_3$

170 160 150 140 130 120 110 100 90 80 70 60 50 40 30 20 10 0

$^{31}P\{^1H\}$-NMR CDCl$_3$

70 60 50 40 30 20 10 0 −10 −20
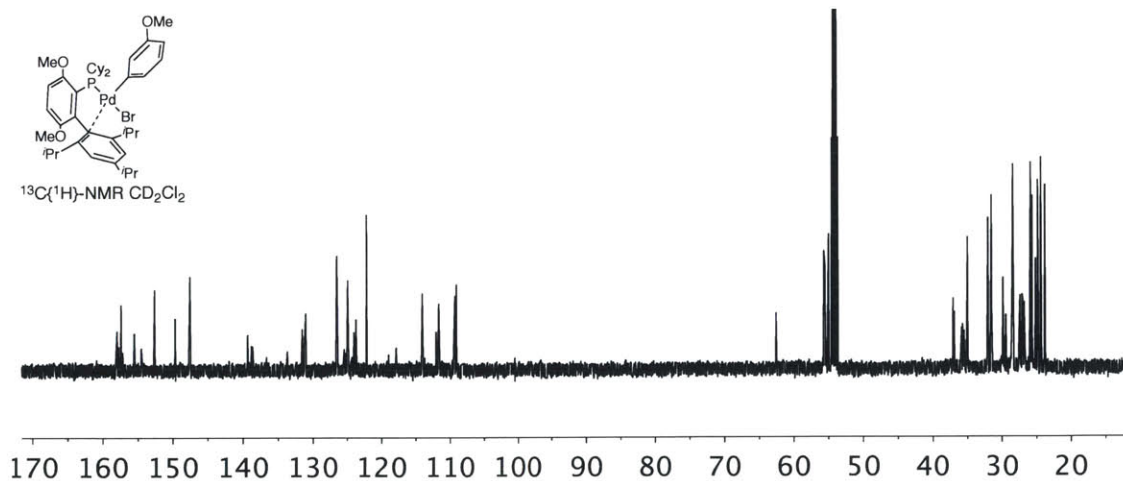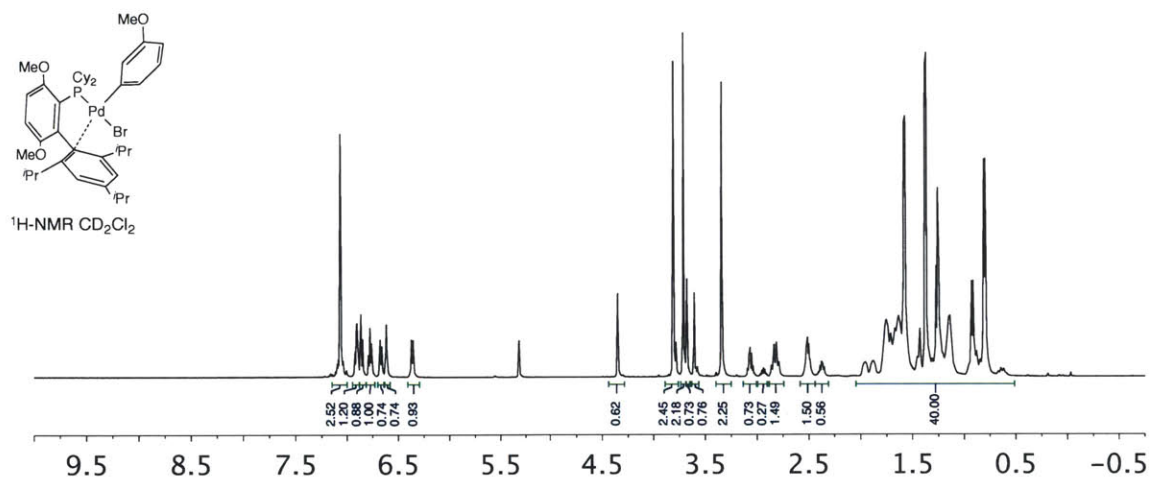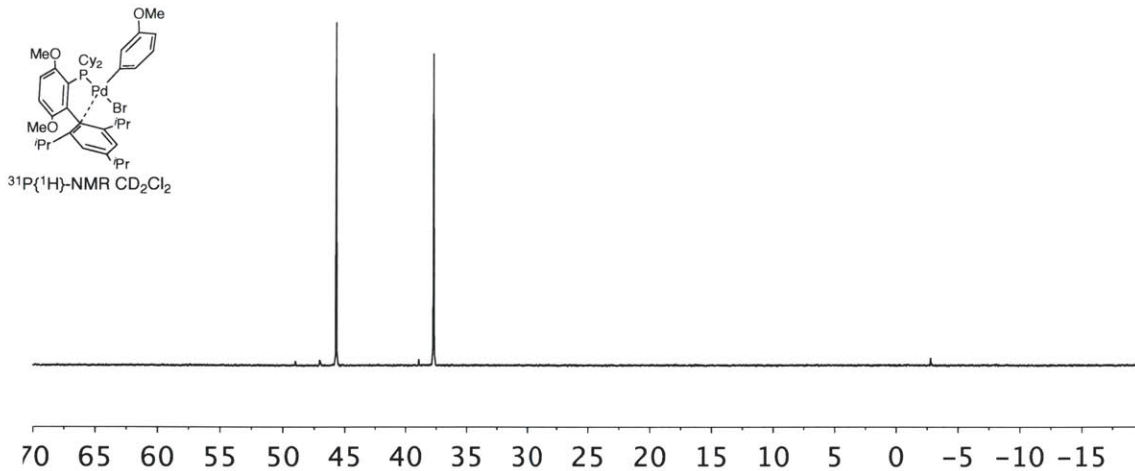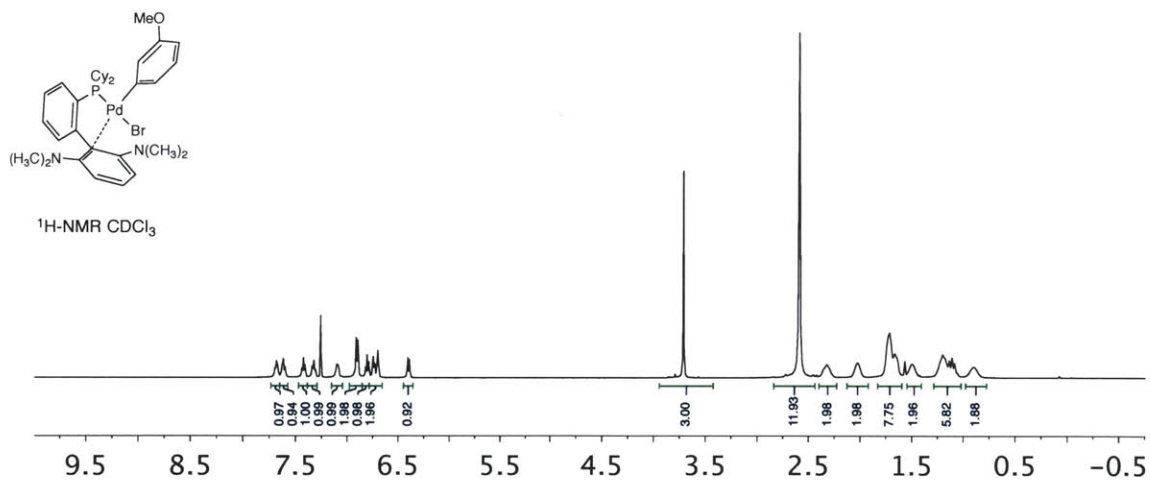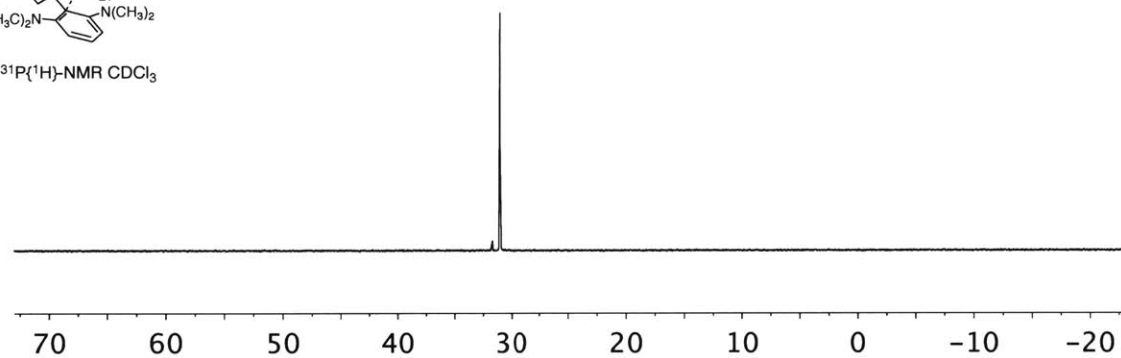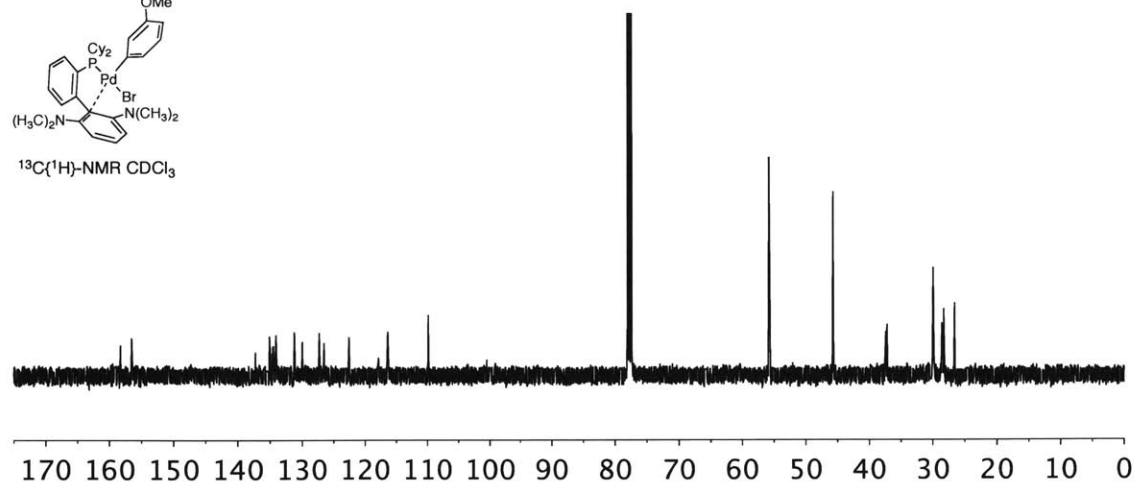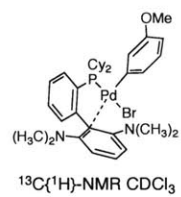
1.4.16.4. Ligand Amido Complexes

1.4.16.4.1. SPhos(Pd)(Ar-*m*OMe)(NPh$_2$) Amido Complex A2

^{1}H-NMR C$_6$D$_6$

^{13}C{^{1}H}-NMR C$_6$D$_6$

^{31}P{^{1}H}-NMR C$_6$D$_6$

119
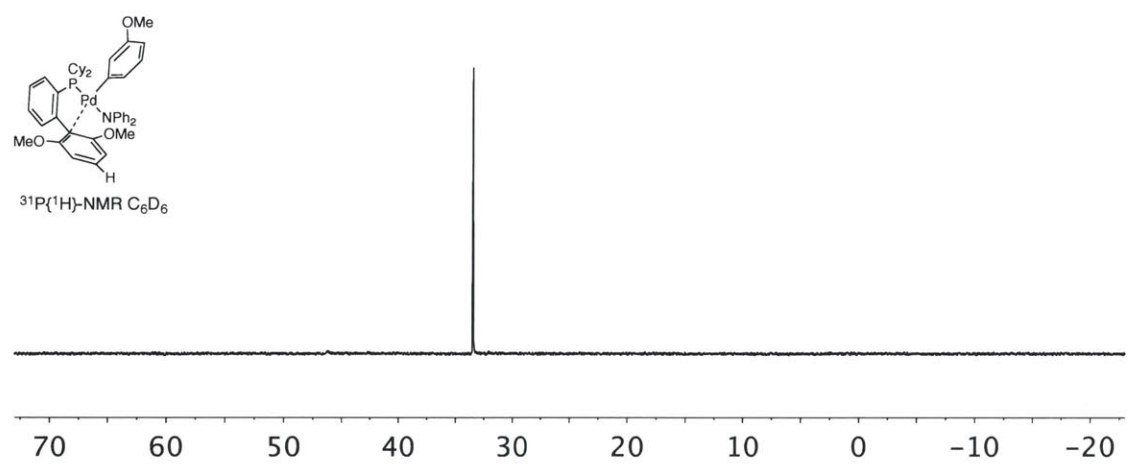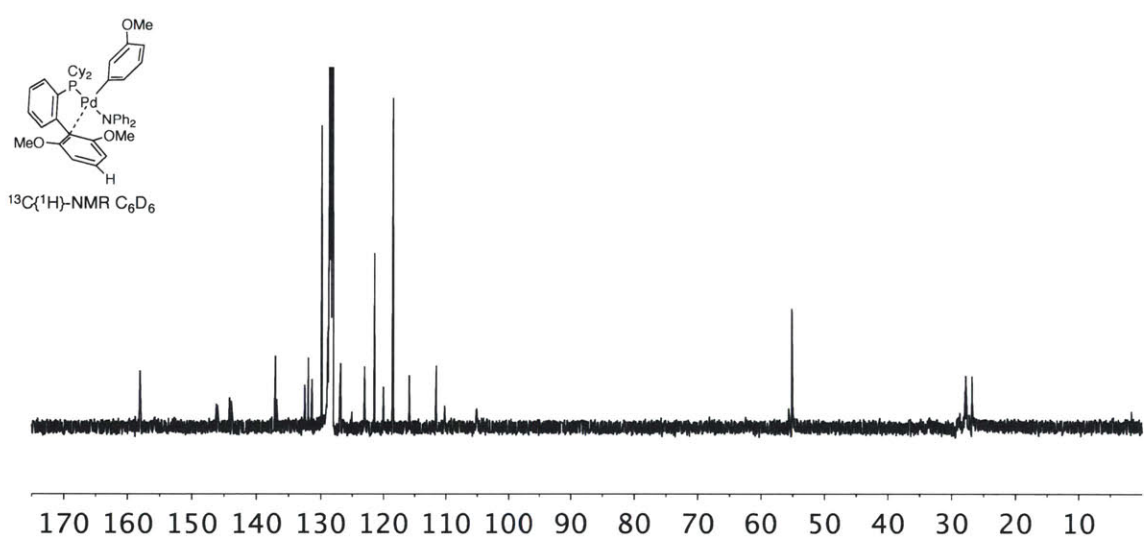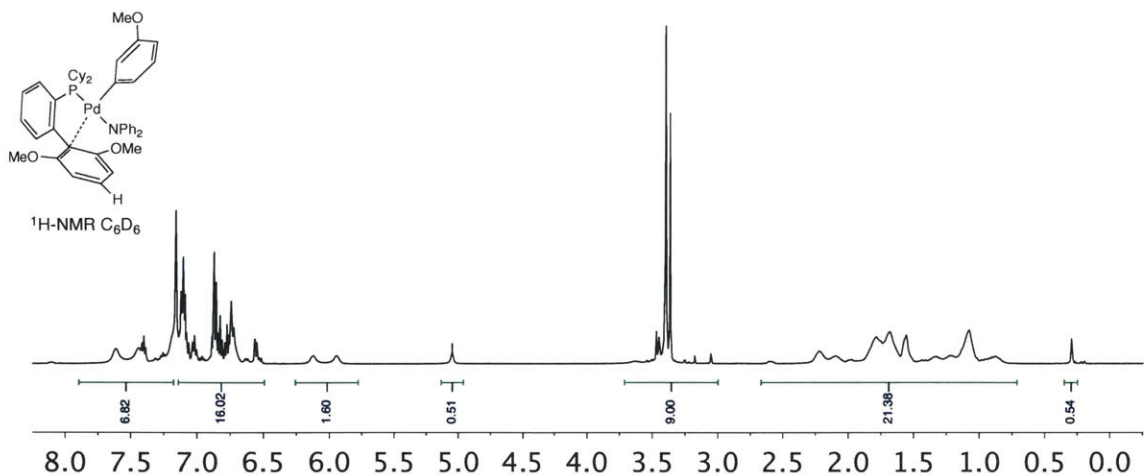
1.4.16.4.2.   Hybrid(Pd)(Ar-*m*OMe)(NPh₂) Amido Complex A3

^{1}H-NMR C₆D₆

^{13}C{^{1}H}-NMR C₆D₆
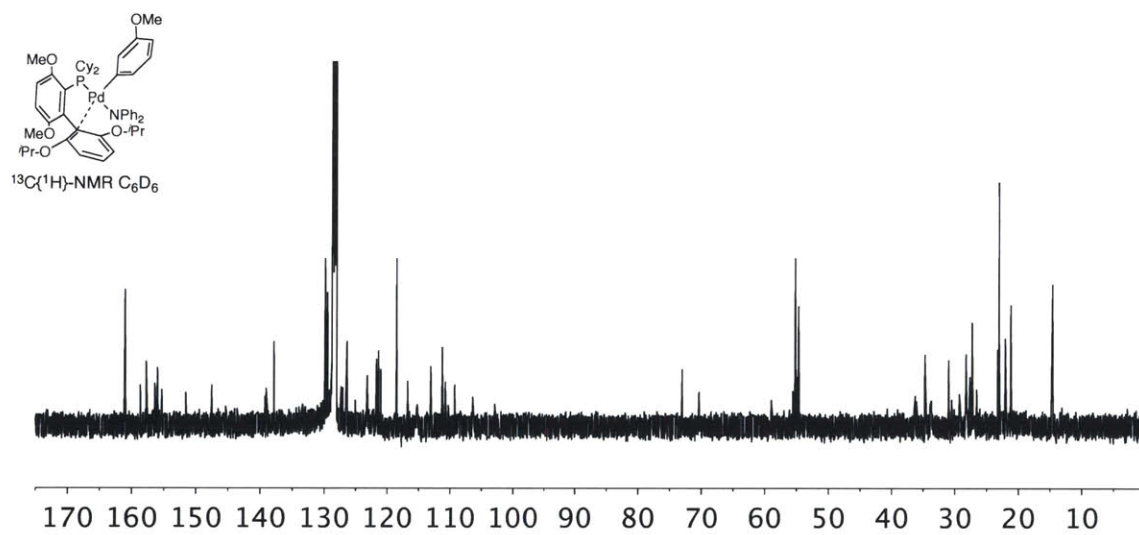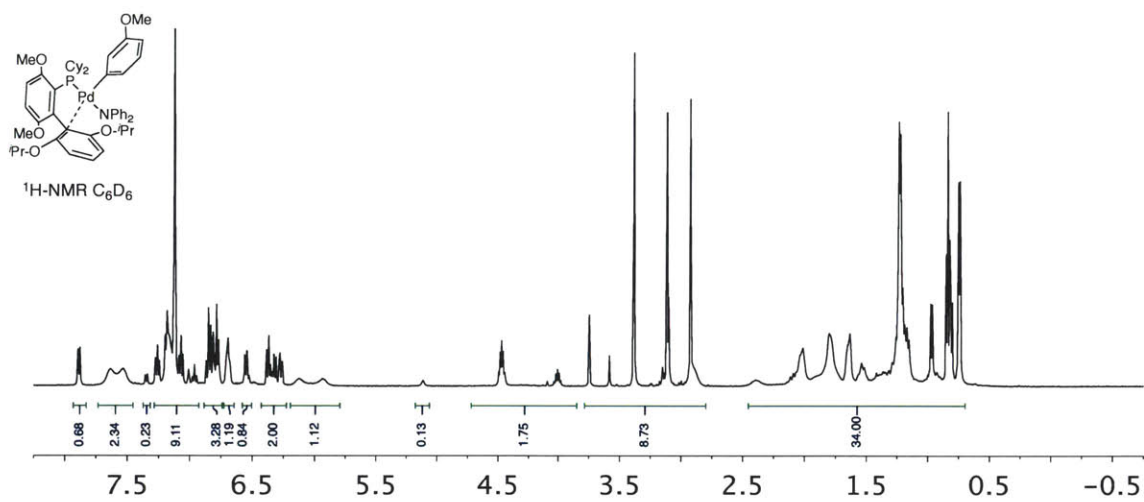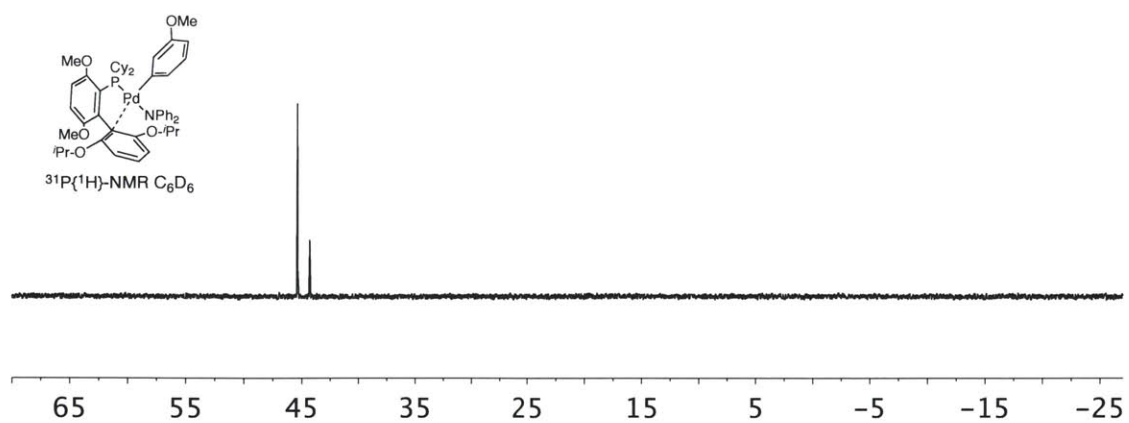
$^{31}P\{^1H\}$-NMR C_6D_6

1.4.16.4.3.   MethoxySPhos(Pd)(Ar-*m*OMe)(NPh$_2$) Amido Complex A4

^1H-NMR C_6D_6

7.09   17.60   12.00   36.14

$^{13}C\{^1H\}$-NMR C_6D_6
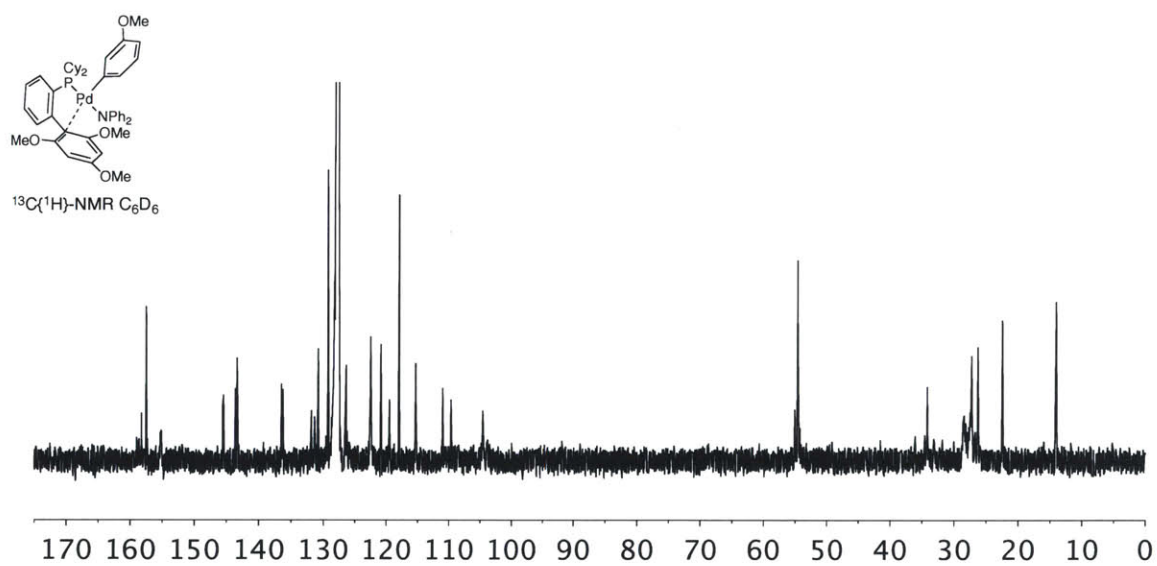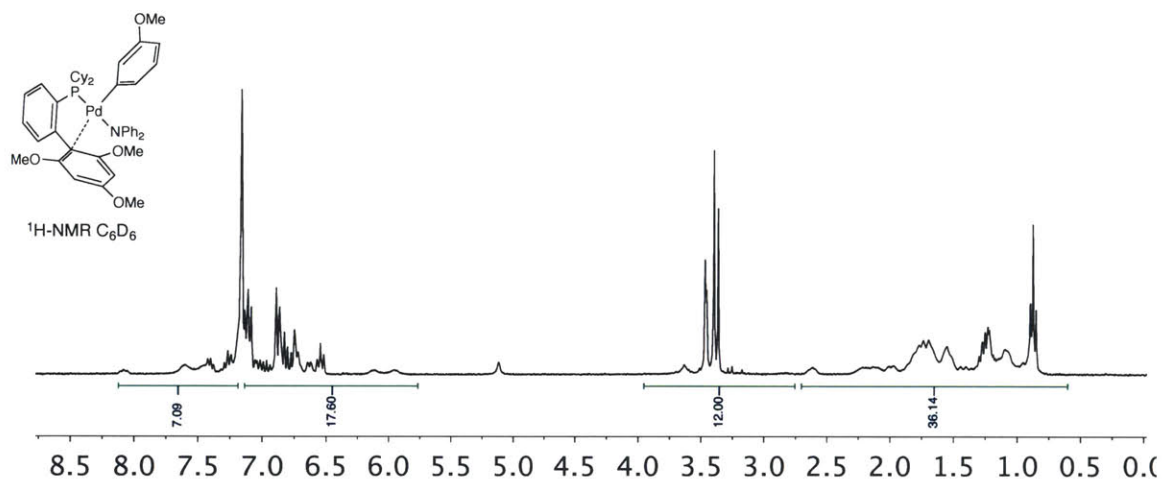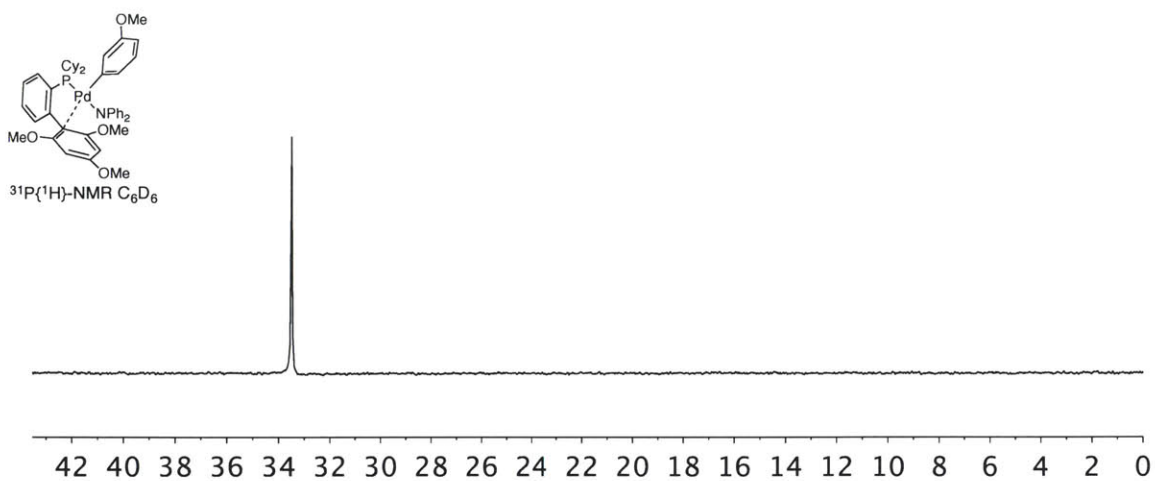
$^{31}P\{^1H\}$–NMR C_6D_6

1.4.16.4.4. AminoSPhos(Pd)(Ar-*m*OMe)(NPh₂) Amido Complex A5

^1H-NMR C_6D_6

^{13}C{^{1}H}-NMR C$_6$D$_6$

170 160 150 140 130 120 110 100 90 80 70 60 50 40 30 20 10

^{31}P-NMR C$_6$D$_6$

70 60 50 40 30 20 10 0 −10 −20
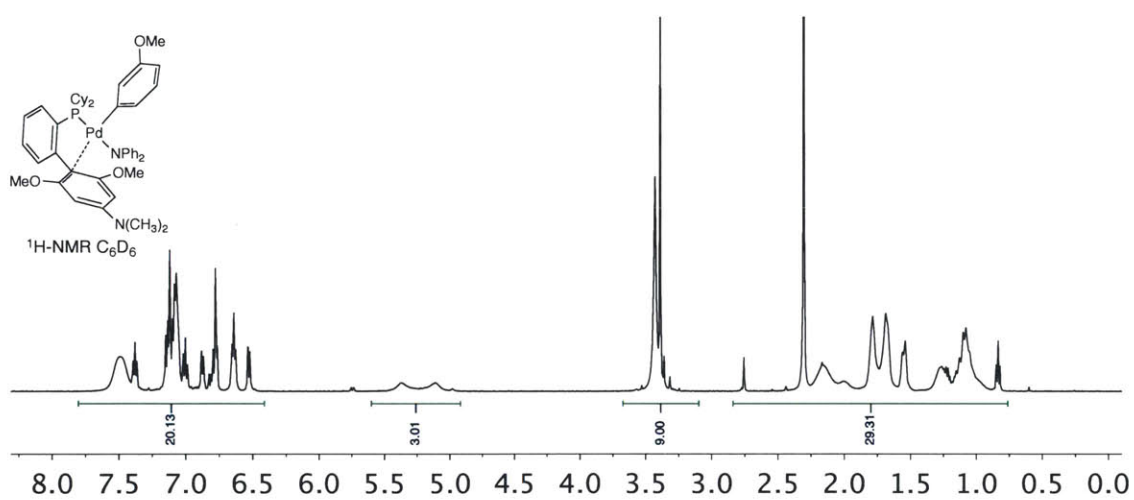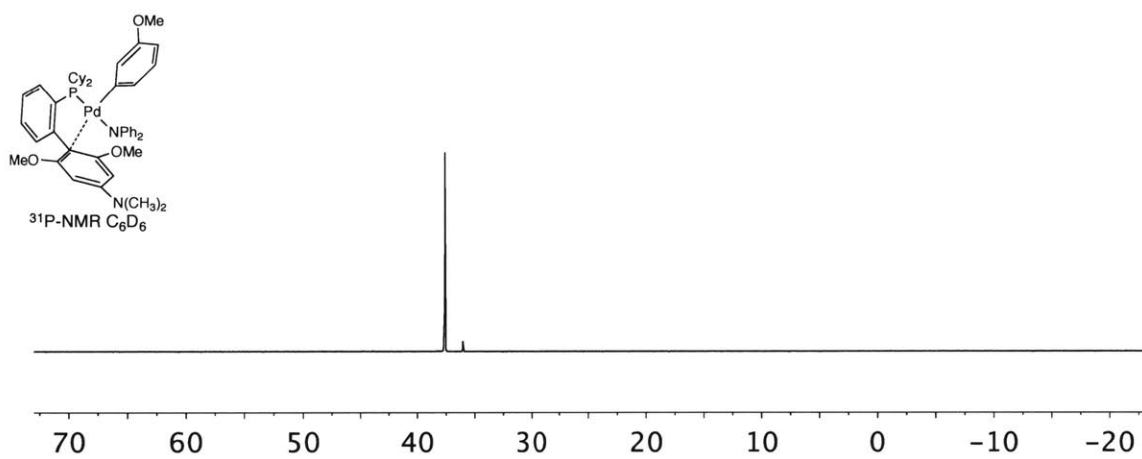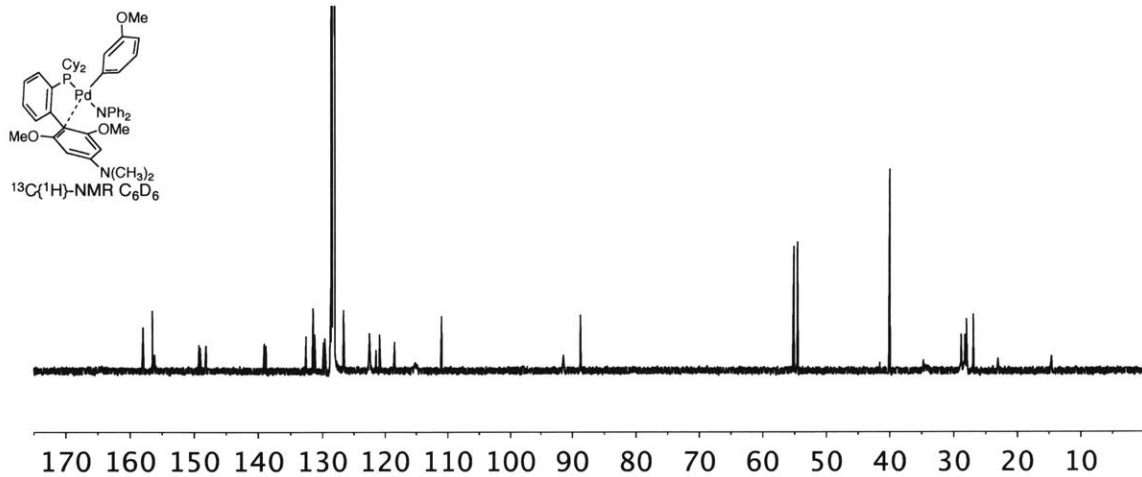
1.4.16.5. Ligand Synthesis

1.4.16.5.1. Ligand L5 AminoSPhos
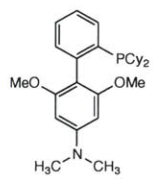
^{1}H-NMR CDCl$_3$
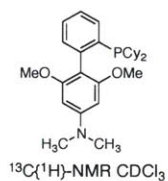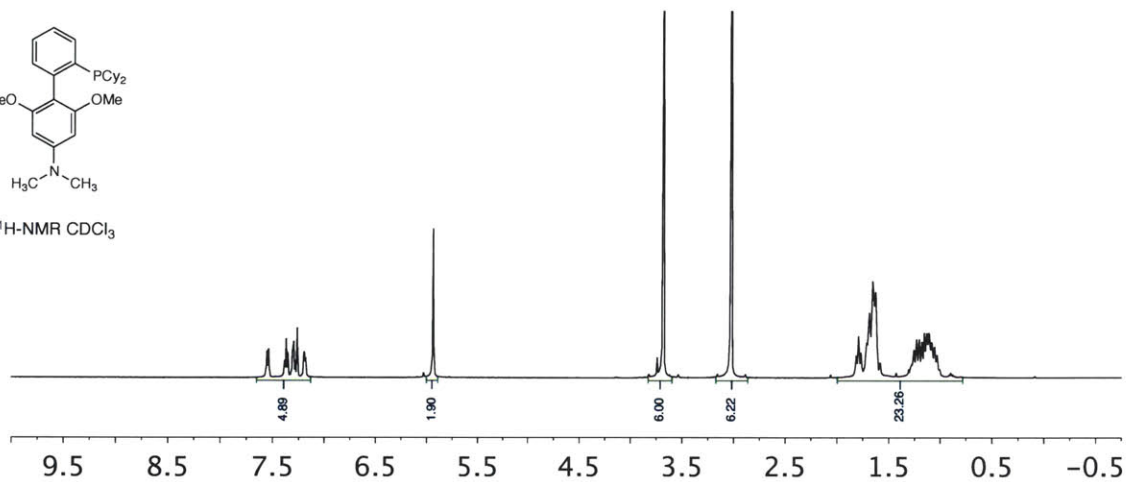
^{13}C{^{1}H}-NMR CDCl$_3$
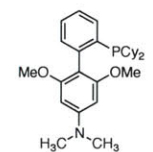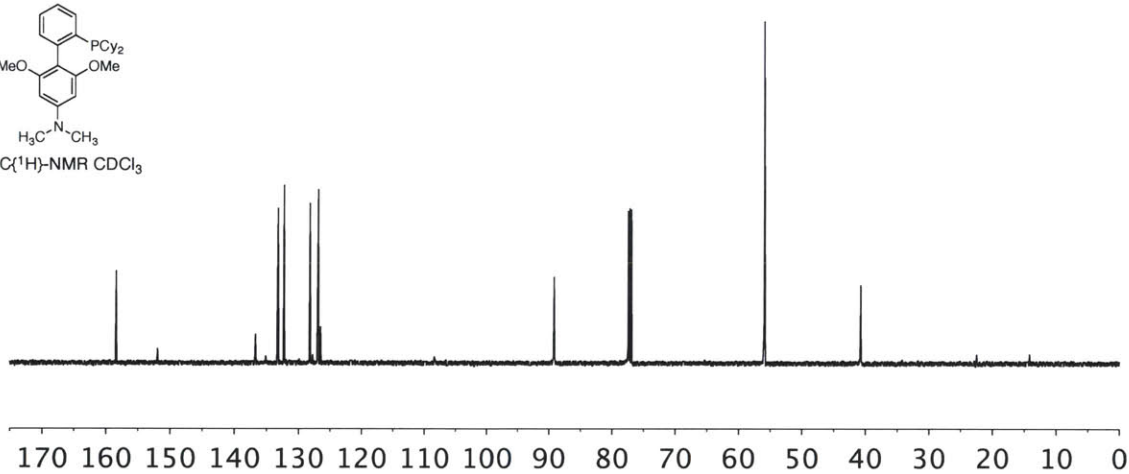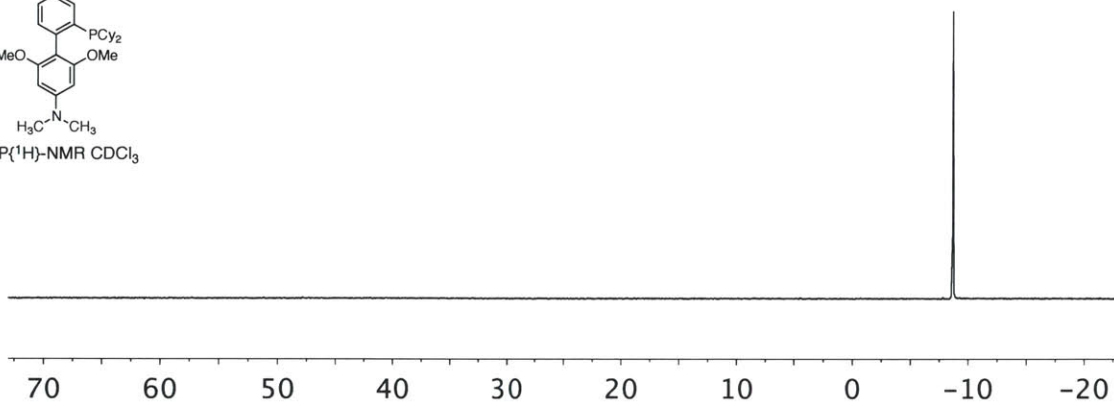
^{31}P{^{1}H}-NMR CDCl$_3$

1.4.16.5.2.   Ligand L5 AminoSPhos Biaryl Precursor
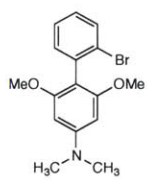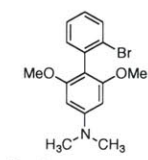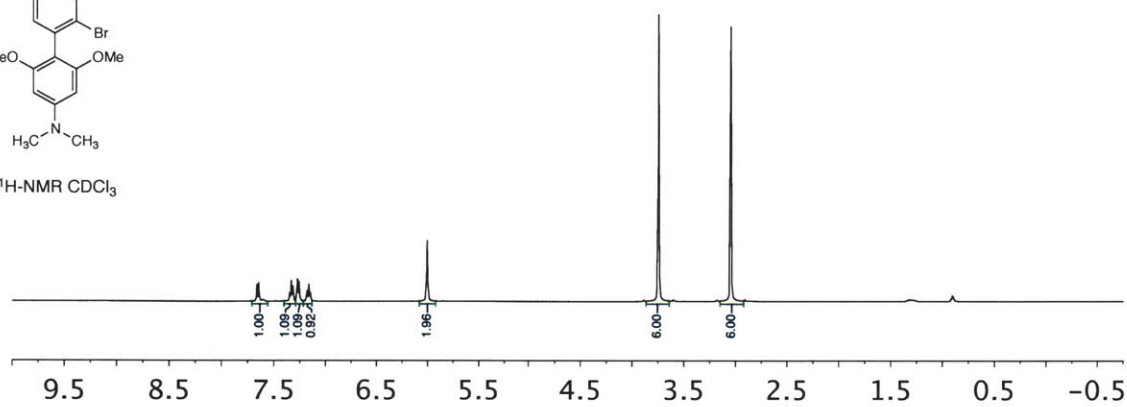
¹H-NMR CDCl₃
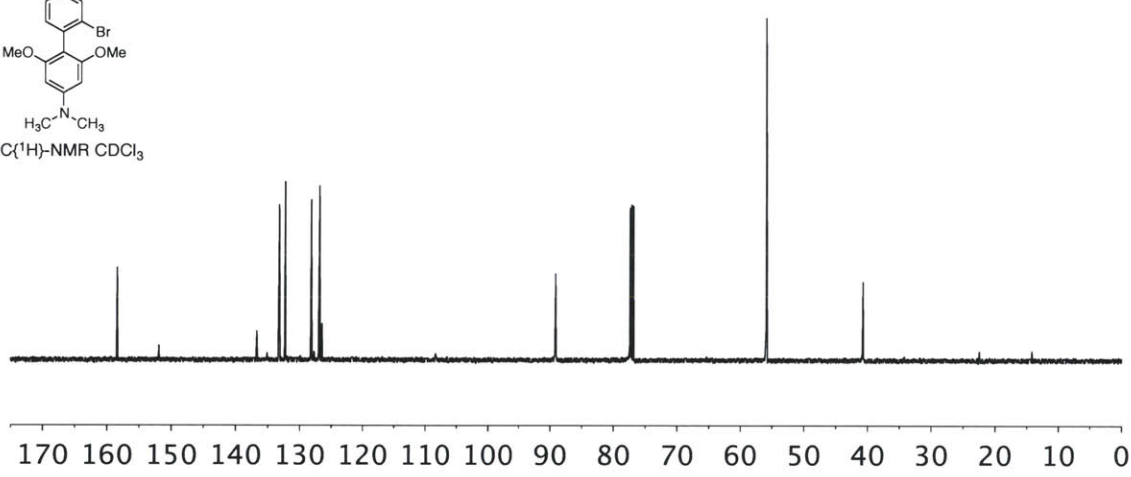
¹³C{¹H}-NMR CDCl₃

1.4.16.5.3.   Ligand L5 AminoSPhos "Lower" Aryl Ring

MeO ⟍ ⟋ OMe

H₃C ⟍N⟋ CH₃

¹H-NMR CCl₂D₂

3.01

6.58

6.45

7.5 7.0 6.5 6.0 5.5 5.0 4.5 4.0 3.5 3.0 2.5 2.0 1.5 1.0 0.5 0.0

MeO ⟍ ⟋ OMe

H₃C ⟍N⟋ CH₃

¹³C{¹H}-NMR CD₂Cl₂

240 220 200 180 160 140 120 100 80 60 40 20 0 −20 −40

1.4.16.5.4.   Hybrid Ligand L3

OMe

MeO—[ring]—PCy₂

iPr-O—[ring]—O-iPr

¹H-NMR CDCl₃

0.89 1.00 0.93 1.90 2.00 3.03 2.93 1.87 8.08 24.19

9.5 8.5 7.5 6.5 5.5 4.5 3.5 2.5 1.5 0.5 −0.5

OMe

MeO—[ring]—PCy₂

iPr-O—[ring]—O-iPr

¹³C{¹H}-NMR CDCl₃

170 160 150 140 130 120 110 100 90 80 70 60 50 40 30 20 10 0

OMe

MeO—[ring]—PCy₂

iPr-O—[ring]—O-iPr

³¹P{¹H}-NMR CDCl₃

70 60 50 40 30 20 10 0 −10 −20
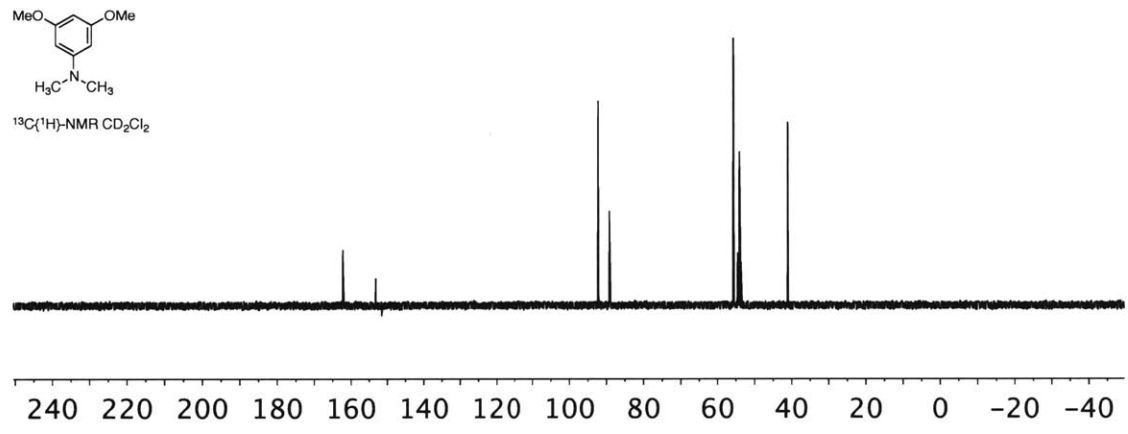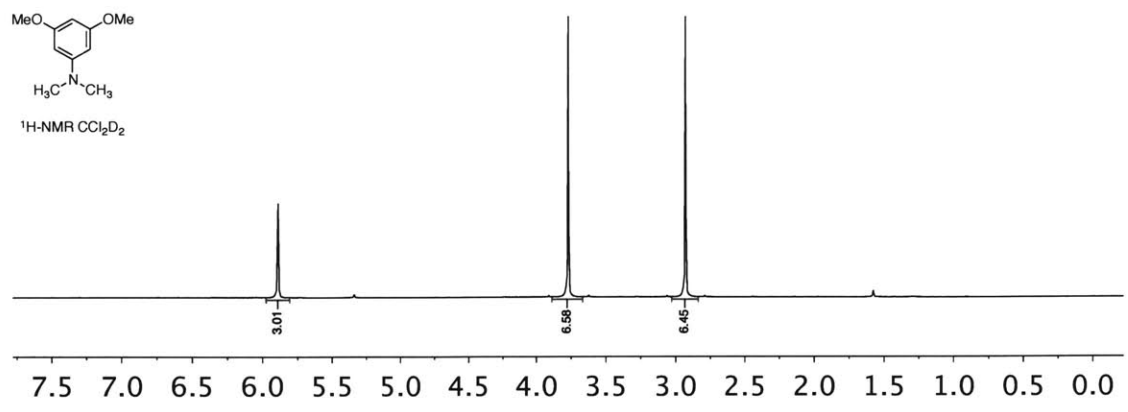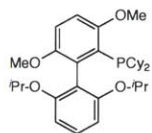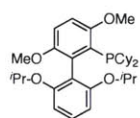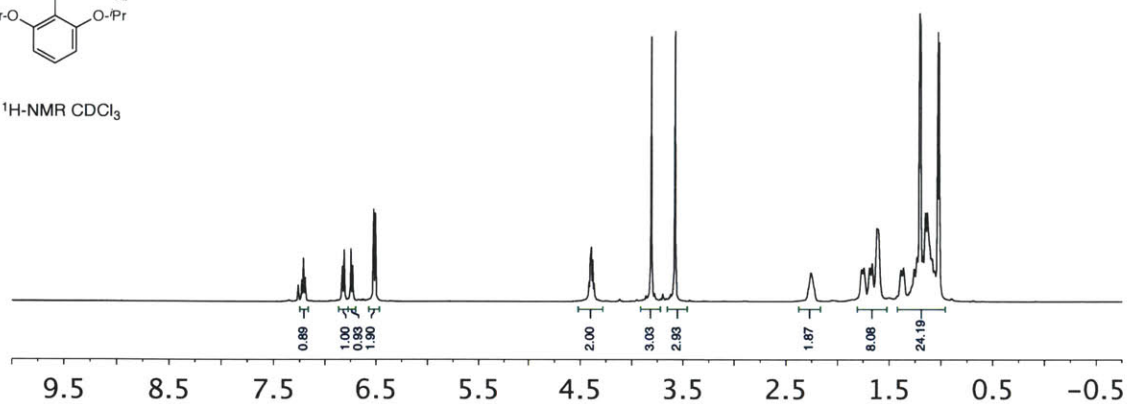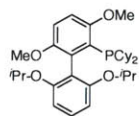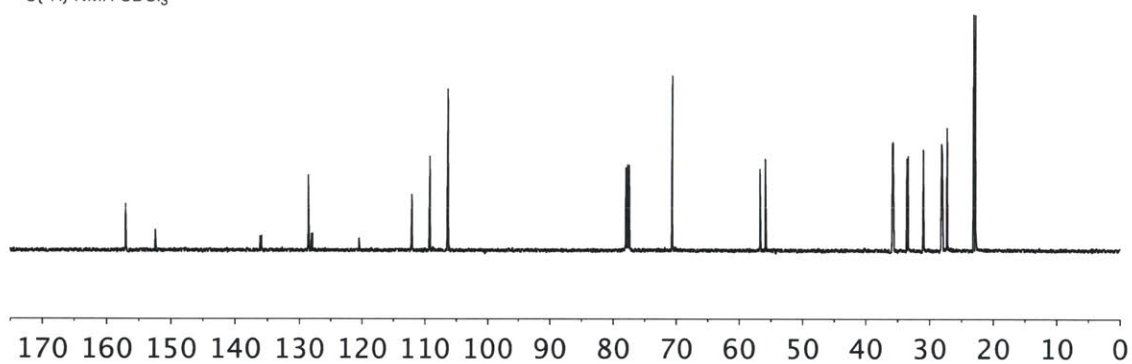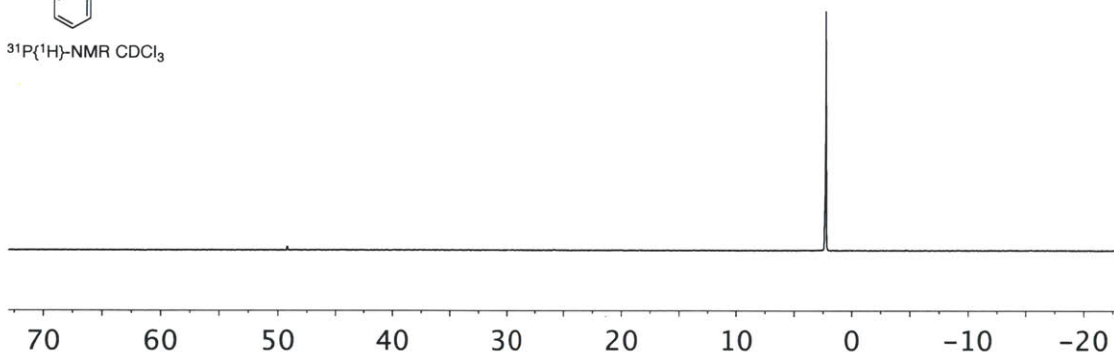
1.4.16.5.5.   BrettPhos Hybrid Ligand L3 Biaryl Precursor
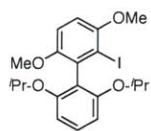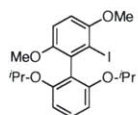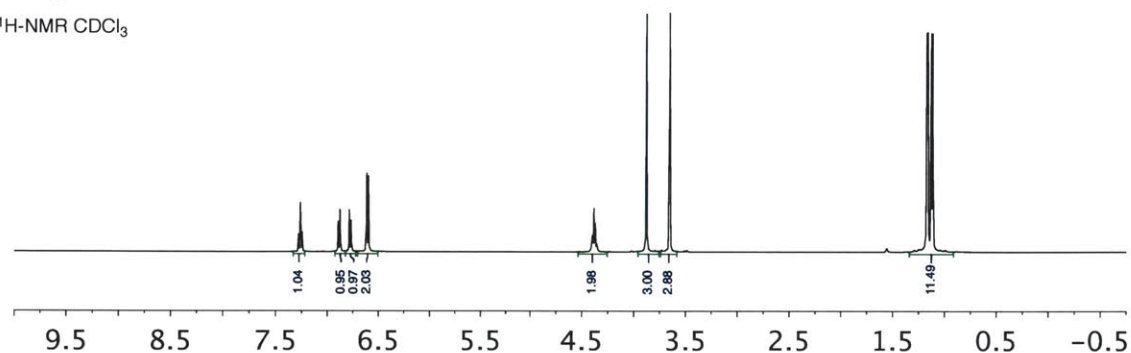
¹H-NMR CDCl₃

¹³C{¹H}-NMR CDCl₃
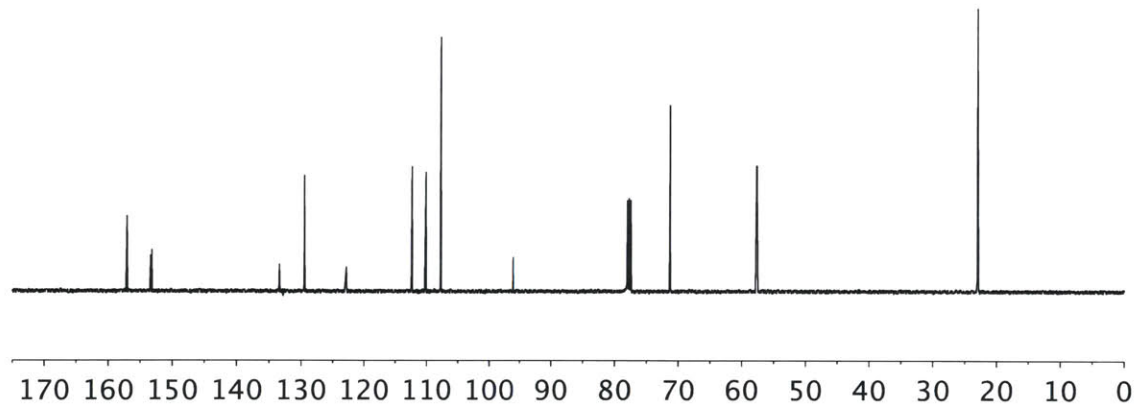
1.5. References

1) a) Schlummer, B.; Scholz, U. *Adv. Synth. Catal.* **2004**, *346*, 1599. b) Surry, D. S.; Buchwald, S. L. *Angew. Chem., Int. Ed.* **2008**, *47*, 6338 c) Wolfe, J. P.; Wagaw, S.; Marcoux, J.-F.; Buchwald, S. L. *Acc. Chem. Res.* **1998**, *31*, 805. c) Affouard, C.; Crockett, R. D.; Diker, K.; Farrell, R. P.; Gorins, G.; Huckins, J. R.; Caille, S. *Org.*

Process Res. Dev. **2015**, *19*, 476. d) Buchwald, S. L.; Mauger, C.; Mignani, G.; Scholz, U. *Adv. Synth. Catal.* **2006**, *348*, 23. e) Surry, D. S.; Buchwald, S. L. *Chem. Sci.* **2011**, *2*, 27. f) Federsel, H.-J.; Hedberg, M.; Qvarnstrom, F. R.; Tian, *Org. Process Res. Dev.* **2008**, *12*, 512. g) Cooper, T. W. J.; Campbell, I. B.; Macdonald, S. J. F. *Angew. Chem., Int. Ed.* **2010**, *49*, 8082. h) Roughley, S. D.; Jordan, A. M. *J. Med. Chem.* **2011**, *54*, 3451. i) Walters, W. P.; Green, J.; Weiss, J. R.; Murcko, M. A. *J. Med. Chem.* **2011**, *54*, 6405.

2) a) Guram, A. S.; Rennels, R. A.; Buchwald, S. L. *Angew. Chem., Int. Ed.,* **1995**, *34*, 1348. b) Louie, J.; Hartwig, J. F. *Tetrahedron Lett.* **1995**, *36*, 3609. c) Kosugi, M.; Kameyama, M.; Migita, T. *Chem. Lett.* **1983**, 927.

3) a) Boncella, J. M.; Villanueva, L. A. *J. Organometal. Chem.* **1994**, *465*, 297. b) Villanueva, L. A.; Abboud, K. A.; Boncella, J. M. *Organometallics* **1994**, *13*, 3921. c) Stambuli, J. P.; Incarvito, C. D.; Buhl, M.; Hartwig, J. F. *J. Am. Chem. Soc.* **2004**, *126*, 1184. d) Klinkenberg, J. L.; Hartwig, J. F. *J. Am. Chem. Soc.* **2010**, *132*, 11830. e) Yamashita, M.; Hartwig, J. F. *J. Am. Chem. Soc.* **2004**, *126*, 5344. f) Driver, M. S.; Hartwig, J. F. *J. Am. Chem. Soc.* **1995**, *117*, 4708. g) Driver, M. S.; Hartwig, J. F. *J. Am. Chem. Soc.* **1997**, *119*, 8232. h) Driver, M. S.; Hartwig, J. F. *J. Am. Chem. Soc.* **1996**, *118*, 7217.

4) a) Reductive Elimination, R. Hoffmann, in IUPAC. *Frontiers of Chemistry*, ed. K. J. Laidler, Pergamon Press, Oxford 1982, 247-263. b) Tatsumi, K. ; Hoffmann, R. ; Yamamoto, A. and Stille, J. K. *Bull. Chem. Soc., Japan*, **1981,** *54*, 1857.

5) The values determined in this study are comparable to those found for platinum based reductive eliminations. The $\Delta H^{\ddagger}$ and $\Delta S^{\ddagger}$ for the reductive elimination of biaryl from $Pt(PPh_3)_2(C_6H_4\text{-}pCH_3)_2$ has been reported to be 17.6 kcal/mol and -23 cal /(mol K). For the reductive elimination of ethane from $Pt(Me_3I(PMePh_2)_2)$, the reported values are 31 kcal/mol and 21 cal /(mol K). For the reductive elimination of 1,1,1-trifluoroethane from *cis*-$PtH(CH_2CF_3)(PPh_3)_2$ the reported values range from 25.4 to 23.9 kcal/mol and 7.8 to 2 cal /(mol K) and are dependent upon the reaction solvent. For references, see a) Brown, M. P.; Puddephatt, R. J.; Upton, C. E. E. *J. Organomet. Chem.* **1973**, *49*, C61. b) Braterman, P. S.; Cross, R. J.; Young, G. B. *J. Chem. Soc., Dalton Trans.* **1977**, 1892. c) Michelin, R. A.; Faglia, S.; Uguagliati, P. *Inorg. Chem.* **1983**, *22*, 1831.

6) a) Vicente, J.; Arcas, A.; Bautista, D.; Jones, P.G.; *Organometallics* **1997**, *16*, 2127. b) Casado, A. L.; Espinet, P. *Organometallics* **1998**, *17*, 954. c) for *trans*-effect see,

Langford, C. H.; Gray, H. B. *Ligand Substitution Processes*, 1966., and references therein, d) the *trans*-configuration has been shown to be energetically accessible for this class of ligands if the alkyl substituent on the phosphine are *tert*-butyl, see Milner, P. J.; Maimone, T. J.; Su, M.; Chen, J.; Muller, P.; Buchwald, S. L. *J. Am. Chem. Soc.* **2012**, *134*, 19922

7) We found no systematic difference between different batches. The reactions performed with 3-chloroanisole were done with the same batch of **OA1a**.

8) Chloride ions have been shown to also have an effect on palladium catalysis: (a) Amatore, C.; Jutand, A.; *Acc. Chem. Res.* **2000**, *33*, 314. (b) Kozuch, S.; Amatore, C.; Jutand, A.; Shaik, S. *Organometallics* **2005**, *24*, 2319. (c) Amatore, C.; Jutand, A.; Suarez, A. *J. Am. Chem. Soc.* **1993**, *115*, 9531. (d) Amatore, C.; Azzabi, M.; Jutand, A. *J. Am. Chem. Soc.* **1991**, *113*, 8375. (e) Jutand, A. *Appl. Organometal. Chem.* **2004**, *18*, 574.

9) a) Mann, G.; Baranano, D.; Hartwig, J. F.; Rheingold, A. L.; Guzei, I. A. *J. Am. Chem. Soc.* **1998**, *120*, 9205. b) Hartwig, J. F. *Inorg. Chem.* **2007**, *46*, 1936.

10) Biscoe, M. R.; Fors, B. P.; Buchwald, S. L. *J. Am. Chem. Soc.* **2008**, *130*, 6686.

11) Reid, S. M.; Boyle, R. C.; Mague, J. T.; Fink, M. J. *J. Am. Chem. Soc.* **2003**, *125*, 7816.

12) Presumably, the L_2Pd^0 complex is not stable in the presence of air particularly so in solution. Thus, a small amount of 3-iodoanisole was added to catalyst solution to form the palladium(II) complex *in situ.*

13) Barder, T. E.; Buchwald, S. L. *J. Am. Chem. Soc.* **2007**, *129*, 12003.

14) a) Ruiz-Castillo, P.; Blackmond, D. G.; Buchwald, S. *J. Am. Chem. Soc.* **2015**, *137*, 3085. b) Park, N. H.; Vinogradova, E. V.; Surry, D. S.; Buchwald, S. L. *Angew. Chem. Int. Ed* **2015**, *54*, 8259.

2. Oxidative Addition

2.1. Introduction:

Most studies of the C–N cross-coupling reaction focus on the "on-cycle" palladium intermediates. The reaction is commonly described in terms of elementary steps such as

oxidative addition,[1] amine binding,[2] deprotonation,[3] and reductive elimination.[4] These reaction steps describe the transformations between different "on-cycle" intermediates (Figure 1-1).

For the oxidative addition step (I to II), previous investigations into the role of the aryl halide and supporting phosphine ligand indicate a range of observed rate laws for oxidative addition of palladium(0) complexes with the aryl halide. Such a variation in rate laws between different electrophiles (ArI, ArBr, and ArCl) for a complex such as $((o\text{-tolyl})_3P)_2Pd$ suggests that more than one Pd(0) species may undergo oxidative addition with the aryl halide.[1e] A study by Klabunde demonstrated that palladium(0) atoms undergo oxidative addition to C_6F_5Cl, CH_3COCl, $n\text{-}C_3F_7I$,and several other organic substrates at temperatures of 77 K.[1k] This experiment suggests that phosphine ligands facilitate the oxidative addition step by preventing the aggregation and formation of palladium metal (palladium black). A study by Hartwig, has shown that the amine (N-methylpiperazine) can participate as a supporting ligand during the oxidative addition step. As shown in the results of this chapter, this observation will have implications for an L1-based palladium catalyzed reaction.

The reaction steps involved in the formation of II to III have also been described with publications rationalizing amine selectivity and amine binding to the palladium(II) center.[2] A publication by the Buchwald group studied the selectivity of different amines by exposing an (L2)Pd(Ph)Cl complex (5 mol %) to a solution of NaO^tamyl, chlorobenzene, and a binary mixture of dissimilar amines (e.g., morpholine/n-propylamine or morpholine/piperidine). This study rationalized the difference in selectivity in terms of Curtin-Hammett type kinetics.

For the case of reductive elimination from the amido complex (IV to I), the electronic effects of the coupling partners and the role of supporting ligand have been thoroughly explored. Our own studies of an L1-based palladium catalyst revealed that the amido complex (IV) was the resting state for the cross-coupling of diarylamines with different aryl halides. As previously mentioned, Hoffman employed EHT calculations elucidating the role of different molecular orbitals in facilitating this product-producing step.[3k-l] The theoretical calculations rationalized the ease by which T-shaped complexes undergo reductive elimination when compared to similar square planar complexes. With the lower aryl ring acting as hemi-labile coordinating group, our own studies demonstrated that the biaryl ligand exhibits rates of reductive elimination intermediate between bidentate and monodentate ligands. An electron-rich lower aryl ring better approximates a bidentate ligand and thus retarded the rate reductive elimination. One can imagine a scenario in which the "lower" aryl ring is displaced by a more nucleophilic ligand (e.g., the amine substrate or a second palladium complex) thus forming an "off-cycle" palladium

131

reservoir that must undergo an intramolecular substitution with the lower aryl ring to form an intermediate capable of reductive elimination (see Scheme 1-2).

Having discussed the "on-cycle" intermediates and reaction steps we turn our attention to "off-cycle" processes. Though often given secondary consideration, catalyst decomposition, catalyst activation, and the formation of "off-cycle" or dormant palladium species are also important in the understanding of the overall catalytic reaction. While amine displacement of the supporting phosphine ligand has been invoked to account for catalyst deactivation, few detailed mechanistic studies addressed this important process.[4] The consequences of an "off-cycle" palladium species, the presence of different palladium(II) stereoisomers, or bimolecular palladium interactions have not been thoroughly investigated for C–N cross-coupling reactions. In fact, we will show in this chapter that the formation of "off-cycle" palladium species can dominate the reaction kinetics.

Unlike studies investigating the kinetics of stoichiometric complexes, our approach is to investigate the overall catalytic cycle. This has both advantages and disadvantages. The overall rate of reaction is a function of *all* the elementary steps and their corresponding rate constants. For some reaction examples, the overall rate of reaction is dominated by one (or two) of these rate constants. Under such a circumstance, it is easy to "assign" a dominant resting state and rate-determining step. Indeed, this was the case with the coupling of diphenylamine and 3-bromoanisole for a RuPhos (**L1**) based palladium catalyst. However, what is probably more often the case, at various points of the reaction progression different elementary steps may influence the overall rate of the reaction. Thus the rate law may differ from beginning to the end of a reaction. Such a behavior cannot reasonably be determined or predicted from stoichiometric kinetic studies. Unfortunately in cases such as this, it is extremely challenging to determine the rate-determining step(s) and their corresponding rate constants. As pointed out by Halpern, this approach has often lead to various proposed mechanisms which are contradictory yet can adequately describe the observed kinetics of the same reaction.[5]

In addition to the aforementioned considerations, one must also consider how the catalytic cycle is initiated. The employment of $Pd(OAc)_2$ or $Pd_2(dba)_3$ can convolute the kinetics of the formation of the active catalyst with the kinetics of the reaction itself.[6] Palladium acetate must first be reduced to generate the active catalyst and for the case of $Pd_2(dba)_3$ the dibenzylideneacetone is not an innocent ligand.[1a,7] Sequential additions of substrate to a reaction have been used to probe the steady-state level of active catalyst. However, this is not without its problems since these subsequent additions also increase the volume of the reaction

and thus may convolute the results. With the ability to synthesize palladium oxidative addition complexes (**II**), we believed that this presumptive "on-cycle" intermediate would be a useful mechanistic tool that would pre-empt the question of catalyst activation and interfering ligands.

In line with the above arguments concerning initiation of the catalytic reaction, the "temperature-trajectory" of the reaction can also play a role. At room temperature, the addition of "on-cycle" catalyst (e.g., oxidative addition complex **OA1a**) can perform several turnovers before forming a less kinetically competent "off-cycle" palladium species. Upon heating to the desired reaction temperature (e.g., 80 °C), these "off-cycle" species can then reform the active catalyst and the reaction will go to completion. If the same reaction is performed by adding the catalyst at the reaction temperature (e.g., 80 °C), the formation of "off-cycle" palladium will undoubtedly occur but the rate of this process compared to "on-cycle" kinetic processes will differ compared to the same reaction initiated at ambient temperatures. Thus these otherwise identical reactions will have different reaction rates and reaction times. Such a scenario may be encountered when kinetic studies are carried out by observation with NMR where all the reagents and catalyst are typically added at room temperature (and then heated to reaction temperature). The NMR experiment may not reproduce the results obtained by performing the kinetic study in a reaction calorimeter where the catalyst is added to the reagents at the reaction temperature.

With these considerations in mind, we chose to study the coupling of different amines with a RuPhos (**L1**) based palladium catalyst.[8] Given the utility and structural diversity of biaryl monophosphine ligands for which **L1** is one example, a kinetic study employing these ligands could identify problematic reaction steps with this ligand class. By use of model reactions that afford high yields, we had hoped to avoid complicating competitive processes that would interfere with our analysis (e.g., parasitic reduction of the aryl halide, competitive C–O coupling, etc.). We initially selected diphenylamine, *N*-methylaniline, and morpholine as model secondary amine substrates with the expectation that the tertiary amine product would not be a competitive substrate (Scheme 2-1). The use of primary amines (aniline, *n*-propylamine, etc.) was initially avoided since **L1**-based palladium catalysts are known to not be selective and anticipated the formation of the secondary amine product to itself be a competitive (and thus interfering) substrate for the C–N coupling reaction.

Scheme 2-1 Model reactions for secondary amines used in this study
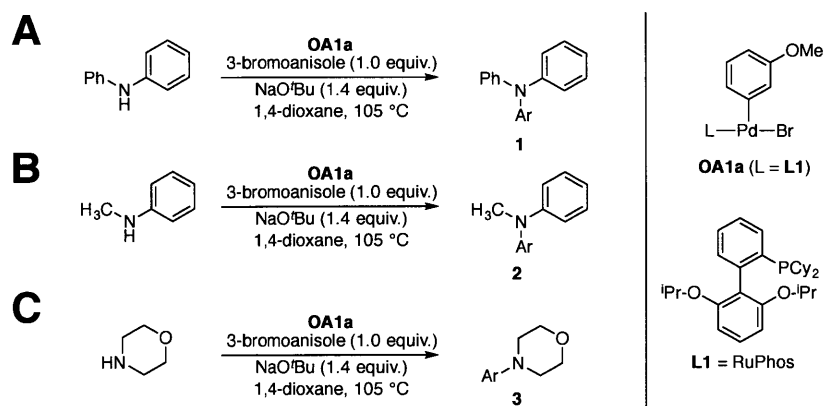
2.2. Results:

2.2.1. Kinetic Evidence for Off-Cycle Palladium

To examine the kinetics of these reactions, calorimetry was used as a primary tool.[9] As previously described, a (concentrated) solution containing **OA1a** was injected in a preheated solution containing all other reagents (amine, aryl halide, and base). The resultant observed power output signal was used as a proxy for the rate of reaction. Gas chromatography analysis of the reaction mixture was used to evaluate the yield/conversion of the reaction.

As described in chapter 1, the cross-coupling reaction of diphenylamine with an aryl halide mediated by a RuPhos (**L1**) based palladium catalyst gave zero-order kinetics consistent with reductive elimination as a rate-determining step. Doubling the amount of **OA1a** doubled the rate and the addition of excess **L1** did not appreciably affect the reaction rate. A ^{31}P-NMR experiment indicated a single species at 33 ppm that matched that of the independently synthesized complex (**A1a**) (Figure 2-1).

134
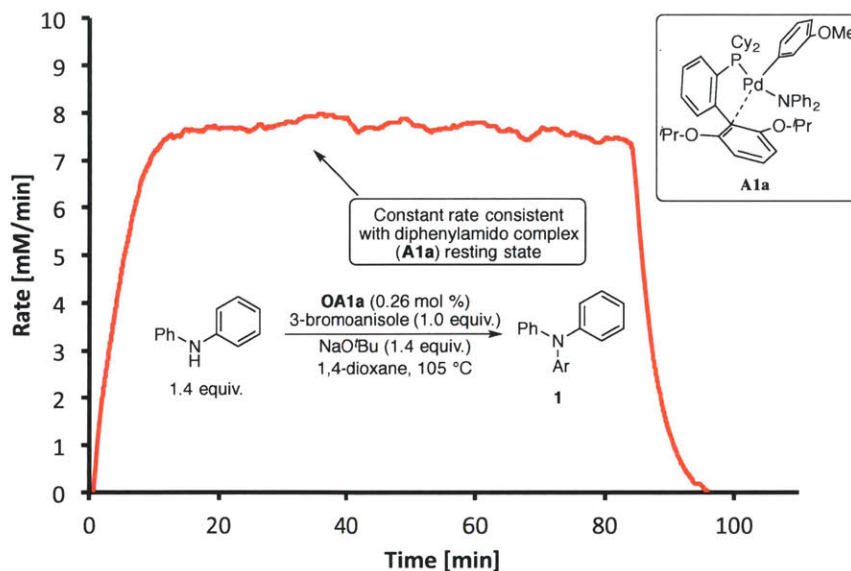
Figure 2-1 Near constant reaction rate consistent with diphenylamido complex resting state and reductive elimination as the rate-determining step.

With these results in hand, we then examined the coupling of a more nucleophilic amine, *N*-methyl aniline. As expected, the rate constant for reductive elimination of the corresponding *N*-methyl anilide complex ($k_{RE,(CH3)N(Ph)}$ > 500 1/min) is at least two orders of magnitude greater than the diphenylamido complex (**A1a**) ($k_{RE,NPh2}$ = 4.4 1/min). However, the rate law for this reaction is not consistent with the prototype mechanism (Figure 1-1). We noted a fast initial rate followed by what is referred to as the plateau region where the reaction proceeds at a near constant rate (Figure 2-2). Furthermore, the time for the reaction to go to completion was highly sensitive to the catalyst loading. Unlike the reaction of diphenylamine, the rate was not directly proportional to the catalyst loading.

135
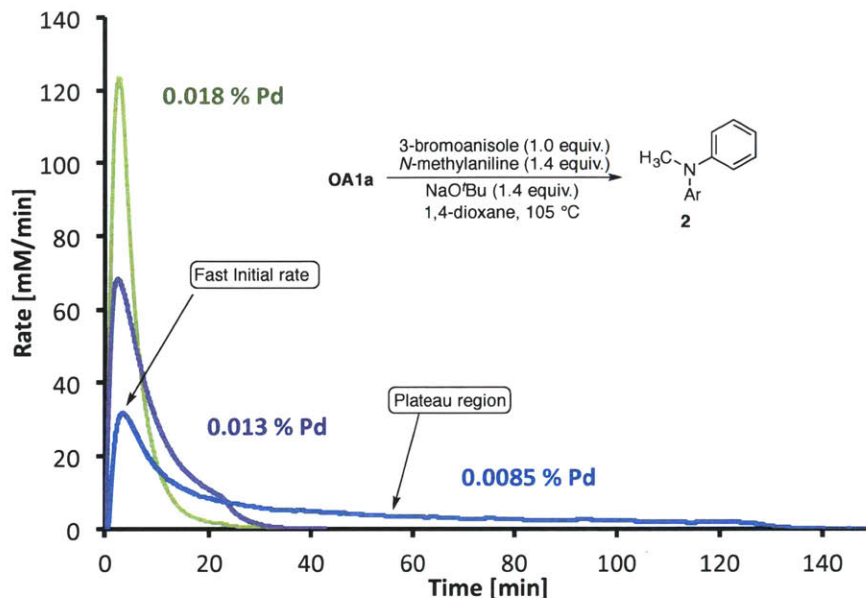
Figure 2-2 Cross-coupling of *N*-methylaniline and 3-bromoanisole with an **OA1a** based catalyst.

Having investigated the N-methylaniline reaction, the reaction of morpholine as a coupling partner with 3-bromoanisole was carried out (Scheme 2-1C, Figure 2-3). When compared to the reaction with *N*-methyl aniline, the reaction of morpholine required an order of magnitude more catalyst to achieve similar reaction times. This reaction was characterized by a fast initial rate followed by a plateau region and a similar non-linear dependence on average rate to catalyst loading. Interestingly, there was a slight and consistent increase in the reaction rate immediately prior to the complete consumption of the limiting reagent (aryl halide). As was done for the reaction of diphenylamine (Scheme 2-1A, Figure 2-1), we performed some experiments with additional **L1**. Unlike the reaction of diphenylamine, the time for the reaction to go to completion decreased with added **L1** (Figure 2-3B).
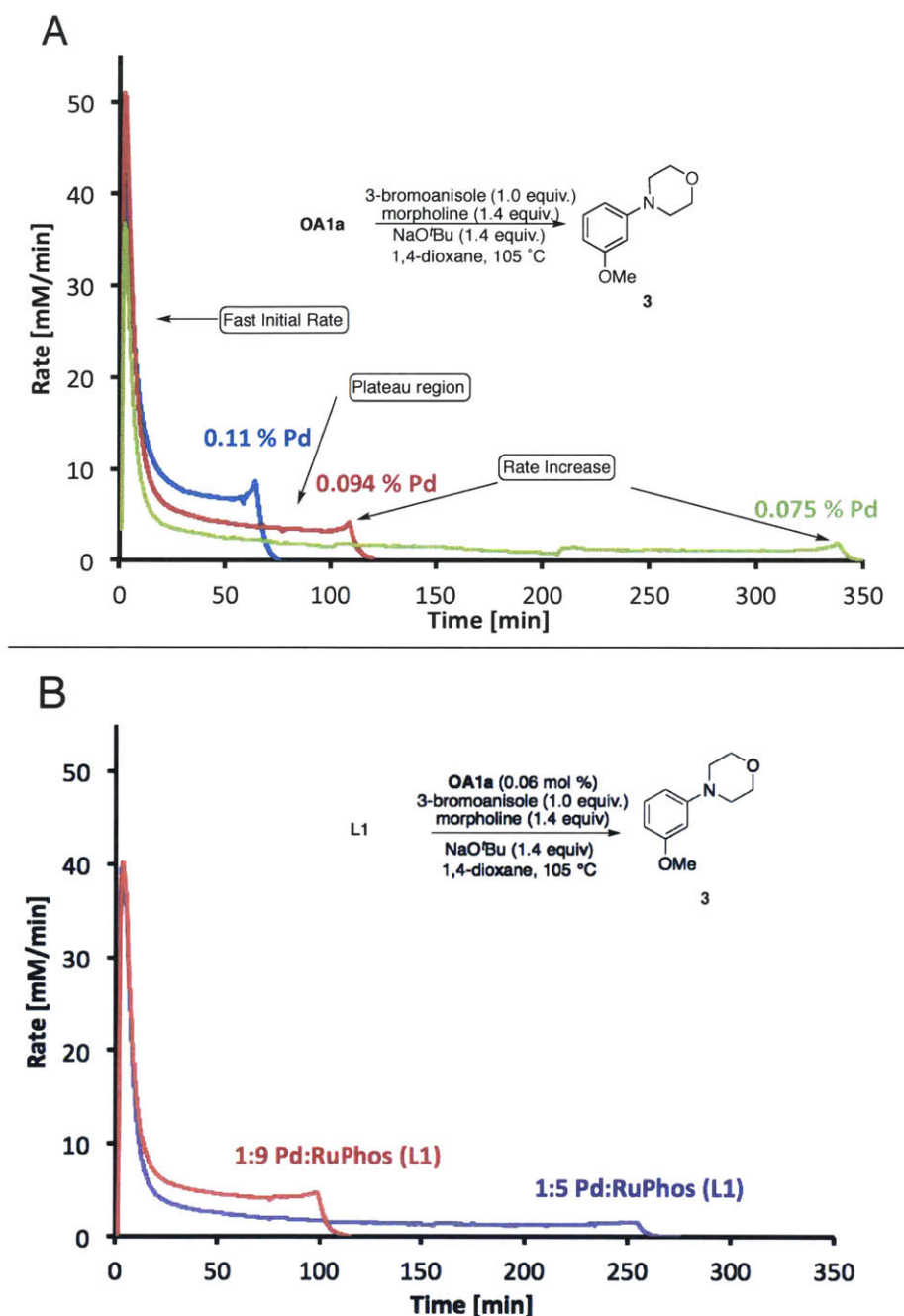
Figure 2-3 A) Cross-coupling of morpholine and 3-bromoanisole with **OA1a** based catalyst. B) Cross-coupling reaction of morpholine and 3-bromoanisole with exogenous RuPhos (**L1**) ligand.

Given that **OA1a** is a presumptive catalytic intermediate, it can be reasonably argued that *all* the palladium is initially "on-cycle" which manifests as the rapid initial rate. The observed decrease and plateau region is not consistent with the prototype C–N coupling mechanism (Figure 1-1) but is more consistent with the formation of an "off-cycle" palladium intermediate for

which the formation of the active "on-cycle" catalyst becomes the rate-determining step. The effect of added ligand **L1** is consistent with the formation of active catalyst by re-association of the **L1** with an "off-cycle" palladium species that is not ligated to a phosphine ligand. The strong non-linear behavior in reaction rate is consistent with interactions between palladium species and/or interactions between palladium and **L1**. The rapid increase in rate near the end of the reaction is consistent with an inverse dependence on the aryl halide, which will be discussed later in this thesis.

Further investigation into the cross-coupling reaction of morpholine with 3-bromoanisole reveals that catalysis occurs readily at ambient temperatures. Thus for the morpholine reaction, a 1 mol % catalyst loading of **OA1a** affords a yield of approximately 20 mol % in the first 20 minutes. Monitoring by ^{31}P-NMR at -9 ppm indicates that a significant portion (~60 %) of the supporting ligand (**L1**) is not associated with the palladium (Table 2-46). The elementary steps describing the transformation of **I** to **II** to **III** to **IV** and then to **I** again are facile under these conditions. Thus, the incomplete conversion is a consequence of the formation of "off-cycle" palladium species which are not kinetically competent at 20 °C.

2.2.1. Variation of amine and supporting ligand

Comparison of the kinetic profiles shown in Figure 2-1, Figure 2-2, and Figure 2-3 of the model reactions suggests that amine nucleophilicity or a correlated parameter plays a major role in the displacement of **L1** from one of the "on-cycle" palladium intermediates. Given the results for the morpholine-based reaction at ambient temperatures, we wondered if this was a general behavior for different amine classes

By calorimetry, the **OA1a** based cross-coupling reaction of 3-bromoanisole with various amine types was evaluated. With the exception of the reaction of diphenylamine where the diphenylamido complex **A1a** is stable to reductive elimination at 20 °C, all other amine types afforded some product. The reaction of the weakly nucleophilic *N*-methylaniline went to completion within 90 minutes. For the more nucleophilic amines, the reactions with *n*-propylamine, di-*n*-butylamine, and *iso*-propylamine afforded small amounts of product within a short time frame (~ 10 minutes) after which no further reaction was observed. The reaction of aniline was found to have a no rate after 50 minutes. The *tert*-butylamine based reaction exhibited an observable rate after two hours, which suggests that sterically hindered amines are

less able to sequester the palladium as an "off-cycle" palladium intermediate. These results suggest that neither reductive elimination nor amine binding to the palladium center are problematic steps.[10]

Scheme 2-2 Cross-coupling reaction of different amines with **OA1a** catalyst. Rates monitored by calorimetry.

Entry	HNR^{1}R^2	Conv. [%]	Yield [%]
1	diphenylamine	0	0
2	N-methylaniline	100	98
3	morpholine	30	30
4	n-dibutylamine	4	trace
5	aniline	17	16
6	n-propylamine	4	trace
7	iso-propylamine	1	trace
8	tert-butylamine	15	13
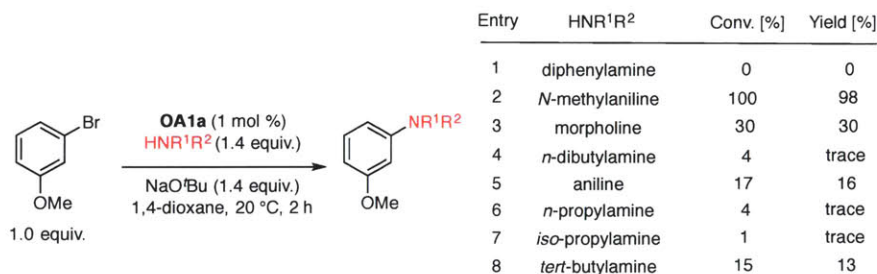
Having established that reactions with several types of amines afford product but do not go to completion at ambient temperatures (Scheme 2-2), we investigated some structurally similar biaryl supporting ligands. A conclusion indicating that the observed kinetic behavior was somehow unique to RuPhos (**L1**) would limit the utility of this study. We thus employed the cross-coupling of *n*-propylamine with 3-bromoanisole at 20 °C with some other ligands employed in the Buchwald laboratory. Employing pre-catalyst or oxidative addition complexes for XPhos (**L7/P7**) or the RuPhos-BrettPhos Hybrid (**L3/OA3**) afforded only trace amounts of product.[11-15]

Scheme 2-3 Biaryl supporting ligands evaluated for the model cross-coupling reaction of 3-bromoanisole and *n*-propylamine
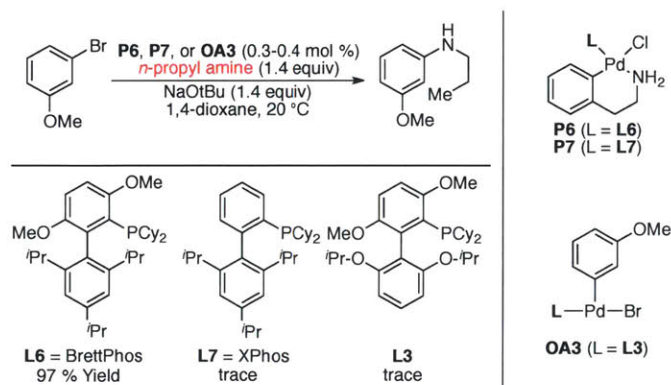
Only the BrettPhos-based catalyst (**L6/P6**) afforded product and complete conversion under these conditions (see Figure 2-35). Like the RuPhos-based reaction of morpholine (Figure 2-3), we observed a fast initial rate followed by a plateau region. There was an increase

139

in reaction rate in the middle of the plateau region, which suggests a complicated reaction mechanism likely due to palladium-palladium interactions (Figure 2-35). Increasing the reaction temperature to 105 °C and by employing **OA6**, we observed a qualitatively similar kinetic pattern to that seen for the RuPhos (**L1**) based morpholine reaction (compare Figure 2-3 and Figure 2-4). Based on the data presented in Scheme 2-2, Figure 2-3, and Figure 2-4, we conclude that different amine types and different ligand types generate analogous "off-cycle" palladium species.
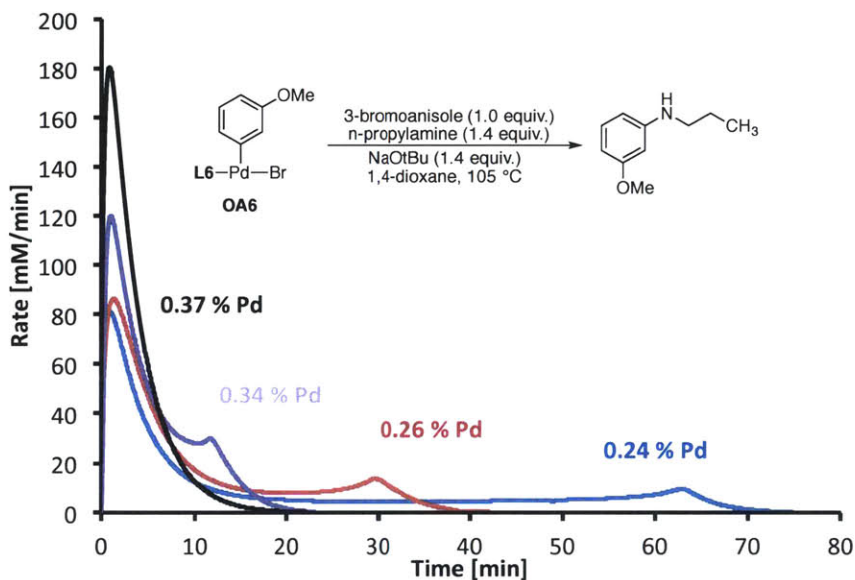
Figure 2-4 Cross-coupling reaction of 3-bromoanisole with *n*-propylamine mediated by a BrettPhos-based catalyst (**OA6**).

As we shall see later in this chapter, there is not a single "off-cycle" palladium species but rather a distribution of at least two palladium complexes at least one of which is phosphine ligated. For the RuPhos (**L1**) based coupling of *n*-propylamine and 3-bromoanisole at 20 °C, these phosphine ligated complexes are not kinetically competent and can be trapped and observed by ^{31}P-NMR (Figure 2-10). In the case of BrettPhos (**L6**) based palladium catalysts, these phosphine-ligated species are apparently kinetically competent at room temperature allowing for the formation of the "on-cycle" alkylamido complex, which undergoes reductive elimination at room temperature. Though the hybrid ligand (**L3**) did not afford a kinetically competent catalyst under these same conditions (Scheme 2-3), it seems that the methoxy substituent at the C3-position for the **L6** ligand facilitates an intramolecular ligand substitution that allows the "off-cycle" species to re-enter the catalytic cycle. Similar to the RuPhos (**L1**) based reaction, free ligand was observed by ^{31}P-NMR for the BrettPhos (**L6**) based reaction. The addition of excess **L6** at 20 °C did not improve the reaction rate which indicates that once

the supporting ligand is displaced from the palladium center it cannot re-associate with the palladium to form an "on-cycle" intermediate. This paralleled the experiment with the RuPhos/morpholine reaction at 30 °C where additional **L1** also did not affect the reaction rate (Figure 2-5). Thus for ambient temperatures, once the supporting ligand has been displaced, it cannot re-associate with "off-cycle" palladium.
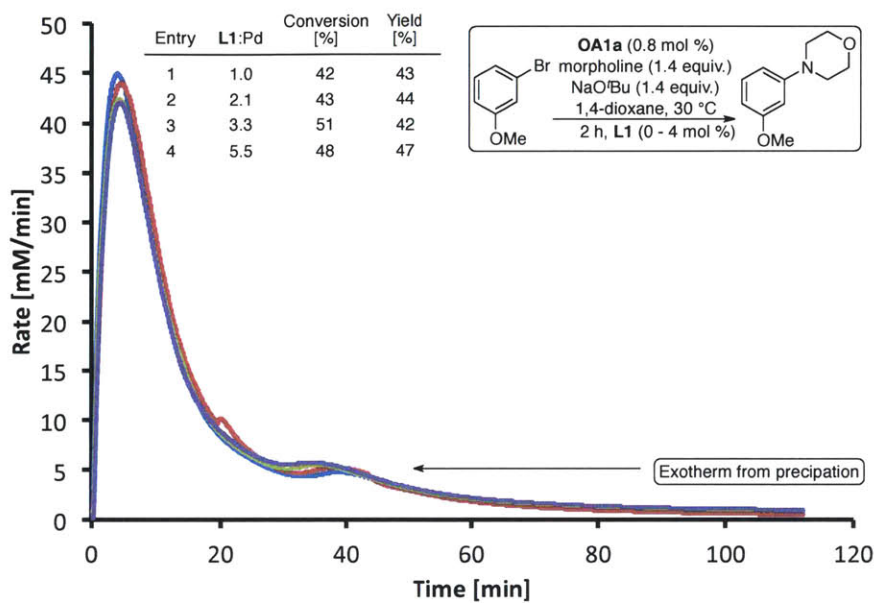
Figure 2-5 Coupling reaction with morpholine and 3-bromoanisole at 30 °C. Yield was not a function of added ligand **L1**.

We were also interested to see if these results could be applicable to other bidentate ligand systems. Oxidative addition complexes of ^{t}ButylBrettPhos, DalPhos, S-BINAP were synthesized for use as catalyst sources. In the case of ^{t}ButylBrettPhos, the coupling of 3-bromoanisole and n-propylamine proceeded selectively and rapidly to completion within 10 minutes.[16]

141
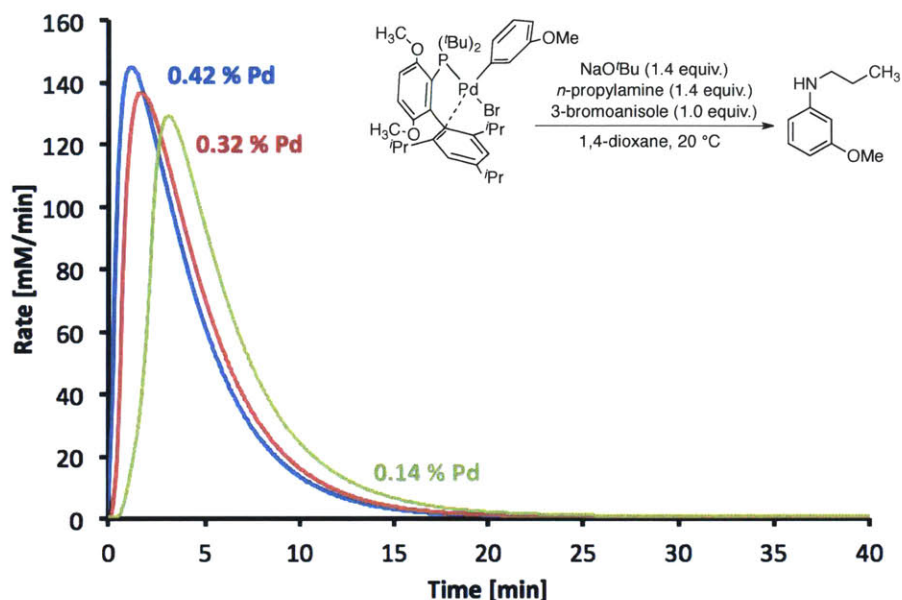
Figure 2-6 Cross-coupling reaction of 3-bromoanisole with *n*-propylamine with a 'ButylBrettPhos-based palladium catalyst. Yields were over 90 % and the reactions were selective with negligible formation of diarylated amine

The coupling of *N*-methylpiperazine with bromobenzene using an S-BINAP based catalyst proceed to completion at 60 °C for a range of catalyst loadings (Figure 2-7).[17] Depending on the catalyst loading, the reaction proceeded to *accelerate* as the reaction progressed. Given that the BINAP-OA complex is a presumptive "on-cycle" intermediate such a result indicated an inverse dependence on one or more substrates. Furthermore, we found that this acceleration was diminished at lower catalyst loadings, which is suggestive of competitive (leading to a less kinetically competent intermediate) and turnover dependent side reaction. Finally, the reaction was found to have reproducible "bumps" during the reaction progression (most apparent for catalyst loadings ranging from 0.22 mol% to 0.31 mol%). These results are not consistent with the prototype reaction mechanism (Figure 1-1) and are not an obvious function of substrate concentrations. Looking forward, these curves are qualitatively similar to the curves where *OA1a was employed in the coupling of morpholine and 3-bromoanisole (Figure 2-17).
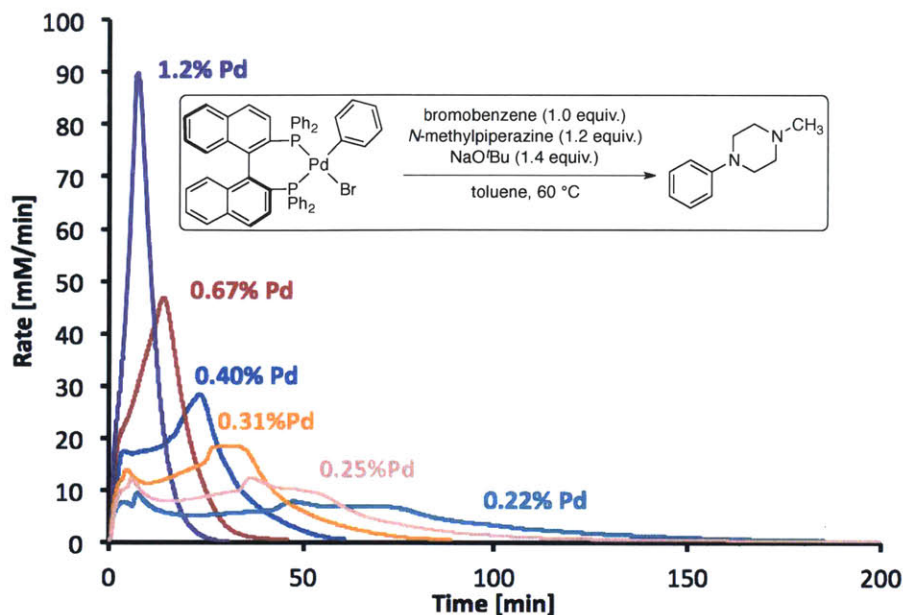
Figure 2-7 Cross-coupling of bromobenzene with *N*-methylpiperazine mediated by an S-BINAP based catalyst. Yields were above 90 % for all reactions.

Finally, the DalPhos-based oxidative addition complex was used to facilitate the coupling of *n*-octylamine and bromobenzene at 105 °C (Figure 2-8). The kinetics of this reaction were found to be nonlinear in catalyst loading. A catalyst loading of 0.24 mol %, the time for the reaction to go to completion would be 230 minutes and at a catalyst loading of 0.49 mol % the time would be 50 minutes (Figure 2-8A). Though *n*-octylamine is more nucleophilic than *N*-methylaniline, the progression of the reaction qualitatively matches the kinetics of a RuPhos (**L1**) based coupling of 3-bromoanisole with *N*-methylaniline (Figure 2-2). The substitution of chlorobenzene for bromobenzene or the addition of exogenous DalPhos ligand improved the reaction rate and decreased the time for the reaction to go to completion (Figure 2-8B).
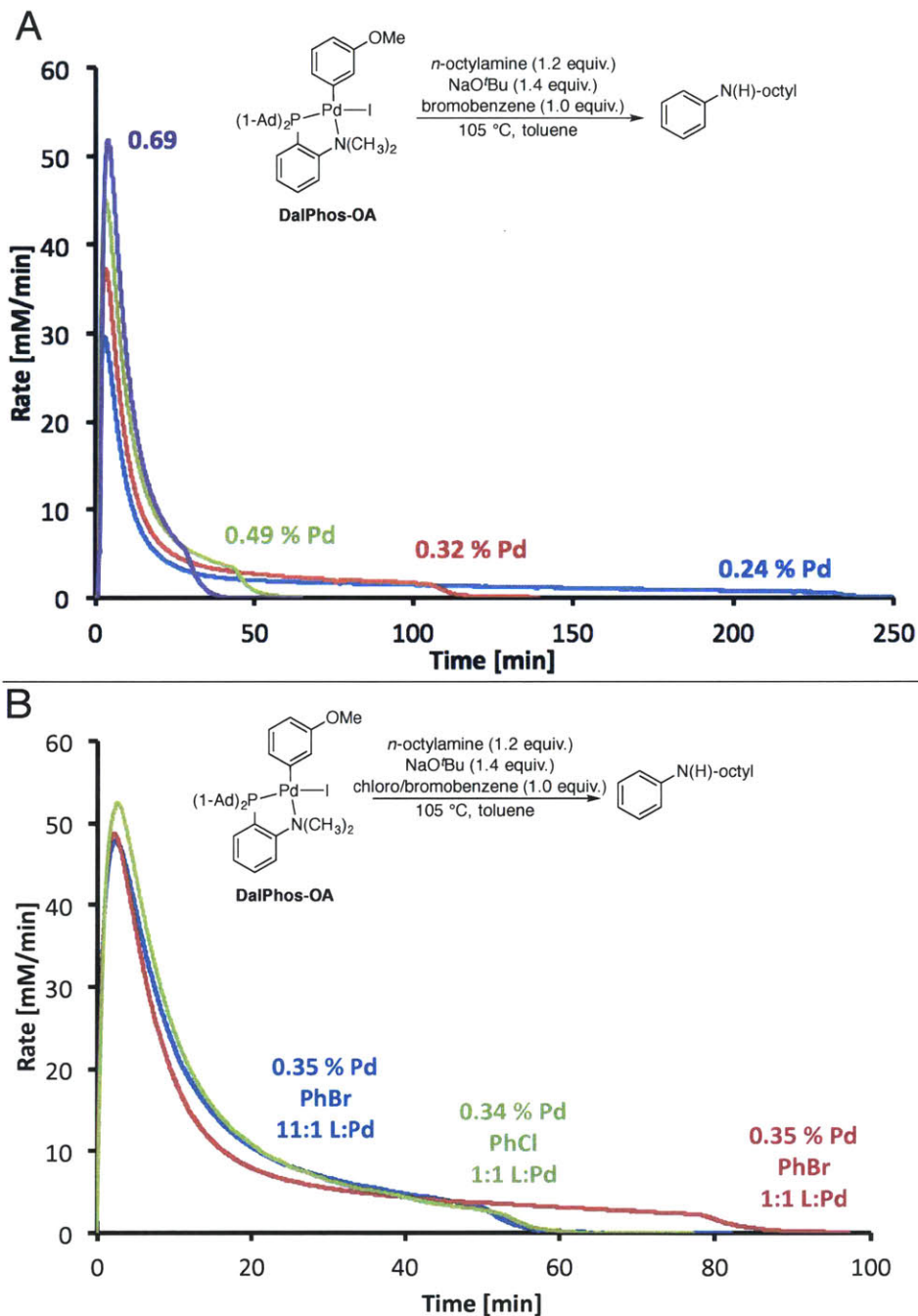
Figure 2-8 Cross-coupling reaction of bromo/chlorobenzene with *n*-octylamine by a DalPhos-based palladium catalyst. A) The cross-coupling reaction of bromobenzene with *n*-octylamine at different catalyst loadings. B) Substitution of chlorobenzene for bromobenzene or the addition of exogeneous DalPhos leads to a (small) increase in reaction rate.

We also investigated a RuPhos (**L1**) based cross-coupling reaction of *n*-propylamine and bromobenzene and a similar reaction of aniline with bromobenzene. In both circumstances, we noted kinetics that give the same characteristic pattern as the coupling of morpholine and 3-bromoanisole mediated by an **L1**-based catalyst. Catalysts based on BrettPhos (**L6**) are

144

reported to selectively arylate primary amines and afford only trace amounts of the tertiary amine product.[18] Catalysts based on RuPhos (**L1**) are reported to be unselective and furnish mixtures of the tertiary and secondary arylated amines. For the example of *n*-propylamine, the poor selectivity of the **L1** based catalyst was apparent as the reaction afforded approximately 25% diarylated product (Figure 2-9). However, when coupling the aniline with bromobenzene it was found that **OA1a** furnished a selective catalyst (Figure 2-9B) with only trace amounts of triphenylamine. These reactions demonstrate that RuPhos (**L1**) and BrettPhos (**L6**) clearly have overlapping mechanistic pathways with multiple amines and aryl bromides.
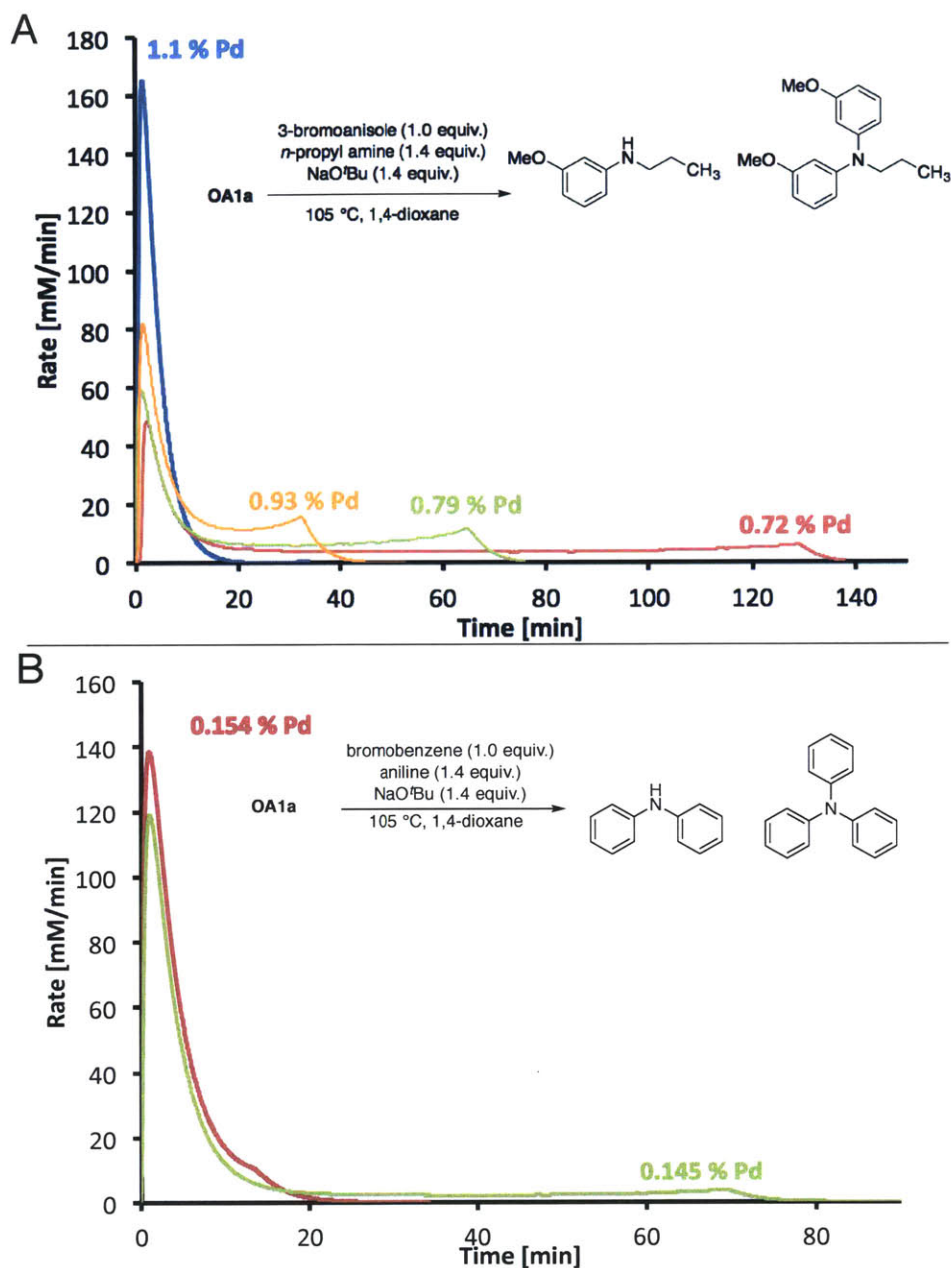
Figure 2-9 A) The cross-coupling of 3-bromoanisole and *n*-propylamine with a RuPhos (**L1**) based palladium catalyst. Yield were above 90 % with the diarylated product accounting for ~25 % of the overall yield. B) The cross-coupling of aniline with bromobenzene mediated by a RuPhos (**L1**) based palladium catalyst. Yields were above 90 % with the triphenylamine being only present in trace amounts. Note the *very* strong dependence on reaction time with catalyst loading.

2.2.2. Formation of "Off-Cycle" Palladium

Given the evidence for "off-cycle" palladium species obtained thus far from kinetic studies of the catalytic reactions employing RuPhos (**L1**), we wished to investigate the

146

sequence of steps by which these species are generated. The reaction with morpholine is not suitable for these studies since this reaction undergoes several turnovers (~20) at ambient temperatures (Scheme 2-2). We therefore selected for further investigation, the related reaction of *n*-propylamine with 3-bromoanisole. We wished to ascertain which reagents (base, amine and aryl halide) were necessary for the displacement of **L1** from the palladium center. We thus performed a series of experiments that were monitored by ^{31}P-NMR.

To confirm the displacement of **L1** from the palladium center, **OA1a** was exposed to a solution containing the reagents necessary for the catalytic reaction (NaO*t*Bu, *n*-propylamine, and aryl halide) (Figure 2-10A). It was thus confirmed that **L1** was quickly displaced from the palladium center.[19] GC analysis of the reaction mixture indicated the formation of the coupled product arising from C–N reductive elimination. The "yield" of free ligand accounted only for 16 % of the total available **L1**. Phosphine ligated palladium was observed at 42 to 48 ppm in the presence of the displaced **L1** at -9 ppm. Since no further turnovers were observed, these ligated complexes are not kinetically competent at ambient temperatures.

A second experiment, which exposed **OA1a** to a solution of *n*-propylamine and 3-bromoanisole did not displace significant quantities of the supporting ligand from the palladium center (Figure 2-10B). Only trace amounts of free **L1** were detected. Many ^{31}P-NMR signals were observed at 40 ppm to 55 ppm, which are consistent with previously reported palladium(II) complexes containing both amine and phosphine ligands.[2a] This experiment demonstrated that the amine cannot displace **L1** on the time scale of the catalytic reaction (Figure 2-10A). In a third experiment (Figure 2-10C), **OA1a** was exposed to a solution of NaO*t*Bu and 3-bromoanisole. No free **L1** was observed but a complex mixture of phosphorus containing species (-50 ppm to -35 ppm and 25 ppm to 55 ppm) was formed. These experiments suggest that the formation of the "off-cycle" species does not occur directly from an amine bound oxidative complex or from direct attack of **OA1a** by the base.
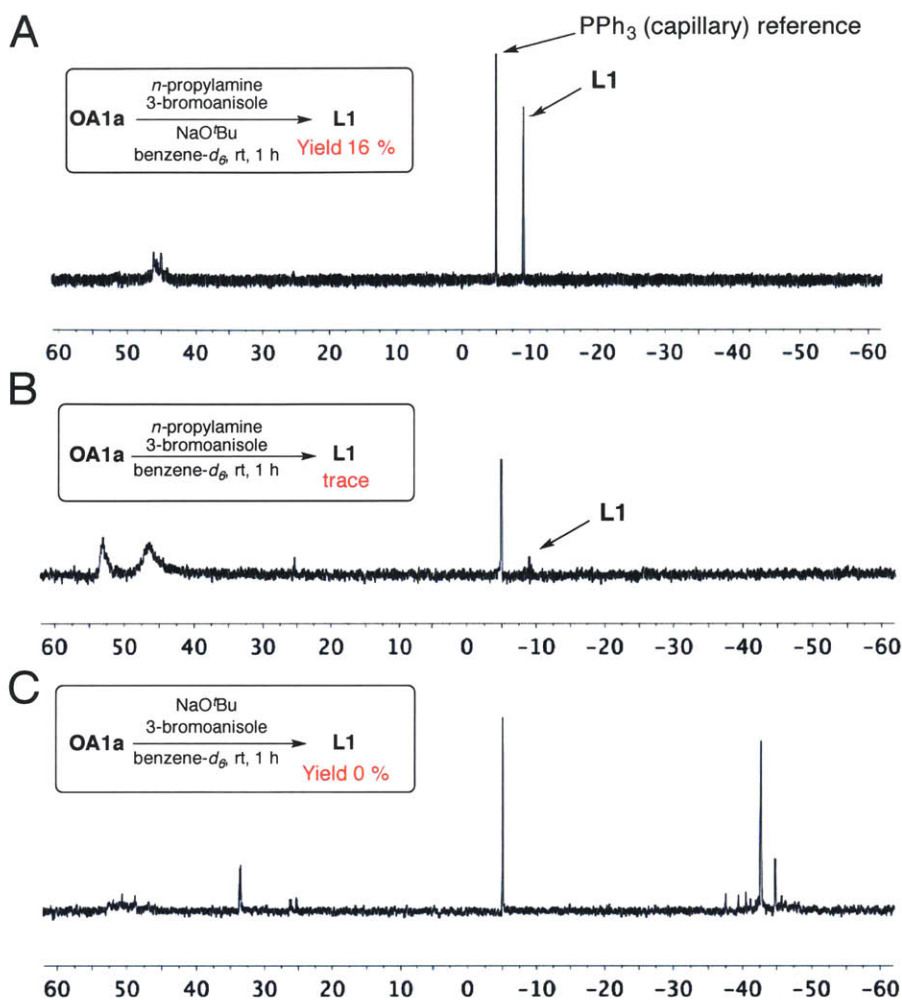
Figure 2-10 A) **OA1a** is exposed to the reagents necessary for a catalytic reaction B) **OA1a** is exposed to a solution of 3-bromoanisole and *n*-propylamine but only trace amounts of **L1** are observed C) **OA1a** is exposed to a solution of NaO*t*Bu and 3-bromoanisole but no free **L1** is observed.

Because these results imply that displacement of **L1** does not occur prior to the formation of the *n*-propylamido complex **A1'** (Figure 2-11), we wished to investigate the sequence of events following the formation of this important intermediate. Due to the instability of **A1'** towards reductive elimination, we generated this complex *in situ* from **A1a**. Thus **A1a** was subjected to a solution of *n*-propylamine and 3-bromoanisole in the absence of NaO*t*Bu. This resulted in the eventual disappearance of the ^{31}P-NMR signal of **A1a** (33 ppm) and the appearance of the ^{31}P-NMR signal for **L1** corresponding to a "yield" of 9.4 % relative to the initially bound ligand present in **A1a**. Thus, this experiment demonstrates that the presence of NaO*t*Bu is not a required reactant for the displacement of **L1** and that the formation of the "off-cycle" palladium species likely occurs after reductive elimination of **A1'**.

148
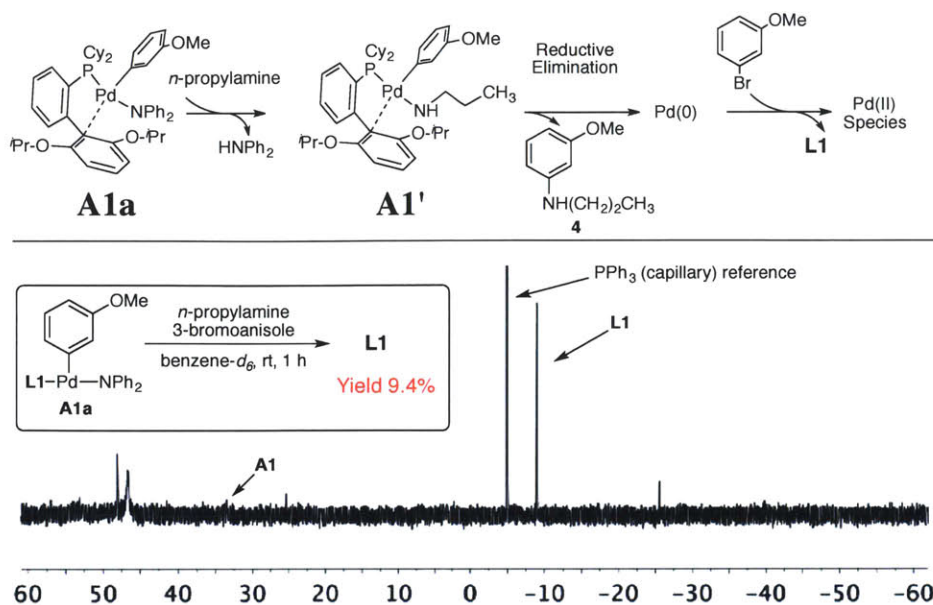
Figure 2-11 *In Situ* amine ligand exchange followed by reductive elimination leading to the displacement of **L1** from the palladium center. Catalyst loading of **A1a** corresponds to approximately ~5 mol %

To gain further insight into the nature of the "off-cycle" palladium species, we revisited the addition of **OA1a** to a 1,4-dioxane solution of NaO*t*Bu, *n*-propylamine, and 3-bromoanisole at 20 °C. As shown in Figure 2-12, analysis of the crude reaction mixture by GC showed the formation of **4** (0.96 equiv. relative to **OA1a**), in conjunction with consumption of the aryl halide (1.3 equiv. relative to **OA1a**). The equivalents of cross-coupled product formed and aryl halide consumed were independent of the initial concentration of **OA1a**. These data demonstrate that **OA1a** forms the amido complex **A1'** which then cleanly undergoes reductive elimination. Since a further 1.3 equivalents of aryl halide are consumed, but no further (product producing) turnovers are observed at room temperature. This result suggests that a majority of the palladium is in the form of "off-cycle" palladium(II) state.[20]
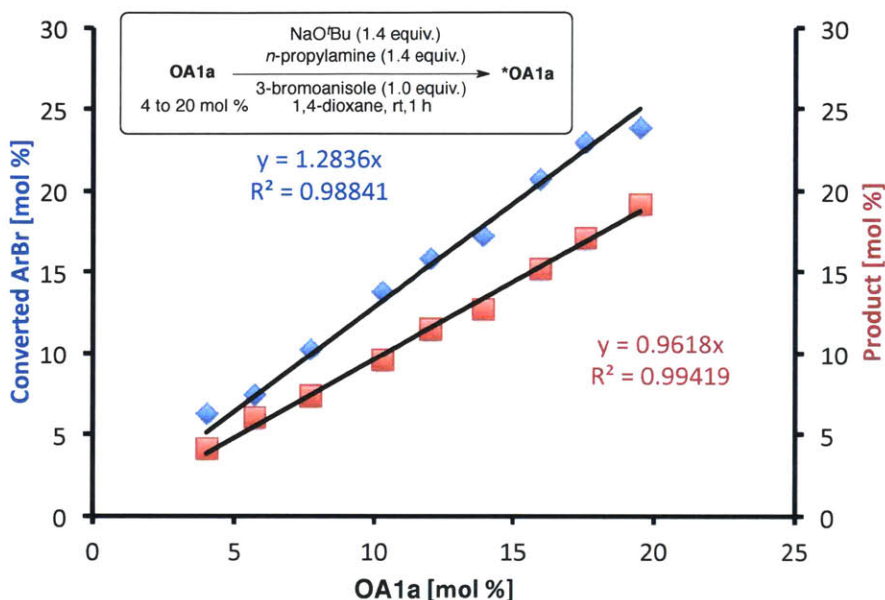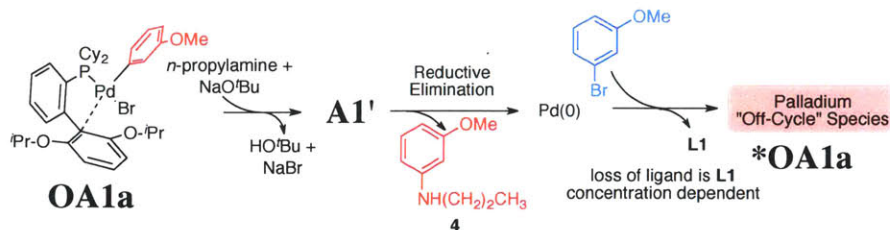
Figure 2-12 Yield of product and consumption of 3-bromoanisole for various concentrations of **OA1a**. Note that 1.3 equivalent (relative to **OA1a**) is consumed.

Based on the "yield" of **L1** displaced from the metal center relative to **OA1a**, we concluded that a collection of "off-cycle" palladium complexes is formed. We thus investigated the role of the initial concentration of **OA1a** on the outcome of the displaced of **L1**. In the experiment shown below (Figure 2-13), **OA1a** is quantitatively consumed for every data point. However, as the initial concentration of **OA1a** increases, the percentage of displaced **L1** decreases (relative to the initial quantity of **OA1a**). The dependence of the percentage of **L1** displaced on the initial concentration of **OA1a** suggests that palladium-palladium and/or palladium-**L1** interactions play a role in the formation of the "off-cycle" palladium species and thus determines the distribution of these species.

150
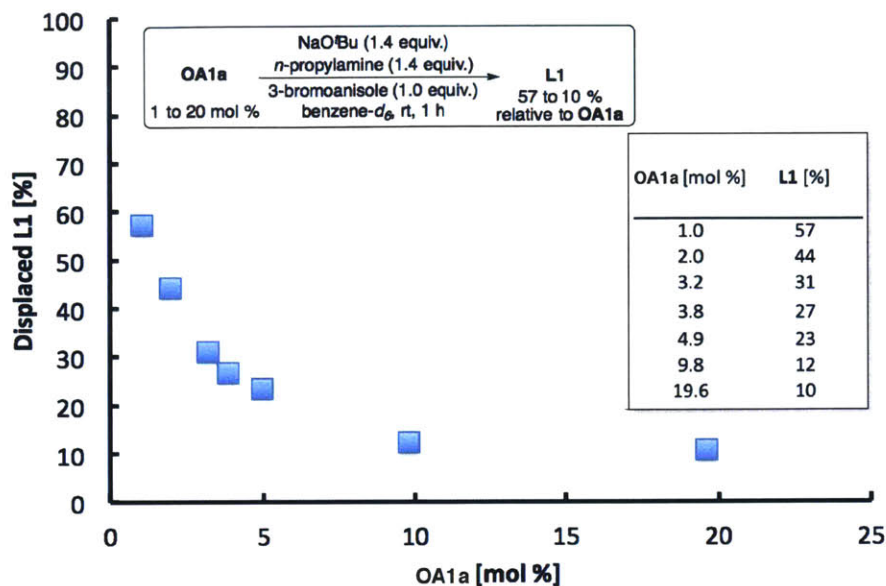
Figure 2-13 Yield of displaced **L1** by exposing **OA1a** to a solution of *n*-propylamine, NaO*t*Bu, and 3-bromoanisole. Quantification of displaced **L1** was by ^{31}P-NMR.

Building on these results, we wanted to determine whether the distribution of these "off-cycle" palladium species was a consequence of kinetic or thermodynamic control. If the "off-cycle" palladium species were in dynamic equilibrium with the displaced **L1**, then the addition of **L1** to the reaction mixture should have an effect on this presumed equilibrium. If additional **L1** does not affect the amount of displaced **L1**, it would indicate that some of these species are kinetically trapped. Furthermore, any palladium-**L1** interaction should result in a change in the distribution of "off-cycle" palladium species when exogenous **L1** is present at the beginning of the reaction. Thus, we compared (by monitoring with ^{31}P-NMR) a reaction with additional **L1** to a reaction where the additional **L1** was omitted. After taking into account the exogenous **L1** added, we found that the amount of **L1** liberated from **OA1a** was the same within experimental error with the control reaction. We thus conclude the distribution of "off-cycle" palladium is controlled by palladium-palladium interactions and is likely responsible for the effect of the initial concentration of **OA1a** on the kinetically controlled displacement of **L1**. These conclusions are also in part supported by the kinetic studies of the catalytic system where the additional ligand had no effect on the yield or conversion of the reaction at ambient temperatures.

With these results in hand, we can begin to offer some mechanistic proposals that account for the experimental data presented thus far. Hartwig has previously shown that for a BINAP-based palladium(0) complex the amine can participate as a ligand during oxidative addition of the aryl halide.[21] We believe that a similar process is occurring in our experimental

151

system and propose that the amine binding immediately following reductive elimination of **IV** leads to the formation of **I'** (Scheme 2-4). Computational studies, for other Pd(0) complexes, have shown that the formation of the *trans*-oxidative addition complex (**II'**) can be kinetically competitive with the formation of the *cis*-oxidative addition complex (**II***) even though the *trans*-isomer is significantly higher in energy than the *cis*-isomer.[22] Because of the greater *trans*-effect of the aryl group, we expect that the P–Pd bond is weakened in complex **II'**. Thus, ligand substitution of **L1** by an amine nucleophile may compete with the isomerization of **II'** to the lower energy *cis*-isomer (**II***). We defer discussion of potential palladium–palladium interactions until later in this thesis.

Scheme 2-4 A) Reductive elimination of **IV** affords at least two kinds of Pd(0) complex **I** and **I'** which undergo interconversion B) Oxidative addition to **I'** can afford either the *trans*-isomer **II'** or the *cis*-isomer **II***.
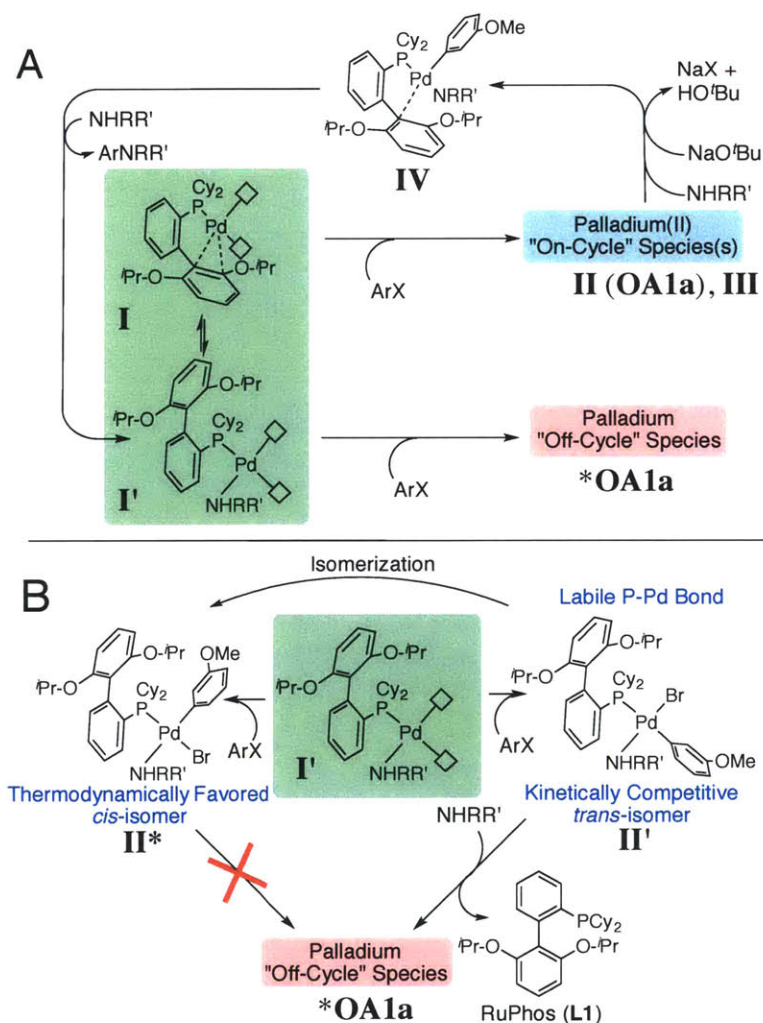
With this proposal in hand, we wished to examine the oxidative addition reaction step using stoichiometric complexes. Based on the work of Fink,[23] we proceeded to synthesize an L_2Pd^0

complex from a (tmeda)Pd(CH$_3$)$_2$ for **L1** and CyJohnPhos **L8** (Figure 2-14). As previously reported, we confirmed that the **L8**-based complex in the presence of an aryl bromide (bromobenzene) for 2 hours *did not* undergo appreciable oxidative addition with the aryl halide. Subjecting the **L8**-based complex (~ 20 mol%) to a solution of bromobenzene (1 equiv.) and *n*-propylamine (1.4 equiv.) afforded an amine ligated Pd(II) (via consumption of the bromobenzene) within an hour as determined by GC with *n*-dodecane as an internal standard. This result demonstrates that the presence of the amine accelerated the rate of oxidative addition for this **L8** based-complex. These results contrast with an analogous system employing an analogous L$_2$Pd(0) BINAP based complex where it was shown the presence of *N*-methyl piperazine *retarded* the rate of oxidative addition to bromobenzene.[21]

Given these results we turned out attention to a set of similar experiments using RuPhos **L1**. Unlike the **L8**-based complex, the **L1**-based complex readily underwent oxidative addition to bromobenzene with a reaction time on the order of 20 to 30 minutes at 25 °C. A single x-ray crystal structure of the **L1**-based L$_2$Pd(0) complex, showed that the lower aryl ring is moved away from the palladium center (Figure 2-14B). Though perhaps inappropriate to extrapolate from a solid state structure, the discrepancy in rates of oxidative addition may be attributed to conformational differences in solution.
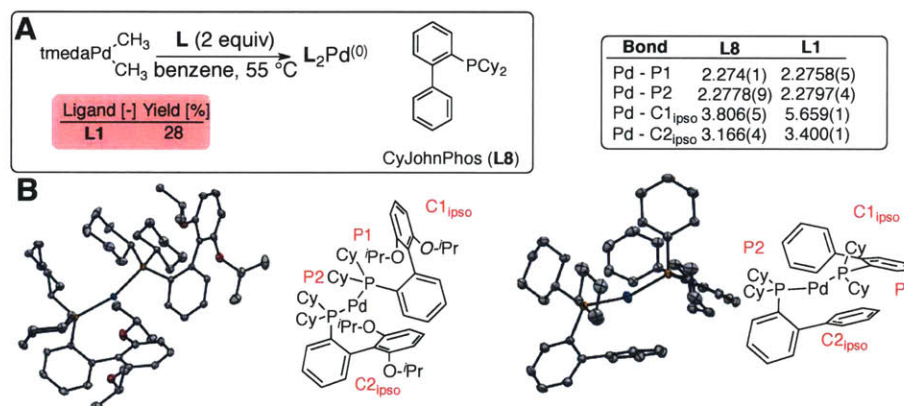
Figure 2-14 A) Yields for the formation of L$_2$P(0) from RuPhos (**L1**) and CyJohnPhos (**L8**) B) ORTEP diagrams and bond length for respective L$_2$Pd(0) complexes. Bond lengths are reported in Angstroms. ORTEP diagram for **L8** reproduced from reference 23

As shown in Figure 2-15, the oxidative addition of the **L1**-based complex to bromobenzene afforded the formation of the independently synthesized **OA1b** as observed by ^{31}P-NMR. Quantification of the "free" **L1** (at -9 ppm) confirmed that for this reaction the loss of *one and*

153

only one equivalent of **L1** (relative to the starting $L_2Pd(0)$ complex). Addition of excess *n*-propyl amine *after* the complete formation of **OA1b** did not afford significant amounts additional free **L1**.
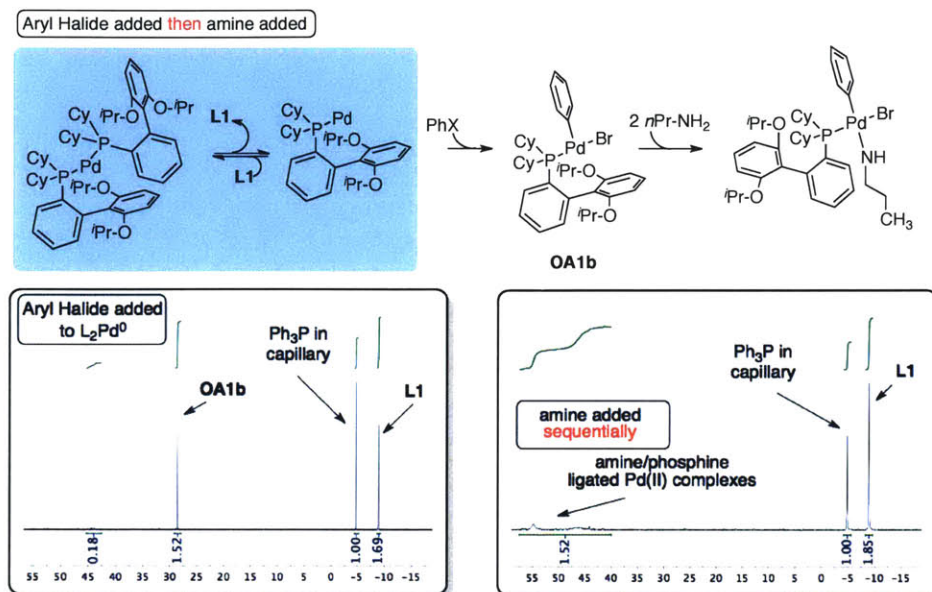
Figure 2-15 $L_2Pd(0)$ complex (L = **L1**) was exposed to a bezene-d_6 solution of bromobenzene after which (~ 1 h) *n*-propylamine was added.

As shown in Figure 2-16, the oxidative addition of $(L1)_2Pd(0)$ in the presence of both bromobenzene and *n*-propylamine gives rise to amine and phosphine ligated palladium(II) complexes. Quantification of the "free" **L1** (at -9 ppm) showed the loss of far more than equivalent of **L1** (relative to the starting material). Thus for both reaction conditions the formation of a Pd(II) is quantitative (as determined by parallel GC experiments) but the product distributions are not identical.
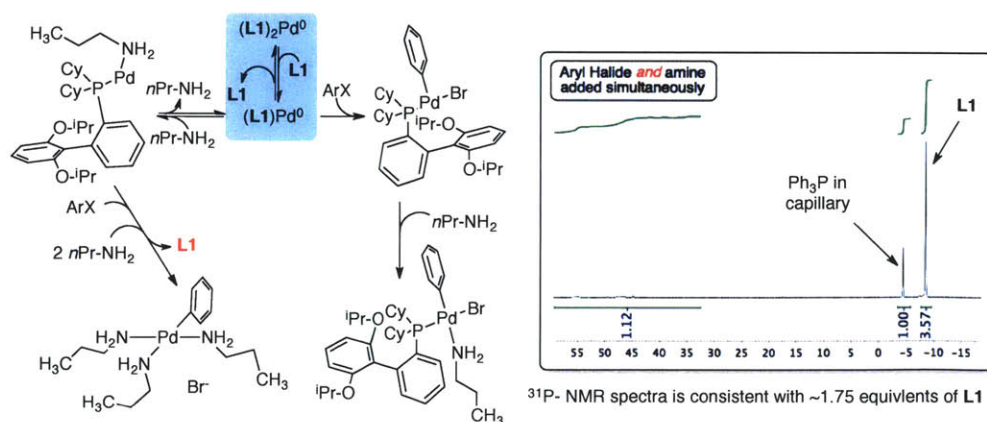
Figure 2-16 ^{31}P-NMR spectra of a $L_2Pd(0)$ complex exposed to a solution of n-propylamine and bromobenzene simultaneously leading to the loss of more than one equivalent of **L1**.

154

2.2.3. Steady State Kinetic Analysis

After investigating some of the elementary reaction steps of the palladium-catalyzed reaction of *n*-propylamine with 3-bromoanisole, the kinetic consequences of the proposed mechanism were further examined with the morpholine system. The fast initial rate of the reaction with morpholine when **OA1a** is employed mitigates the utility of the "excess" experiments.[9a] At elevated catalyst concentrations, the initial rate of the reaction is so fast that the reaction goes to completion prior to reaching the steady-state plateau region. At sufficiently low catalyst concentrations, only weak substrate dependences are observed for the plateau region. As previously described, we found that the reaction of *n*-propylamine can be used to efficiently generate "off-cycle" complexes ***OA1a** from **OA1a**. The employment of ***OA1a** would allow us to initiate the catalytic cycle from a near steady-state condition as shown in Scheme 2-5.

Scheme 2-5 Different methods of initiation for the cross-coupling reaction of morpholine and 3-bromoanisole.
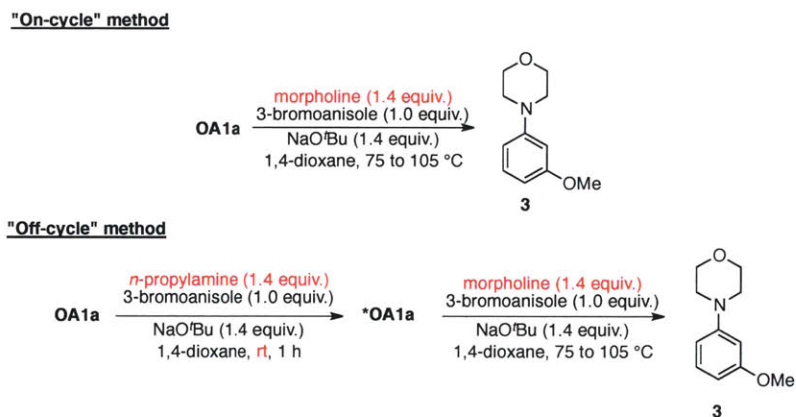
Using different concentrations of ***OA1a**, we found that the rate increase observed at the end of the reaction is preserved while the fast initial rate is suppressed (Figure 2-17). For both the "on-cycle" and "off-cycle" methods, low catalyst concentrations (~0.1 mol % at 105 °C) have the same limiting behavior where the reaction rate has a weak dependence on substrate concentration that manifests as a near constant rate (plateau region).

155
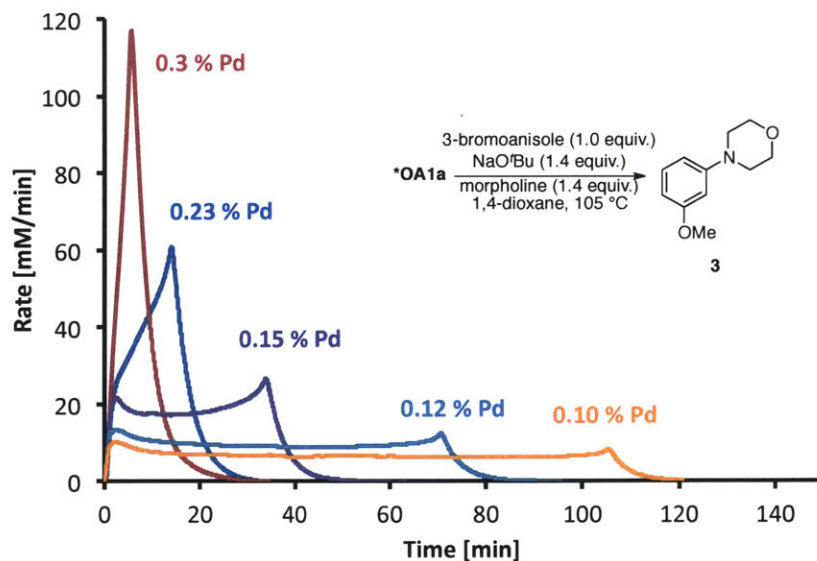
Figure 2-17 Cross-coupling reaction of 3-bromoanisole and morpholine initiated by ***OA1a.**

Investigations into the concentration dependence of the reaction with morpholine were performed at higher catalyst loadings and at a lower temperature (75 °C).[24] Variation of the initial concentration of morpholine revealed the anticipated dependence on amine concentration. As shown in Figure 2-18B, the reaction rate was essentially independent of morpholine concentration above 1.3 M while below 1.3 M there was an apparent inverse dependence. Moreover, comparing different experiments in Figure 2-18B, we note that when the morpholine concentration is 0.4 M (indicated with a dashed line), the rate decreases with increasing aryl halide concentration. This observation is consistent with an inverse dependence on the concentration of aryl halide and would explain why the three curves (red, green, blue) do not overlap.

156
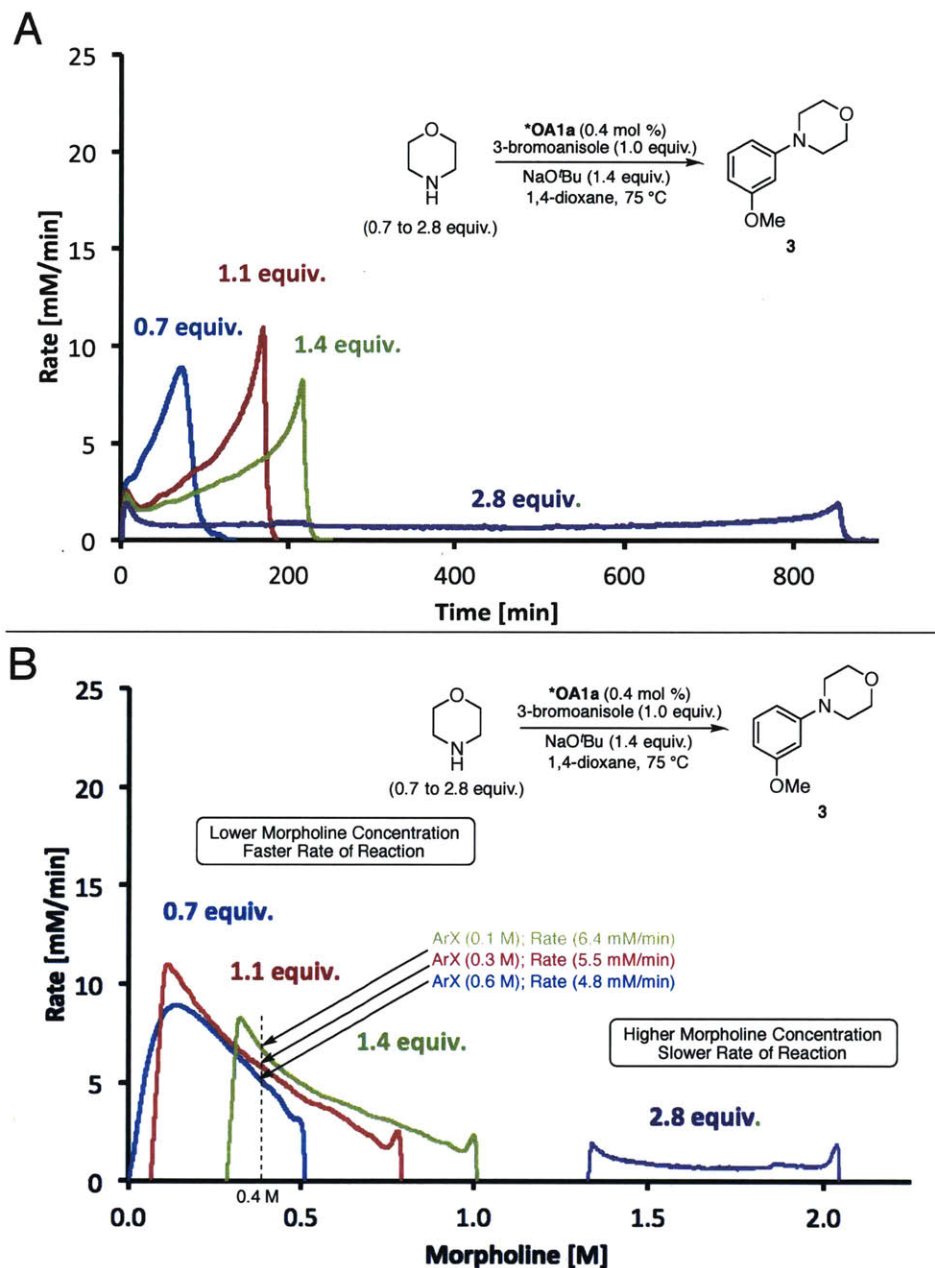
Figure 2-18 A) Cross-coupling reaction of morpholine with 3-bromoanisole with various initial concentrations of morpholine. B) The rate plotted as a function of morpholine concentration. Note that the reactions progress from right to left.

We can rationalize the inverse dependence on amine by its ability to influence the relative amounts of **I** and **I'**, which will affect the formation rate of "off-cycle" palladium. Since the rate constants for oxidative addition of **I** and **I'** should differ, the concentration or reactivity of the aryl halide should affect the relative proportion of oxidative addition through **I** and **I'**, and thus the global kinetic profile. This hypothesis is supported by the observation that for many of the reactions (see Figure 2-3), there is a rapid increase in rate at the end of the reaction that

157

corresponds to the complete consumption of the limiting reagent (aryl halide). Such a feature suggests that at low concentration (or low reactivity) of aryl halide, oxidative addition through complex **I** is favored.

To further confirm the inverse dependence on aryl halide, reactions employing ***OA1a** with different initial concentrations of 3-bromoanisole were compared. As shown in Figure 2-19, an inverse dependence on aryl halide concentration was observed. The reaction employing an initial 3-bromoanisole concentration of 0.95 M (blue line) proceeded at roughly half the rate of a reaction employing an initial concentration of 0.36 M (red line).[25] Furthermore, substitution of the less reactive 3-chloroanisole resulted in a dramatic increase in rate resulting in a reaction time of approximately 20 minutes compared to 3 hours for the aryl bromide. Despite, the well-established lower reactivity of aryl chlorides, this behavior is not without precedent. Previously studies have attributed the improvement in overall reaction rate to the greater ease of "transmetallation" of the chloride relative to the bromide in forming the amido complex (**IV**).[26] The current experiment suggests that improvement in overall reaction rate is due to the preference for oxidative pathway via complex **I**.[27-31]
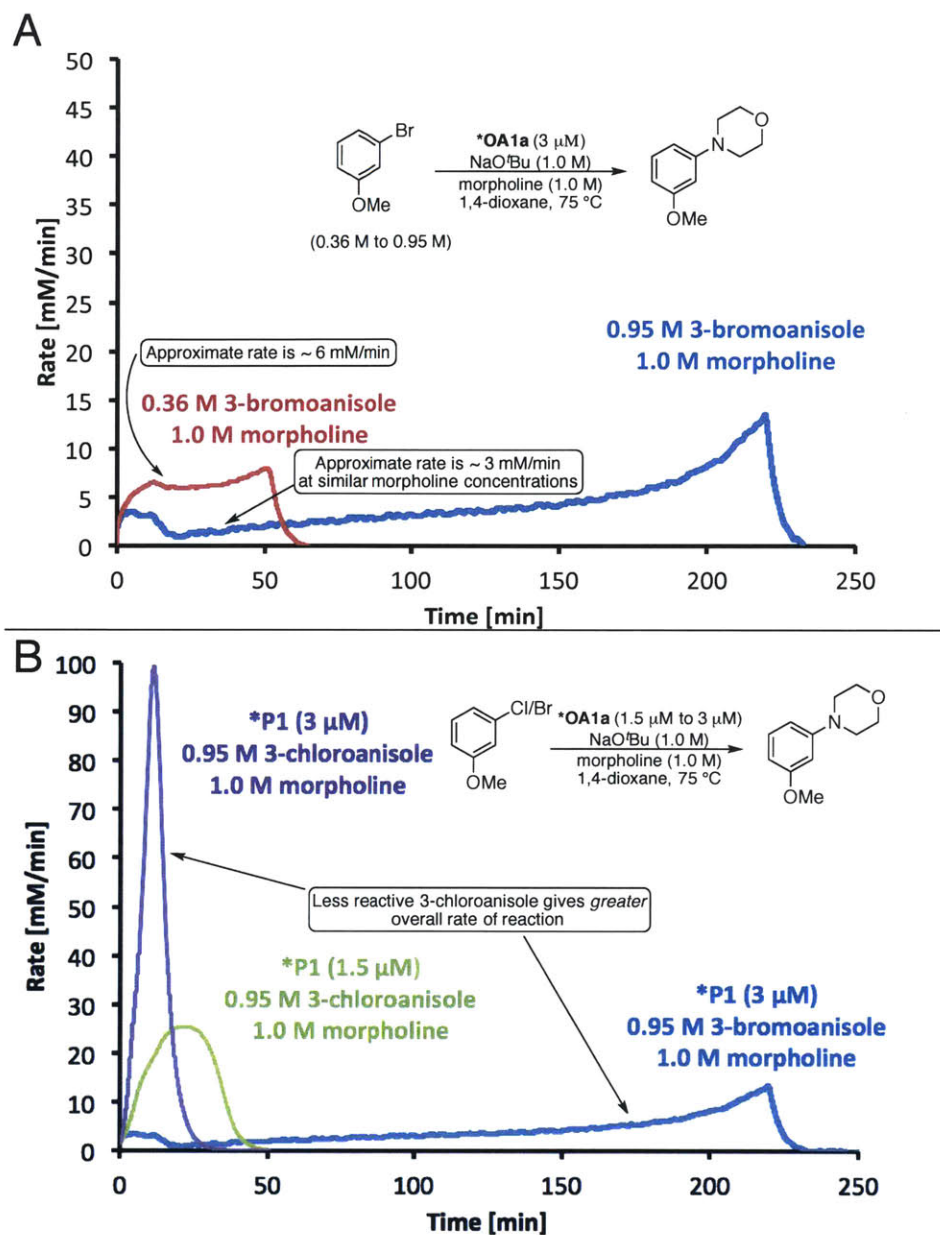
Figure 2-19 A) Cross-coupling reaction of morpholine and 3-bromoanisole with different initial concentrations of 3-bromoanisole B) The employment of the less reactive 3-chloroanisole affords a greater overall reaction rate.

2.2.4. Kinetic Modeling

Experiments have shown that the rate law is: 1) not linear in concentration of either **OA1a** or *OA1a, 2) dependent upon the catalyst source (e.g., **OA1a** vs *OA1a), 3) inversely dependent on the catalyst concentration of both amine and aryl halide at temperatures higher than 75 °C

and 4) displays positive order on the concentration of added **L1** (but not at ambient temperatures).[32]

Elementary steps have been proposed that can account for much of this behavior with the caveat that the proposed model remains an incomplete description of the mechanism. We modeled the "off-cycle" species as two different Pd(II) "off-cycle" complexes (**V** and **VI**). The complex **V** is proposed to be an amine bound Pd(II) complex. We are uncertain as to the structure of the dimeric complex(es) **VI**, but the unknown species observed at 45 ppm by ^{31}P-NMR prompted the invocation of this intermediate. Furthermore, the strong dependence of displaced **L1** on the initial concentration of **OA1a** which we attribute to palladium-palladium interaction is partly captured in our model by a bimolecular interaction between **V** and **II'**. Thus for high concentration of catalyst, the formation of **VI** occurs more readily, while lower concentration of catalyst should favor a greater proportion of **V** (and free **L1**). Additional assumptions regarding the formation of **I** and **I'** (green box) were also necessary. The formation of **I'** from **IV** and interconversion between **I** and **I'** are plausible but simplified relationship among several possibilities (see Scheme 2-6 and Scheme 2-8).

With these approximations in mind, the full rate law was derived from the scheme below. Only kinetically relevant substrate species (and corresponding rate constants) are highlighted in blue. A single set of rate constants were chosen to give a qualitative fit to the experimental data at 75 °C. The rate constant k_{L1} relative to other rate constants was set to ensure that re-association of **V** with **L1** to form "on-cycle" intermediate **IV** is the slowest step in the process. The oxidative addition rate constants were chosen so that $k_{OA1} \gg k_{OA2}$, indicating that **I** is more reactive than **I'** towards oxidative addition. Furthermore, this assumption is necessary to obtain the inverse dependence on aryl halide. Thus at low concentration (or low reactivity) of aryl halide, oxidative addition via **I** is favored and will manifest as a rapid increase in overall rate of catalyst near the end of the reaction. To make the interconversion rate of **I** and **I'** comparable to the rate of oxidative addition k_F/k_R was specified to be near unity and the ratios k_{D2}/k_{D1} and k_{OA1}/k_R were fitted to the experimental data. The rate law was then evaluated using the Runge-Kutta algorithm implemented in the MATLAB software package.

Scheme 2-6 Proposed mechanism incorporating off-cycle species
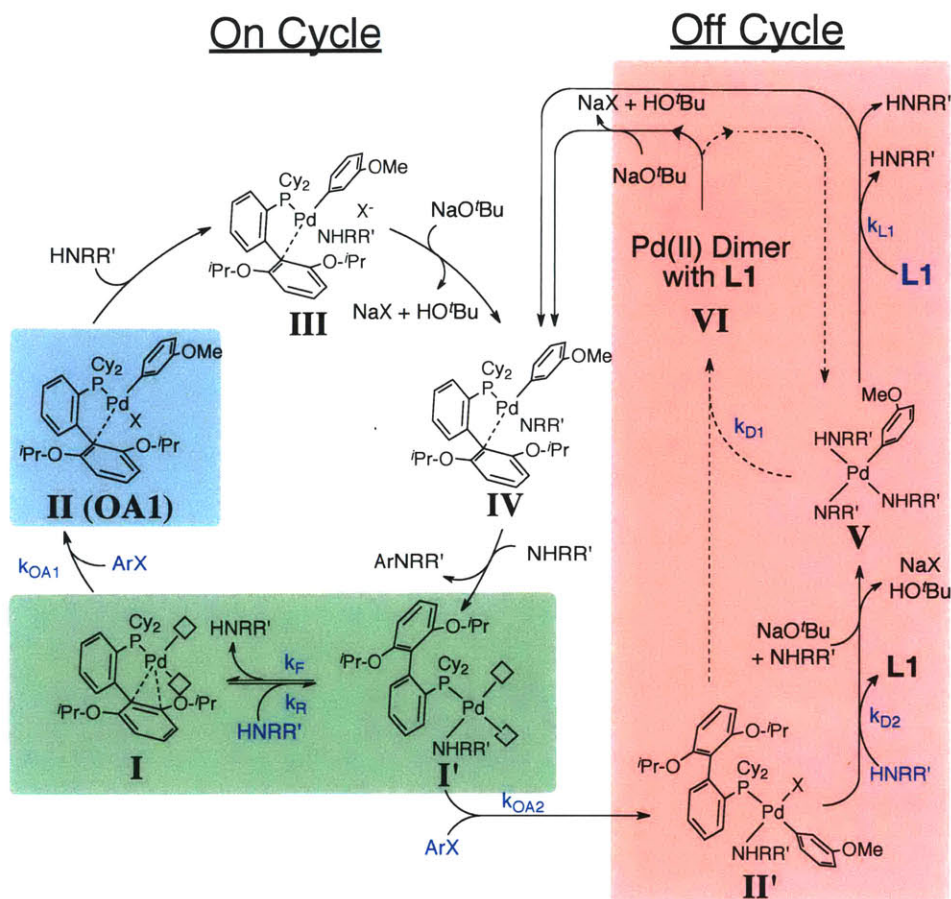
As shown in Figure 2-20, the simulated rate is strongly affected by the catalyst loading and whether the reaction is started using either "off-cycle" ***OA1a** or "on-cycle" **OA1a** palladium. Both of these phenomena were observed in our experimental data as well. Using the same rate constants, the model simulation is able to qualitatively reproduce the dependence upon amine concentration as shown in Figure 2-20 (compare to Figure 2-18) while reproduction of the inverse dependence upon aryl halide is less satisfactory (Figure 2-24). Simulation of added ligand gives a linear relationship with inverse reaction time but overestimates the dependence when compared to the experimental data (Figure 2-44). Further meaningful improvements to this model will require more detailed studies towards the identification of these "off-cycle" catalytic species.
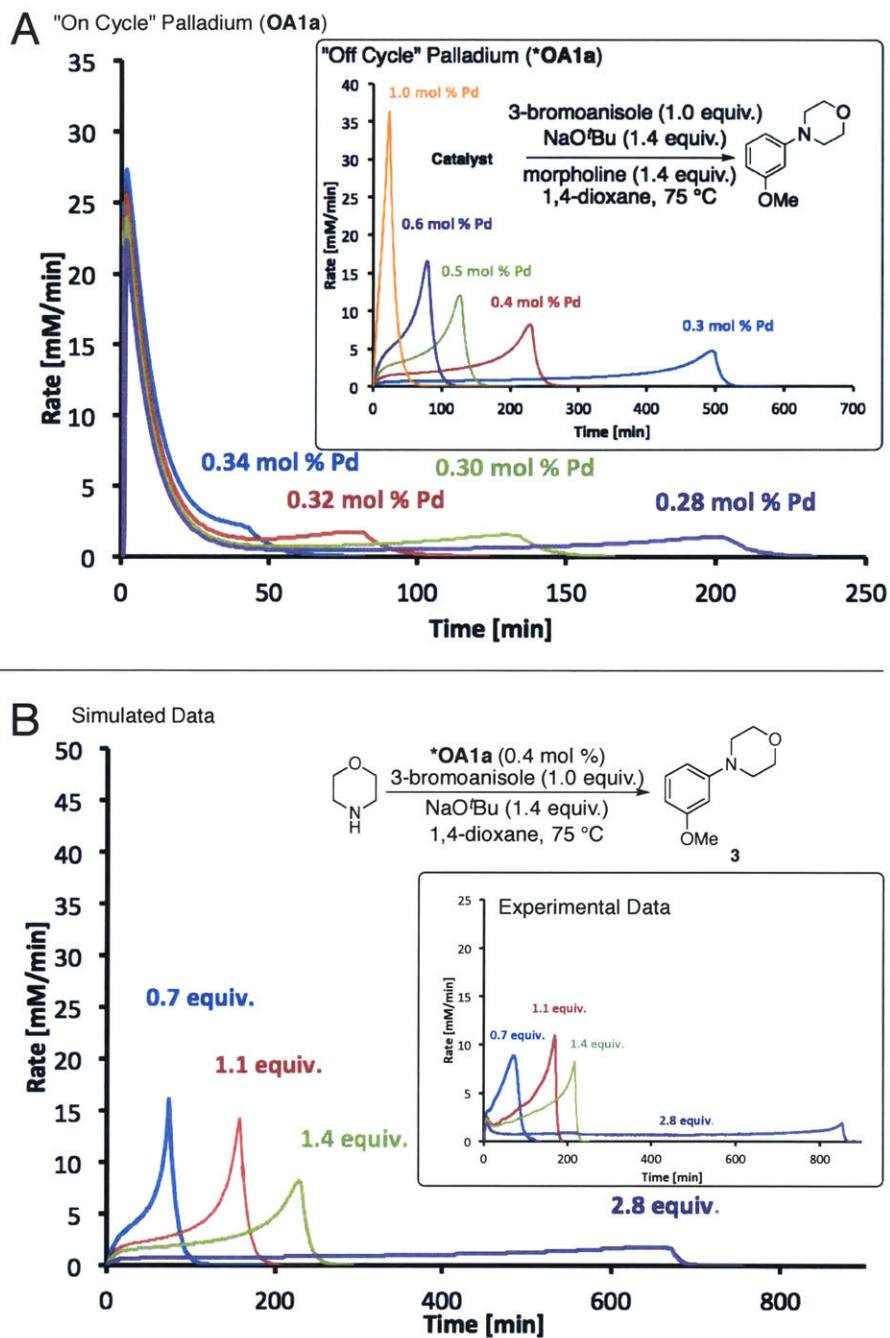
Figure 2-20 A) Simulated rate of reaction with "On-Cycle" palladium. Chart Inset contains the simulated rate of reaction with "Off-Cycle" palladium B) Simulated rate of reaction with "Off-Cycle" palladium and various initial concentrations of amine. Chart inset contains a reproduction of the experimental data.

162

2.3. Summary

Even for simple substrates, the C–N cross-coupling reaction is significantly more complex than the catalytic cycle usually presented suggests (Figure 1-1). Arguments based only on "on-cycle" elementary reaction steps can be misleading when "off-cycle" palladium species act as catalyst reservoirs. Attempts to optimize the reaction rates by increasing the concentration (or reactivity) of the amine substrates and aryl halides can lead to diminished reaction rates. Merely conducting the reaction under more dilute conditions can lead to a greater rate of reaction. Given that a palladium catalyst readily affords product at room temperature for various amines is evidence that "on-cycle" elementary steps are sufficiently rapid *and that suppressing the formation of the "off-cycle" or dormant catalyst states is an important consideration in reaction optimization.*

Furthermore, we have shown that multiple ligand, amine, and aryl halide combinations that give overlapping kinetic profiles. The results presented in this chapter indicate that the formation of the amido complex (**IV**) from an "off-cycle" palladium(II) species is the rate-determining step in a number of reactions. Identification of these "off-cycle" complexes and investigation of their chemistries is a key step towards gaining a complete understanding of these reactions.

2.4. Experimental

2.4.1. Derivation of Rate law

Scheme 2-7 Proposed partial mechanism with Off-Cycle Species (reproduced from Scheme 2-6)
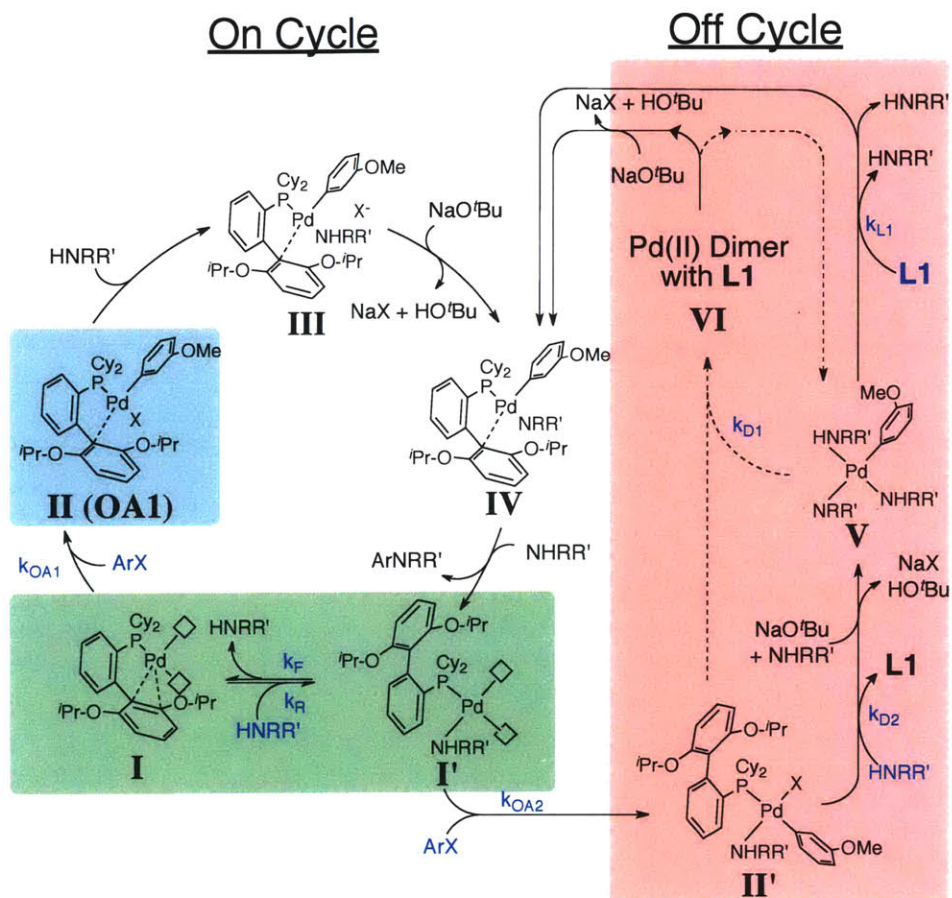
Starting from the scheme above, we write the following differential equations to describe the reaction network as seen in equation 1.1. Here we have replaced the roman numerals (**I**, **II**, **IV**, etc) with Arabic (e.g., [1], [1']) numerals where brackets indicating units of concentration. The first equation gives the rate of reaction by accounting for the consumption of aryl halide. The parameter c is a quantity relating conversion relative to a reference concentration $[ArX]_o$. The kinetic parameters (for now) are written without reference to substrate concentrations. A differential equation (rate law) for species [4] (**IV**) is not directly written- we assume that **IV** leads directly to **I'**. The same argument is used for **II(OA1)** which leads directly to **I'**. Likewise in this scheme, we also assume that **VI** leads immediately to **V** and **I'**.

164

$$\frac{d}{dt}\begin{bmatrix} [ArX]_o c \\ [1] \\ [1'] \\ [2'] \\ [5] \end{bmatrix} = \begin{bmatrix} k_{OA1} & k_{OA2} & 0 & 0 \\ -(k_F + k_{OA1}) & k_R & 0 & 0 \\ k_F + k_{OA1} & -(k_R + k_{OA2}) & k_{D1} & k_{L1} \\ 0 & k_{OA2} & -(k_{D1} + k_{D2}) & 0 \\ 0 & 0 & k_{D2} & -k_{L1} \end{bmatrix}\begin{bmatrix} [1] \\ [1'] \\ [2'] \\ [5] \end{bmatrix} \qquad 2.1$$

We make the following steady state assumptions for [2], thus converting the 4th differential equation into an algebraic one.

$$\frac{d[2']}{dt} = 0 = k_{OA2}[1'] - (k_{D1} + k_{D2})[2] \rightarrow \frac{k_{OA2}}{(k_{D1} + k_{D2})}[1'] = [2'] \qquad 2.2$$

Application of equation **2.2** leads to the new matrix.

$$\frac{d}{dt}\begin{bmatrix} ArX_o c \\ [1] \\ [1'] \\ [5] \end{bmatrix} = \begin{bmatrix} k_{OA1} & k_{OA2} & 0 \\ -(k_F + k_{OA1}) & k_R & 0 \\ k_F + k_{OA1} & -k_R - k_{OA2} + k_{D1}\dfrac{k_{OA2}}{(k_{D1} + k_{D2})} & k_{L1} \\ 0 & k_{D2}\dfrac{k_{OA2}}{(k_{D1} + k_{D2})} & -k_{L1} \end{bmatrix}\begin{bmatrix} [1] \\ [1'] \\ [5] \end{bmatrix} \qquad 2.3$$

We make a similar steady state assumption for [1], thus converting the 2nd differential equation into an algebraic equation.

$$\frac{d[1]}{dt} = 0 = -(k_F + k_{OA1})[1] + k_R[1'] \rightarrow \frac{k_R}{k_F + k_{OA1}}[1'] = [1] \qquad 2.4$$

Application of this equation leads to the new matrix

$$\frac{d}{dt}\begin{bmatrix} -ArX_o c \\ [1'] \\ [5] \end{bmatrix} = \begin{bmatrix} k_{OA1}\dfrac{k_R}{k_F + k_{OA1}} + k_{OA2} & 0 \\ -k_{OA2} + \dfrac{k_D k_{OA2}}{(k_{D1} + k_{D2})} & k_{L1} \\ \dfrac{k_{D2} k_{OA2}}{(k_{D1} + k_{D2})} & -k_{L1} \end{bmatrix}\begin{bmatrix} [1'] \\ [5] \end{bmatrix} \qquad 2.5$$

We now begin to explicitly write out the substrate dependencies in terms of dimensionless parameters

$$k_{OA1} \rightarrow k'_{OA1}(X_0 - c) \qquad\qquad 2.6a$$

$$k_{OA2} \rightarrow k'_{OA2}(X_0 - c) \qquad\qquad 2.6b$$

$$k_F \rightarrow k'_F(A_0 - c) \qquad\qquad 2.6c$$

$$k_{L1} \rightarrow k'_{L1} \frac{[Pd]_0}{[ArX]_o} (< 5 > +L_o)$$ 2.6d

$$k_{D1} \rightarrow k'_{D1} \frac{[Pd]_0}{[ArX]_o} < 5 >$$ 2.6e

$$k_{D2} \rightarrow k'_{D2}(A_0 - c)$$ 2.6f

$$k_R \rightarrow k'_R$$ 2.6g

We note that

$$< 5 > [Pd]_0 = [5]$$ 2.7a

$$< 1' > [Pd]_0 = [1']$$ 2.7b

Application of equations **2.6a-2.6g** to equation **2.5** yields equation **2.8**

$$\frac{d}{dt}\begin{bmatrix} ArX_o c \\ [1'] \\ [5] \end{bmatrix} = \begin{bmatrix} k'_{OA1}(X_0 - c)\frac{k'_R}{k'_F(A_0 - c) + k'_{OA1}(X_0 - c)} + k'_{OA2}(X_0 - c) & 0 \\ -k'_{OA2}(X_0 - c) + \frac{k'_{D1}\frac{[Pd]_0}{[ArX]_o} < 5 > k_{OA2}(X_0 - c)}{\left(k'_{D1}\frac{[Pd]_0}{[ArX]_o} < 5 > +k'_{D2}(A_0 - c)\right)} & k'_{L1}\frac{[Pd]_0}{[ArX]_o}(< 5 > +L_o) \\ \frac{k'_{D2}(A_0 - c)k'_{OA2}(X_0 - c)}{\left(k'_{D1}\frac{[Pd]_0}{[ArX]_o} < 5 > +k'_{D2}(A_0 - c)\right)} & -k'_{L1}\frac{[Pd]_0}{[ArX]_o}(< 5 > +L_o) \end{bmatrix}\begin{bmatrix} [1'] \\ [5] \end{bmatrix}$$ 2.8

Simplification and substitution of equation **2.7** into equation **2.8** yields....

$$\frac{d}{dk_{L1}t}\begin{bmatrix} \frac{[ArX]_o}{[Pd]_0}c \\ < 1' > \\ < 5 > \end{bmatrix} = \begin{bmatrix} \frac{k'_{OA1}}{k'_{L1}}\frac{k'_R(X_0 - c)}{k'_F(A_0 - c) + k'_{OA1}(X_0 - c)} + \frac{k'_{OA2}}{k'_{L1}}(X_0 - c) & 0 \\ \frac{k'_{OA2}}{k'_{L1}}(c - X_0) + \frac{k'_{OA2}}{k'_{L1}}\frac{\frac{k'_{D1}}{k'_{D2}}\frac{[Pd]_0}{[ArX]_o} < 5 > (X_0 - c)}{\left(\frac{k'_{D1}}{k'_{D2}}\frac{[Pd]_0}{[ArX]_o} < 5 > +(A_0 - c)\right)} & \frac{[Pd]_0}{[ArX]_o}(< 5 > +L_o) \\ \frac{k'_{OA2}}{k'_{L1}}\frac{(A_0 - c)(X_0 - c)}{\left(\frac{k'_{D1}}{k'_{D2}}\frac{[Pd]_0}{[ArX]_o} < 5 > +(A_0 - c)\right)} & -\frac{[Pd]_0}{[ArX]_o}(< 5 > +L_o) \end{bmatrix}\begin{bmatrix} < 1' > \\ < 5 > \end{bmatrix}$$ 2.9

Further rearrangement yields....

$$\frac{d}{dk_{L1}t}\begin{bmatrix} \frac{[ArX]_o}{[Pd]_0}c \\ < 1' > \\ < 5 > \end{bmatrix} = \begin{bmatrix} \left(\frac{k'_{OA1}}{k'_{OA2}}\frac{1}{\frac{k'_F}{k_R}(A_0 - c) + \frac{k'_{OA2}}{k_R}\frac{k'_{OA1}}{k'_{OA2}}(X_0 - c)} + 1\right)(X_0 - c) & 0 \\ (c - X_0) + \frac{\frac{[Pd]_0}{[ArX]_o} < 5 > (X_0 - c)}{\left(\frac{[Pd]_0}{[ArX]_o} < 5 > +\frac{k'_{D2}}{k'_{D1}}(A_0 - c)\right)} & \frac{[Pd]_0}{[ArX]_o}(< 5 > +L_o) \\ \frac{\frac{k'_{D2}}{k'_D}(A_0 - c)(X_0 - c)}{\left(\frac{[Pd]_0}{[ArX]_o} < 5 > +\frac{k'_{D2}}{k'_{D1}}(A_0 - c)\right)} & -\frac{[Pd]_0}{[ArX]_o}(< 5 > +L_o) \end{bmatrix}\begin{bmatrix} \frac{k'_{OA2}}{k'_{L1}} < 1' > \\ < 5 > \end{bmatrix}$$ 2.10

Finally, we cast this into a form amenable to computer implementation. We should note that the second and third equations of **2.11** are linearly dependent and that the first column of the Jacobian contains only zero elements.

$$\frac{d}{dk'_{L1}t}\begin{bmatrix}\frac{[\text{ArX}]_o}{[\text{Pd}]_0}c \\ <1'> \\ <5>\end{bmatrix} = \begin{bmatrix} 0 & \left(\frac{k'_{OA1}}{k'_{OA2}}\frac{1}{\frac{k'_F}{k'_R}(A_0-c)+\frac{k'_{OA2}}{k'_R}\frac{k'_{OA1}}{k'_{OA2}}(X_0-c)}+1\right)(X_0-c) & 0 \\ 0 & (c-X_0)+\frac{\frac{[\text{Pd}]_0}{[\text{ArX}]_o}<5>(X_0-c)}{\left(\frac{[\text{Pd}]_0}{[\text{ArX}]_o}<5>+\frac{k'_{D2}}{k'_{D1}}(A_0-c)\right)} & \frac{[\text{Pd}]_0}{[\text{ArX}]_o}(<5>+L_o) \\ 0 & \frac{\frac{k'_{D2}}{k'_D}(A_0-c)(X_0-c)}{\left(\frac{[\text{Pd}]_0}{[\text{ArX}]_o}<5>+\frac{k'_{D2}}{k'_{D1}}(A_0-c)\right)} & -\frac{[\text{Pd}]_0}{[\text{ArX}]_o}(<5>+L_o) \end{bmatrix}\begin{bmatrix} c \\ \frac{k'_{OA2}}{k'_{L1}}<1'> \\ <5>\end{bmatrix}$$

2.11

This system of equations (equation **2.11**) has the following two possible initial conditions

$$\text{"On-Cycle" } initial\ condition\ \begin{bmatrix} c \\ <1'> \\ <5>\end{bmatrix} = \begin{bmatrix}0\\1\\0\end{bmatrix} when\ k'_{L1}t=0 \qquad \text{2.12a}$$

$$\text{"Off-Cycle" } initial\ condition\ \begin{bmatrix} c \\ <1'> \\ <5>\end{bmatrix} = \begin{bmatrix}0\\0\\1\end{bmatrix} when\ k'_{L1}t=0 \qquad \text{2.12b}$$

A total of 13 dimensionless groups for this model are as follows[33]:

$$<1'>,<5>,c,X_0,A_0,L_0,\frac{[\text{Pd}]_0}{[\text{ArX}]_o},k'_{L1}t,\frac{k'_{OA1}}{k'_{OA2}},\frac{k'_{OA2}}{k'_{L1}} \qquad \text{2.13}$$

$$\frac{k'_{OA2}}{k'_R},\frac{k'_F}{k_R},\frac{k'_{D2}}{k'_D} \qquad \text{2.14}$$

The parameter $<1'>$ represents the dimensionless concentration of Species I' and $<5>$ represents the dimensionless concentration of Species **5** which are the only two "allowed" species in the mathematical model. These parameters can take allowed values between zero and one but their sums must equal one. The c parameter represents a dimensionless conversion relative to a reference concentration $[\text{ArX}]_o$. The value of c can take values between zero up to the lesser value (limiting reagent) of X_0 or A_0. (Typically X_0 is set to one equivalent and A_0 is set to 1.4 equivalents so that the value of c is between zero and one.) The parameters X_o and A_o represent aryl halide equivalents and amine equivalents relative to the reference (dimensioned) concentration $[\text{ArX}]_o$ which is specified at 0.73 M. The parameter L_0 represents the number of "added" ligand equivalents relative to the (dimensioned) concentration $[\text{Pd}]_0$. The ratio $\frac{[\text{Pd}]_0}{[\text{ArX}]_o}$ represents the (dimensionless) molar fraction of palladium relative to the (dimensioned) reference concentration. The dimensionless parameter $\frac{k'_{OA1}}{k'_{OA2}}$ is set to a value of 200, which indicates that oxidative addition through pathway OA1 is faster than OA2. The

dimensionless parameter $\frac{k'_{OA2}}{k'_{L1}}$ is set to a value of 10. Further increases in this value do not change the simulation results[1] but can cause numerical instability in the Runge-Kutta algorithm used as implemented by MATLAB. The parameter $k'_{L1}t$ represents a dimensionless time, thus equation **2.11** is solved in this dimensionless time coordinate and given the actual experimental time k'_{L1} is then determined.

This leaves the following dimensionless groups to be determined. Given that the reaction rate is a strong function of amine (as shown in Figure 2-18), we compute the following estimate-

$$\frac{[Pd]_0}{[ArX]_o} < 5 > \approx \frac{k'_{D2}}{k'_D}(A_0 - c) \rightarrow \frac{\frac{[Pd]_0}{[ArX]_o} < 5 >}{(A_0 - c)} \approx \frac{k'_{D2}}{k'_D} \rightarrow \frac{k'_{D2}}{k'_D} \sim \left(0.004 * \frac{1}{1.4}\right) \qquad 2.15$$

We also make the following estimate

$$\frac{k'_F}{k_R}(A_0 - c) \approx \frac{k'_{OA2}}{k'_R}\frac{k'_{OA1}}{k'_{OA2}}(X_0 - c) \rightarrow \frac{k'_F}{k_R}1.4 \approx \frac{k_{OA2}}{k_R}200 * 1 \qquad 2.16$$

Based on the experimental observation that the morpholine based reaction gives 20 to 30 turnovers at room temperature we estimate the parameter $\frac{k'_{OA2}}{k'_R}$ to have a value of 0.05 thus based on equation **2.16** we would estimate $\frac{k'_F}{k'_R}$ temperature to have a value of 7.1. Keeping in mind that these two dimensionless groups are compensating parameters (see the Jacobian of equataton 1.11 (1st row 2nd column)), an alternative method would be to set $\frac{k'_F}{k'_R}$ to unity and thus obtain an estimate for $\frac{k'_{OA2}}{k'_R}$. Based on these initial estimates, two of the parameters were fitted the experimental values in the manuscript in order to obtain the final parameters summarized in the table below.

Table 2-1 Parameters for Kinetic Simulations

Kinetic Parameters	Value	Note
$\frac{k'_{OA1}}{k'_{OA2}}$	200 [-]	Estimated
$\frac{k'_{OA2}}{k'_{L1}}$	10 [-]	Estimated

$\dfrac{k'_F}{k'_R}$	1 [-]	Estimated
$\dfrac{k'_{D2}}{k'_D}$	0.0118 [-]	Fitted from initial estimate
$\dfrac{k'_{OA2}}{k'_R}$	0.001 [-]	Fitted from initial estimate
k'_{L1}	0.596 [1/min]	Chosen to correspond to experimental time
$[ArX]_o$	0.73 M	Reference concentration; constant

With these parameters a MATLAB script was run to solve Equation **2.11** and the rates were plotted as a function of dimensionless time. A convolution by use of a Fourier transform was applied to the simulated rate data in order to better reproduce the calorimeter's response factor. This data was then plotted in Excel and converted to dimensioned coordinates- Rate in terms of M/min and time in terms of minutes.

2.4.2. Simulation Results
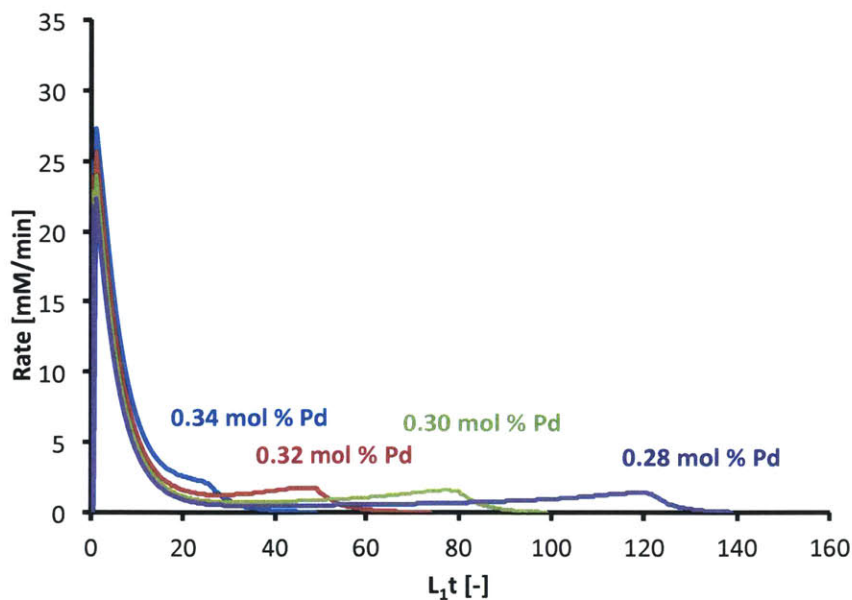
Figure 2-21 Simulated rates in terms of dimensionless time at various concentration of palladium catalyst. Initial condition is given by equation 2.12a. Kinetic parameters are given in Table 2-1. ($A_0 = 1.3$ and $X_0 = 1.0$)
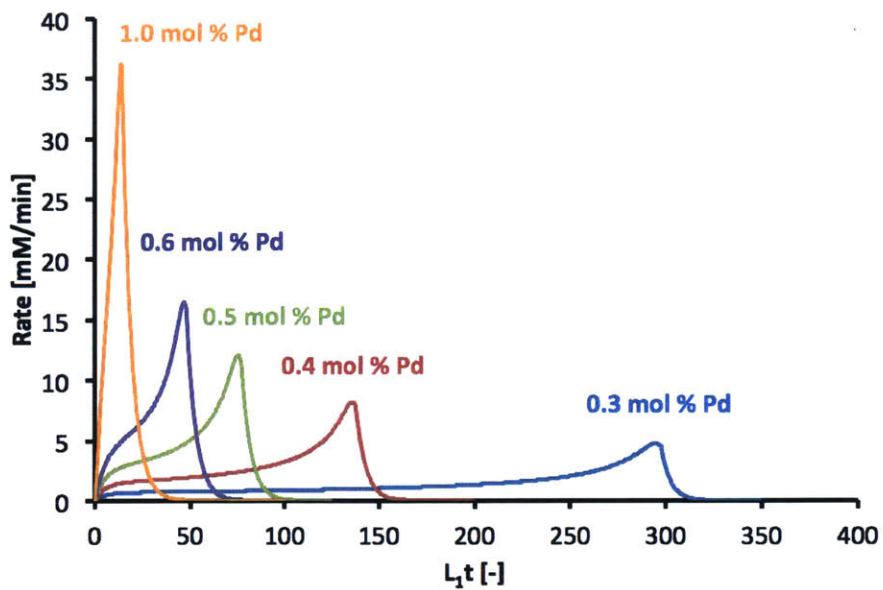
Figure 2-22 Simulated rates as a function of dimensionless time. Initial conditions given by equation 2.12b. Kinetic parameters are otherwise unchanged.
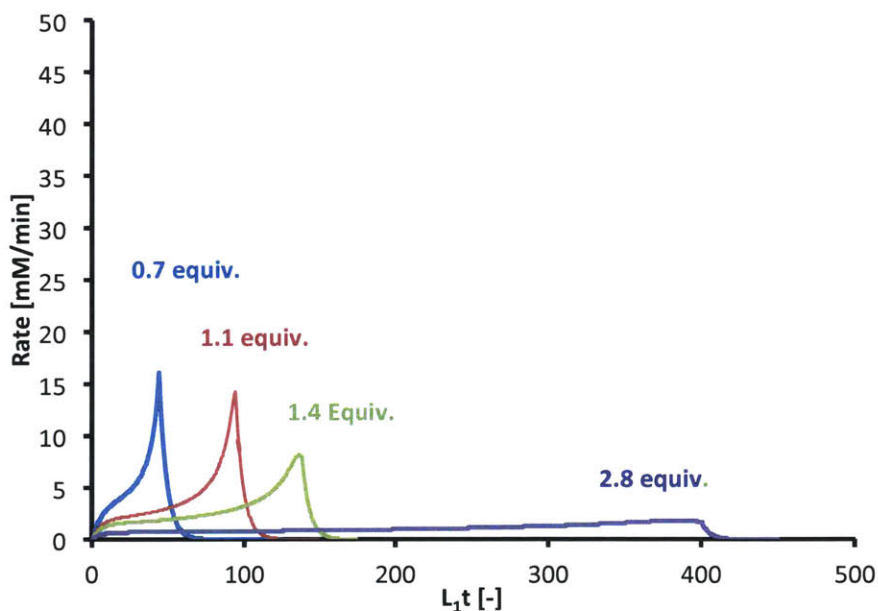
Figure 2-23 Simulated rate as a function of dimensionless time. Initial condition is given by equation 2.12b. Concentration of palladium is 0.4 mol % relative to reference concentration. Curves refer to different amine equivalent: 0.7 (blue), 1.1 (ref), 1.4 (green) and 2.8 (purple)

170
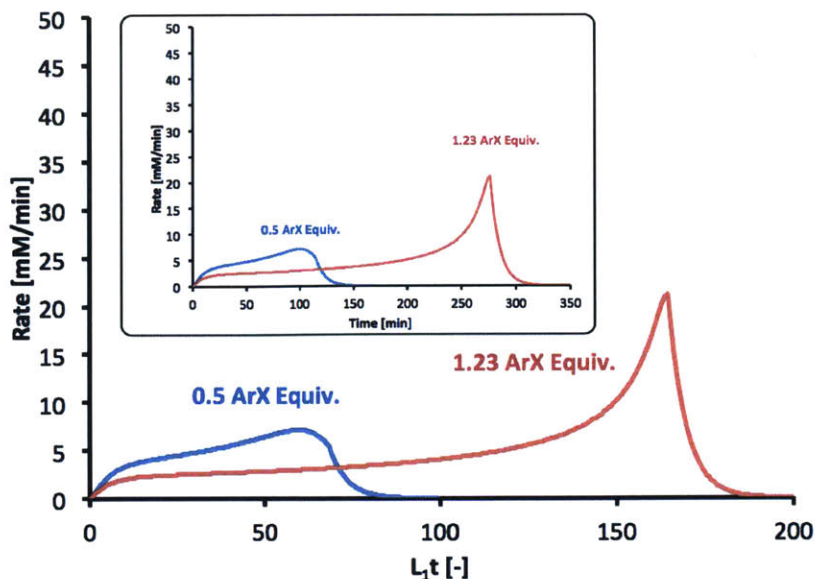
Figure 2-24 Simulated rate as a function of dimensionless time. Inset shows same graph as function of time in minutes. Initial condition is given by equation 2.12b. Palladium concentration is 0.4 mol % relative to reference concentration $[ArX]_0 = 0.73M$.
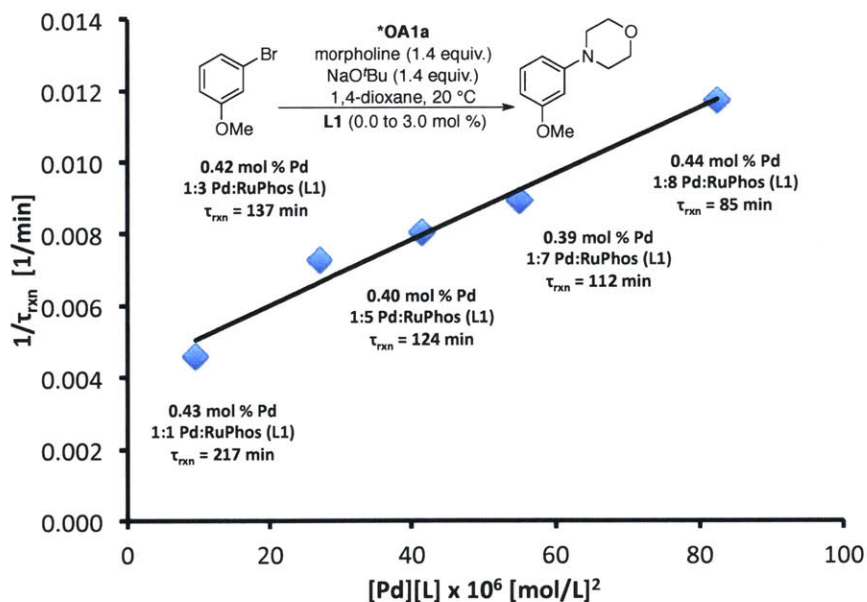
Figure 2-25 Experimental Data plotting reciprocal reaction time.

2.4.3. Approximations in the model for Pd(0) Complexes.

With even modest numbers of (compensating) parameters in a model, *it is easy to simulate most any kind of behavior*. However, in the absence of corroborative experimental evidence (i.e. kinetic experiments of *individual steps)* many different combinations of kinetic parameters will

yield similar results. A more realistic model (Scheme 2-8) may thus include different Pd(0) species in addition to Complex **I** and Complex **I'** with which further "adjustments" could be made to achieve a better fit to the experimental data but we felt a simpler model would more effectively rationalize and communicate our experimental results (Scheme 2-6). We have presented a more exhaustive scheme below where those species labeled with a green box are the same as those presented in the manuscript.

It is important to point out that the amido complex **IV** undergoes reductive elimination to form complex **O** which is contained in the grey box of Scheme 2-8. This intermediate **O** can then form a series of complexes **I'**, **A**, **B**, **C** which all can undergo oxidative addition to form **II'**. This same intermediate can also form **I**, which is in the yellow box of Scheme 2-8. In the manuscript, the yellow box (Scheme 2-8) is represented as a single species **I**. In the manuscript, the grey box (Scheme 2-8) is represented as a single species **I'**.

With significant mathematical effort, the fitted rate constants (Table 2-1) could be recast in terms of the elementary processes described in Scheme 2-8. This would require application of a detailed balance for each elementary step, which imposes some mathematical constraints but will result in an underdetermined set of equations.[2] Nonetheless, we can take this scheme and by use of scaling arguments show a set of differential equations (rate laws) that match in form equation 2.11

Scheme 2-8 Exhaustive Scheme of Palladium(0) Species.
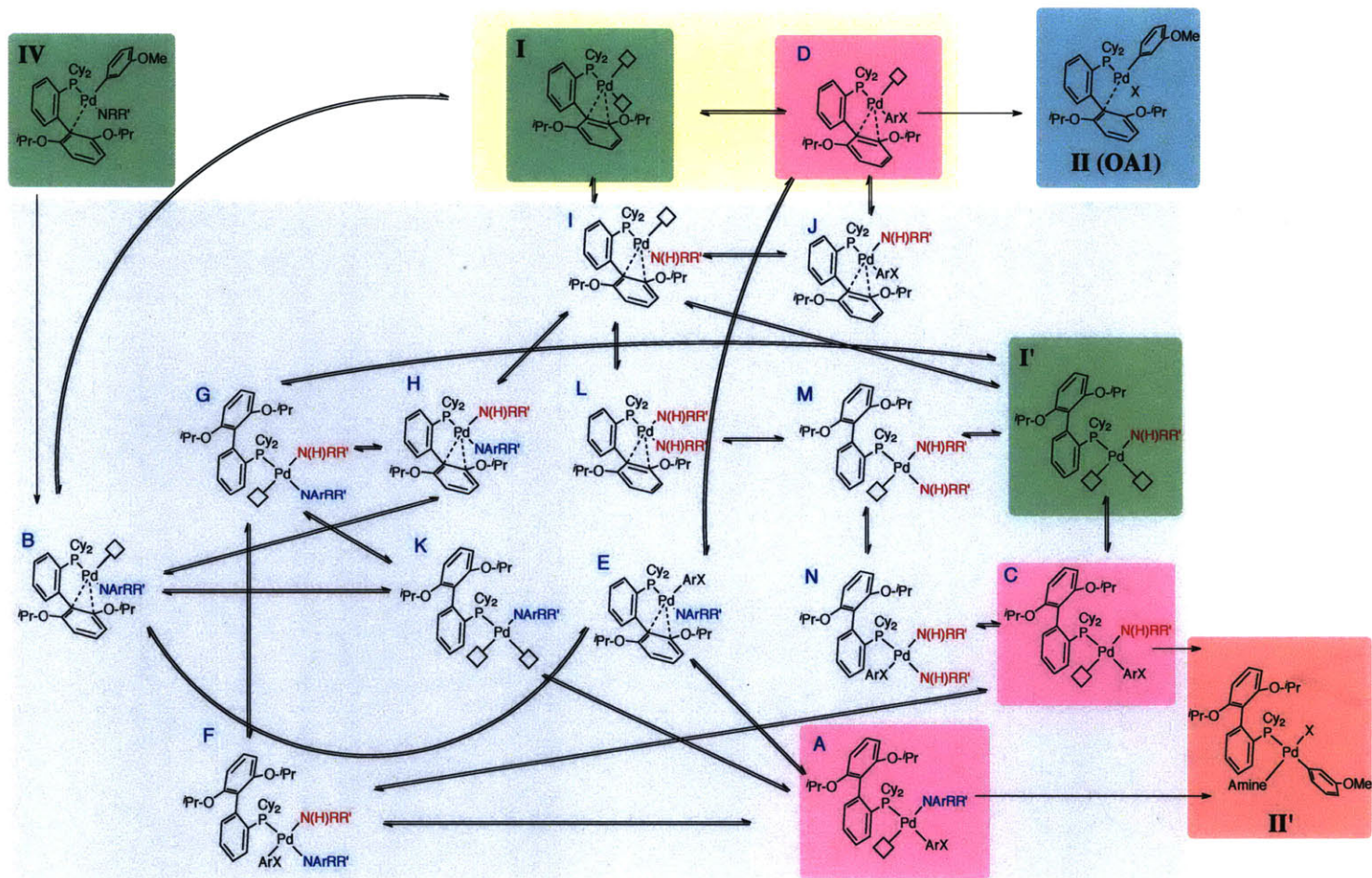
Green Boxes are complexes presented in the manuscript
Pink Boxes are Complexes which can undergo oxidative addition
Grey box indicates those species which are represented by **I'** in the manuscript
Yellow box indicates those species which are represented by **I** in the manuscript

Note: The binding mode of the aryl halide to the palladium is not explicitly stated but may be bound to the pi system or directly to the halide. Not all potential stereoisomers are listed.

ArX	Aryl Halide
NArRR'	Cross coupled product
N(H)RR'	Amine Substrate

We start by defining the following auxiliary functions, $\mathcal{F}$ (grey box; Scheme 2-8) and $\mathcal{H}$ (yellow box; Scheme 2-8).

$$\mathcal{H} = [1] + [D] \qquad\qquad 2.17$$

$$\mathcal{F} = [1'] + [A] + [B] + [C] + [E] + [F] + [G] + [H] + [I] + [J] + [K] + [L] + [M] \\ + [N] \qquad\qquad 2.18$$

We give an example for how rate constants are written for the elementary reaction steps of Scheme 2-8. For the conversion of Species K to Species A, the rate constant is $k_{K,A}$ and the rate constant for the reverse reaction is written as $k_{A,K.}$ In the interest of saving space in an already complicated reaction diagram, these rate constants are not explicitly written in Scheme 2-8.

We thus begin to define the following relationships in terms of our 1st order rate constants as in equation 2.11.

$$\overline{k_{OA1}} = \frac{k_{D,II}[D]}{\mathcal{H}} \qquad\qquad 2.19$$

Since $\mathcal{H}$ is defined as the sum of [1] and [D] then we would expect that the ratio of [D] to $\mathcal{H}$ be proportional to the amount of aryl halide so that k_{OA1} is proportional to the amount of aryl halide. Another rate constant can thus be defined as follows

$$\overline{k_F} = \frac{k_{DJ}[Amine][D]}{\mathcal{H}} + \frac{k_{[1]I}[Amine][1]}{\mathcal{H}} + \frac{k_{DE}[PROD][D]}{\mathcal{H}} + \frac{k_{[1]O}[PROD][1]}{\mathcal{H}} \qquad 2.20$$

The highlighted terms are proportional the amount of amine thus making $\overline{k_F}$ proportional to the amount of amine. The 3rd and 4th terms are in proportion to the amount of product that is not as nucleophilic as the amine and thus should not contribute significantly to the rate constant. Another rate constant can thus be defined as follows

$$\overline{k_R} = \frac{k_{JD}[J]}{\mathcal{F}} + \frac{k_{I[1]}[I]}{\mathcal{F}} + \frac{k_{ED}[E]}{\mathcal{F}} \qquad\qquad 2.21$$

The highlighted terms are not proportional to any of the substrates. The function $\mathcal{F}$ should be proportional to the amount of amine and thus the concentration of **J** and **I** (which are part of $\mathcal{F}$

and contain amine as a ligand) should also be proportional to the amount of amine. The last term contains the concentration of **E** which, a complex which includes as a ligand the cross-coupled product from reductive elimination. Thus its contribution to the rate constant should be small. From these arguments, would give the rate constant $\overline{k_R}$ no dependence on any substrates. This brings us to our final kinetic constant…

$$\overline{k_{OA2}} = \frac{k_{OA,A}[A]}{\mathcal{F}} + \frac{k_{OA,C}[C]}{\mathcal{F}} \qquad 2.22$$

The concentration of **A** should be proportional the amount of product amine (blue species; Scheme 2-8) which should not be as effective a ligand as the substrate amine (red species; Scheme 2-8). Based on this argument we can ignore the contribution of the 1st term. For the second term, the concentration of Species **C** should be in proportion to the concentration of ArX. Most of the species in $\mathcal{F}$ do not contain aryl halide as a ligand. Thus we would expect the rate constant $\overline{k_{OA2}}$ to be in proportional to the concentration of aryl halide.

Using equations 2.17 to 2.22, we can write the system of differential equations in a form very similar to equation 2.11 for our catalytic cycle. Thus given our scaling arguments for equations 2.19 and 2.22 Scheme 2-8 can be reasonably represented by the mechanism given in Scheme 2-16.

$$\frac{d}{dt}\begin{bmatrix} [ArX]_o c \\ \mathcal{H} \\ \mathcal{F} \\ [2'] \\ [5] \end{bmatrix} = \begin{bmatrix} \overline{k_{OA1}} & \overline{k_{OA2}} & 0 & 0 \\ -(\overline{k_F} + \overline{k_{OA1}}) & \overline{k_R} & 0 & 0 \\ \overline{k_F} + \overline{k_{OA1}} & -(\overline{k_R} + \overline{k_{OA2}}) & k_{D1} & k_{L1} \\ 0 & \overline{k_{OA2}} & -(k_{D1} + k_{D2}) & 0 \\ 0 & 0 & k_{D2} & -k_{L1} \end{bmatrix} \begin{bmatrix} \mathcal{H} \\ \mathcal{F} \\ [2'] \\ [5] \end{bmatrix} \qquad 2.23$$

2.4.4. MATLAB Script Files

What follows are the script files used to generate the simulated rate data.

```
function Objective2 = BatchScript2(min_arg)


    Param.PdArX = 0.004; %experiment
    Param.A0 = 1.4; % experiment
    Param.X0 = 1.0; % experiment
    Param.L0 = 0; %experiment

    Param.ArX0 = 0.73;   %constant

    Param.kOA1kOA2 = 200;


    Param.kOA2kL2 = 10;

    Param.kFkR =1*abs(min_arg(1));
    Param.kOA2kR = 2*0.0059*abs(min_arg(2));
    Param.kd2kd = 0.001*abs(min_arg(3));


    IVP =0.1 ;


    Param.plot =1;
    Param.SpeciesPlot = 0;
    Param.plot_script = 'r';
    Param.Save = 1;
    Param.Filename ='out.csv';
    if(1)
    Param.convolution = 0.2;
    else
        Param.convolution = 0;
    end


    L0_data = [0 2 4 6 7];
    Pd_data = [0.0043 0.0042 0.0040 0.0039 0.0044];
    time_data = [217 137 124 112 85];
    Color_data = ['r' 'k' 'k' 'k' 'k'];
    Names  = ['out1a.csv'; 'out1b.csv'; 'out1c.csv'; 'out1d.csv' ;'out1e.csv'];

    L0_data2 = [0 0 0 0];
    A0_data2 = [0.7 1.1 1.4 2.8];
    Pd_data2 = [0.0040 0.0040 0.0040 0.0040];
    time_data2 = [85 190 230 875];
    Color_data2 = ['b' 'r' 'g' 'm'];
    Names2  = ['out2a.csv'; 'out2b.csv';'out2c.csv' ;'out2d.csv'];

    L0_data3 = [0 0 0];
    A0_data3 = [1.4 1.4 1.4];
    Pd_data3 = [0.00405 0.004059 0.004];
    X0_data3 = [0.5 1.23 1.0];

    time_data3 = [50 225 10];
    Color_data3 = ['b' 'r' 'g'];
    Names3  = ['out3a.csv'; 'out3b.csv'; 'out3c.csv'];
```

```matlab
    L2 = 1.2; % should be 1.2 from 12
    L2t = 450;
 if(Param.plot)
   figure();
   hold on;
 end
 for i = 1:5
  Param.plot_script = Color_data(i);
  Param.L0 = L0_data(i);
  Param.PdArX = Pd_data(i);
  Param.Filename = Names(i,:);
  Time0(i) =FullODEScript2(IVP,L2t,Param);
  Objective1a(i) = Time0(i) /(L2*time_data(i))-1;
 end
 if(Param.plot)
 figure();
 hold on;
 plot((Pd_data/0.0043).*(1+L0_data),1./ Time0,'+');
 end
 if(Param.plot)
  figure();
  hold on;
 end
 for i = 1:4
   Param.plot_script = Color_data2(i);
   Param.L0 = L0_data2(i);
   Param.A0 = A0_data2(i);
   Param.PdArX = Pd_data2(i);
     Param.Filename = Names2(i,:);
   Objective1b(i) = FullODEScript2(IVP,L2t,Param)/(L2*time_data2(i))-1;
 end
 if(Param.plot)
   figure();
   hold on;
 end

  for i = 1:3

    Param.plot_script = Color_data3(i);
    Param.L0 = L0_data3(i);
    Param.A0 = A0_data3(i);
    Param.X0 = X0_data3(i);
    Param.PdArX = Pd_data3(i);
    Param.Filename = Names3(i,:);

    Objective1c(i) = FullODEScript2(IVP,L2t,Param)/(L2*time_data3(i))-1;
  end

  if(Param.plot)
   figure();
   hold on;
  end
  Pd_data4 = [0.003  0.004 0.005 0.006 0.007 0.01];
  Color_data4 = ['k' 'k' 'r' 'b' 'm' 'r'];
  Names4 = [  'out4a.csv'; 'out4b.csv'; 'out4c.csv'; 'out4d.csv'; 'out4e.csv'; 'out4f.↙
csv']   ;
  for i = 1:length(Pd_data4)
```

177

```matlab
        Param.plot_script = Color_data4(i);
        Param.L0 = 0;
        Param.A0 = 1.4;
        Param.X0 = 1.0;
        Param.PdArX = Pd_data4(i);
        Param.Filename = Names4(i,:);
        FullODEScript2(IVP,L2t,Param);
    end

    %Compute On Cycle vs Off-Cycle
    Color_data5 = ['r' 'b' 'g' 'm' 'b' 'b' 'b'];
    Names5 = ['out5a.csv';'out5b.csv'; 'out6a.csv' ; 'out6b.csv' ; 'out6c.csv'; 'out6d.↵
csv';'out6e.csv'];
    Pd_Data5 = [0.004 0.004 0.0034 0.0032 0.0030 0.0028 0.0025 ];
    if(Param.plot)
     figure();
     hold on;
    end
    for i = 1:length(Pd_Data5)
      Param.plot_script = Color_data5(i);
      Param.L0 = 0;
      Param.A0 = 1.4;
      Param.X0 = 1.0;
      Param.PdArX = Pd_Data5(i);
      Param.Filename = Names5(i,:);
      if(i == 1 || i == 2)
          IVP = 1;
          if(i == 2)
              IVP = 0.1;
          end
          FullODEScript2(IVP,L2t,Param);
      else
           if(Param.plot && i==3)
            figure();
            hold on;
          end
          IVP = 1;
          FullODEScript2(IVP,L2t,Param);

      end

    end


    Objective1a = Objective1a .* Objective1a;
    Objective1a = sum(Objective1a);

    Objective1b = Objective1b .* Objective1b;
    Objective1b = sum(Objective1b);

    Objective1c = Objective1c .* Objective1c;
    Objective1c = sum(Objective1c);
```

178

```
Objective2 =  Objective1b  + Objective1c + Objective1a

 return;
```

```matlab
function [RxnTime,turnover,c,F,IV,kT] = FullODEScript2(IVP,kL2t,Param)
if(IVP ==1)
    Initial_value = [0 1 0]; %On Cycle conditions
else
    Initial_value = [0 0 1]; %Off Cycle conditions
end

default_opt = odeset();
if(Param.convolution)
    [kT,Y] = ode45(@FullODESet2b,[0:0.5:kL2t], Initial_value,default_opt,Param);
else
    [kT,Y] = ode45(@FullODESet2b,[0 kL2t], Initial_value,default_opt,Param);
end

c = Y(:,1);
F = Y(:,2);
IV = Y(:,3);

rate = zeros(1,length(kT));

for i = 1:length(Y(:,1))
    tmp = FullODESet2b(0,[Y(i,1) Y(i,2) Y(i,3)],Param);
    rate(i) = Param.ArX0 * tmp(1);
end
if(Param.convolution)
    convolution = transpose(exp(-abs(Param.convolution)*kT))   ;
    rate = ifft(fft(rate).*fft(convolution))./(length(rate).*Param.convolution);
end

if(Param.plot)
    %figure()
    plot(kT,rate,Param.plot_script,'LineWidth',3);
    xlabel('Dimensionless Time (kL2t)')
    ylabel('Rate dc/d(k1t) * ArXo')
    %hold on;
    %plot(kT,c,'c','LineWidth',3);
end
if(Param.SpeciesPlot)
    % figure();
    plot(kT,IV,Param.plot_script,'LineWidth',3);
    xlabel('Dimensionless Time (kL2t)');
    ylabel('Concentration');

end
RxnTime = -1;
for i = 1:1:length(Y(:,1))
    if(Y(i,1) > 0.97*Param.A0 || Y(i,1) > 0.96*Param.X0)
        RxnTime = kT(i);
        break;
    end
end
temp = zeros(length(rate),2);

if(Param.Save)
%rate(2) = 0;
    for i = 1:length(rate)
        temp(i,1) = kT(i);
        temp(i,2) = rate(i);
```

```
    end
%    length(rate)
    csvwrite(Param.Filename,temp);
end
return
```

```matlab
function dx = FullODESet2(t,x,external_param)
%easier to follow
c = x(1);
F = x(2);
IV = x(3);
if(c < 0)
    c = 0 ;
end
if(c > external_param.X0 || c > external_param.A0)
    if(external_param.X0 < external_param.A0)
        c = external_param.X0;
    else
        c = external_param.A0;
    end
end
if(IV < 0)
    IV = 0;
end
if(IV > 1)
    IV = 1;
end
if(F < 0)
    F = 0;
end
if(F > 1)
    F = 1;
end

if(c > 0.97*external_param.X0 || c > 0.97*external_param.A0)
    dx = [0 0 0];
    return ;
end

%Different Parameters
PdArX = external_param.PdArX;
kd2kd = external_param.kd2kd;
%kRkF = external_param.kRkF;
A0 = external_param.A0;
X0 = external_param.X0;
L0 = external_param.L0;


kOA1kOA2 = external_param.kOA1kOA2;
ArX0 = 0.73;


kOA2kL2 = external_param.kOA2kL2 ;
kOA2kR= external_param.kOA2kR;
kFkR= external_param.kFkR;
%IVP =0.5 ;



%Intermediate Results

%T = 1 + kOA2kd2*(X0-c)/((kdkd2/(A0-c)+1)*(1+kRkF/(A0-c)));
```

```
%Jacobian
J11 = 0;
J21 = 0;
J31 = 0;
J12 = kOA2kL2*(X0-c)*(1+kOA1kOA2/(kFkR*(A0-c)+kOA2kR*kOA1kOA2*(X0-c))) ;
J22a = kOA2kL2*(c-X0);
J22b = kOA2kL2*PdArX*IV*(X0-c)/(PdArX*IV+kd2kd*(A0-c));
J22 = J22a+J22b;
J32 = kOA2kL2*kd2kd*(A0-c)*(X0-c)/(PdArX*IV+kd2kd*(A0-c));

J13 = 0;
J23 = PdArX*(IV+L0);
J33 = -PdArX*(IV+L0);

%don't multiply by c because I didn't divide by c
dx(1) = (J11 + J12 * F + J13 * IV)*PdArX;
dx(2) = J21 + J22 * F + J23 * IV ;
dx(3) = J31 + J32 * F + J33 * IV;
dx = transpose(dx);
```

183

2.4.5. Calorimetry and NMR Procedures

2.4.5.1.   Off-Cycle (*OA1) Method.

Procedure for "off-cycle" method is the similar to calorimetry procedure given in chapter 1 of this thesis. The solution for *OA1a is described as follows: The In a nitrogen-filled glove box, weighed amounts of n-propyl amine (1.4 equiv.), NaOtBu (1.4 equiv.), and 3-bromoanisole (1.0 equiv.) were loaded into a screw cap test tube. For each equivalent of 3-bromoanisole was added 1.0 g of 1,4-dioxane. The stock solution was used across multiple experiments. The complex **OA1a** (20 mol %) was added to aliquots of this solution were added to and the mixture allowed to sit for 1 h at room temperature to form *OA1a. Syringes were loaded with this stock solution and weighed. The syringes were removed from the glove box and then used in the calorimetry experiment.

2.4.5.2. ^{31}P-NMR Quantification Experiments

A measured amount of triphenylphosphine was dissolved in benzene-d_6 (purchased from Cambridge Isotopes labs). This solution was then partitioned into capillaries that were then flame sealed. A capillary was inserted into the NMR tube during the experiment. A stock solution of NaOtBu, n-propylamine, benzene-d_6, and 3-bromoanisole was then made in the glove box. Calibration of the capillaries was performed by dissolving a known amount of RuPhos (**L1**) into an aliquot of stock solution. Relaxation time was set to 60 seconds. Inverse gated decoupling was applied. A total of 64 repetitions (for adequate signal to noise ratio) were acquired giving an experiment time of approximately 1 h.

2.4.6. Calorimetry at 105 °C

2.4.6.1.   Coupling of N-methylaniline with 3-bromoanisole

Following Procedure in section 2, a stock solution of 3-bromoanisole (2.78 g, 14.9 mmol), N-methyl aniline (2.22 g, 20.7 mmol) and NaOtBu (2.02 g, 21.0 mmol) in 1,4-dioxane (14.8 g) was partitioned into 3 separate reaction vials and loaded into the calorimeter. After equilibration, the

catalyst solutions were introduced via syringe. Catalyst solution A: **OA1a** (10.7 mg, 14.1 μmol) in toluene (5.02 g), 2.13 mg/g. Catalyst solution B: **OA1a** (10.6 mg, 14.0 μmol) in toluene (5.02 g), 2.11 mg/g.
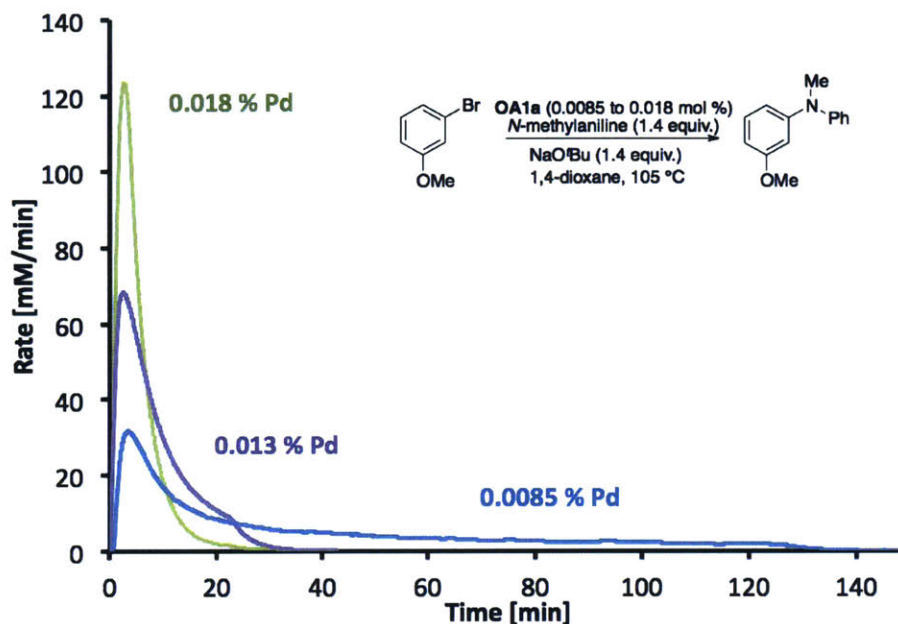
Figure 2-26 Rate of reaction for different catalyst (**OA1a**) loadings

Table 2-2 Stock Solution

Weight [g]	Name [-]	Conc [mmol/g]
2.0246	NaO^{t}Bu	0.97
2.2237	N-methylaniline	0.95
2.7841	3-bromoanisole	0.68
14.8073	1,4-dioxane	

Table 2-3 Catalyst Solutions

Catalyst Label [-]	**OA1a** [mg]	Toluene [g]	Conc. [mg/g]
A	10.7	5.0218	2.13
B	10.6	5.0205	2.11

185

Table 2-4 Run Summary

Catalyst Label [-]	Channel [-]	Stock Solution [g]	Loaded [g]	Unloaded [g]	Injection [g]	ArX [mmol]	Pd [%]
A	B3	3.0169	2.7386	2.6460	0.0926	2.06	0.0126
A	B4	3.1087	2.7906	2.6553	0.1353	2.12	0.0179
B	B4'	3.0318	2.7157	2.6525	0.0632	2.07	0.0085

Table 2-5 GC Data

Channel [-]	Dodecane [mg]	N-methyl aniline [pA s]	ArX [pA s]	Dodecane [pA s]	Product [pA s]	Yield [%]
B3	148.6	85.3	0.0	180.1	425.8	97
B4	150.8	82.8	0.0	180.2	426.6	95
B4'	150.3	75.9	0.0	158.5	368.6	96

Table 2-6 Energy Density

Channel [-]	Energy [J]	Energy Density [kJ/mol]
B3	445	216
B4	434	205
B4'	367	177

2.4.6.2.   OA1a catalyzed coupling of morpholine with 3-bromanisole

Following general procedure (see section 2.4.3), a stock solution of 3-bromoanisole (3.74 g, 20.0 mmol), morpholine (2.43 g, 27.9 mmol) and NaO*t*Bu (2.70 g, 28.1 mmol) in 1,4-dioxane (20.0 g) was partitioned into 3 separate reaction vials and loaded into the calorimeter. After equilibration, the catalyst solutions were introduced via syringe. Catalyst solution A: **OA1a** (17.0 mg, 22.4 μmol) in benzene (1.00 g), 16.7 mg/g. Catalyst solution B: **OA1a** (15.2 mg, 20.1 μmol) in benzene (1.01 g), 14.8 mg/g. Catalyst solution C: **OA1a** (12.9 mg, 17.0 μmol) in benzene (1.02 g), 12.5 mg/g.

186
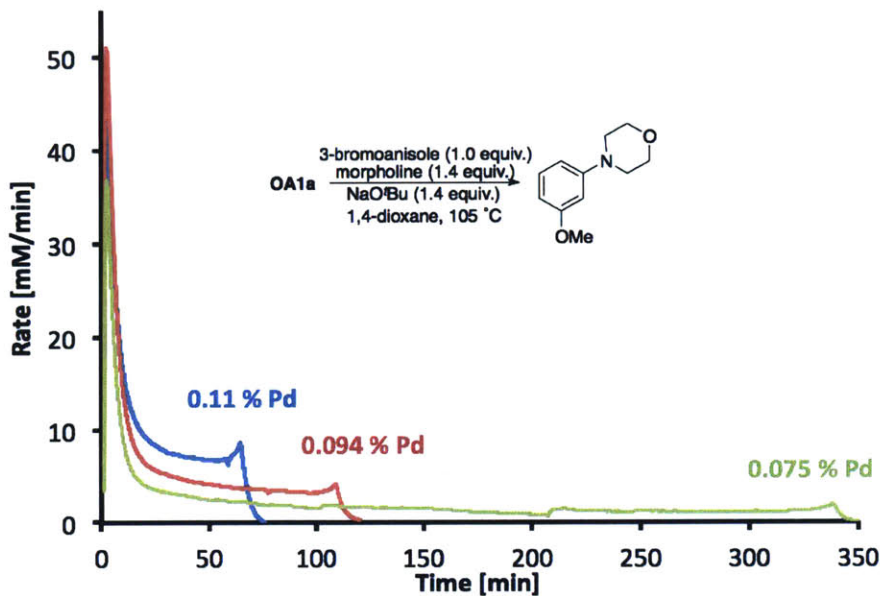
Figure 2-27 Rate of Reaction for different catalyst (**OA1a**) loadings

Table 2-7 Stock Solution

Weight [g]	Name [-]	Conc [mmol/g]
2.4387	morpholine	0.97
2.6990	NaO^{t}Bu	0.97
3.7429	3-bromoanisole	0.69
20.01	1,4-dioxane	

Table 2-8 Catalyst Solution

Catalyst Label [-]	**OA1a** [mg]	Benzene [g]	Concentration [mg/g]
A	17.0	1.0006	16.7
B	15.2	1.0146	14.8
C	12.9	1.0207	12.5

Table 2-9 Run Summary

Catalyst Label [-]	Channel #	Stock Sol [g]	Syringe Weight Loaded [g]	Syringe Weight Unloaded [g]	Injection Mass [g]	Catalyst [mg]	ArX [mmol]	Pd [mol %]
A	A1	4.1916	2.7492	2.6077	0.1415	2.36	2.90	0.107
B	A2	4.1909	2.7793	2.639	0.1403	2.07	2.90	0.094
C	A3	4.2404	2.7383	2.6045	0.1338	1.67	2.94	0.075

Table 2-10 Energy Density

Channel #	Energy [J]	Energy Density [kJ/mol]
A1	496	171
A2	595	205
A3	485	165

Table 2-11 GC Data

Channel #	Dodecane [mg]	Dodecane [pA s]	Product [pA s]	Yield [%]
A1	95.8	35.16	111.35	92
A2	137.1	51.10	117.46	95
A3	153.7	71.11	150.76	97

2.4.6.3. OA1a catalyzed coupling of morpholine with 3-bromanisole and added RuPhos L1

Following General Procedure A, a stock solution of 3-bromoanisole (3.74 g, 20.0 mmol), morpholine (2.43 g, 27.9 mmol) and NaOtBu (2.70 g, 28.1 mmol) in 1,4-dioxane (20.0 g) was partitioned into 2 separate reaction vials and loaded into the calorimeter. After equilibration, the catalyst solutions were introduced via syringe. The stock catalyst solution of **OA1a** was made with varied amounts of extra ligand **L1**. Catalyst solution A: **OA1a** (100.9 mg, 133 μmol) in benzene (10.0 g). Catalyst solution B: Catalyst Solution **A** (2.008 g) with **L1** (48.7 mg, 104 μmol). Catalyst solution C: Catalyst Solution **A** (2.0033 g) with **L1** (97.1 mg, 208 μmol).
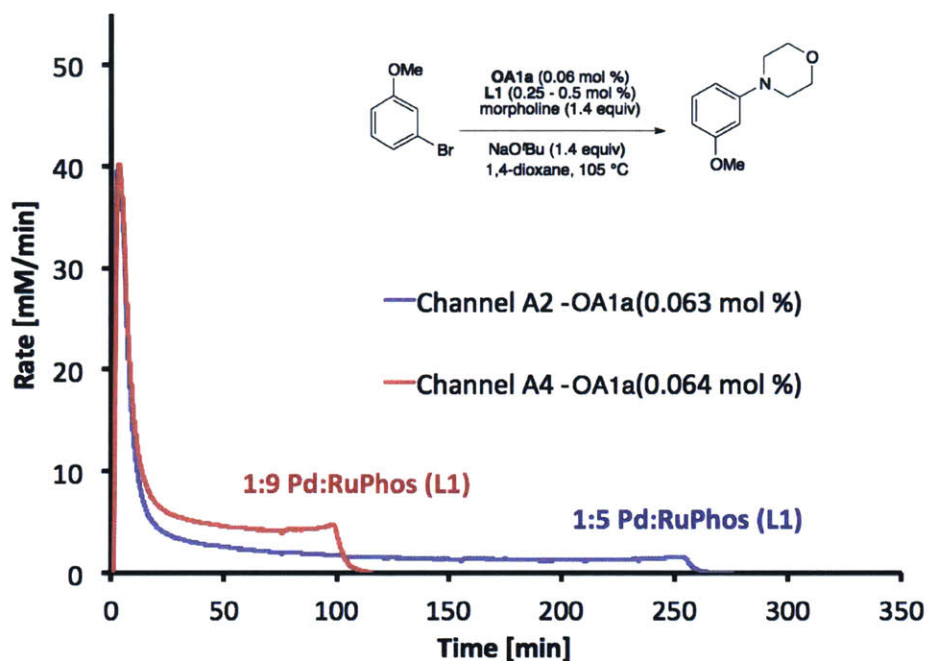
Figure 2-28 Rate of reaction with additional ligand **L1**

Table 2-12 Stock Solution

Weight [g]	Name [-]	Conc. [mmol/g]
2.4345	morpholine	0.97
2.6944	NaOᵗBu	0.97
3.7475	3-bromoanisole	0.69
20.0200	1,4-dioxane	

Table 2-13 Catalyst Solution

Catalyst Label [-]	OA1a [mg]	RuPhos (L1) [mg]	Benzene [g]	Solution Label A [g]	OA1a [mg/g]	Excess/Added RuPhos (L1) [mg/g]	Ratio [L1:Pd]
A	100.9	0	10.0034	N/A	10.0	0.0	1.00
B	N/A	48.7	N/A	2.008	9.7	23.7	4.95
C	N/A	97.1	N/A	2.0033	9.5	46.2	8.90

Table 2-14 Run Summary

Catalyst Label [-]	Channel [#]	Stock Sol [g]	Syringe Loaded [g]	Syringe Unloaded [g]	Injection [g]	ArX [mmol]	Pd [mol %]	Ratio [L:Pd]
B	A2	4.2003	2.773	2.6303	0.1427	2.91	0.063	4.95
C	A4	4.2051	2.7566	2.6086	0.148	2.92	0.064	8.90

Table 2-15 GC Data

Channel [#]	Dodecane [mg]	Dodecane [pA s]	Product [pA s]	Yield [%]
A2	145.2	98.38	222.94	99
A4	135.8	55.20	135.77	>99

Table 2-16 Energy Density

Channel [-]	Energy [J]	Energy Density [kJ/mol]
A2	671	230
A4	666	228

2.4.6.4. DalPhos-based Pd catalyzed coupling of *n*-octylamine and bromobenzene

Following General Procedure A, a stock solution of bromobenzene (2.32 g, 14.9 mmol), *n*-octyl amine (2.31 g, 17.9 mmol) and NaO^{t}Bu (2.00 g, 20.8 mmol) in toluene (14.81 g) was partitioned into 4 separate reaction vials and loaded into the calorimeter. After equilibration, the catalyst solutions were introduced via syringe. Catalyst Solution: **DalPhos-OA** (41.1 mg, 54.0 μmol) in THF (1.01 g), 39.2 mg/g.
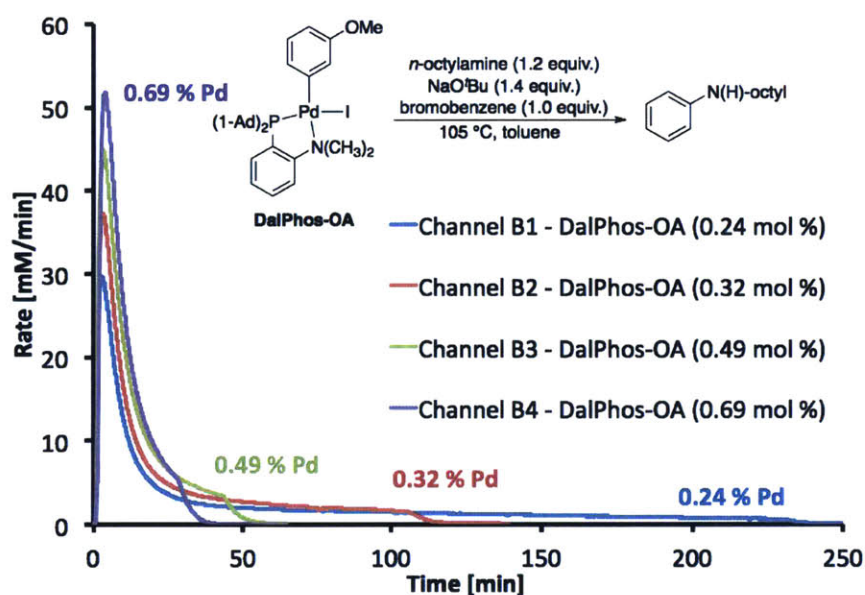
Figure 2-29 Reaction rate at different DalPhos-based catalyst loadings

190

Table 2-17 Stock Solution

Weights [g]	Name [-]	Conc [mmol/g]
2.3247	bromobenzene	0.69
1.9979	NaO^{t}Bu	0.97
2.3053	n-octylamine	0.83
14.8125	toluene	

Table 2-18 Catalyst Solution

DalPhos-OA [mg]	THF [g]	Conc. [mg/g]
41.1	1.0087	39.2

Table 2-19 Run Summary

Channel [#]	Stock Solution [g]	Syringe Weight [g]	Unloaded [g]	Injection Weight [g]	ArX [mmol]	Pd [%]
B1	3.0091	2.724	2.6276	0.0964	2.07	0.24
B2	3.0144	2.7701	2.6416	0.1285	2.08	0.32
B3	3.0059	2.8271	2.6293	0.1978	2.07	0.49
B4	3.0095	2.9035	2.6258	0.2777	2.07	0.69

Table 2-20 GC Data

Channel [#]	dodecane [mg]	dodecane [pA s]	Product [pA s]	Yield [%]
B1	141.6	164.1	422.1	>99
B2	156.6	197.4	473.0	>99
B3	150.2	164.6	421.5	>99
B4	146.9	133.9	336.5	>99

Table 2-21 Energy Density

Channel [#]	Energy [J]	Energy Density [kJ/mol]
B1	453	218
B2	453	218
B3	451	217
B4	422	204

2.4.6.5. DalPhos-based Pd Catalyzed coupling of bromo/chlorobenzene and n-octylamine

Following General Procedure A, a stock solution of bromobenzene (2.32 g, 14.9 mmol), n-octyl amine (2.31 g, 17.9 mmol) and NaOtBu (2.02 g, 21.0 mmol) in 1,4-dioxane (14.80 g) was

191

partitioned into separate reaction vials and loaded into the calorimeter. A second stock solution of chlorobenzene (1.69 g, 15.0 mmol), n-octylamine (2.30 g, 17.8 mmol) and NaOtBu (2.02 g, 20.8 mmol) in toluene (14.80 g) was partitioned into a vial and loaded into the calorimeter. After equilibration, the catalyst solutions were introduced via syringe. Catalyst Solution: **DalPhos-OA** (30.3 mg, 39.8 μmol) in THF (0.76 g), 38.3 mg/g.
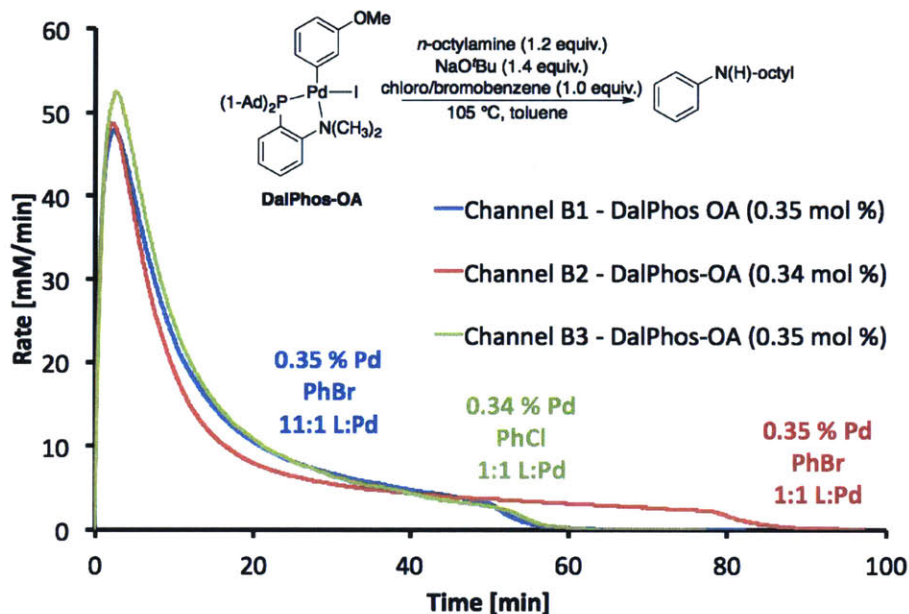
Figure 2-30 Reaction rate at different concentrations of DalPhos-OA catalyst

Table 2-22 Stock Solution for Channels B1 and B2

Weight [g]	Name [-]	Conc. [mmol/g]
2.0212	NaOtBu	0.98
2.3202	bromobenzene	0.69
2.3063	n-octylamine	0.83
14.8033	toluene	

Table 2-23 Stock Solution for Channel B3

Weight [g]	Name [-]	Conc. [mmol/g]
2.0204	NaOtBu	1.01
1.6895	chlorobenzene	0.72
2.2987	n-octylamine	0.86
14.8033	toluene	

Table 2-24 Catalyst Solution

DalPhos-OA [mg]	THF [g]	Conc. [mg/g]
30.3	0.7610	38.29

Table 2-25 Run Summary

Channel [#]	Stock Solution [g]	Syringe Loaded [g]	Syringe Unloaded [g]	Injection Weight [g]	ArX [mmol]	Pd [mol %]	Added DalPhos [mg]	Ratio L:Pd
B1	3.0082	2.7780	2.6329	0.1451	2.09	0.35	32.10	11.41
B2	3.0029	2.7649	2.6188	0.1461	2.08	0.35	0.00	0.00
B3	3.0061	2.7701	2.6235	0.1466	2.18	0.34	0.00	0.00

Table 2-26 GC Data

Channel [#]	Dodecane [mg]	dodecane [pA s]	Product [pA s]	Yield [%]
B1	150.6	205.7	491.1	99
B2	124.2	85.9	249.8	>99
B3	128.7	111.2	330.6	>99

Table 2-27 Energy Density

Channel [#]	Energy [J]	Energy Density [kJ/mol]
B1	409	196
B2	462	222
B3	466	214

2.4.6.6. BrettPhos-based Pd catalyzed coupling of *n*-propylamine with 3-bromoanisole

Following General Procedure A, a stock solution of 3-bromoanisole (2.79 g, 14.9 mmol), *n*-propylamine (1.23 g, 20.8 mmol) and NaO*t*Bu (2.00 g, 20.8 mmol) in 1,4-dioxane (15.02 g) was partitioned into 3 separate reaction vials and loaded into the calorimeter. After equilibration, the catalyst solutions were introduced via syringe. Catalyst Solution A: **OA6** (40.0 mg, 48.3 μmol) in THF (0.9102 g), 42.1 mg/g. Catalyst Solution B: **OA6** (39.1 mg, 47.1 μmol) in THF (0.7057 g), 52.5 mg/g. Catalyst Solution C: **OA6** (39.9 mg, 48.1 μmol) in THF (0.6033 g), 62.0 mg/g.

In a second experiment (Tables 2-33 to 2-34) a stock solution of 3-bromoanisole (2.90 g, 15.5 mmol), *n*-propylamine (1.23 g, 20.9 mmol) and NaO*t*Bu (2.07 g, 21.5 mmol) in 1,4-dioxane (15.01 g) was partitioned into a reaction vials and loaded into the calorimeter. After equilibration, the catalyst solutions were introduced via syringe. Catalyst Solution D: **OA6** (40.1 mg, 48.4 μmol) in THF (0.5928 g), 63.4 mg/g.

193
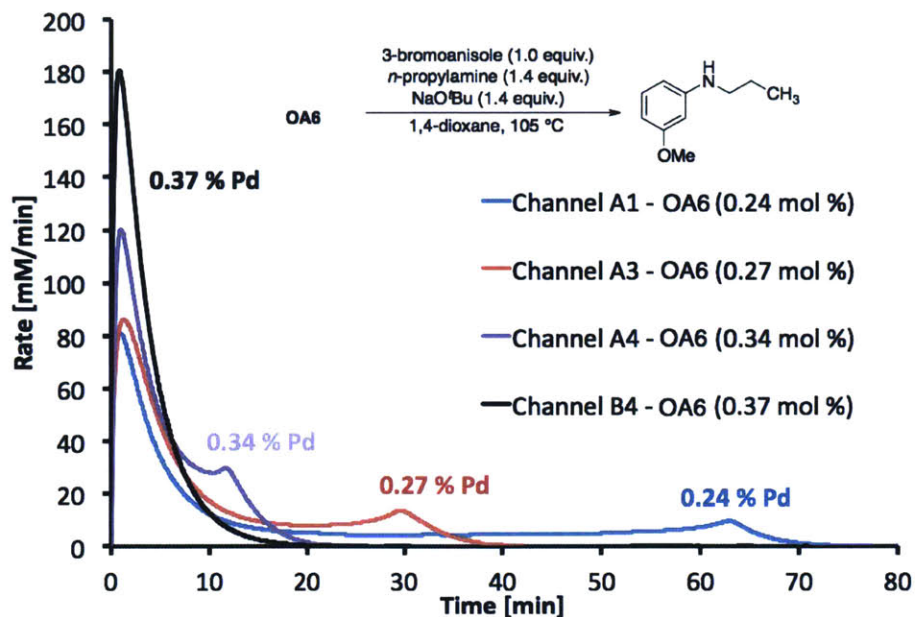
Figure 2-31 Rate of reaction with varying amounts of BrettPhos-Based Catalyst (**OA6**)

Table 2-28 Stock Solution

Weight [g]	Name [-]	Conc [mmol/g]
1.9988	NaO^{t}Bu	0.99
2.7856	3-bromoanisole	0.71
1.229	n-propyl amine	0.99
15.0264	dioxane	

Table 2-29 Catalyst Solution

Channel [#]	OA6 [mg]	THF [g]	Conc. [mg/g]
A1	40.0	0.9102	42.1
A3	39.1	0.7057	52.5
A4	39.9	0.6033	62.0

Table 2-30 Run Summary

Channel [#]	Stock Solution [g]	Syringe [g]	Unloaded [g]	Injection [g]	ArX [mmol]	Pd [%]
A1	3.0023	2.7369	2.6357	0.1012	2.13	0.24
A3	2.9977	2.7401	2.6489	0.0912	2.12	0.27
A4	3.0097	2.7476	2.6470	0.1006	2.21	0.34

194

Table 2-31 Energy Density

Channel [#]	Energy Output [J]	Energy Density [kJ/mol]
A1	419	197
A3	364	172
A4	341	154

Table 2-32 GC Data

Channel [#]	Dodecane [mg]	Dodecane [pA s]	Product [pA s]	Yield [%]
A1	161	220.3	307.2	96
A3	152.9	278.4	413.2	98
A4	143.1	287.9	439.0	90

Table 2-33 Stock Solution for Channel B4

Weight [g]	Name [-]	Conc. [mmol/g]
2.8986	3-bromoanisole	0.73
2.0654	NaO^{t}Bu	1.01
1.2319	n-propyl amine	0.98
15.0107	1,4-dioxane	

Table 2-34 Catalyst Solution for Channel B4

OA6 [mg]	THF [g]	Conc [mg/g]
40.1	0.5928	63.4

Table 2-35 Run Summary for Channel B4

Stock Sol [g]	Syringe [g]	Unloaded [g]	Injection [g]	ArX [mmol]	Pd [%]
2.9958	2.7543	2.6482	0.1061	2.19	0.37

Table 2-36 Energy Density for Channel B4

Energy [J]	Energy Density [kJ/mol]
422	193

Table 2-37 GC Data for Channel B4

dodecane [mg]	dodecane [pA s]	Product [pA s]	Yield [%]
154.5	185.7	262.4	91

2.4.6.7. BrettPhos-based Pd catalyzed coupling of 3-bromo/chloroanisole and *n*-propylamine

Following General Procedure A, a stock solution of 3-bromoanisole (2.79 g, 14.9 mmol), *n*-propylamine (1.23 g, 20.8 mmol) and NaOtBu (2.00 g, 20.8 mmol) in 1,4-dioxane (15.02 g) was partitioned into 2 separate reaction vials and loaded into the calorimeter. A second stock solution of 3-chloroanisole (2.14 g, 15.01 mmol), *n*-propyl amine (1.23 g, 20.8 mmol) and NaOtBu (2.01 g, 20.9 mmol) in 1,4-dioxane (15.01 g) was partitioned into 2 vials and loaded into the calorimeter. After equilibration, the catalyst solutions were introduced via syringe. Catalyst Solution: **OA6** (99.7 mg, 120 μmol) in THF (2.25 g), 42.4 mg/g.
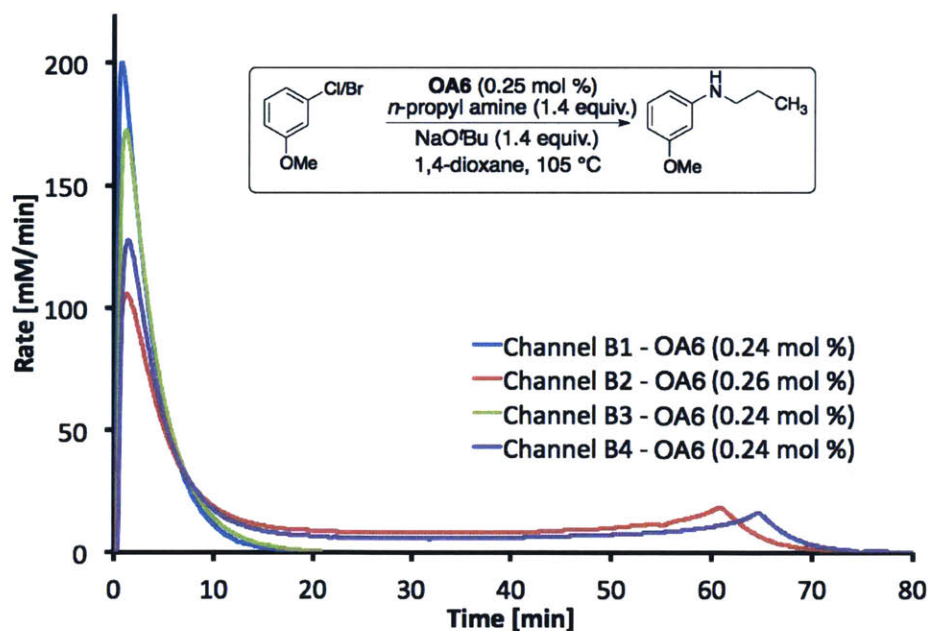

Figure 2-32 BrettPhos (**OA6**) Pd-Catalyzed reactions of 3-chloroanisole with 3-bromoanisole compared.

Table 2-38 Stock Solution (3-chloroanisole)

Weight [g]	Name [-]	Conc. [mmol/g]
2.1358	3-chloroanisole	0.74
2.0074	NaO^{t}Bu	1.03
1.2307	n-propyl amine	1.02
15.0131	1,4-dioxane	

Table 2-39 Stock Solution (3-bromoanisole)

Weight [g]	Name [-]	Conc. [mmol/g]
1.9988	NaO^{t}Bu	0.99
2.7856	3-bromoanisole	0.71
1.229	n-propyl amine	0.99
15.0264	1,4-dioxane	

Table 3-40 Catalyst Solution

OA6 [mg]	THF [g]	Conc. [mg/g]
99.7	2.2523	42.4

Table 2-41 Run Summary

ArX [-]	Channel [#]	Stock Solution [g]	Syringe [g]	Unloaded [g]	Injection [g]	ArX [mmol]	Pd [%]
3-chloroanisole	B1	3.0042	2.7610	2.6570	0.1040	2.21	0.24
3-bromoanisole	B2	2.9942	2.7374	2.6314	0.1060	2.12	0.26
3-chloroanisole	B3	3.0120	2.7479	2.6458	0.1021	2.21	0.24
3-bromoanisole	B4	3.0207	2.7723	2.6715	0.1008	2.14	0.24

Table 2-42 Energy Density

Channel [#]	Energy Output [J]	Energy Density [kJ/mol]
B1	363	165
B2	262	124
B3	480	217
B4	287	134

197

Table 2-43 GC Data

Channel [#]	Dodecane [mg]	Dodecane [pA s]	Product [pA s]	Yield [%]
B1	145.4	272.5	435.5	96
B2	147.9	308.1	446.1	92
B3	145.9	172.2	280.8	98
B4	150.4	179.9	263.4	94

2.4.6.8. ^{31}P-NMR Quantification at 20 °C for OA1a coupling of morpholine/n-propylamine with 3-bromoanisole.

Four ^{31}P-NMR experiments were performed. First a stock solution of triphenylphosphine in deuterated benzene was sealed in a glass capillary. This capillary was placed in an NMR tube with a stock solution of RuPhos (**L1**) in benzene-d_6 (Experiment #1). The NMR experiment was performed and the observed phosphorus signal for **L1** was quantitated and referenced to the signal for the triphenylphosphine. This capillary was used in subsequent experiments.

A stock solution (Solution A) of n-propylamine, NaOtBu, 3-bromoanisole, and benzene-d_6 was added to **OA1a** in experiment #2. This same stock solution (Solution A) was added to **OA1a** and **L1** in experiment #3. Comparison of the exp. #2 and exp. #3 does not support the presence of a dynamic equilibrium (*vide infra*) between free **L1** and a phosphine ligated palladium species,

Finally a stock solution (Solution B) of morpholine, NaOtBu, 3-bromoanisole, and benzene-d_6 was added to **OA1a** in experiment #4. Quantification by ^{31}P-NMR indicated 60 % of the supporting ligand could be accounted for as free ligand **L1**.

Table 2-44 Stock Solutions

Stock Solution A			Stock Solution B	
Weight [g]	Name [-]		Weight [g]	Name [-]
0.4006	3-bromoanisole		0.1329	NaO^{t}Bu
0.1790	n-propyl amine		0.1960	3-bromoanisole
0.2876	NaO^{t}Bu		0.1237	morpholine
2.0060	benzene-d_6		1.0080	benzene-d_6

Table 2-45 Run Summary

Exp #	OA1a [mg]	RuPhos (L1) [mg]	Sol Name [-]	Sol Weight [g]	Conc L1 (from OA1a) [mg/g]	Conc (added) L1 [mg/g]
1	0	12.5	benzene-d_6	1.1168	0.00	11.07
2	15.7	0	A	0.9001	10.54	0.00
3	15.8	6.1	A	0.9066	10.53	6.57
4	5.6	0	B	0.9901	3.46	0.00

Table 2-46 ^{31}P-NMR Data and Yield Calculations

Exp #	Measured ^{31}P-NMR Signal at -9 ppm (referenced to capillary standard)	Calculated Max L1 ^{31}P-NMR Signal (from OA1a)	Calculated Max L1 ^{31}P-NMR Signal (from added L1)	Yield of L1 [%]
1	1.42	N/A	N/A	N/A
2	0.41	1.35	0.00	30
3	1.19	1.35	0.84	26
4	0.27	0.44	0.00	61

Equilibrium calculation for experiments #2 and #3

Taking experiment #2 we can calculate a presumed equilibrium constant for free ligand using an equilibrium relationship. Given that we can account for 30 % free ligand we can calculate a K value of 0.1286 as seen below.

$$K = \frac{[L1][Pd]}{[PdL]} \Rightarrow K = \frac{(0.3)(0.3)}{1 - 0.3} = 0.1286$$

Thus as we have done for experiment #3 where we have added a concentration of extra **L1** ligand (Table 45; last column) corresponding to a significant portions of the concentration. If the

equilibrium assumption were justified, we would anticipate a "free" ligand yield of 14 %. Instead the measured value indicates a yield of 26 % (Table 3-46; Exp #3) which is comparable to the 30 % yield of the control reaction. This result suggests that the ligand association **L1** is not at dynamic equilibrium.

$$\frac{(x + 0.62)(x)}{1 - x} = 0.1286 \Rightarrow x = 0.14$$

2.4.7. Calorimetry at Low Temperatures

2.4.7.1. OA1a based coupling of different amines with 3-bromoanisole at 20 °C.

In a nitrogen-filled glove box, weighed amounts of aryl halide, amine, base, and solvent were charged into separate 16 mL vials (Wheaton Vial, 16 mL E-C Vial, Cat # 224706). The vials were equipped with a stir bar and then sealed with a silicon rubber/Teflon laminated septum (ThermoScientific, 10/90 FOR18-400, B7995-18). The part number for retaining cap for each septum/vial was manufactured by Kimble-Chase (part # 73804-18400). The vials were removed from the glove box and loaded into the calorimeter controlled at a temperature of 20 °C. A reaction vial containing pure solvent was loaded into reference channel of the calorimeter.

Separately, (multiple) solutions of **OA1a** were prepared by the addition of the palladium complex into toluene or other appropriate solvent in a 4 mL Vial (Wheaton 4 mL E-C Vial Cat # 224742). The masses of the palladium complex and solvent were recorded. Syringes equipped with a 6-inch needle were then loaded with the catalyst solution and weighed. After thermal equilibration of the reaction vials (~1 h) into the preheated calorimeter, the catalyst solution was injected through the septum to start the reactions. The syringes were weighed again to calculate the total amount of catalyst injected into the reaction. An equal mass of pure solvent was injected into the reference channel.

The vials were removed after 2 hours time, a weighed amount of n-dodecane was added and the mixture *immediately* analyzed by gas chromatography.
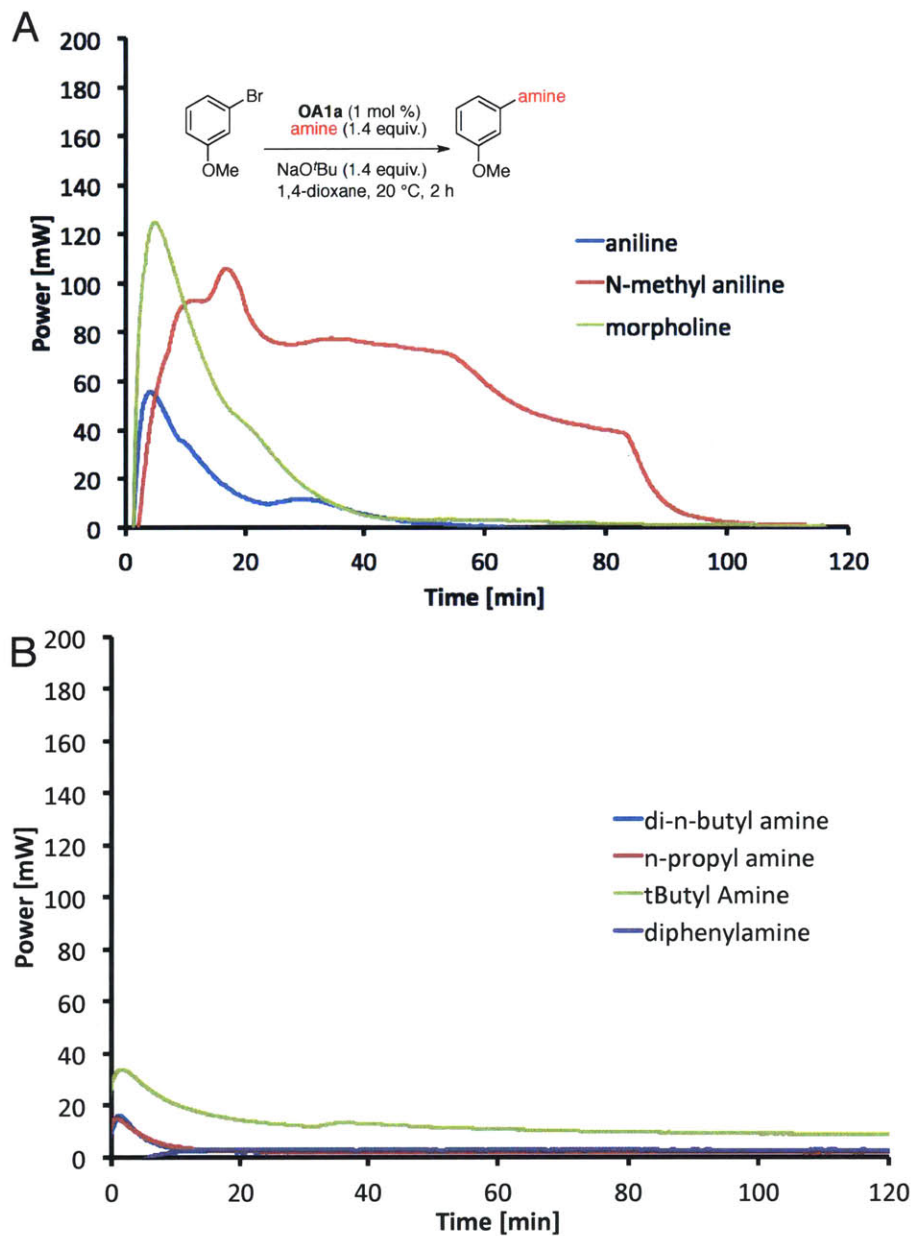
Figure 2-33 Power output from calorimeter for various amine types

Table 2-47 Catalyst Solution

Catalyst Label [-]	OA1a [mg]	CH$_2$Cl$_2$ [g]	Conc. [mg/g]
A	100.8	0.9063	100.1
B	102.1	0.9165	100.2

Table 2-48 Run Summary

Catalyst Label [-]	Name [-]	Amine [g]	NaO^{t}Bu [g]	3-bromoanisole [g]	1,4-dioxane [g]	Total [g]	Syringe Loaded [g]	Syringe Unloaded [g]	Injectin Weight [g]	ArX [mmol]	Pd [%]
A	aniline	0.2453	0.2520	0.3464	1.8566	2.7003	2.7945	2.6457	0.1488	1.85	1.06
A	N-methylaniline	0.2801	0.2530	0.3456	1.8644	2.7431	2.8172	2.6728	0.1444	1.85	1.03
A	morpholine	0.2285	0.2552	0.3465	1.8545	2.6847	2.7822	2.6356	0.1466	1.85	1.04
B	n-dibutylamine	0.3376	0.2530	0.3476	1.8600	2.7982	2.8293	2.6821	0.1472	1.86	1.05
B	n-propylamine	0.1522	0.2515	0.3453	1.8584	2.6074	2.7818	2.6514	0.1304	1.85	0.93
B	^{t}butylamine	0.1918	0.2538	0.3496	1.8703	2.6655	2.8191	2.6728	0.1463	1.87	1.03
B	dipheny amine	0.5496	0.2512	0.3882	1.8723	3.0613	2.8235	2.6808	0.1427	2.08	0.91

Table 2-49 GC Data

Name [-]	Dodecane [mg]	Dodecane [pA s]	3-bromoanisole [pA s]	Product [pA s]	Conversion [%]	Yield [%]
aniline	103.5	154.4	192.1	59.0	17	16
N-methylaniline	103.3	82.8	0.0	253.5	100	98
morpholine	95.2	178.8	204.0	127.9	30	33
n-dibutylamine	125.3	181.1	216.0	4.7	4	trace
n-propylamine	145.9	265.9	268.2	trace	4	trace
^{t}butylamine	138.0	281.5	271.2	62.1	15	13
diphenylamine	160.5	307.5	333.9	0.0	0	0
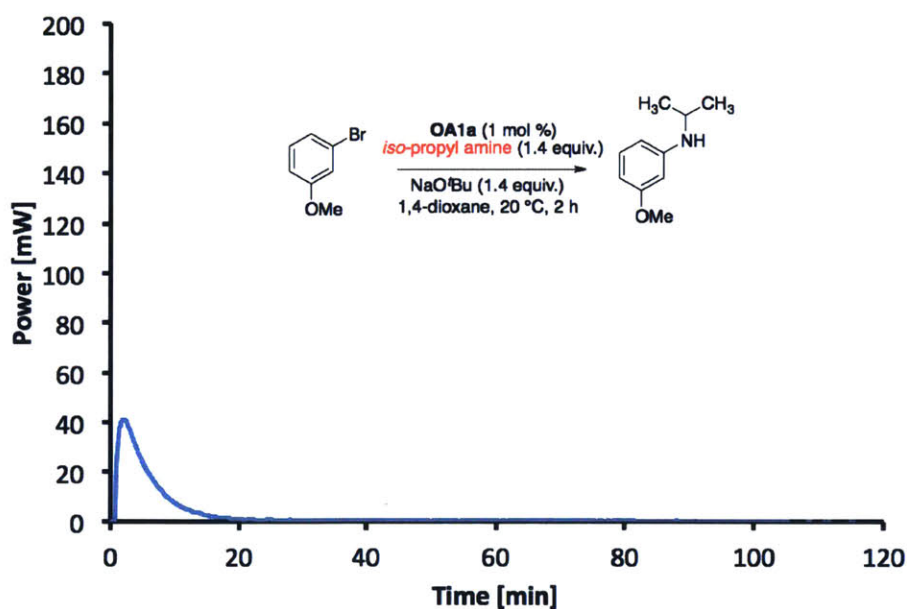
Figure 2-34 Power output from calorimeter for iso-propylamine reaction

Table 2-50 Run Summary

iso-propylamine [g]	NaO^{t}Bu [g]	3-bromoanisole [g]	1,4-dioxane [g]	Total [g]	Syringe Loaded [g]	Unloaded [g]	Injection Weight [g]	ArX [mmol]	Pd [%]
0.1639	0.2698	0.3862	2.008	2.8279	2.8309	2.6769	0.154	2.07	1.11

Table 2-51 Catalyst Solution

OA1a [mg]	CH$_2$Cl$_2$ [g]	Conc. [mg/g]
50.0	0.3924	113.02

Table 2-52 GC Data

Name [-]	dodecane [mg]	dodecane [pA s]	3-bromoanisole [pA s]	Product [pA s]	Conversion [%]	Yield [%]
iso-propylamine	96.4	50.86	89.98	trace	1.0	trace

2.4.7.2. Ligand screening with *n*-propylamine and 3-bromoanisole at 20 °C

Following General Procedure A, a stock solution of 3-bromoanisole (3.74 g, 20.0 mmol), *n*-propylamine (1.63 g, 27.7 mmol) and NaO*t*Bu (2.69 g, 28.0 mmol) in 1,4-dioxane (20.0 g) was partitioned into separate reaction vials and loaded into the calorimeter. After equilibration, the catalyst solutions were introduced via syringe. Catalyst Solution A: **P7** (30.5 mg, 41.3 μmol) in CH$_2$Cl$_2$ (0.5021 g), 57.3 mg/g. Catalyst Solution B: **P6** (30.0 mg, 42.3 μmol) in CH$_2$Cl$_2$ (0.5021 g), 56.4 mg/g. Catalyst Solution C: **OA1a** (29.8 mg, 39.3 μmol) in CH$_2$Cl$_2$ (0.5029 g), 55.9 mg/g. Catalyst Solution D: **OA3** (29.7 mg, 36.3 μmol) in CH$_2$Cl$_2$ (0.5349 g), 52.6 mg/g.
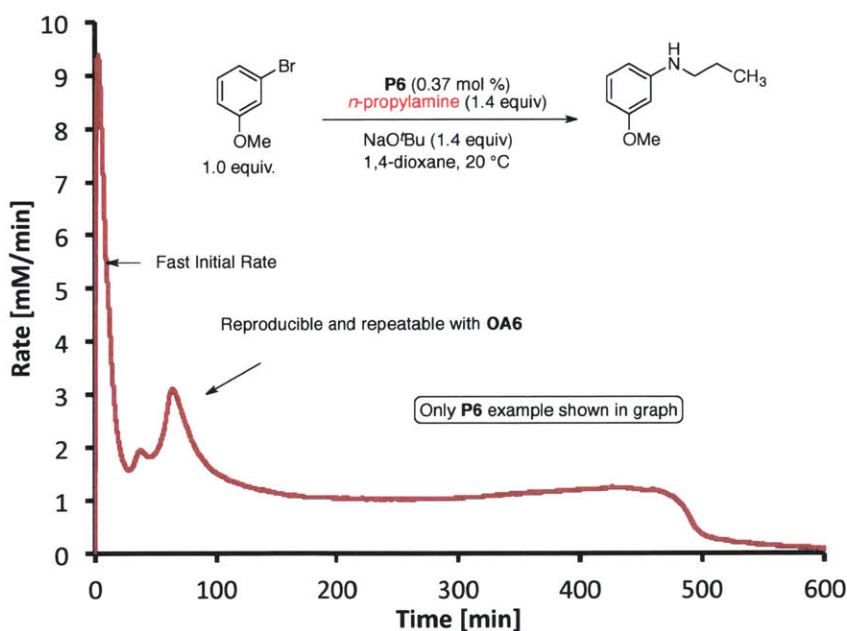
Figure 2-35 Reaction rate for BrettPhos (**P6**) based cross-coupling of n-propylamine and 3-bromoanisole

Table 2-53 Stock Solution

Reagent [g]	Name [-]	Conc. [mmol/g]
1.6323	*n*-propylamine	0.98
2.6891	NaO^{t}Bu	1.00
3.7412	3-bromoanisole	0.71
20.021	1,4-dioxane	

Table 2-54 Catalyst Solutions

Catalyst Label [-]	Name [-]	Catalyst [mg]	CH$_2$Cl$_2$ [g]	Conc. [mg/g]
A	XPhos- G1 Precat (**P7**)	30.5	0.5021	57.3
B	BrettPhos-G1 Precat (**P6**)	30.0	0.5021	56.4
C	Ruphos OA (**OA1a**)	29.8	0.5029	55.9
D	Hybrid OA (**OA3**)	29.7	0.5349	52.6

Table 2-55 Run Summary Data

Catalyst Label [-]	Channel ID #	Stock Sol [g]	Syringe Loaded [g]	Syringe Unloaded [g]	Injection Mass [g]	ArX [mmol]	Pd [mol %]
A	A1	4.2325	2.8247	2.6706	0.1541	3.02	0.40
B	A2	4.2215	2.8063	2.6478	0.1585	3.01	0.37
C	A3	4.2134	2.8234	2.6699	0.1535	3.00	0.38
D	A4	4.2293	2.8033	2.6631	0.1402	3.01	0.30

Table 2-56 Energy Data

Channel #	Energy [J]	Energy Density [kJ/mol]
A2	701	233

204

Table 2-57 GC Data

Channel #	Dodecane [mg]	Dodecane [pA s]	3-bromoanisole [pA s]	Product [pA s]	Conversion [%]	Yield [%]
A1	105.2	109.60	249.30	18.93	5	5
A2	162.5	181.73	0.00	376.49	100	97
A3	149.1	117.65	203.88	1.45	0	1
A4	146.6	115.68	202.15	1.20	0	0

2.4.7.3. ^{t}BuBrettPhos-based Pd catalyzed coupling of *n*-propylamine and 3-bromoanisole at 20 °C

Following General Procedure A, a stock solution of 3-bromoanisole (2.80 g, 15.0 mmol), *n*-propyl amine (1.37 g, 23.2 mmol) and NaO*t*Bu (2.02 g, 21.0 mmol) in 1,4-dioxane (15.0 g) was partitioned into separate reaction vials and loaded into the calorimeter. After equilibration, the catalyst solutions were introduced via syringe. Catalyst Solution: **^{t}BuBrettPhos-OA** (38.9 mg, 50.0 *μ*mol) in THF (0.5148 g), 70.3 mg/g.
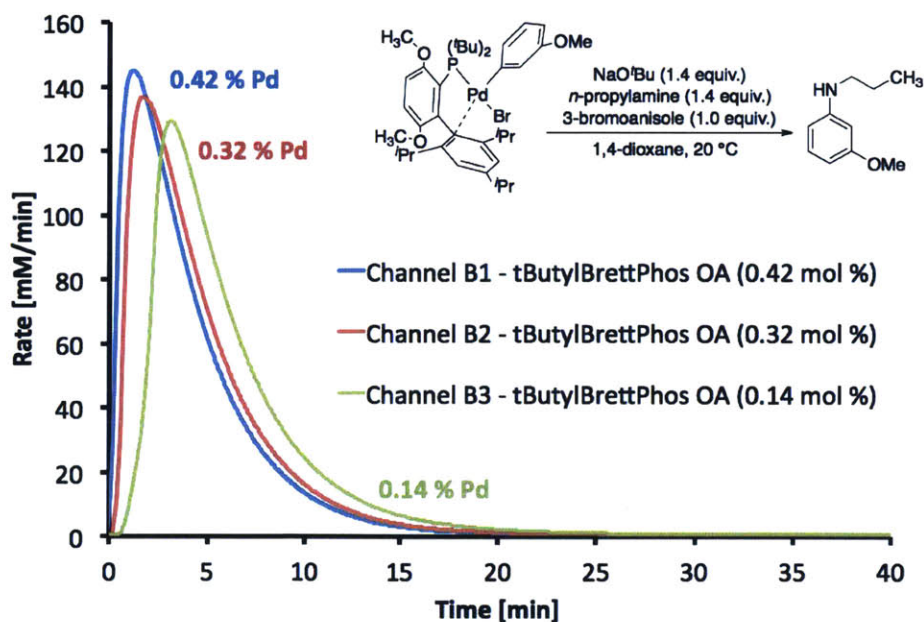
Figure 2-36 *t*ButylBrettPhos-based coupling of 3-bromoanisole with *n*-propylamine

Table 2-58 Stock Solution

Weight [g]	Name [-]	Conc. [mmol/g]
2.0164	NaOᵗBu	0.99
2.8025	3-bromoanisole	0.71
1.3658	*n*-propylamine	1.09
14.9815	1,4-dioxane	

Table 2-59 Catalyst Solution

Catalyst [mg]	THF [g]	Conc [mg/g]
38.9	0.5148	70.3

Table 2-60 Run Summary

Channel [#]	Stock Solution [g]	Syringe Loaded [g]	Syringe Unloaded [g]	Injection [g]	ArX [mmol]	Pd [%]
B1	3.0206	2.7467	2.6464	0.1003	2.14	0.42
B2	3.0331	2.7235	2.6482	0.0753	2.15	0.32
B3	3.0166	2.7065	2.674	0.0325	2.14	0.14

Table 2-61 Energy Density

Channel [#]	Energy [J]	Limiting Reagent [mmol]	Energy Density [kJ/mol]
B1	511	2.14	239
B2	498	2.15	232
B3	492	2.14	231

Table 2-62 GC Data

Channel [#]	Dodecane [mg]	Dodecane [pA s]	Product [pA s]	Yield [%]
B1	137	217.6	397.3	94
B2	151.8	162.9	269.4	94
B3	138.6	172.6	304.2	96

206

2.4.7.4. S-BINAP-based Pd catalyzed coupling of *N*-methylpiperazine and bromobenzene at 60 °C.

Following General Procedure A, a stock solution of bromobenzene (2.34 g, 15.0 mmol), *N*-methyl piperazine (1.80 g, 18.0 mmol) and NaO*t*Bu (2.01 g, 20.9 mmol) in toluene (15.0 g) was partitioned into separate reaction vials and loaded into the calorimeter. After equilibration, the catalyst solutions were introduced via syringe. Catalyst Solution A: **BINAP-OA** (25.3 mg, 28.6 *µ*mol) in benzene (0.4092 g), 58.2 mg/g. Catalyst Solution B: **BINAP-OA** (24.7 mg, 27.9 *µ*mol) in benzene (0.6025 g), 39.4 mg/g. Catalyst Solution C: **BINAP-OA** (25.4 mg, 28.7 *µ*mol) in benzene (0.8090 g), 30.4 mg/g. Catalyst Solution D: **BINAP-OA** (25.7 mg, 29.0 *µ*mol) in benzene (0.5150 g), 47.5 mg/g. Catalyst Solution E: **BINAP-OA** (49.7 mg, 56.2 *µ*mol) in benzene (0.5020 g), 90.1g/g. Catalyst Solution F: **BINAP-OA** (48.8 mg, 55.1 *µ*mol) in benzene (0.2508 g), 162.9 mg/g.
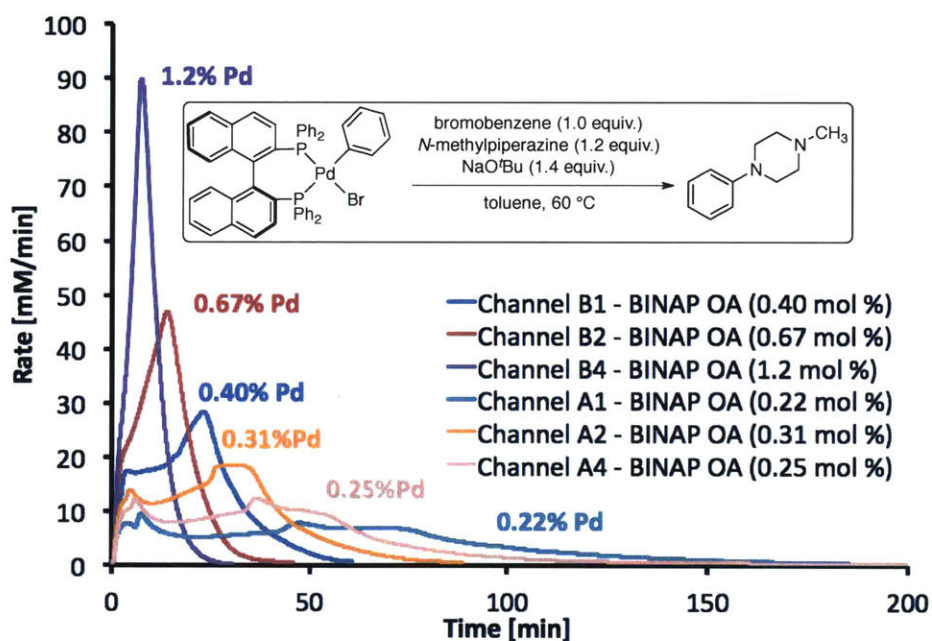
Figure 2-37 Rate of reaction for different catalyst loadings

Table 2-63 Stock Solution

Weight [g]	Name [-]	Conc [mmol/g]
2.0061	NaO^{t}Bu	0.99
2.3407	bromobenzene	0.71
1.8010	N-methylpiperazine	0.85
15.0024	toluene	

Table 2-64 Catalyst Solution

Catalyst Label [-]	Catalyst [mg]	Benzene [g]	Conc [mg/g]
A	25.3	0.4092	58.2
B	24.7	0.6025	39.4
C	25.4	0.8090	30.4
D	25.7	0.5150	47.5
E	49.7	0.5020	90.1
F	48.8	0.2508	162.9

Table 2-65 Run Summary

Catalyst Label [-]	Channel [#]	Stock Solution [g]	ArX [mmol]	Syringe Weight [g]	Unloaded [g]	Injection [g]	Pd [%]
A	A1	3.0143	2.14	2.8462	2.7754	0.0708	0.22
B	A2	3.0131	2.14	2.8362	2.6859	0.1503	0.31
C	A4	3.0111	2.14	2.826	2.671	0.155	0.25
D	B1	3.0172	2.14	2.856	2.6968	0.1592	0.40
E	B2	3.0359	2.15	2.812	2.6706	0.1414	0.67
F	B4	3.0307	2.15	2.8025	2.6567	0.1458	1.25

Table 2-66 GC Data

Channel [#]	Dodecane [mg]	Dodecane [pA s]	Product [pA s]	Yield [%]
A1	128.0	123.5	197.3	>99
A2	150.7	102.3	156.9	89
A4	158.7	139.4	187.1	97
B1	138.0	87.7	130.0	>99
B2	172.0	109.9	125.5	>99
B4	163.0	104.0	155.2	86

Table 2-67 Energy Density

Channel [#]	ArX [mmol]	Energy [J]	Energy Density [kJ/mol]
A1	2.14	500	234
A2	2.14	503	235
A4	2.14	498	233
B1	2.14	507	237
B2	2.15	490	227
B4	2.15	498	232

2.4.7.5. OA1a catalyzed coupling of morpholine with 3-bromoanisole (30 °C) and Excess Ligand (L1)

Following General Procedure A, a stock solution of 3-bromoanisole (3.47 g, 18.6 mmol), morpholine (2.26 g, 25.9 mmol) and NaOtBu (2.50 g, 26.0 mmol) in 1,4-dioxane (18.70 g) was partitioned into separate reaction vials and loaded into the calorimeter. Extra ligand **L1** was added to each reaction vial. After equilibration, the catalyst solutions were introduced via syringe. Catalyst Solution: **OA1a** (197.1 mg, 260 μmol) in CH_2Cl_2 (1.4981 g), 116.3 mg/g.
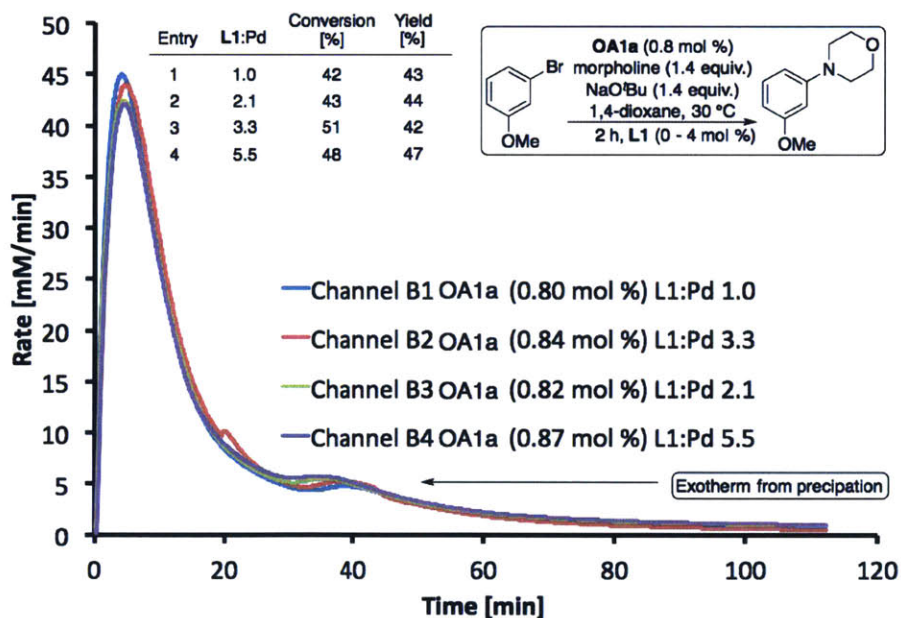
Figure 2-38 Effect of Added ligand **L1** on rate and conversion

209

Table 2-68 Stock Solution

Reagent [g]	Name [-]	Conc [mmol/g]
2.5011	NaO^{t}Bu	0.97
2.2640	morpholine	0.97
3.4700	3-bromoanisole	0.69
18.7003	1,4-dioxane	

Table 2-69 Catalyst Solution

OA1a [mg]	CH$_2$Cl$_2$ [g]	Conc. [mg/g]
197.1	1.4981	116.3

Table 2-70 Run Summary

Channel #	Stock Sol. [g]	RuPhos (L1) [mg]	Syringe Loaded [g]	Syringe Unloaded [g]	Injection [g]	ArX [mmol]	Pd [%]	L1:Pd
B1	4.0133	0	2.8168	2.6723	0.1445	2.76	0.80	1.00
B2	3.9931	25.2	2.8303	2.68	0.1503	2.75	0.84	3.35
B3	4.004	11.3	2.8212	2.6736	0.1476	2.76	0.82	2.07
B4	4.0105	50.4	2.82	2.6624	0.1576	2.76	0.87	5.47

Table 2-71 Energy Density (Note: Does not take into account incomplete conversion)

Channel #	Energy [J]	Energy Density [kJ/mol]
B1	303	110
B2	300	109
B3	309	112
B4	337	122

Table 2-72 GC Data

Channel #	dodecane [mg]	3-bromoanisole [pA s]	dodecane [pA s]	Product [pA s]	Conversion [%]	Yield [%]
B1	109.9	106.83	88.51	109.01	42	45
B2	96.2	120.21	102.94	141.06	51	44
B3	77.8	81.54	48.80	86.74	43	46
B4	100.8	158.47	132.49	195.24	48	49

2.4.7.6. Comparison of the reaction 3-bromo/iodo/chloroanisole with morpholine at 20 °C

General Procedure A was followed. Four stock solutions were prepared for each individual condition (Tables 2-73 – 2-76). The vials were allowed to equilibrate before injecting catalyst solutions. The reaction was allowed to run for exactly 2 h and then analyzed by gas chromatography.
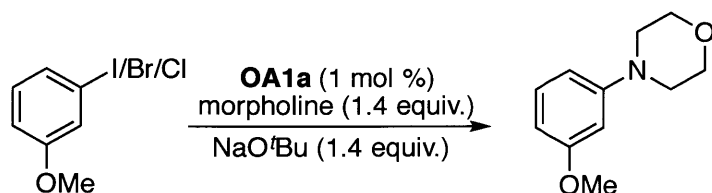
Table 2-73 Stock Solution for Entry 1

Reagent [g]	Name [-]	Conc. [mmol/g]
1.0026	NaO^{t}Bu	1.00
1.0661	3-chloroanisole	0.72
0.9175	morpholine	1.01
7.4321	1,4-dioxane	

Table 2-74 Stock Solution for Entry 2

Reagent [g]	Name [-]	Conc. [mmol/g]
0.9997	NaO^{t}Bu	0.97
1.3905	3-bromoanisole	0.69
0.9128	morpholine	0.97
7.4667	toluene	

Table 2-75 Stock Solution for Entry 3

Reagent [g]	Name [-]	Conc. [mmol/g]
1.008	NaO^{t}Bu	1.01
1.0605	3-chloroanisole	0.71
0.9028	morpholine	1.00
7.4482	toluene	

Table 2-76 Stock Solution for Entry 4

Reagent [g]	Name [-]	Conc. [mmol/g]
1.0008	NaO^{t}Bu	0.94
1.7143	3-iodoanisole	0.66
0.9083	morpholine	0.94
7.4746	toluene	

Table 2-77 Catalyst Solution

OA1a [mg]	CH₂Cl₂ [g]	Conc [mg/g]
149.4	1.4097	95.82

Table 2-78 Run Summary

Entry [-]	Solvent [-]	ArX [-]	Solution Weight [g]	Syringe [g]	Syringe Unloaded [g]	Injection Weight [g]	ArX [mmol]	Pd [mol %]	Catalyst [mg]	Syringe Loaded [g]
1	1,4-dioxane	3-choroanisole	2.4940	2.559	2.6679	0.1497	1.79	1.06	14.34	2.8176
2	toluene	3-bromoanisole	2.5100	2.5773	2.6808	0.1476	1.73	1.08	14.14	2.8284
3	toluene	3-chloroanisole	2.5282	2.5254	2.626	0.1552	1.81	1.09	14.87	2.7812
4	toluene	3-iodoanisole	2.4997	2.511	2.6556	0.1516	1.66	1.16	14.53	2.8072

Table 2-79 GC Data

Entry [-]	Solvent [-]	ArX [-]	ArX [pA s]	Dodecane [pA s]	Product [pA s]	Conversion [%]	Yield [%]
1	1,4-dioxane	3-choroanisole	125.9	154.7	64.7	32	27
2	toluene	3-bromoanisole	198.7	207.7	62.3	19	18
3	toluene	3-chloroanisole	129.7	122.4	54.4	26	24
4	toluene	3-iodoanisole	125.8	163.9	63.8	31	26

2.4.7.7. Displaced RuPhos (L1) from as function of OA1a

In a nitrogen-filled glove box, a stock solution of NaO*t*Bu (0.8163 g, 8.50 mmol), *n*-propylamine (0.4980 g, 8.4 mmol), 3-bromoanisole (1.1208 g, 5.99 mmol), and benzene-d_6 (6.00 g) was charged to a screw cap test tube. Separately a reference solution of RuPhos (**L1**) (14.7 mg, 31.5 μmol) and the stock solution (0.9221 g) was used to calibrate a sealed capillary filled with a triphenylphosphine solution (in benzene-d_6). The stock solution was added to a weighed quantity of **OA1a.** This solution after ~20 minutes this solution was transferred to an NMR tube equipped with the calibrated capillary. The tube was sealed with a polyethylene cap, the cap was wrapped with parafilm, and then removed from of the glove box and a ^{31}P-NMR experiment was used to quantify the amount of free ligand at -9 ppm (referenced to 85 % H₃PO₄ (aq.) at 0 ppm) relative to the PPh₃ reference integral at -5 ppm. The phosphorus NMR experiment was

performed with inverse gated decoupling, a relaxation time of 60 s and a total of 64 transients for an adequate signal to noise ratio.
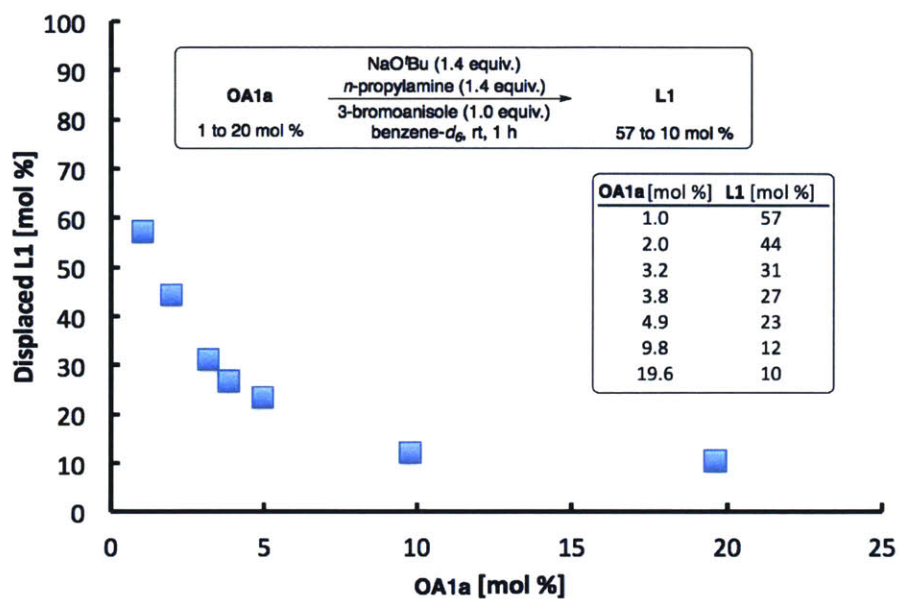
Figure 2-39 Yield of **L1** with respect to varying concentration of **OA1a**.

Table 2-80 Stock Solution for ^{31}P-NMR Experiments

Weights [g]	Name [-]
0.498	*n*-propyl amine
1.1208	3-bromoanisole
0.8163	NaO^{t}Bu
6.0016	d_6-benzene

Table 2-81 Solution for Capillary Calibration

14.7	[mg] of RuPhos
0.9221	[g] Stock Solution
0.9368	Total [g]

Table 2-82 Run Data (Last entry gives calibration results for capillary)

OA1a [mg]	OA1a [mol %]	OA1a [mmol/g]	Stock Solution [g]	L1 [31] P-Integral at -9 ppm (normalized to reference)
5.6	1.04	0.0074	0.996	1.15
10.7	1.98	0.0141	1.0031	1.69
17.2	3.17	0.0226	1.0049	1.90
20.9	3.82	0.0271	1.0145	1.97
26.5	4.95	0.0351	0.9936	2.22
53.6	9.79	0.0695	1.0155	2.29
108.9	19.61	0.1393	1.0298	3.95
Calibration	N/A	0.0337 (L1)	N/A	9.11

2.4.7.8. GC experiments with OA1a

In a nitrogen-filled glove box, weighed amounts of NaO*t*Bu (1.00 g, 10.5 mmol), 3-bromoanisole (1.40 g, 7.49 mmol), 1,4-dioxane (7.52 g), and *n*-propylamine (0.62 g, 10.5 mmol) were charged to a screw cap test tube. An aliquot of this mixture (5.92 g) was then added to *n*-dodecane (0.45 g) to make a new stock solution. Aliquots of this stock solution were then added to varying amounts of **OA1a** (Table S85).   After 1 h, the mixtures were then analyzed by gas chromatography.
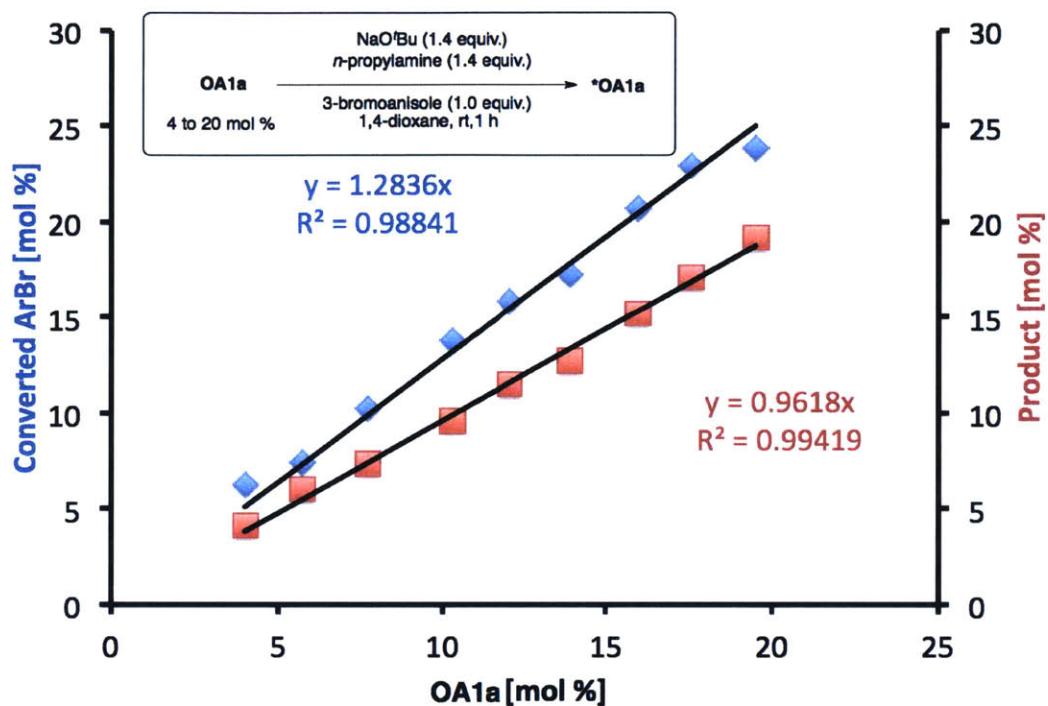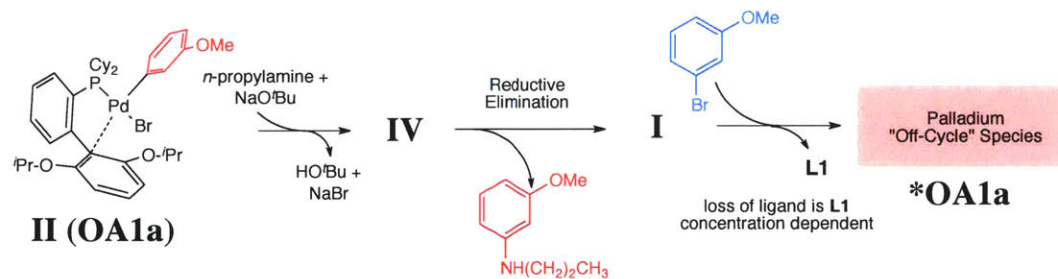
Figure 2-40 Consumption of 3-bromoanisole as a function of **OA1a**

Table 2-83 Stock Solution A

Reagent [g]	Name [-]	Conc. [mmol/g]
1.0063	NaO^{t}Bu	0.99
1.4006	3-bromoanisole	0.71
0.6183	n-propyl amine	0.99
7.5198	1,4-dioxane	

Table 2-84 Stock Solution B

Reagent [g]	Name [-]	Conc. [mg/g]
5.9183	Stock Sol. A	N/A
0.4476	dodecane	70.31

Table 2-85 GC Data

Entry [-]	dodecane [mg]	3-bromoanisole [pA s]	dodecane [pA s]	Product [pA s]	Diarylated Product [pA s]
Stock	N/A	349.2	448.8	0.0	0.0
1	36.29	667.2	915.1	48.3	0.0
2	36.90	869.2	1207.3	94.2	0.0
3	36.64	722.7	1034.7	98.1	0.0
4	35.59	645.8	963.1	119.0	0.0
5	36.30	860.1	1313.9	193.6	0.0
6	36.02	753.7	1171.0	191.4	0.0
7	35.62	759.7	1232.5	240.8	8.6
8	35.37	765.8	1278.4	281.5	29.9
9	36.15	949.8	1604.2	395.3	20.6

Table 2-86 Run Summary

Entry [-]	OA1a [mg]	Stock Sol B [g]	ArX [mmol]	OA1a [µmol]	OA1a [mol %]	Conv. [%]	ArX [mmol]	"Missing" ArX [µmol]	Cross-coupled Product Yield [µmol]	Cross-coupled Product Yield [%]
Stock	0	N/A	N/A	0	0	0.00	N/A	N/A	0.00	0.00
1	10.3	0.5161	0.341	13.59	3.99	6.27	0.32	21.38	14.17	4.10
2	15	0.5248	0.347	19.79	5.71	7.45	0.32	25.82	21.32	6.07
3	20.1	0.5211	0.344	26.52	7.71	10.22	0.31	35.16	25.72	7.38
4	26.1	0.5062	0.334	34.43	10.30	13.81	0.29	46.15	32.55	9.61
5	31.1	0.5162	0.341	41.03	12.04	15.85	0.29	54.02	39.60	11.47
6	35.7	0.5123	0.338	47.10	13.92	17.26	0.28	58.40	43.58	12.71
7	40.5	0.5066	0.335	53.43	15.97	20.76	0.27	69.45	51.50	15.20
8	44.2	0.503	0.332	58.31	17.56	23.00	0.26	76.38	57.65	17.13
9	50.2	0.5142	0.340	66.23	19.50	23.89	0.26	81.11	65.94	19.17

2.4.7.9. GC Experiments with diphenylamido complex

In a nitrogen-filled glove box, weighed amounts of 3-bromoanisole (0.5606 g, 3.0 mmol), benzene (3.08 g), n-propylamine (0.25 g, 4.2 mmol), and n-dodecane (0.31 g) were charged to a screw cap test tube. Aliquots of this stock solution were added to weighed quantities of the diphenylamido complex and mixed (Table 2-90). These solutions were allowed to stand for 2.5 h before analysis by gas chromatography. Note the amount of 3-bromoanisole consumed is 0.45 equivalent relative to the amount of initial **A1a**. Also note that the amount of cross-coupled product is consistent with 0.37 equivalents of cross-coupled product. Such results indicate the

formation of an inactive palladium(II) dimer formation (the product of turnovers affects the rate of reaction).
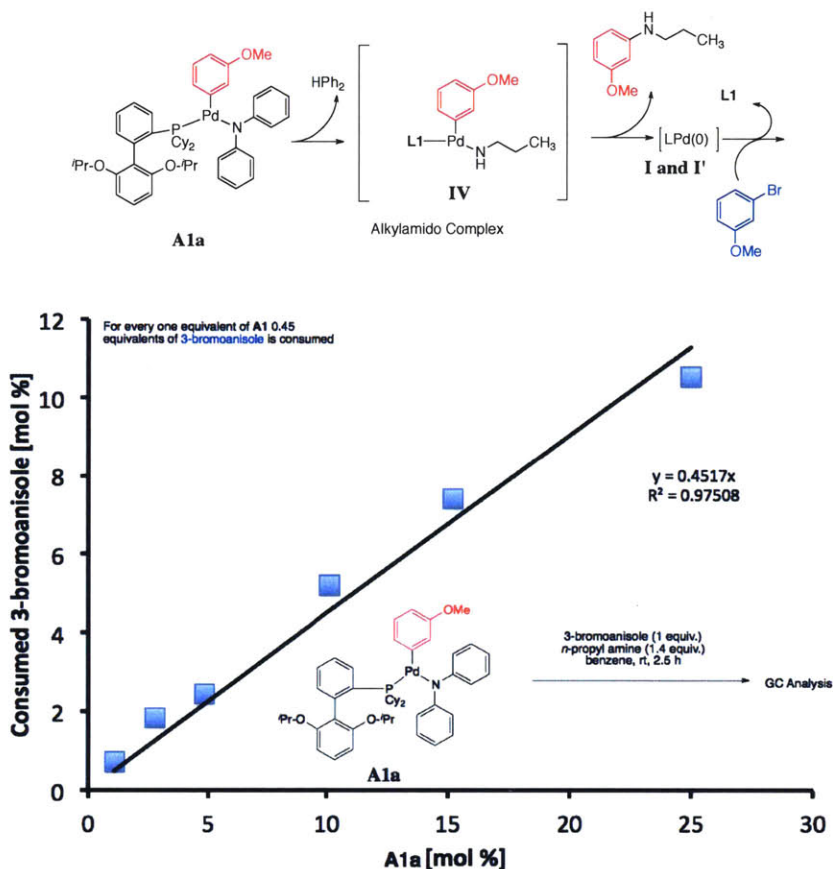
Figure 2-1 Consumption of 3-bromoanisole as a function of amido complex (**A1a**)
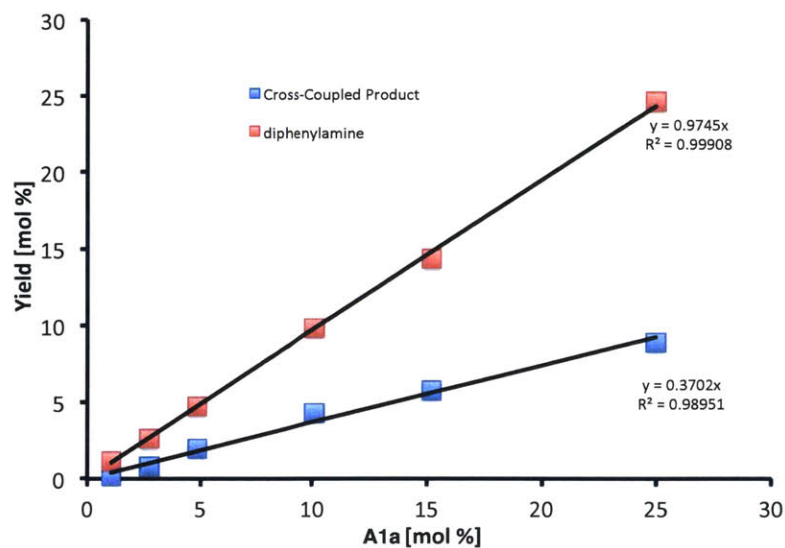
Figure 2-41 Formation of diphenylamine (displaced from amido complex) and cross-coupled product

Table 2-87 Stock Solution

Weight [g]	Name [-]	Conc. [mmol/g]
0.3061	*n*-dodecane	
0.56059	3-bromoanisole	0.72
0.2468	*n*-propylamine	1.00
3.0791	benzene	

Table 2-88 Experiment Summary

Label [-]	**A1a** [mg]	Stock Solution [g]	Pd [mol %]
A	5.6	0.8483	1.08
B	14.4	0.8573	2.77
C	25.3	0.8600	4.85
D	9.7	0.1577	10.10
E	18.7	0.2032	15.21
F	25.3	0.1668	24.98

Table 2-89 GC Data

Label [-]	3-bromoanisole [pA s]	*n*-dodecane [pA s]	Product [pA s]	Diphenylamine [pA s]
Stock	112.23	132.80	0.00	0.00
A	210.87	251.34	0.53	4.52
B	136.40	164.42	1.44	6.70
C	178.46	216.49	4.52	16.01
D	51.98	64.90	2.98	10.14
E	119.46	152.69	9.49	34.62
F	79.08	104.61	9.93	40.80

Table 2-90 Experiment Summary

Label [-]	Pd [mol %]	Conversion ArX [mol %]	Product Yield [mol %]	Diphenylamine yield [mol %]
A	1.08	0.73	0.20	1.14
B	2.77	1.84	0.82	2.58
C	4.85	2.46	1.96	4.67
D	10.10	5.23	4.30	9.87
E	15.21	7.43	5.83	14.33
F	24.98	10.55	8.90	24.65

2.4.8. Experiments using *OA1a and Excess Experiments

2.4.8.1. Variation of *OA1a loading at 105 °C

Following General Procedure B, a stock solution of 3-bromoanisole (3.78 g, 20.2 mmol), morpholine (2.44 g, 28.0 mmol) and NaOtBu (2.70 g, 28.2 mmol) in 1,4-dioxane (20.00 g) was partitioned into separate reaction vials and loaded into the calorimeter. A second stock solution of 3-bromoanisole (3.74 g, 20.0 mmol), morpholine (2.46 g, 28.3 mmol) and NaOtBu (2.68 g, 28.0 mmol) in 1,4-dioxane (20.00 g) was partitioned into separate reaction vials and loaded into the calorimeter. After equilibration, the catalyst solutions were introduced via syringe. Catalyst Solution A: **OA1a** (26.6 mg, 35.1 μmol) in the amine stock solution (0.514 g), 49.22 mg/g. Catalyst Solution B: **OA1a** (31.7 mg, 41.8 μmol) in the amine stock solution (0.501 g), 59.5 mg/g. Catalyst Solution C: **OA1a** (16.2 mg, 21.4 μmol) in the amine stock solution (0.527 g), 29.8 mg/g. Catalyst Solution E: **OA1a** (12.4 mg, 16.4 μmol) in the amine stock solution (0.510 g), 23.8 mg/g. Catalyst Solution F: **OA1a** (9.6 mg, 12.7 μmol) in the amine stock solution (0.5100 g), 18.5 mg/g.
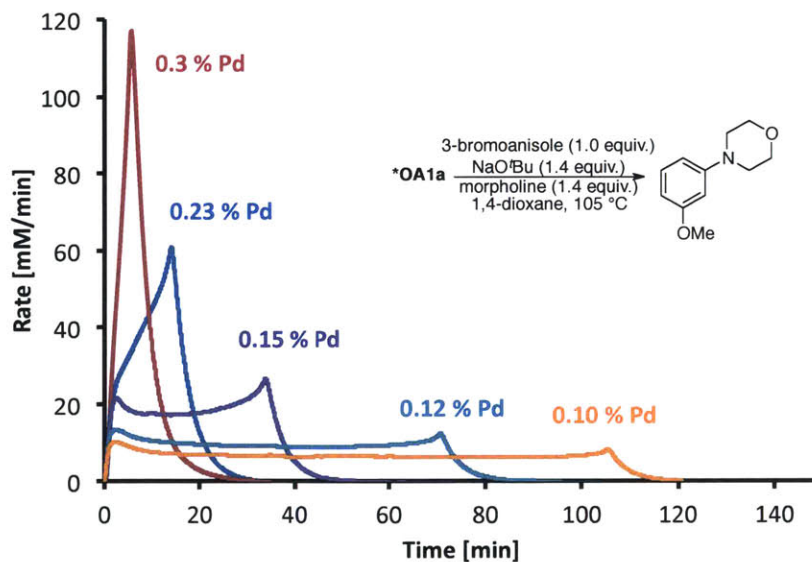
Figure 2-42 Rate of Reaction for varying amount of *OA1a

Table 2-91 Stock Solution

Weight [g]	Name [-]	Conc [mmol/g]
2.4365	morpholine	0.97
3.7855	3-bromoanisole	0.70
2.7030	NaO^{t}Bu	0.97
20.0002	1,4-dioxane	

Table 2-92 Catalyst Solution

Catalyst Label [-]	OA1a [mg]	Amine Solution [g]	Catalyst [mg/g]
A	26.6	0.5138	49.22
B	31.7	0.501	59.51
C	16.2	0.5267	29.84

Table 2-93 Run Summary

Catalyst Label [-]	Channel #	Solution Weight [g]	Loaded Syringe [g]	Unloaded Syringe [g]	Injection Weight [g]	ArX [mmol]	Pd [mol %]
A	A1	4.2306	2.7326	2.6263	0.1063	3.03	0.23
B	A2	4.2006	2.7514	2.6368	0.1146	3.01	0.30
C	B2	4.202	2.7361	2.6231	0.113	3.02	0.15

Table 2-94 GC Data

Channel [-]	Dodecane [mg]	Dodecane [pA s]	Product [pA s]	Yield [%]
A1	134.9	142.9	345.0	98
A2	135.5	125.2	283.6	93
B2	148.1	129.7	289.3	99

Table 2-95 Energy Density

Channel [-]	Energy [J]	Energy Density [kJ/mol]
A1	632	208
A2	622	206
B2	691	229

220

Table 2-96 Stock Solution

Weight [g]	Name [-]	Conc. [mmol/g]
2.4632	morpholine	0.98
2.6843	NaO^{t}Bu	0.97
3.7413	3-bromoanisole	0.69
20.0020	1,4-dioxane	

Table 2-97 Catalyst Solution

Catalyst Label [-]	OA1a [mg]	Amine Solution [g]	Catalyst Solution [mg/g]
E	12.4	0.5097	23.8
F	9.6	0.51	18.5

Table 2-98 Run Summary

Catalyst Label [-]	Channel #	Stock Solution [g]	Syringe Loaded [g]	Syringe Unloaded [g]	Injection Weight [g]	ArX [mmol]	Pd [%]
E	A3	4.2668	2.7414	2.627	0.1144	2.95	0.12
F	A4	4.2272	2.7477	2.6283	0.1194	2.93	0.10

Table 2-99 Energy Density

Channel #	Energy [J]	Energy Density [kJ/mol]
A3	712	241
A4	737	252

221

2.4.8.2. Variation of Morpholine Concentration at 75 °C

Following General Procedure B, solutions for each reaction vial (Tables 2-100 to 2-103) were made with morpholine, 3-bromoanisole (or 3-chloroanisole), NaOtBu, and 1,4-dioxane. After equilibration, the catalyst solutions were introduced via syringe. Catalyst Solution: **OA1a** (101 mg, 133 μmol) in the amine stock solution (1.17 g), 79.6 mg/g.
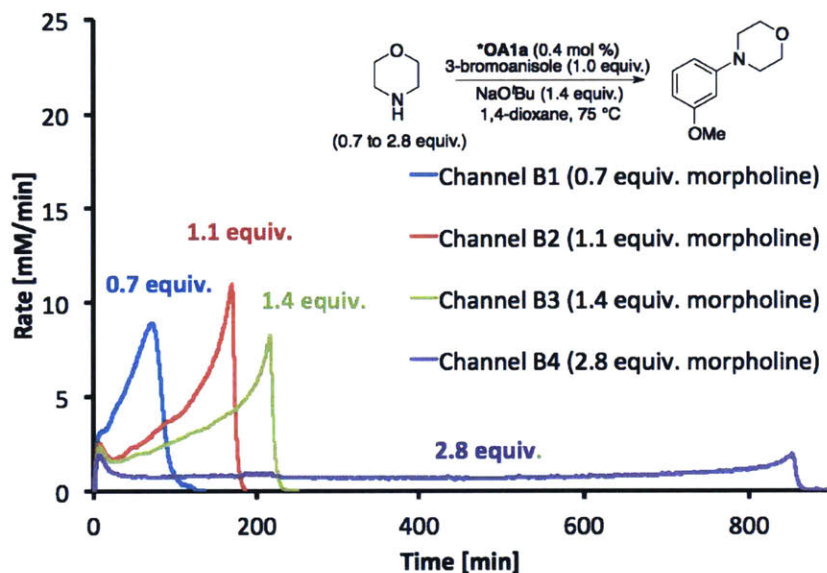
Figure 2-43 Rate of reaction with different equivalents of morpholine

Table 2-100 Stock Solution for Channel B1

Reagent [g]	Name [-]	Conc. [mmol/g]
0.4959	NaOtBu	0.96
0.6927	3-bromoanisole	0.69
0.2268	morpholine	0.48
3.9612	1,4-dioxane	

Table 2-101 Stock Solution for Channel B2

Reagent [g]	Name [-]	Conc. [mmol/g]
0.5009	NaOtBu	0.97
0.6965	3-bromoanisole	0.69
0.3528	morpholine	0.76
3.8128	1,4-dioxane	

222

Table 2-102 Stock Solution for Channel B3

Reagent [g]	Name [-]	Conc. [mmol/g]
0.5117	NaO'Bu	0.99
0.6959	3-bromoanisole	0.69
0.4502	morpholine	0.96
3.7200	1,4-dioxane	

Table 2-103 Stock Solution for Channel B4

Reagent [g]	Name [-]	Conc. [mmol/g]
0.5119	NaO'Bu	0.99
0.6905	3-bromoanisole	0.69
0.9112	morpholine	1.95
3.3100	1,4-dioxane	

Table 2-104 Catalyst Solution

OA1a [mg]	Amine Sol. [g]	Conc. [mg/g]
100.9	1.1672	79.57

Table 2-105 Run Summary

Channel [-]	Stock Solution [g]	Syringe Loaded [g]	Syringe Unloaded [g]	Injection [g]	Pd [%]	ArX (or Amine) [mmol]
B1	4.1995	2.7459	2.6448	0.1011	0.37	**2.04**
B2	4.2351	2.7775	2.6803	0.0972	0.35	2.94
B3	4.2485	2.7788	2.6746	0.1042	0.37	2.94
B4	4.2486	2.7739	2.6658	0.1081	0.39	2.92

Table 2-106 GC Data

Channel [-]	Dodecane [mg]	3-bromanisole [pA s]	Dodecane [pA s]	Product [pA s]	ArBr Conversion [%]	Yield [%]
B1	151.2	29.4	93.8	132.4	80	95
B2	152.6	0.0	194.3	408.9	100	99
B3	150.1	0.0	164.5	355.0	100	100
B4	144.4	0.0	162.9	356.6	100	98

Table 2-107 Energy Density (Note: Takes into account limiting reagent for Channel B1)

Channel [-]	Energy [J]	Energy Density [kJ/mol]
B1	468	230
B2	618	210
B3	626	213
B4	652	224

2.4.8.3. Variation of ArX concentration at 75 °C

Following General Procedure B, solutions for each reaction vial (Tables 2-108 to 2-111) were made from morpholine, 3-bromoanisole (or 3-chloroanisole), NaOtBu, and 1,4-dioxane. After equilibration, the catalyst solutions were introduced via syringe. Catalyst Solution: **OA1a** (106 mg, 35.1 μmol) in the amine stock solution (1.06 g), 90.7 mg/g.
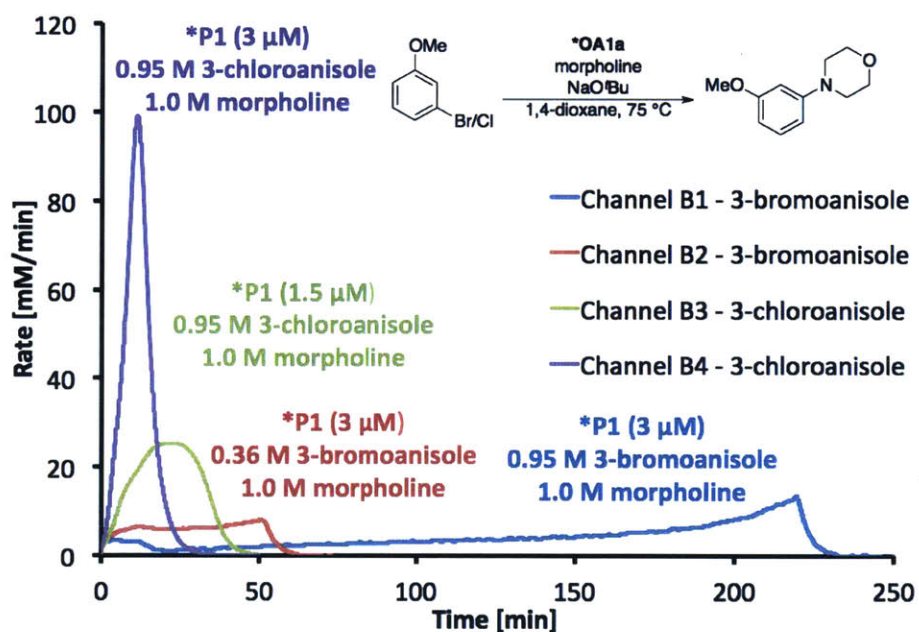

Figure 2-44 Reaction rate for different aryl halide concentration and types

Table 2-108 Stock Solution for Channel B1

Reagent [g]	Name [-]	Conc [mmol/g]
1.0129	NaO^{t}Bu	0.98
0.9024	morpholine	0.96
1.8110	3-bromoanisole	0.90
7.0368	1,4-dioxane	

Table 2-109 Stock Solution for Channel B2

Reagent [g]	Name [-]	Conc. [mmol/g]
1.0227	NaO^{t}Bu	0.99
0.9099	morpholine	0.97
0.6942	3-bromoanisole	0.34
8.1457	1,4-dioxane	

Table 2-110 Stock Solution for Channel B3

Reagent [g]	Name [-]	Conc. [mmol/g]
1.0203	NaO^{t}Bu	0.99
0.9038	morpholine	0.96
1.0530	3-chloroanisole	0.69
7.8037	1,4-dioxane	

Table 2-111 Stock Solution for Channel B4

Reagent [g]	Name [-]	Conc. [mmol/g]
1.0047	NaO^{t}Bu	0.99
0.907	morpholine	0.99
1.3707	3-chloroanisole	0.91
7.2595	1,4-dioxane	

Table 2-112 Stock Solution for Catalyst

OA1a [mg]	Amine Sol. [g]	Conc. [mg/g]
106	1.0622	90.74

Table 2-113 Run Summary

Channel #	Stock Solution [g]	Loaded Syringe [g]	Unloaded Syringe [g]	Injection Weight [g]	Cat [mg]	Arx [mmol]	Pd [mol %]	Pd [mM]
B1	4.2146	2.7033	2.5992	0.1041	9.45	3.79	0.33	3.15
B2	4.2086	2.7556	2.657	0.0986	8.95	1.45	0.81	2.91
B3	4.2096	2.6888	2.6364	0.0524	4.75	2.89	0.22	1.52
B4	4.2009	2.7771	2.6692	0.1079	9.79	3.83	0.34	3.17

225

Table 2-114 GC Data

Channel #	Dodecane [mg]	Dodecane [pA s]	Product [pA s]	Yield [%]
B1	106.8	115.0	441.7	95.0
B2	107	133.9	202.0	98.0
B3	108.1	121.6	370.0	>99
B4	111.2	81.3	323.1	>99

Table 2-115 Energy Density

Channel #	Energy [J]	Energy Density [kJ/mol]
B1	777	205
B2	294	203
B3	615	213
B4	817	213

2.4.8.4. *OA1a catalyzed coupling of 3-Iodoanisole and n-propylamine at 75 °C

Following General Procedure B, a stock solution of 3-iodoanisole (4.09 g, 17.6 mmol), morpholine (2.15 g, 24.7 mmol) and NaO*t*Bu (2.37 g, 24.7 mmol) in toluene (14.12 g) was partitioned into 4 separate reaction vials and loaded into the calorimeter. After equilibration, the catalyst solutions were introduced via syringe. Catalyst Solution A: **OA1a** (53.6 mg, 70.7 μmol) in the amine stock solution (0.5512 g) with **L1** (56.3 mg, 121 μmol), 81.1 mg/g. Catalyst Solution B: **OA1a** (48.8 mg, 64.4 μmol) in the amine stock solution (0.564 g), 79.7 mg/g. Catalyst Solution C: **OA1a** (49.3 mg, 65.0 μmol) in the amine stock solution (0.543 g), 83.3 mg/g. Catalyst Solution D: **OA1a** (27.4 mg, 36.1 μmol) in the amine stock solution (0.551 g), 47.4 mg/g.
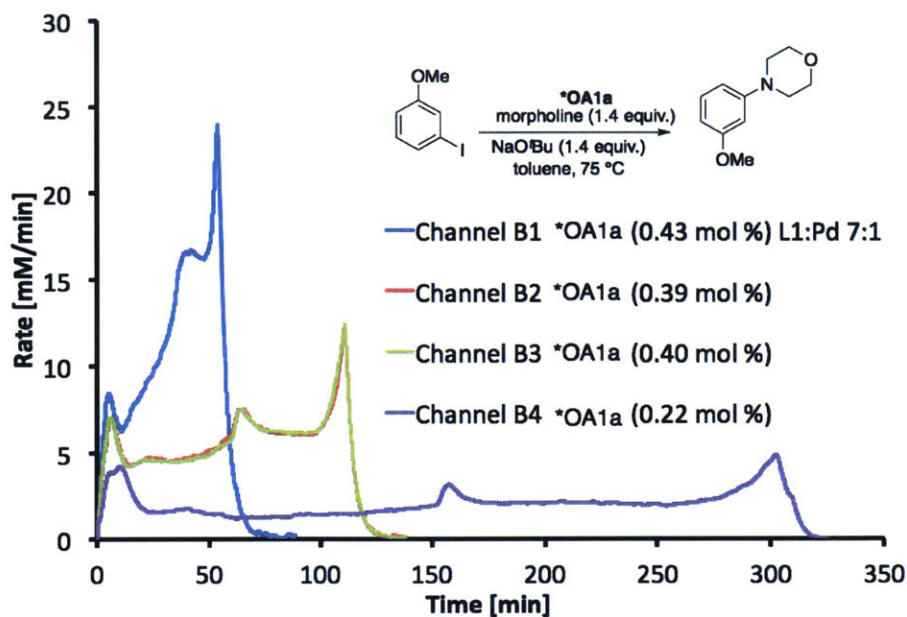
Figure 2-45 Cross-Coupling of 3-iodoanisole with morpholine mediated by *OA1a

Table 2-116 Stock Solution

Reagent [g]	Name [-]	Conc. [mmol/g]
2.3739	NaO^{t}Bu	1.09
2.1487	morpholine	1.09
4.0905	3-iodoanisole	0.77
14.1221	toluene	

Table 2-117 Catalyst Stock Solution

Catalyst Label [-]	OA1a [mg]	RuPhos (L1) [mg]	Amine Sol. [g]	Conc. [mmol/g]
A	53.6	56.3	0.5512	81.08
B	48.8	0	0.5637	79.67
C	49.3	0	0.5425	83.31
D	27.4	0	0.5507	47.40

Table 2-118 Run Summary

Catalyst Label [-]	Channel #	Weight [g]	Loaded Syringe [g]	Unloaded [g]	Injection Weight [g]	Pd [%]	ArX [mmol]
A	B1	4.159	2.7807	2.6514	0.1293	0.43	3.21
B	B2	4.283	2.763	2.6414	0.1216	0.39	3.31
C	B3	4.1274	2.8036	2.6869	0.1167	0.40	3.19
D	B4	4.173	2.7459	2.6345	0.1114	0.22	3.22

227

Table 2-119 GC Data

Channel #	Dodecane [mg]	Dodecane [pA s]	Product [pA s]	Yield [%]
B1	146.3	167.82	404.76	96
B2	152.4	214.84	523.93	99
B3	137.9	121.95	316.90	99
B4	124.6	145.14	429.38	100

Table 2-120 Energy Density

Channel #	Energy [J]	Energy Density [kJ/mol]
B1	675	210
B2	723	219
B3	690	217
B4	735	228

2.4.8.5. Variation of NaOtBu concentration at 75 °C

Following General Procedure B, solutions for each reaction vial (Tables 2-120 – 2-121) were made with morpholine, 3-bromoanisole, NaOtBu, and 1,4-dioxane. After equilibration, the catalyst solutions were introduced via syringe. Catalyst Solution: **OA1a** (102.4 mg, 135 μmol) in the amine stock solution (1.0611 g), 88.0 mg/g. Catalyst Solution: **OA1a** (53.4 mg, 70.4 μmol) in the amine stock solution (0.5570 g), 87.5 mg/g. *Note: Oscillations in graph (red line) are an artifact of poor tuning (of the temperature controller +/- 0.1 °C) for the circulating bath.*
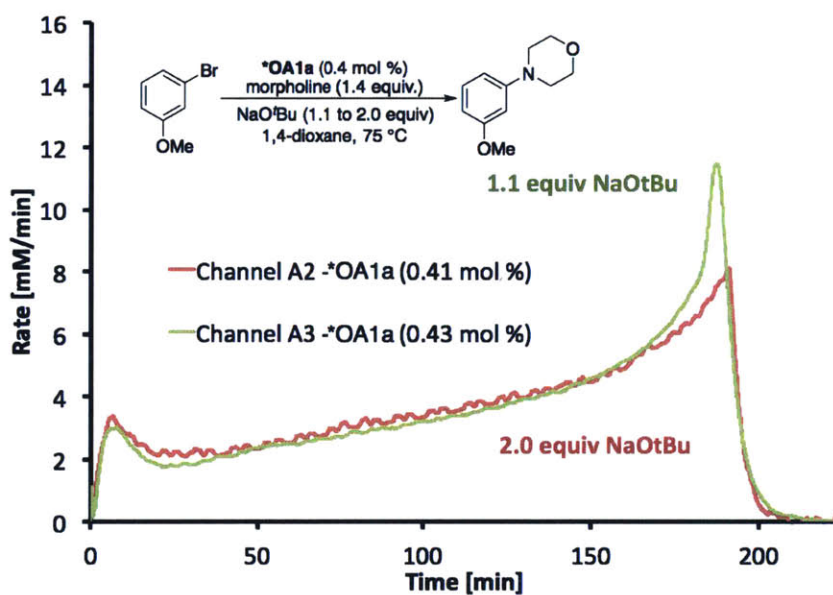

Figure 2-46 Rate of reaction at different concentrations of NaOtBu

228

Table 2-121 Stock Solution for A2

Reagent [g]	Name [-]	Conc. [mmol/g]
1.0121	NaO^{t}Bu	0.77
1.1493	morpholine	0.97
1.7708	3-bromoanisole	0.69
9.7033	1,4-dioxane	

Table 2-122 Stock Solution for A3

Reagent [g]	Name [-]	Conc. [mmol/g]
1.0068	NaO^{t}Bu	1.39
0.6342	morpholine	0.97
0.9718	3-bromoanisole	0.69
4.9090	1,4-dioxane	

Table 2-123 Stock Solution for *OA1a

Channel [-]	OA1a [mg]	Amine Sol. [g]	Conc. [mg/g]
A2	102.4	1.0611	88.0
A3	53.4	0.5570	87.5

Table 2-124 Run Summary

Channel [-]	Stock Solution [g]	Loaded Syringe [g]	Unloaded Syringe [g]	Injection [g]	ArX [mmol]	Pd [mol %]
A2	4.2087	2.7442	2.6422	0.1020	2.92	0.41
A3	4.2121	2.7536	2.6465	0.1071	2.91	0.43

Table 2-125 Energy Density

Channel [-]	Energy [J]	Energy Density [kJ/mol]
A2	604	207
A3	590	203

Table 2-126 GC Data

Channel [-]	Dodecane [mg]	Dodecane [pA s]	Product [pA s]	Yield [%]
A2	112.9	57.7	157.7	96
A3	105.2	46.1	143.4	102

229

2.4.8.6. Variation of excess RuPhos (L1) concentration at 75 °C

Following General Procedure B, a stock solution of 3-bromoanisole (3.74 g, 20.0 mmol), morpholine (2.43 g, 27.9 mmol) and NaO*t*Bu (2.69 g, 28.0 mmol) in 1,4-dioxane (20.0 g) was partitioned into separate reaction vials and loaded into the calorimeter. Extra ligand **L1** was added to the various reaction vials (Table 2-128). After equilibration, the catalyst solutions were introduced via syringe. Catalyst Solution: **OA1a** (92.5 mg, 122 μmol) in the amine stock solution (1.07 g), 79.4 mg/g.
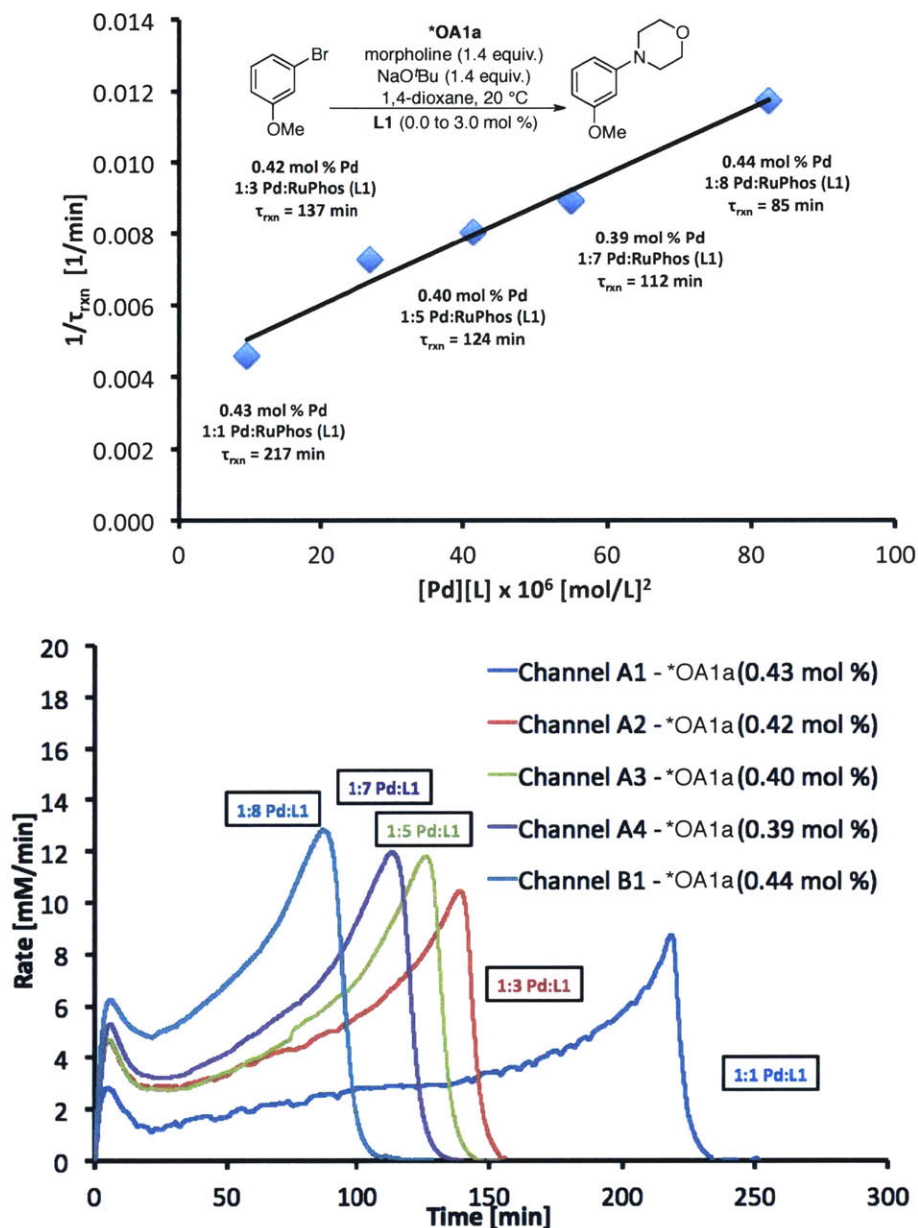

Figure 2-47 Effect of added ligand for a reaction initiated using *OA1a

Table 2-127 Stock Solution for Calorimetry Run

Reagent [g]	Name [-]	Conc [mmol/g]
2.6884	NaO'Bu	0.97
3.7423	3-bromoanisole	0.69
2.4330	morpholine	0.97
20.0024	1,4-dioxane	

Table 2-128 Stock Catalyst Solution

OA1a [mg]	Amine Sol. [g]	Conc. [mg/g]
92.5	1.0725	79.40

Table 2-129 Run Summary Data

Channel #	Stock Solution [g]	RuPhos (L1) [mg]	Loaded Syringe [g]	Unloaded Syringe [g]	Injection Weight [g]	ArX [mmol]	Pd [%]	RuPhos (L1) [%]
A1	4.2198	0.0	2.76	2.64	0.12	2.91	0.43	0.00
A2	4.2116	11.1	2.73	2.62	0.12	2.91	0.42	0.82
A3	4.2169	21.5	2.76	2.65	0.11	2.91	0.40	1.59
A4	4.2066	31.5	2.76	2.66	0.11	2.90	0.39	2.33
B1	4.2195	42.0	2.75	2.63	0.12	2.91	0.44	3.10

Table 2-130 Run Summary Data for Reciprocal Plot

Channel #	$[Pd][L] \times 10^6$ $[M]^2$	$1/Tau_{rxn}$ [1/min]	Tau_{rxn} [min]
A1	9.57	0.0046	217
A2	27.14	0.0073	137
A3	41.34	0.0080	124
A4	55.11	0.0089	112
B1	82.48	0.0117	85

Table 2-131 Energy Density

Channel #	Energy [J]	Energy Density [kJ/mol]
A1	590	203
A2	583	201
A3	559	192
A4	572	197
B1	634	218

Table 2-132 GC Data

Channel #	Dodecane [mg]	Dodecane [pA s]	Product [pA s]	Yield [%]
A1	109.1	77.73	229.79	>99
A2	114.6	76.36	211.50	99.00
A3	107.3	55.35	169.02	>99
A4	104.2	41.52	129.36	>99
B1	102.4	47.02	146.17	99.00

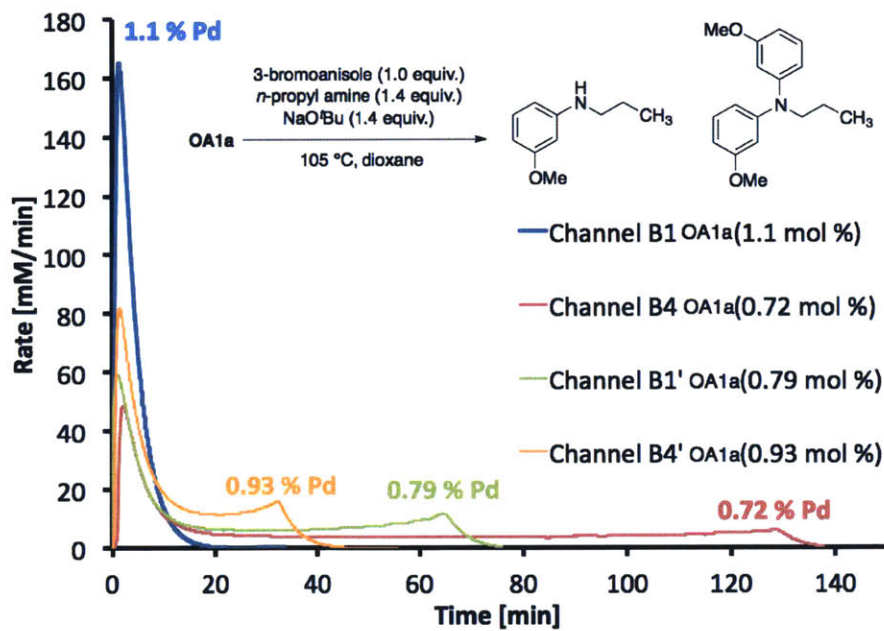## 2.4.8.7. Coupling of n-propylamine with 3-bromoanisole by RuPhos (L1) based catalyst

Figure 2-48 Coupling of *n*-propyl amine with 3-bromoanisole mediated by **OA1a** catalyst

Table 2-133 Stock Solution for Channels B1 and B4

Weight [g]	Name [-]	Conc [mmol/g]
2.0214	NaO^{t}Bu	1.01
1.231	n-propyl amine	1.00
2.7889	3-bromoanisole	0.71
14.886	1,4-dioxane	

Table 2-134 Stock Solution for Channels B1' and B4'

Weight [g]	Name [-]	Conc [mmol/g]
2.015	NaO^{t}Bu	1.00
1.2349	n-propyl amine	1.00
2.7873	3-bromoanisole	0.71
14.886	1,4-dioxane	

Table 2-135 Catalyst Solutions

Channel [#]	OA1a [mg]	THF [g]	Conc. [mg/g]
B1	173.2	0.9101	159.88
B4	39	0.3215	108.18
B1'	41.6	0.3017	121.18
B4'	51.6	0.3067	144.01

Table 2-136 Run Summary

Channel [#]	n-dodecane [mg]	3-bromoanisole [pA s]	dodecane [pA s]	Arylated Product [pA s]	Diarylated Product [pA s]	Arylated Product [%]	Diarylated Product [%]	Pd [%]
B1	151.6	0	77.31	88.78	23.74	69	24	1.05
B4	130.1	0	55.56	75.73	15.04	71	27	0.72
B1'	144.9	0	71.71	91.47	19.32	74	27	0.79
B4'	157.6	0	66.51	78.46	18.05	74	25	0.93

Table 2-137 Energy Density

Channel [#]	Energy [J]	Limiting Reagent [mmol]	Energy Density [kJ/mol]
B1	430	2.15	200
B4	386	2.14	180
B1'	414	2.14	193
B4'	426	2.15	198

233

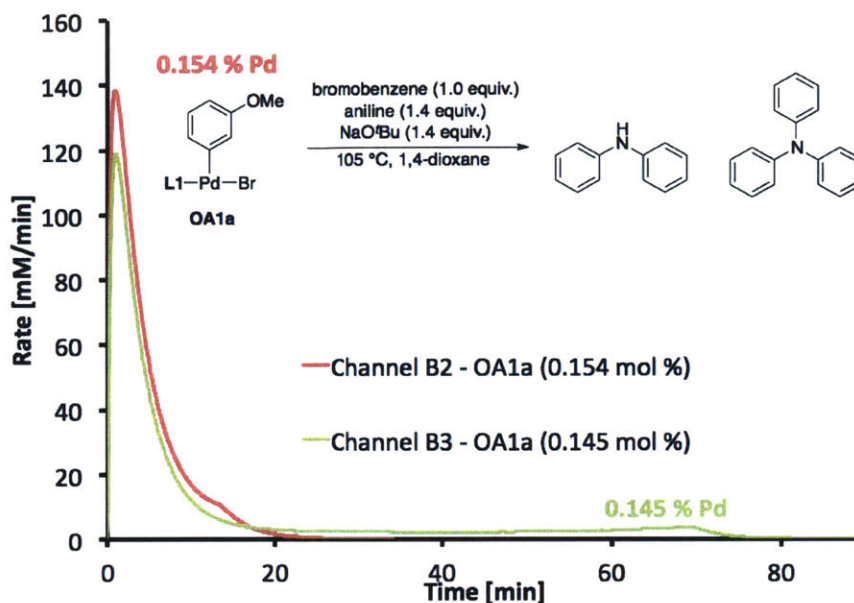## 2.4.8.8.   Coupling of aniline with bromobenzene

Figure 2-49 Coupling of aniline with bromobenzene mediated by **OA1a**. Note the tiny catalyst range- 0.154 to 0.145 mol %.

Table 2-138 Stock Solution

Weight [g]	Name [-]	Conc. [mmol/g]
2.0005	NaO^{t}Bu	0.99
1.9269	aniline	0.98
2.3232	bromobenzene	0.70
14.889	1,4-dioxane	

Table 2-139 Catalyst Solution

OA1a [mg]	THF [g]	Conc [mg/g]
23.2	0.9093	24.88
24.3	1.0923	21.76

Table 2-140 Run Summary

Channel [#]	Stock Solution [g]	ArX [mmol]	Syringe [g]	Unloaded [g]	Weight [g]	Pd [mol %]
B2	3.0069	2.12	2.7706	2.671	0.0996	0.154
B3	3.0422	2.14	2.7533	2.6454	0.1079	0.145

Table 2-141 Energy

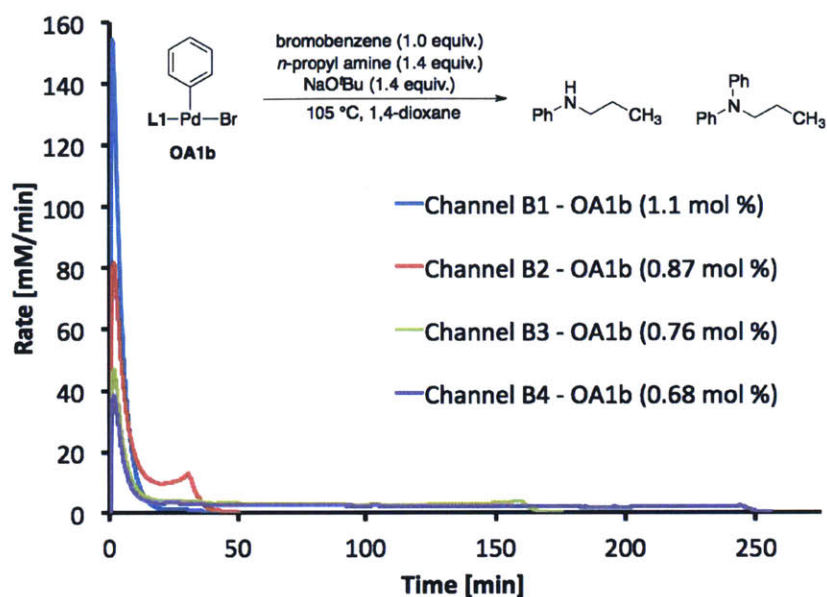| Channel [#]	Energy [J]	ArX [mmol]	Energy Density [kJ/mol]
B2	402	2.12	190
B3	409	2.14	191

234

Figure 2-50 Rate of reaction for coupling of n-propyl amine and bromobenzene by **OA1b**

Table 2-142 Stock Solution

Weight [g]	Reagent [-]	Conc. [mg/g]
2.0069	NaO^{t}Bu	1.01
2.3427	bromobenzene	0.73
1.2283	n-propyl amine	1.01
0.1971	n-dodecane	
14.8835	1,4-dioxane	

Table 2-143 Catalyst Solution

OA1b [mg]	THF [g]	Conc. [mg/g]
56.1	0.5996	85.6
49.7	0.6138	74.9
42.8	0.604	66.2
36.8	0.6054	57.3

Table 2-144 Run Summary

Channel [#]	Stock Solution [g]	ArX [mmol]	Syringe Loaded [g]	Unloaded [g]	Injection [g]	Pd [mol %]
B1	3.0216	2.20	2.8535	2.6562	0.1973	1.06
B2	3.0157	2.19	2.8551	2.6704	0.1847	0.87
B3	2.9993	2.18	2.8506	2.6674	0.1832	0.76
B4	3.0012	2.18	2.8373	2.6486	0.1887	0.68

Table 2-145 GC Data (Note: dodecane [mg] is calculated from table 3-143)

235

Channel [#]	dodecane [mg]	dodecane [pA s]	Product [pA s]	Diarylated Product [pA s]	Biphenyl [pA s]
B1	28.83	26.84	159.71	55.31	0.82
B2	28.77	32.08	191.51	55.25	2.85
B3	28.62	27.45	164.84	39.77	4.37
B4	28.63	23.70	137.40	33.46	3.90

Table 2-146 Energy Density

Channel [#]	Energy [J]	ArX [mmol]	Energy Density [kJ/mol]
B1	528	2.20	240
B2	531	2.19	242
B3	578	2.18	265
B4	672	2.18	308

2.4.8.9.   Coupling of *n*-propylamine with chlorobenzene
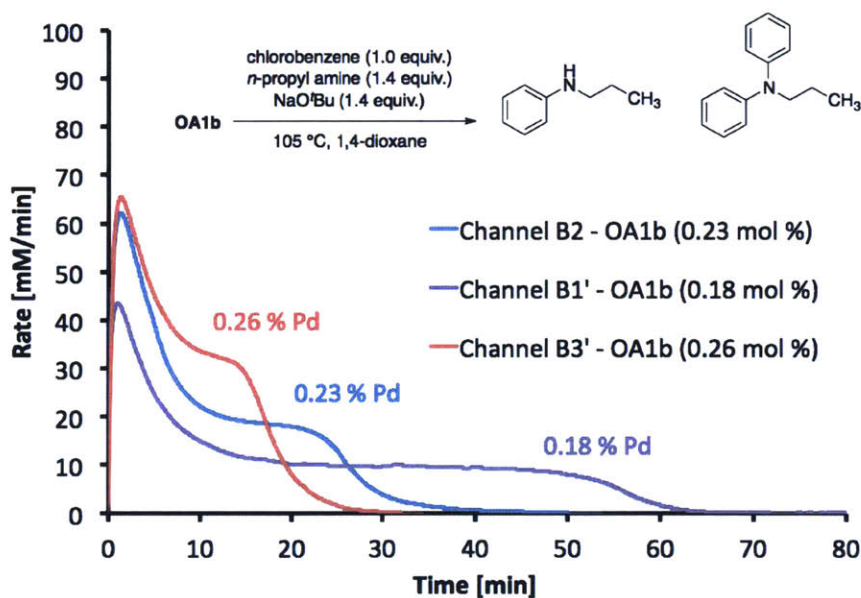
Figure 2-51 Cross-coupling reaction of chlorobenzene and *n*-propylamine mediated by a RuPhos based catalyst (**OA1b**)

Table 2-147 Stock Solution

Weight [g]	Reagent [-]	Conc. [mmol/g]
1.9911	NaO^{t}Bu	1.06
1.6512	chlorobenzene	0.76
1.2129	*n*-propyl amine	1.05
14.654	1,4-dioxane	

236

Table 2-148 Catalyst Solution

Channel [#]	OA1b [mg]	THF [g]	Conc. [mg/g]
B1', B3'	19.2	0.9123	20.6
B2	19.2	0.9396	20.0

Table 2-149 Run Summary

Channel [#]	Stock Solution [g]	Syringe [g]	Unloaded [g]	Injection [g]	ArX [mmol]	Pd [mol %]
B1'	2.0165	2.7753	2.6775	0.0978	1.52	0.18
B3'	2.0138	2.8277	2.6882	0.1395	1.52	0.26
B2	2.0299	2.7950	2.6692	0.1258	1.53	0.23

Table 2-150 GC Summary

Channel [#]	n-tetradecane [mg]	n-tetradecane [pA s]	N-propylaniline [pA s]	N-phenyl-N-propylaniline [pA s]	N-propylaniline [%]	N-phenyl-N-propylaniline [%]
B1'	101.5	139.38	182.09	47.01	76	23
B3'	118.9	203.90	227.75	59.72	76	23
B2	111.8	248.85	290.33	84.76	74	25

Table 2-151 Energy Data

Channel [#]	Energy [J]	Limiting Reagent [mmol]	Energy Density [kJ/mol]
B1'	336	1.52	220
B3'	330	1.52	217
B2	417	1.53	272

2.4.9. Synthesis of Pd(0) and amino bound Pd(II) Complexes
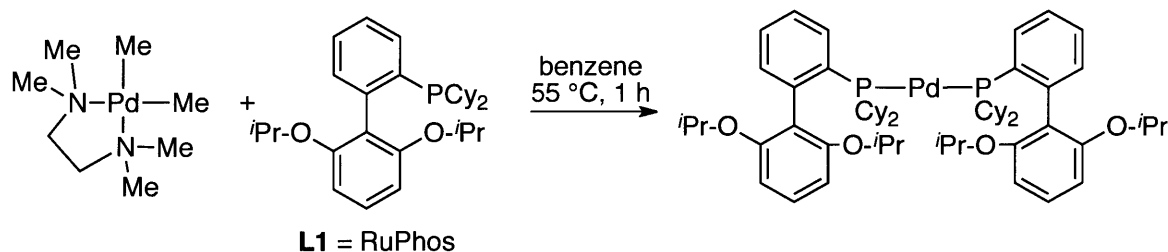
L1 = RuPhos

In a nitrogen filled glove box, tmedaPd(CH₃)₂ (388.9 mg, 1.54 mmol), RuPhos **L1** (1.4395 g, 3.09 mmol) and benzene (6 mL) was added to a screw cap test tube. A teflown stir bar was charged to the test tube and the tube closed with a Teflon/silicon septum and cap. The tube was taken out of the glove box and heated in an oil bath at 55 °C for 2 h. The solution was taken back into the glove box and filtered through celite. After which the solvent was removed under

237

vacuum to give a dry foam. A *minimum* of pentane (~ 7 mL) was added after which the solid went into solution. Over the course of one hour a precipitant formed. The pentane was decanted and the product washed with pentane (7 mL) and dried under vacuum. Product was a yellow solid (447.5 mg, 28 % yield, 0.43 mmol). Proton spectra not assigned- see plot. ^{13}C **NMR** (126 MHz, Toluene-d_8) δ 157.46 (br), 155.94 (br), 107.53 (br), 104.57 (br), 71.40. 68.42, 58.26, 49.63 (br), 45.19 , 38.74 (br), 35.54 (br), 32.84 (br), 32.19 (br), 31.73 (br), 30.60 (br), 27.49 (br), 26.93 (br), 22.32 , 22.19 , 21.84 , 21.56. ^{31}P **NMR** (202 MHz, Toluene-d_8) δ 44.10 (s), -9 (s), 70 – 10 (br).

General Procedure for (o-tolyl)₃PPd(Ar)X

In a nitrogen-filled box, a round bottom flask (100 mL) was charged with Pd(dba)₂ (1.00 g) and P(o-tolyl)₃ (1.11 g). A teflon stir bar was added and then an excess of aryl halide (~ 4 mL) was added followed by the benzene solvent (60 mL). The reaction was allowed to stir for 1 hour after which the mixture was removed from the glove box and filtered through celite to remove any insolubles material. The benzene solvent was then removed with the aid of a rotary evaporator and replaced with diethyl ether (60 mL). The ether solution was allowed to site overnight during which the intermediate would precipitate. *Note: Precipitation of the product is quite sluggish. Sonication can be used to induce nucleation.* The resultant product was isolated by filtration and then dissolved in *n*-propyl amine (5 mL). This solution was allowed to stir for an additional day after which pentane (20 mL) was added to precipitate the product as a white powder. *Note: Precipitation of product is again quite sluggish. Scratching the side of the flask can induce precipitation.* Precipitation was allowed to occur overnight. The product was washed twice more with pentane (2 x 20 mL) and the yield recorded.
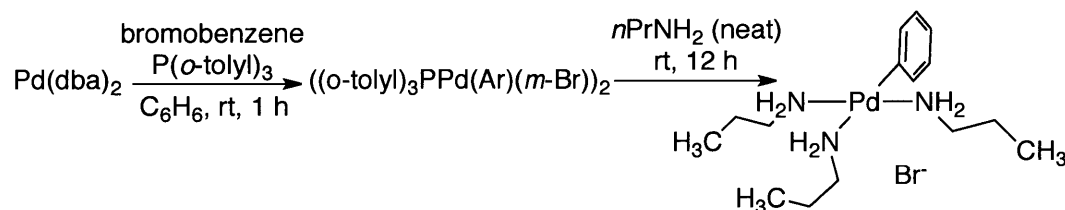
Following the general procedure, the reaction of Pd(dba)$_2$ (1.00 grams, 1.74 mmol) and P(o-tolyl)$_3$ (1.11 g, 3.65 mmol) with bromobenzene (4 mL) afforded the intermediate (781 mg). Without further characterization, the intermediate was carried forward by reaction with n-propyl amine (5 mL). Precipitation into pentane yields the product (406 mg, 0.92 mmol, 53 %) as a white solid. ^{1}H NMR (500 MHz, Toluene-d_8) δ 7.35 – 7.21 (m, 3H), 7.09 (s, 1H), 7.03 (q, J = 7.0 Hz, 2H), 6.95 (dd, J = 14.1, 6.8 Hz, 2H), 4.49 (s, 1H), 3.69 (s, 2H), 3.03 – 2.80 (m, 2H), 2.39 (s, 3H), 2.19 – 2.11 (m, 2H), 1.50 – 1.43 (m, 3H), 1.23 (s, 4H), 0.95 (s, 1H), 0.79 (s, 1H), 0.63 (s, 3H), 0.57 (s, 3H). ^{13}C NMR (126 MHz, Toluene-d_8) δ 153.25, 152.65, 135.33, 124.55, 46.93, 44.85, 27.63, 27.21, 25.96, 25.65, 12.83, 11.90, 11.67, 11.42.
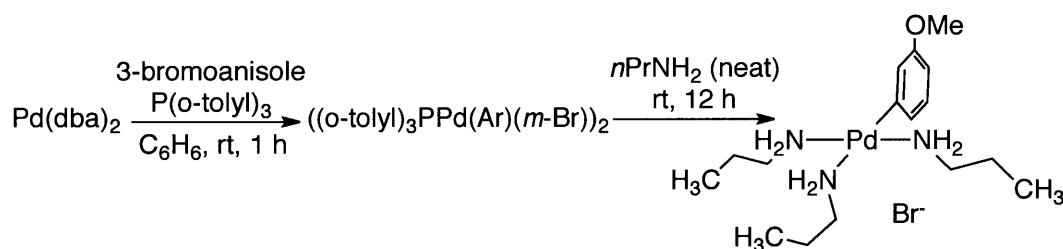

Following the general procedure, the reaction of Pd(dba)$_2$ (1.00 grams, 1.74 mmol) and P(o-tolyl)$_3$ (1.11 g, 3.65 mmol) with 3-bromoanisole (4 mL) afforded the intermediate (762 mg). Without further characterization, the intermediate was carried forward by reaction with n-propyl amine (5 mL). Precipitation into pentane yields the product (341 mg, 0.73 mmol, 42 %) as a white solid. ^{1}H-NMR (500 MHz, Toluene-d_8) δ 7.22 – 7.02 (m, 1H), 7.04 – 6.89 (m, 5H), 6.51 (d, J = 6.7 Hz, 1H), 4.62 – 4.37 (m, 1H), 3.78 – 3.63 (m, 4H), 3.50 (s, 4H), 3.09 – 2.72 (m, 2H), 2.47 (s, 9H), 2.26 – 2.11 (m, 1H), 2.07 (s, 1H), 1.74 – 1.42 (m, 4H), 1.40 – 1.18 (m, 7H), 1.07 – 0.73 (m, 5H), 0.73 – 0.37 (m, 13H). ^{13}C-NMR (126 MHz, Toluene-d_8) δ 158.96 , 154.52 (br), 154.20 (br), 127.46 (br), 121.14 (br), 109.54 , 55.06 (br), 47.82 (br) , 46.94 (br), 44.89 (br) , 27.72 (br), 27.20 (br), 26.00 (br), 25.69 (br) , 12.82 (br) , 11.90 (br), 11.70 (br), 11.44 (br). **Elemental**: Calculated, C(40.82) H(7.28), Found: C(40.81) H(7.14):

L (1 equiv)
ArX (excess)
Cyclohexane

L-Pd-Br

L = tBuBrettPhos

OMe

MeO   PtBu$_2$

^{i}Pr ^{i}Pr

^{i}Pr
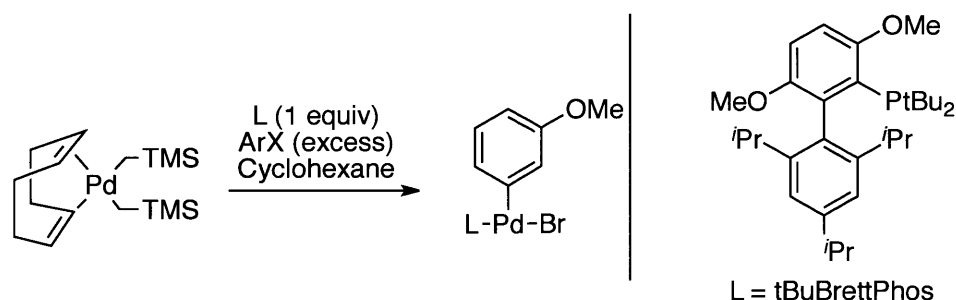
In a nitrogen filled glove box, ^{t}BuBrettPhos (110.9 mg, 0.23 mmol) was charged to a screw cap test tube followed by 3-bromoanisole (100 mg, 0.53 mmol) and the codPd(CH$_2$TMS)$_2$ (88.9 mg, 0.23 mmol). To this mixture was added cyclohexane (~ 3 mL) and a Teflon stir bar. The test tube was sealed with a cap fitted with a Teflon septum and the reaction was allowed to stir overnight at room temperature. The reaction was then taken out of the glove box and pentane (10 mL) was added to the mixture. The pentane was decanted and the product was further washed with pentane (2 x 10 mL). The product was dried under vacuum to yield a yellow powder (106.0 mg, 59 %). *Note: In solution the compound is known to undergo rearrangement.* ^{1}H NMR (500 MHz, CD$_2$Cl$_2$) δ 8.40 – 8.29 (m), 7.74 (s), 7.04 (s), 6.93 (dd, J = 8.9, 2.3 Hz), 6.87 (d, J = 8.9 Hz), 6.70 – 6.67 (m), 6.67 – 6.63 (m), 6.30 – 6.23 (m), 5.82 (d, J = 21.2 Hz), 3.93 (s), 3.79 (s), 3.66 (s,), 3.33 (s), 3.13 – 2.96 (m), 2.67 – 2.53 (m), 1.58 (d, J = 6.8 Hz), 1.55 (s), 1.51 (dd, J = 15.7, 4.0 Hz), 1.37 (dd, J = 17.1, 10.8 Hz), 0.82 (d, J = 6.6 Hz). ^{13}C{^{1}H} NMR (126 MHz, CD$_2$Cl$_2$) δ 161.16 , 157.17 – 156.91 (multiple overlapping peaks), 154.7 – 154.15 (multiple overlapping peaks), 152.56 , 152.44 , 142.38 – 140.69 (multiple overlapping peaks), 138.63 , 135.95 , 133.40 , 129.91 , 129.23 , 128.24 , 128.10 (d, J = 1.5 Hz), 126.36 – 126.20 (br), 125.36 , 125.33 – 124.5 (br), 118.95 , 117.83 , 117.80 116.51 , 115.29 , 114.56 , 114.3 – 114.2 (multiple overlapping peaks) , 114.05 – 113.79 (br), 111.90 , 111.35 – 110.7 (multiple overlapping peaks), 108.12 (br) , 99.17 , 57.54 , 55.87 , 55.53 , 55.40 , 55.37 , 55.00 , 54.79 , 54.56 , 54.42 , 41.73 , 41.63 , 40.47 , 40.37 , 35.09 , 31.91 , 31.10 , 31.05 , 30.87 , 30.82 , 26.14 , 25.08 , 24.94 , 23.22 , 23.18 , 23.12 , 22.7-22.5 (multiple overlapping peaks), 21.72 , 21.67 , 20.60 , 20.43 , 20.38 – 20.25 (multiple overlapping peaks). ^{31}P{^{1}H} NMR (202 MHz, CD$_2$Cl$_2$) δ 82.17, 80.59 , 72.85 – 69.35 (br), 63.31 . ATR-IR (cm^{-1}): 2950, 2890, 2860, 2820, 1610, 1570, 1560, 1450, 1420, 1260, 1230, 1030, 1010, 815, 765, 695. Elemental: Calculated for C$_{38}$H$_{56}$BrO$_3$PPd C(58.65) H(7.25) Found: C(58.36) H(7.26)

(o-toyl)$_3$P—Pd
Br

S-BINAP (1 equiv.)
CH$_2$Cl$_2$, rt
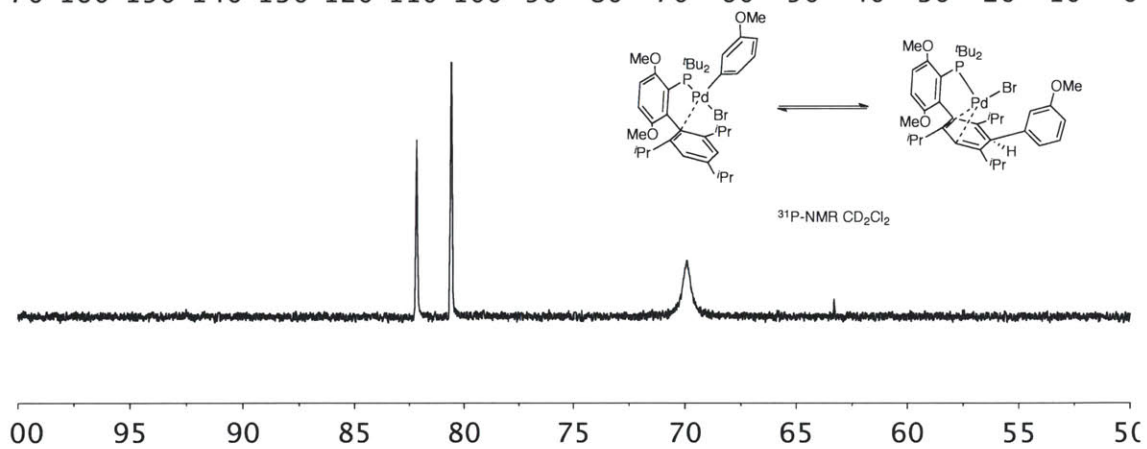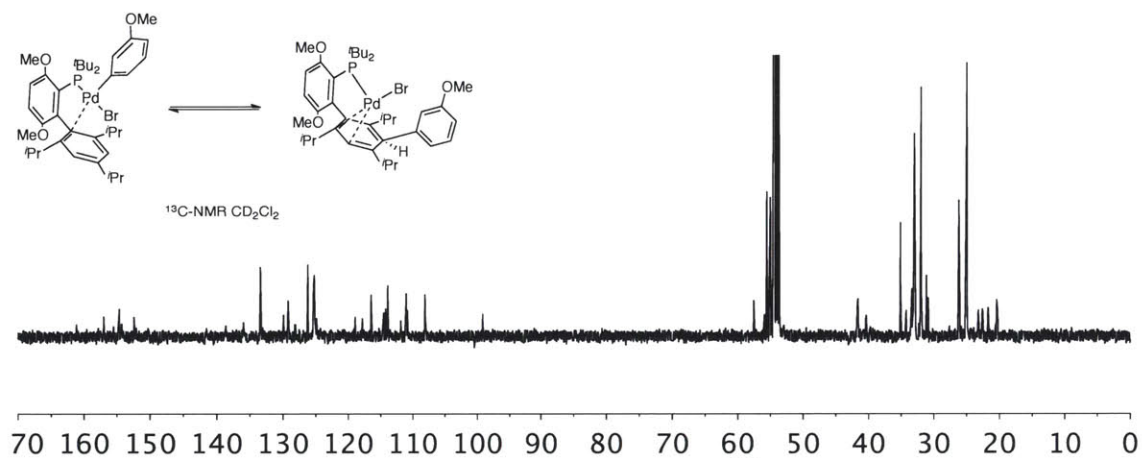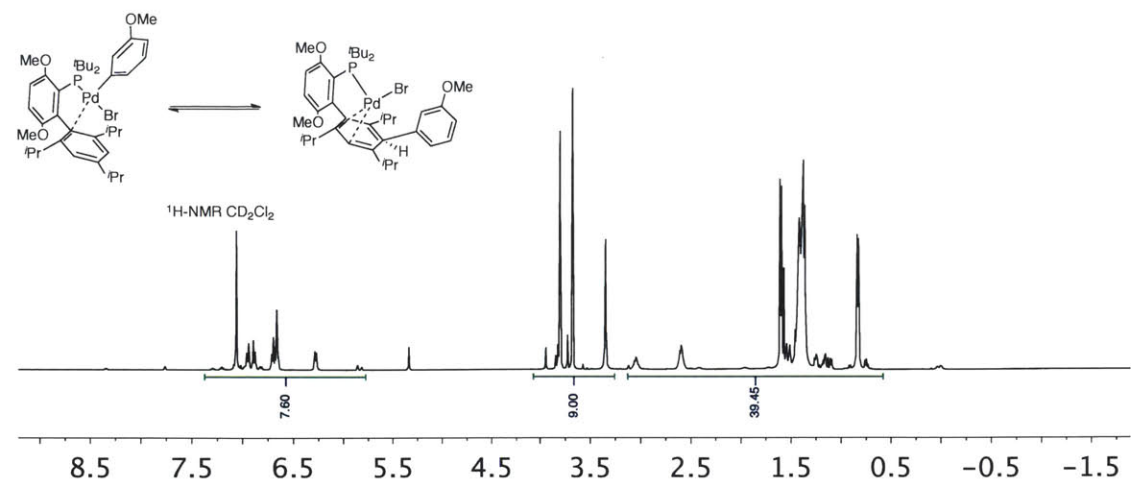
Ph$_2$
P
Pd
P   Br
Ph$_2$

240
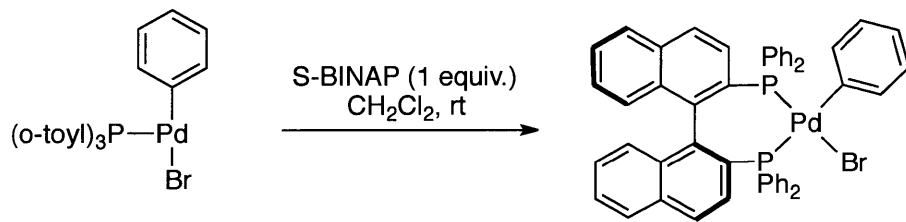
To a 20 mL scintillation vial was added (*o*-tolyl)$_3$PPd(Ph)Br (364 mg, 0.64mmol) and S-BINAP (404 mg, 0.65 mmol), and dichloromethane (~10 mL). The mixture was allowed to stir for 2 h and then the solvent was removed with the aid of a rotary evaporator. The residue was washed with pentane (3 x 20 mL) and dried under high vacuum. The product was a tan solid (540.6 mg, 95 % yield). **^{1}H NMR** (500 MHz, CD$_2$Cl$_2$) δ 7.97 (m, 1H), 7.78 (m, 3H), 7.64 – 7.3 (m, 14H), 7.24 – 7.17 (m, 1H), 7.16 – 7.11 (m, 1H), 7.10 – 6.86 (m, 8H), 6.81 – 6.75 (m, 2H), 6.73 – 6.67 (m, 3H), 6.59 – 6.45 (m, 2H). **^{13}C{^{1}H} NMR** (126 MHz, CD$_2$Cl$_2$) δ 158.06, 158.03, 157.08, 157.04, 139.85, 139.82, 139.75, 139.72, 137.42, 137.40, 137.33, 137.28, 137.24, 136.36, 136.25, 135.92, 135.83, 134.61, 134.54, 134.28, 134.27, 134.16, 134.04, 133.93, 133.88, 133.66, 133.60, 132.94, 132.86, 132.54, 132.47, 132.13, 132.10, 131.98, 131.89, 131.70, 131.68, 131.61, 131.58, 131.56, 131.24, 131.22, 130.57, 130.56, 130.12, 130.10, 129.89, 129.87, 129.76, 129.74, 129.26, 129.21, 129.06, 128.98, 128.79, 128.74, 128.66, 128.58, 128.49, 128.41, 128.38, 128.05, 128.02, 127.96, 127.94, 127.91, 127.90, 127.65, 127.56, 127.41, 127.38, 127.29, 127.22, 126.83, 126.38, 126.08, 123.30 (Observed complexity due to C-P splitting). **^{31}P{^{1}H} NMR** (202 MHz, CD$_2$Cl$_2$) δ 28.29 (d, J = 39.2 Hz), 11.87 (d, J = 39.2 Hz). ATR-IR 3050, 1560, 1500, 1480, 1460, 1430, 1300, 1090, 1020, 995, 811, 725, 691. **Elemental**: Calculated for C$_{50}$H$_{37}$BrP$_2$Pd C(67.77) H(4.21) Found: C(67.48) H(4.34)
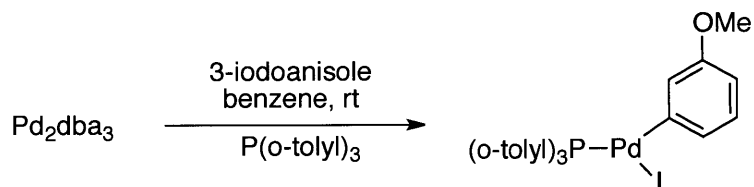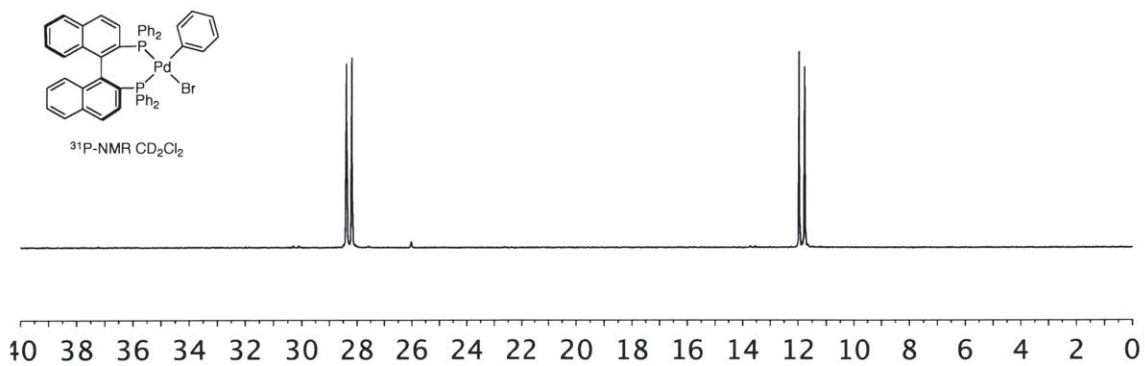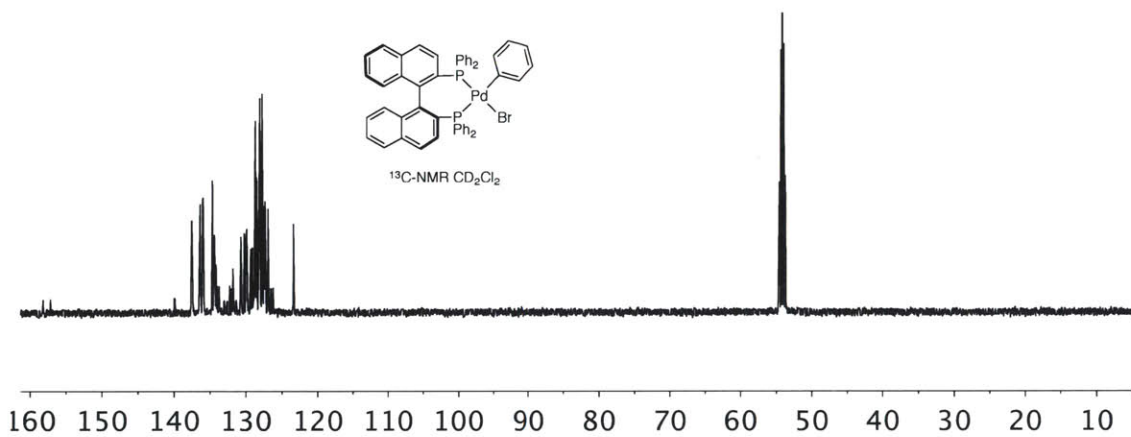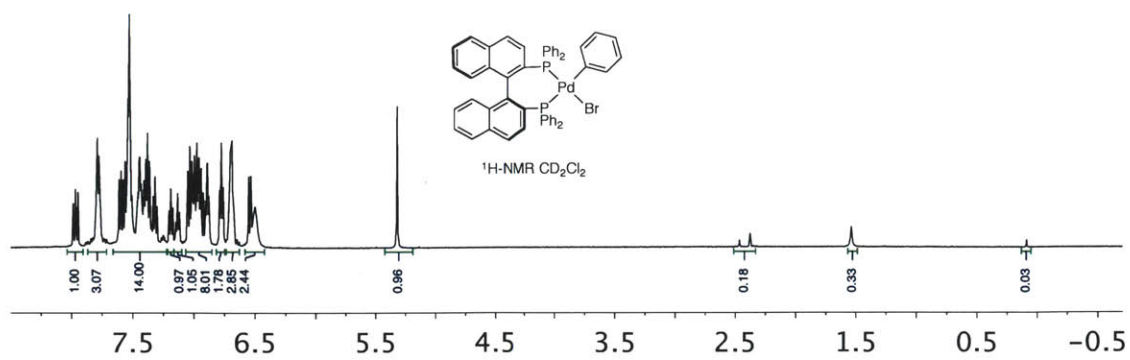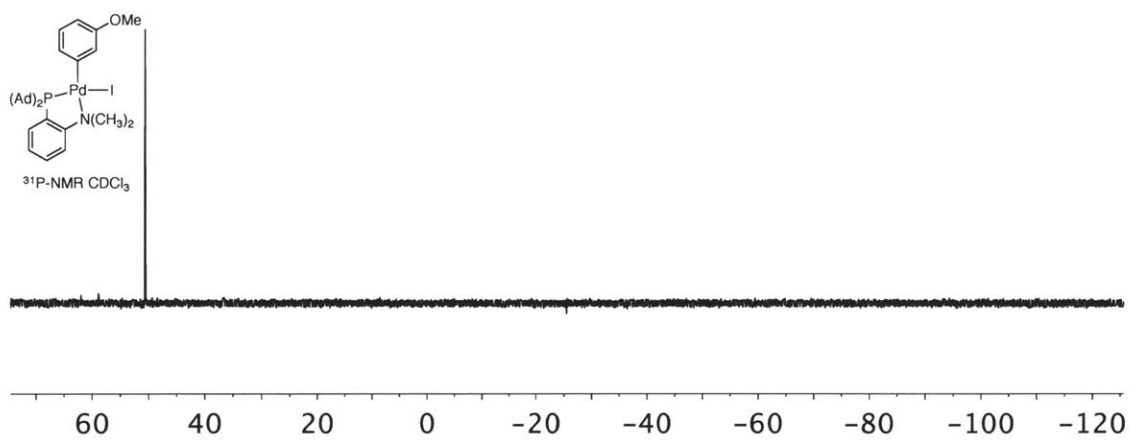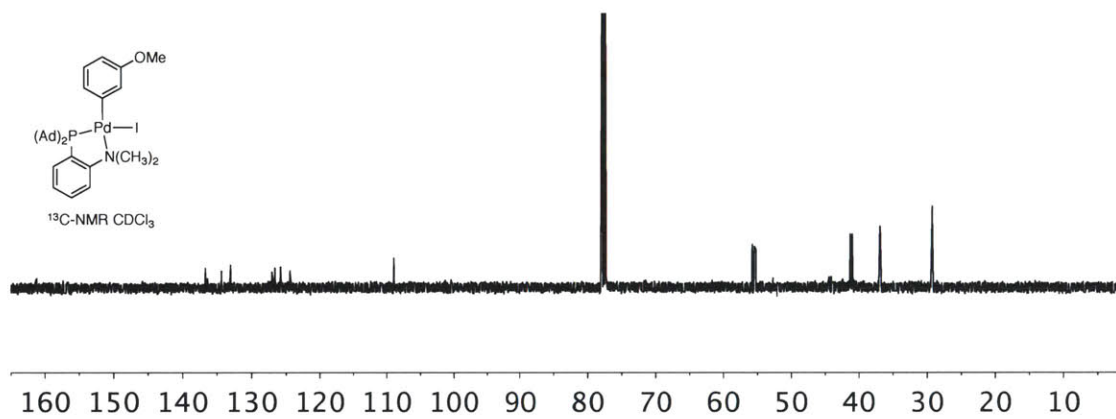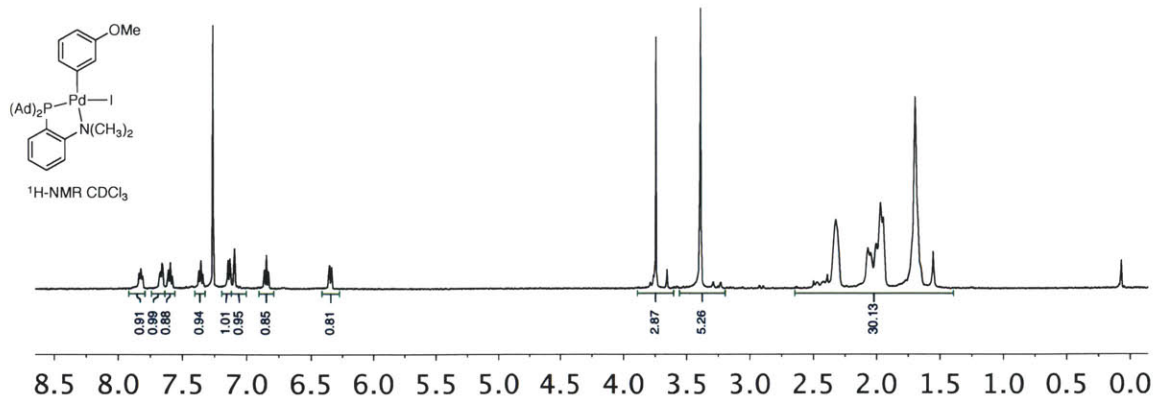

In a nitrogen filled glove box, a round bottom flask (100 mL) was charged with iodoanisole (2.43 g, 10.4 mmol), P(*o*-tolyl)$_3$ (1.33 g, 4.4 mmol), Pd$_2$dba$_3$ (1.04 g, 1.14 mmol) and benzene (~60 mL). The mixture was stirred with a teflon stir bar for 1 h and then filtered through a pad of Celite. The filtrate was taken out of the glove box and the solvent was removed with the aid of a rotary evaporator. To the residue was added diethyl ether (~60 mL) and the mixture was allowed to stand overnight. The resultant orange product (0.864 g, 1.30 mmol) was collected by filtration (59 % Yield). The material was used to synthesize the DalPhos-OA complex. No characterization was carried out.
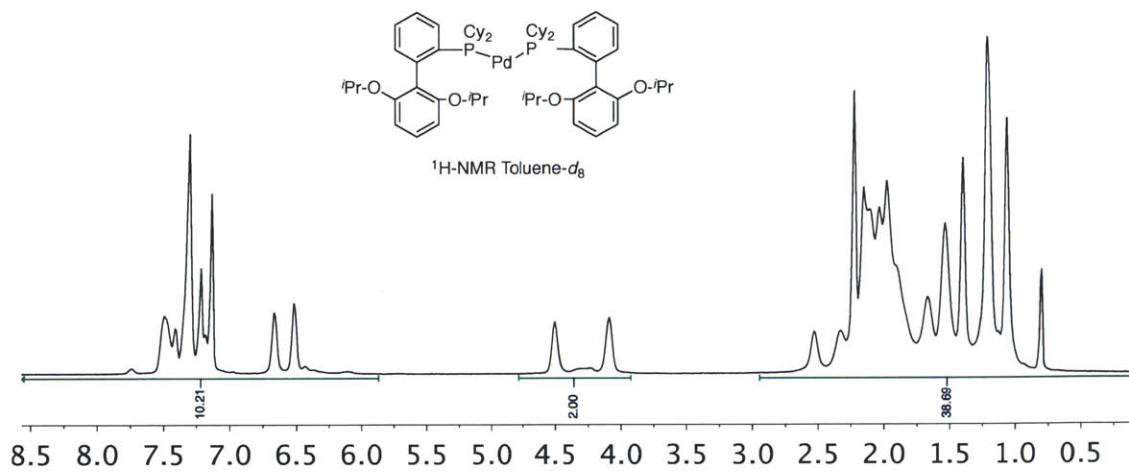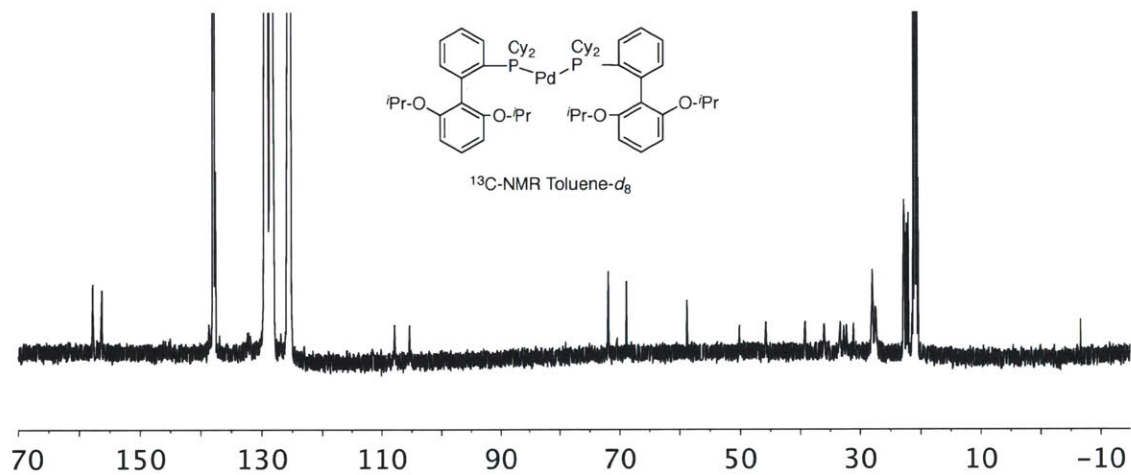
DalPhos (1 equiv.)
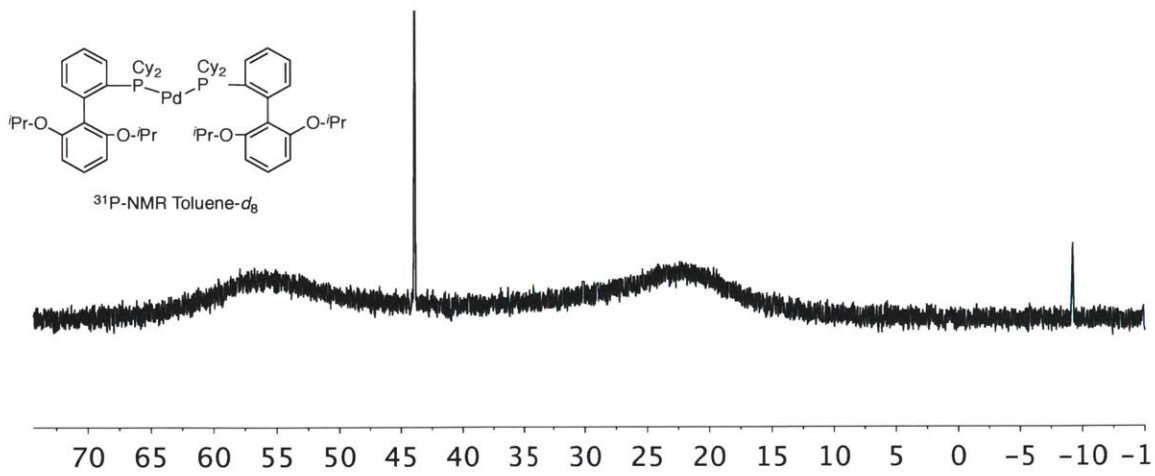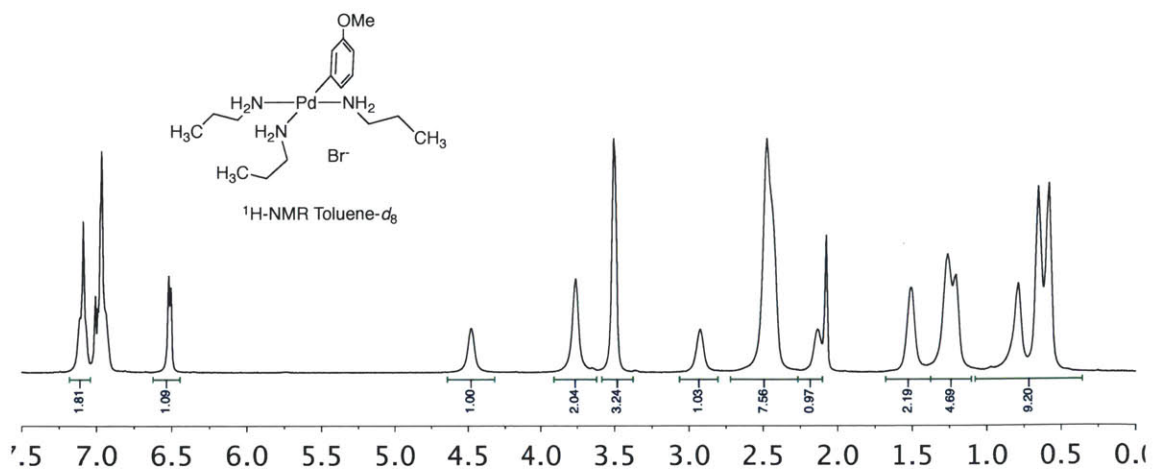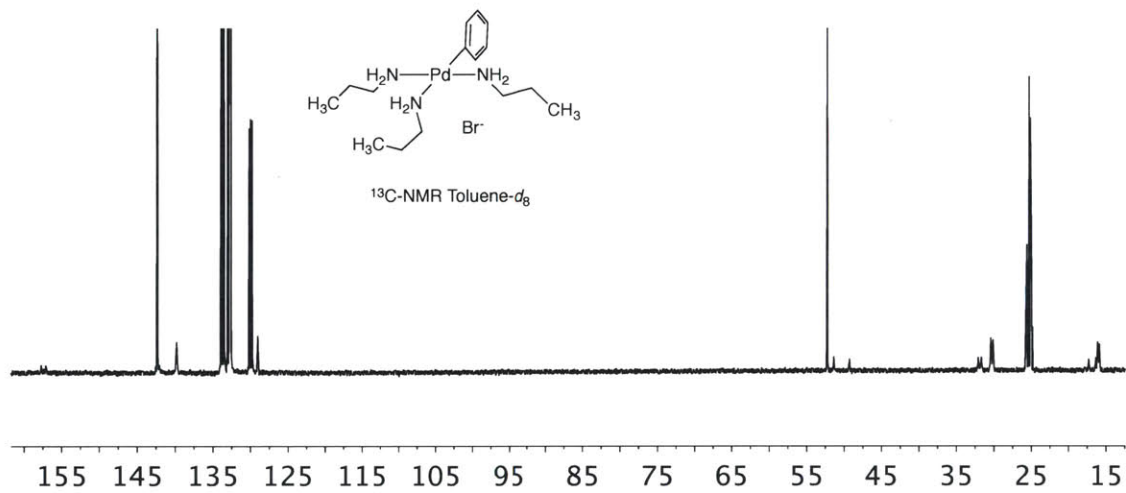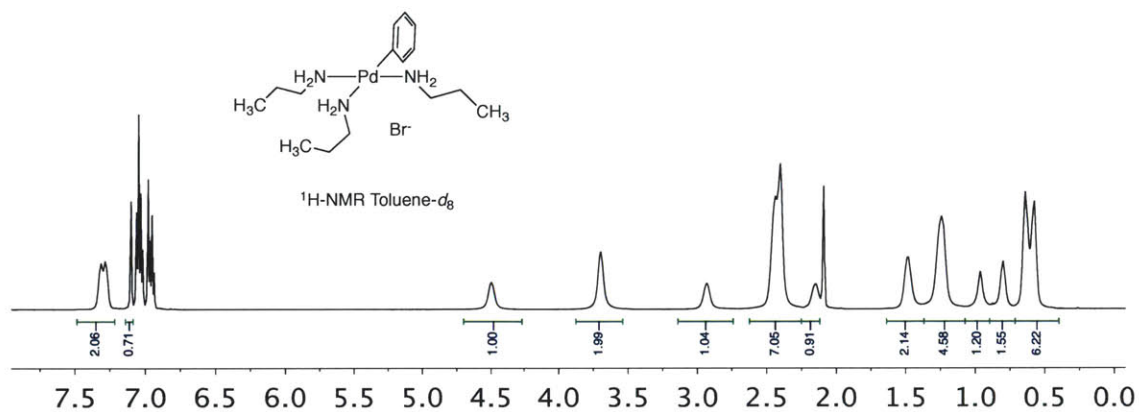CH₂Cl₂, rt

(o-tolyl)₃P—Pd

OMe

Ad
Ad
P—Pd—I
N—CH₃
CH₃

OMe
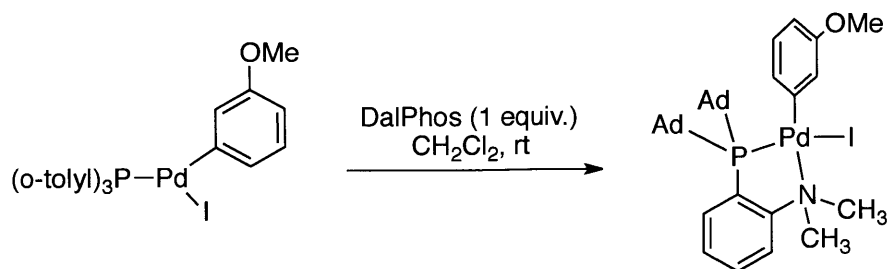
A screw cap test tube was charged with (o-tolyl)₃PPd(Ar)I (231 mg, 0.36 mmol), DalPhos ligand (151 mg, 0.36 mmol), and dichloromethane (~ 5 mL). This mixture was then stirred for 7.5 h after which the solvent was removed with the aid a rotary evaporator. The residue was washed with diethyl ether (2 x 10 mL) and dried under high vacuum. Product was a slightly pink-tan solid (215 mg, 0.28 mmol, 80 % yield). ^{1}H NMR (500 MHz, CDCl₃) δ 7.88 – 7.78 (m, 1H), 7.70 – 7.64 (m, 1H), 7.62 – 7.56 (m, 1H), 7.42 – 7.31 (m, 1H), 7.13 (d, J = 7.8 Hz, 1H), 7.11 – 7.07 (m, 1H), 6.84 (t, J = 7.8 Hz, 1H), 6.39 – 6.31 (m, 1H), 3.74 (s, 2H), 3.39 (s, 3H), 2.62 – 1.24 (m, 26H). ^{13}C{^{1}H} NMR (126 MHz, CDCl₃) δ 164.50 , 160.80 , 160.69 , 136.18 , 136.17 , 133.84 , 133.83 , 132.51 , 132.50 , 126.54 , 126.14 , 126.11 , 125.30 , 125.29 , 123.94 , 123.87 , 108.41 , 55.23 , 54.93 , 54.69 , 43.95 , 43.87 , 43.66 , 43.57 , 40.79 , 40.78 , 40.52 , 40.50 , 36.41 (d, J = 1.1 Hz), 36.35 (d, J = 1.2 Hz), 28.78 , 28.71. ^{31}P{^{1}H} NMR (202 MHz, CDCl₃) δ 50.66. ATR-IR (cm^{-1}): 2900, 2840, 1560, 1460, 1340, 1230, 1030, 971, 766, 741, 695. Elemental: Calculated for C₃₅H₄₇INOPPd C(55.16) H(6.22) Found: C(54.98) H(6.23)

^{1}H-NMR CD$_2$Cl$_2$

7.60 9.00 39.45

8.5 7.5 6.5 5.5 4.5 3.5 2.5 1.5 0.5 −0.5 −1.5

^{13}C-NMR CD$_2$Cl$_2$

70 160 150 140 130 120 110 100 90 80 70 60 50 40 30 20 10 0

^{31}P-NMR CD$_2$Cl$_2$

00 95 90 85 80 75 70 65 60 55 5(

^{1}H-NMR CD$_2$Cl$_2$

^{13}C-NMR CD$_2$Cl$_2$

^{31}P-NMR CD$_2$Cl$_2$

^{31}P-NMR Toluene-d_8

^{13}C-NMR Toluene-d_8

^{1}H-NMR Toluene-d_8

¹H-NMR Toluene-d_8

¹³C-NMR Toluene-d_8
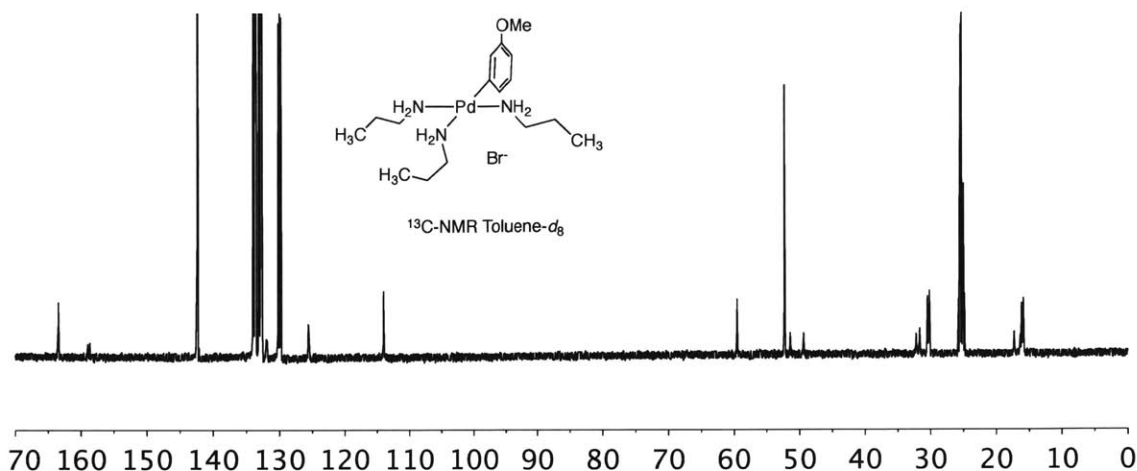

¹H-NMR Toluene-d_8

13C-NMR Toluene-d_8

2.5. References

1) (a) Amatore, C.; Jutand, A.; Khalil, F.; M'Barki, M. A.; Mottier, L. *Organometallics* **1993**, *12*, 3168. (b) Portnoy, M.; Milstein, D. *Organometallics* **1993**, *12*, 1665. (c) Amatore, C.; Pfluger, F. *Organometallics* **1990**, *9*, 2276. (d) Stille, J. K.; Lau, K. S. Y. *Acc. Chem. Res.* **1977**, *10*, 434. (e) Barrios-Landeros, F.; Hartwig, J. F. *J. Am. Chem. Soc.* **2005**, *127*, 6944. (f) Fitton, P.; Rick, E. A. *J. Organometal. Chem.* **1971**, *28*, 287. (g) Foa, M.; Cassar, L. *J. Chem. Soc., Dalton Trans.* **1975**, 2572. (h) Parshall, G. W. *J. Am. Chem. Soc.* **1974**, *96*, 2360 (i) Ariafard, A.; Lin, Z. *Organometallics* **2006**, *25*, 4030 (j) Amatore, C.; Azzabi, M.; Jutand, A. *J. Am. Chem. Soc.* **1991**, *113*, 8375. (k) Klabunde, K.J.; Low, J.Y.F. *J. Am. Chem. Soc.* **1974**, *96*, 7674.

2) (a) Biscoe, M. R.; Barder, T. E.; Buchwald, S. *Angew. Chem., Int. Ed.* **2007**, *46*, 7232. (b) Ferretti, A. C.; Mathew, J. S.; Ashworth, I.; Purdy, M.; Brennan, C.; Blackmond, D. G. *Adv. Synth. Catal.* **2008**, *350*, 1007.

3) (a) Hartwig, J. F. *Inorg. Chem.* **2007**, *46*, 1936. (b) Boncella, J. M.; Villanueva, L. A. *J. Organometal. Chem.* **1994**, *465*, 297. (c) Villanueva, L. A.; Abboud, K. A.; Boncella, J. M. *Organometallics* **1994**, *13*, 3921. (d) Driver, M. S.; Hartwig, J. F. *J. Am. Chem. Soc.* **1995**, *117*, 4708. (e) Koo, K.; Hillhouse, G. L. *Organometallics* **1995**, *14*, 4421. (f) Driver, M. S.; Hartwig, J. F. *J. Am. Chem. Soc.* **1996**, *118*, 4206. (g) Driver, M. S.; Hartwig, J. F. *J. Am. Chem. Soc.* **1997**, *119*, 8232. (h) Yamashita, M.; Hartwig, J. F. *J. Am. Chem. Soc.* **2004**, *126*, 5344. (i) Barder, T. E.; Biscoe, M. R.; Buchwald, S. L. *Organometallics* **2007**, *26*, 2183. (j) Klinkenberg, J. L.;

Hartwig, J. F. *J. Am. Chem. Soc.* **2010**, *132*, 11830. (k) Tatsumi, K.; Hoffman, R.; Yamamoto, A.; Stille, J.K.; *Bull. Chem. Soc. Jpn.* **1981**, *54*, 1857-1867. (l) Reductive Elimination, R. Hoffmann, in IUPAC. *Frontiers of Chemistry*, ed. K. J. Laidler, Pergamon Press, Oxford 1982, 247-263.

4) (a) Widenhoefer, R. A.; Zhong, H. A.; Buchwald, S. *Organometallics* **1996**, *15*, 2745. (b) Widenhoefer, R. A.; Buchwald, S. *Organometallics* **1996**, *15*, 3534. (c) Zhong, H. A.; Widenhoefer, R. A. *Inorg. Chem.* **1997**, *36*, 2610. (d) Wei, C. S.; Davies, G. H. M.; Soltani, O.; Albrecht, J.; Gao, Q.; Pathirana, C.; Hsiao, Y.; Tummala, S.; Eastgate, M. D. *Angew. Chem., Int. Ed.* **2013**, *52*, 5822. (e) Strieter, E. R.; Blackmond, D. G.; Buchwald, S. L. *J. Am. Chem. Soc.* **2003**, *125*, 13978.

5) (a) Halpern, J. *Inorg. Chim. Acta* **1981**, *50*, 11. (b) Mathew, J. S.; Klussman, M.; Iwamura, H.; Valera, F.; Futran, A.; Emanuelsson, E. A. C.; Blackmond, D. G. *J. Org. Chem.* **2006**, *71*, 4711. (c) Hein, J. E.; Armstrong, A.; Blackmond, D. G. *Org. Lett.* **2011**, *13*, 4300. (d) Jimeno, C.; Christmann, U.; Escurdo-Adan, E. C.; Vilar, R.; Pericas, M. A. *Chem. Eur. J.* **2012**, *18*, 16510.

6) (a) Shekhar, S.; Ryberg, P.; Hartwig, J. F.; Mathew, J. S.; Blackmond, D. G.; Strieter, E. R.; Buchwald, S. *J. Am. Chem. Soc.* **2006**, *128*, 3584. (b) Amatore, C.; Jutand, A.; M'Barki, M. A. *Organometallics* **1992**, *11*, 3009 (c) Fors, B. P.; Krattiger, P.; Strieter, E.; Buchwald, S. L. *Org. Lett.* **2008**, *10*, 3505. (d) Amatore, C.; Jutand, A. *J. Organomet. Chem.* **1999**, *576*, 254. (e) Fairlamb, I. J. S.; Kapdi, A. R.; Lee, A. F.; McGlacken, G. P.; Weissburger, F.; Vries, A. H. M. d.; Vondervoort, L. S.-v. d. *Chem. Eur. J.* **2006**, *12*, 8750. (f) Amatore, C.; Broeker, G.; Jutand, A.; Khalil, F. *J. Am. Chem. Soc.* **1997**, *119*, 5176. (g) Melvin, P. R.; Balcells, D.; Hazari, N.; Nova, A. *ACS Catalysis* **2015**, *5*, 5596.

7) (a) Fairlamb, I. J. S.; Kapdi, A. R.; Lee, A. F.; McGlacken, G. P.; Weissburger, F.; Vries, A. H. M. d.; Vondervoor, L. S.-v. d. *Chem. Eur. J.* **2006**, *12*, 8750. (b) Amatore, C.; Jutand, A.; Meyer, G. *Inorg. Chim. Acta* **1998**, *273*, 76. (c) Amatore, C.; Carre, E.; Jutand, A.; M'Barki, M. A. *Organometallics* **1995**, *14*, 1818. (d) Ozawa, F.; Kubo, A.; Hayashi, T. *Chem. Lett.* **1992**, 2177. (e) Mace, Y.; Kapdi, A. R.; Fairlamb, I. J. S.; Jutand, A. *Organometallics* **2006**, *25*, 1795.

8) (a) Milne, J. E.; Buchwald, S. L. *J. Am. Chem. Soc.* **2004**, *126*, 13028. (b) Fors, B. P.; Buchwald, S. L. *J. Am. Chem. Soc.* **2010**, *132*, 15914.

9) (a) Blackmond, D. G. *Angew. Chem., Int. Ed.* **2005**, *44*, 4302. (b) Wadso, I. *Acta Chem. Scand.* **1968**, *22*, 927.

10) Ruiz-Castillo, P.; Blackmond, D. G.; Buchwald, S. *J. Am. Chem. Soc.* **2015**, *137*, 3085. b) Park, N. H.; Vinogradova, E. V.; Surry, D. S.; Buchwald, S. L. *Angew. Chem. Int. Ed* **2015**, *54*, 8259.

11) There are several examples of room temperature palladium catalyzed C–N bond forming reactions: (a) Wolfe, J. P.; Buchwald, S. *J. Org. Chem.* **1997**, *62*, 6066. (b) Old, D. W.; Wolfe, J. P.; Buchwald, S. *J. Am. Chem. Soc.* **1998**, *120*, 9722. (c) Hartwig, J. F.; Kawatsura, M.; Hauck, S. I.; Shaughnessy, K. H.; Alcazar-Roman, L. M. *J. Org. Chem.* **1999**, *64*, 5575. (d) Wolfe, J. P.; Buchwald, S. *Angew. Chem., Int. Ed.* **1999**, *38*, 2413. (e) Stauffer, S. R.; Lee, S.; Stambuli, J. P.; Hauck, S. I.; Hartwig, J. F. *Org. Lett.* **2000**, *2*, 1423. (f) Marion, N.; Navarro, O.; Mei, J.; Stevens, E. D.; Scott, N. M.; Nolan, S. P. *J. Am. Chem. Soc.* **2006**, *128*, 4101 (g) Ogata, T.; Hartwig, J. F. *J. Am. Chem. Soc.* **2008**, *130*, 13848. (h) Biscoe, M. R.; Fors, B. P.; Buchwald, S. L. *J. Am. Chem. Soc.* **2008**, *130*, 6686. (i) Wheaton, C. A.; Bow, J.-P. J.; Stradiotto, M. *Organometallics* **2013**, *32*, 6148

12) Huang, X.; Anderson, K. W.; Zim, D.; Jiang, L.; Klapars, A.; Buchwald, S. L. *J. Am. Chem. Soc.* **2003**, *125*, 6653

13) Fors, B. P.; Watson, D. A.; Biscoe, M. R.; Buchwald, S. L. *J. Am. Chem. Soc.* **2008**, 130, 13552.

14) Isolation of the XPhos **L7** oxidative addition complex is problematic, so a first generation precatalyst **P7** was employed. For comparative purposes, the BrettPhos **L6** first generation precatalyst **P6** was also used. The oxidative addition complex **OA6** for BrettPhos **L6** gave similar results when compared to **P6**. For precatalyst synthesis see reference 11h

15) For the reaction employing **P6** (at 20 °C; Scheme 2), we observed a characteristic fast initial rate as seen in the previous reaction examples. This reaction was repeated with **OA6** catalyst (1 mol %) and monitored by ^{31}P-NMR. Under these conditions, we estimate time for the completion of the reaction to be less than two hours. Free ligand **L6** was observed by ^{31}P-NMR. Due to the continuous formation of precipitating NaBr, quantification of the NMR signal was impractical.

16) By substituting 2-bromotoluene for 3-bromoanisole for the coupling of *n*-propylamine, the reaction proceeded to give several turnovers (~3) before halting. Observation by ^{31}P-NMR indicates the formation of free ligand. Thus there is some indication that tert butyl substituents may for some reactions provide enough stability that the reaction will go to completion quickly but a change of substrates will displace the supporting ligand from the palladium center. We did not focus our studies on this class of ligands, since they are known to undergo rearrangement,

which unnecessarily complicates any in-depth analysis. See Milner, P. J.; Maimone, T. J.; Su, M.; Chen, J.; Muller, P.; Buchwald, S. L. *J. Am. Chem. Soc.* **2012**, *134*, 19922

17) See reference 6a. As an aside, an inverse temperature dependence on the reaction was found. At 0.4 mol% loading at 105 °C the reaction would not go to completion, while the same reaction at 60 °C finished the reaction within an hour. GC-MS of the reaction mixture of the (105 °C) reaction indicated the presence of triphenlyphosphine.

18) (1) (a) Surry, D. S.; Buchwald, S. L. *Chem. Sci.* **2011**, *2*, 27. (b) Hartwig, J. F. *Acc. Chem. Res.* **2008**, *41*, 1534. (c) Hartwig, J. F. *Angew. Chem., Int. Ed.* **1998**, *37*, 2046. (d) Kienle, M.; Dubbaka, S. R.; Brade, K.; Knochel, P. *Eur. J. Org. Chem.* **2007**, 4166. (e) Maiti, D.; Fors, B. P.; Henderson, J. L.; Nakamura, Y.; Buchwald, S. *Chem. Sci.* **2011**, *2*, 57

19) ^{31}P-NMR experiments that quantified the amount of displaced **L1** were performed with inverse gated decoupling and a delay time of 60 seconds. For signal-to-noise ratio of sufficient quality, 64 transients were typically recorded thus giving a measurement time of 1 hour.

20) We also observed some formation of 3,3'-dimethoxybiphenyl and products the related to the scission of the P-C$_{aryl}$ bond of the supporting ligand **L1**. This implies some type of interaction possibly between **II'** and **V** (or **II/OA1**) as shown in Scheme 3-5. Consequently the "off-cycle" palladium species may not be composed of a single Pd(II) species or a single oxidation state. Regardless, the data suggests that the "off-cycle" palladium is predominately Pd(II). (a) Ozawa, F.; Fujimori, M.; Yamamoto, T.; Yamamoto, A. *Organometallics* **1986**, *5*, 2144. (b) Wang, D.; Izawa, Y.; Stahl, S. S. *J. Am. Chem. Soc.* **2014**, *136*, 9914 (c) Albeniz, A. C.; Espinet, P.; Lopez-Cimas, O.; Martin-Ruiz, B. *Chem. Eur. J.* **2005**, *11*, 242. d) Casado, A. L.; Casares, J. A.; Espinet, P. *Organometallics* **1997**, *16*, 5730. e) Asselt, R. v.; Elsevier, C. J. *Organometallics* **1994**, *13*, 1972. f) Ozawa, F.; Hidaka, T.; Yamamoto, T.; Yamamoto, A. *Journal of Organomet. Chem.* **1987**, *330*, 253. g) Parshall, G. W. *J. Am. Chem. Soc.* **1974**, *96*, 2360.

21) Shekhar, S.; Ryberg, P.; Hartwig, J. F. *Organic Letters* **2006**, *8*, 851.

22) (a) Casado, A. L.; Espinet, P. *Organometallics* **1998**, *17*, 954. (b) for *trans*-effect see, Langford, C. H.; Gray, H. B. *Ligand Substitution Processes*, 1966., and references therein, (c) the *trans*-configuration has been shown to be energetically accessible for this class of ligands if the alkyl substituent on the phosphine are *tert*-butyl, see Milner, P. J.; Maimone, T. J.; Su, M.; Chen, J.; Muller, P.; Buchwald, S. L. *J. Am. Chem. Soc.* **2012**, *134*, 19922 (d) For oxidative addition stereochemistry see. Barder, T. E.; Biscoe, M. R.; Buchwald, S. *Organometallics* **2007**, *26*, 2183. (e) Li Z.; Fu, Y.; Guo, Q.-X.; Liu, L. *Organometallics* **2008**, *27*, 4043.

23) Reid, S. M.; Boyle, R. C.; Mague, J. T.; Fink, M. J. *J. Am. Chem. Soc.* **2003**, *125*, 7816.

(24) The lower temperature (75 °C vs. 105 °C) allows for a higher catalyst concentration (0.4 mol % *OA1) to give a reaction time of about 3 hours. At 0.3 mol % (*OA1) at 105 °C, the reaction time is about 10 minutes. Low catalyst loadings will favor weak substrate dependencies (near constant rate) while a higher catalyst loading better demonstrate the inverse dependence upon amine and aryl halide.

25) Experiments were carried out in which the initial concentration of NaOtBu was varied. We did not find any kinetic dependence upon the base at 75 °C and 0.4 mol % *OA1.

(26) We have limited our proposed mechanism to include only two types of palladium(0) and have labeled them as Complex I and Complex I'. There are other palladium(0) complexes which may be kinetically relevant. These potential species are listed in the Scheme 2-8 .

(27) We found that the substitution of the aryl halide (3-chloro/bromo/iodoanisole) at 20 °C (1.0 mol % OA1) did not afford significantly different yields (20 to 30%) or conversions. We also performed several experiments with excess L1 at 30 °C (0.8 mol % OA1), and observed no significant differences in yield (~45 %), which suggests that association of L1 with "off-cycle" palladium is not appreciable at lower temperatures.

(28) Similar behavior was seen for the cross-coupling of 4-bromoanisole vs. 4-chloroanisole with morpholine using an XPhos-based (L2) catalytic system: Barjian, S.; Tom, D. M. E.; Baird, M. C. *Organometallics* **2014**, *33*, 3928. A second system based on a modified biaryl phosphine ligand for the coupling acyclic amides also showed a similar behavior where the reaction rate of the catalytic system was shown to be ArCl > ArBr >> ArI. See Hicks, J. D.; Hyde, A. M.; Cuezva, A. M.; Buchwald, S. *J. Am. Chem. Soc.* **2009**, *131*, 16720.

(29) Chloride ions have been shown to also have an effect on palladium catalysis: (a) Amatore, C.; Jutand, A.; *Acc. Chem. Res.* **2000**, *33*, 314. (b) Kozuch, S.; Amatore, C.; Jutand, A.; Shaik, S. *Organometallics* **2005**, *24*, 2319. (c) Amatore, C.; Jutand, A.; Suarez, A. *J. Am. Chem. Soc.* **1993**, *115*, 9531. (d) Amatore, C.; Azzabi, M.; Jutand, A. *J. Am. Chem. Soc.* **1991**, *113*, 8375. (e) Jutand, A. *Appl. Organometal. Chem.* **2004**, *18*, 574.

(30) The substitution of 3-iodoanisole (in toluene) for 3-bromoanisole gave comparable rates to 3-bromoanisole at 75 °C for a *OA1-based catalyst. For the role of solvent in coupling of aryl iodides see, Fors, B. P.; Davis, N. R.; Buchwald, S. L. *J. Am. Chem. Soc.* **2009**, *131*, 5766.

31) We should also point out that aryl chlorides also exhibit the behavior seen for aryl bromides. By diminishing the catalyst loading for an aryl chloride, we can recover the plateau behavior seen for aryl bromides (Figure 2-51).

32) At ambient temperatures additional L1 did not have an effect on reaction rates.

33) This parameter affects only the initial rate of reaction for the case where the "on-cycle" initial value condition is used. With increasing value the initial simulated reaction rate becomes greater but so does the speed towards the plateau region increase as well.